THE UNIVERSITY of ADELAIDE

Development of Next-Generation Construction Materials with Graphene Additives

Van Dac Ho

Master of Engineering (Civil and Structural)

Bachelor of Civil Engineering

A thesis submitted in fulfilment of the requirements for the degree of Doctor of Philosophy

The University of Adelaide

Faculty of Engineering, Computer and Mathematical Sciences

School of Civil, Environmental and Mining Engineering

September 2020

Development of Next-Generation Construction Materials with Graphene Additives

By:

Van Dac Ho

Supervised by:

Professor Dusan Losic, Ph.D.,
School of Chemical Engineering and Advanced Materials,
The University of Adelaide

Associate Professor (Alex) Ching-Tai Ng, Ph.D.,
School of Civil, Environmental and Mining Engineering,
The University of Adelaide

A thesis submitted in fulfilment of the requirements for the degree of Doctor of Philosophy

School of Civil, Environmental and Mining Engineering
Faculty of Engineering, Computer and Mathematical Sciences
The University of Adelaide
North Terrace, Adelaide, SA 5005, Australia

Email: vandac.ho@adelaide.edu.au

Table of contents

Abstract

The developments of ordinary Portland cement (OPC) composites and alkali-activated binder composites have attracted significant attention in the past decade. Different technologies have been proposed to address current drawbacks of these construction materials (e.g. low tensile strength, flexural strength, and brittleness), reduce the amount of cement consumption or replace OPC products for minimizing the environmental impact of construction materials. Among many additives explored to address these problems, graphene-based materials have emerged in the last few years as one of the most promising additives with many exciting results. However, it is still lacking the depth of understanding the influence of key parameters of graphene materials, such as dosages and sizes, on mechanical and durability properties of the composites, and enhancing mechanism of pristine graphene (PRG) in the cement matrix. Moreover, no study has been reported on the influence of graphene oxide (GO) additives on mechanical and durability properties of fly ash (FA)/ ground granulated blast furnace slag (GGBS) alkali-activated binder (AAB) composites prepared with natural sand (NS) or lead smelter slag (LSS) sand cured at ambient temperature. This thesis consists of a series of studies with the focus on addressing current research gaps and making a contribution to the development of next-generation construction materials using graphene additives.

The first experimental study on the effect of the dosage of an ultra-large size (56μm) of PRG industrially manufactured by an electrochemical process on compressive and tensile strengths of cement-based mortars reveals that the addition of PRG to mortars improves their mechanical properties, with characteristic concentration dependence. The mortar with 0.07% PRG is identified as the optimal concentration, which provides 34.3% and 26.9% improvement in compressive and tensile strength at 28 days, respectively. However, with the further increases in PRG contents, the enhancement of mechanical properties of mortars is limited due to the impact of the van der Waals force on the sedimentation of PRG suspension.

The second study focuses on the size effect of PRG on mechanical strengths of cement-based mortars by considering a variety of PRG sizes, such as 5μm, 43μm, 56μm, and 73μm at the optimal dosage of 0.07% PRG. The study reveals that the mechanical strengths of mortars at 7 and 28 days significantly depend on the sizes of PRG. The mixes with size 56μm and 73μm show a significant influence on both the compressive and tensile strengths of mortars. In contrast, the mix containing size 43μm exhibits a significant increase in tensile strengths only. There are no significant effects on either compressive or tensile strengths for the mix with size 5μm.

The third study presents the proposed reinforcing mechanism and optimized dosage of PRG for enhancing mechanical properties of cement-based mortars. The results confirmed that the strengths of the mortars depend on PRG dosages. The size of PRG has a significant effect on the enhancement rate of the mechanical strengths of the mortars, whereas it does not have a significant influence on the optimized PRG dosage for the mechanical strengths of the cement-based mortars. The dosage at 0.07% PRG is identified as the optimized concentration of PRG for enhancing mechanical strengths. The reinforcing mechanism of PRG in the cement matrix highly depends on the surface area of PRG sheets.

The fourth and fifth studies show the effect of the dosages, sizes, and densities of PRG as well as design mixes on mechanical and durability properties of cement-based mortars cured at short-term and long-term periods. The study reveals that the addition of PRG to mortars can enhance compressive, flexural, and tensile strengths of mortars at different curing ages. The 0.07% PRG is identified as the optimum dosage for enhancing the mechanical strengths of the mortars. Incorporating a small amount of PRG additives into the mortar can improve its durability, such as water absorptions, voids, sulphate expansion, and water penetration depths. The results of the mix containing PRG size 73μm show the best improvement in the mechanical and durability properties of the mortars, followed by that of size 20μm and then size 40μm.

The last experimental study on the influence of GO additive on mechanical and durability properties of AAB mortars containing NS and LSS sand cured at ambient temperature reveals that the increase of GGBS% in AAB results in a significant increase in compressive and tensile strengths, and a decrease in flowability, water absorption and dry shrinkage of the mortars. The results also show that the mortars with 0.05% and 0.1% GO additives provide better mechanical and durability properties compared to the control mixes.

The results generated from this thesis show great potential for using PRG and GO as additives in OPC and AAB composites to develop next-generation construction materials. They not only address the current drawbacks of OPC and AAB composites but also reduce the environmental impact of using OPC and NS.

Statement of Originality

I, Van Dac Ho, certify that this work contains no material which has been accepted for the award of any other degree or diploma in my name, in any universities or other tertiary institutions and, to the best of my knowledge and belief, contains no material previously published or written by another person, except where due reference has been made in the text. In addition, I certify that no part of this work will, in the future, be used in a submission in my name, for any other degree or diploma in any universities or other tertiary institutions without the prior approval of the University of Adelaide and where applicable, any partner institution responsible for the joint-award of this degree.

I acknowledge that copyright of published works contained within this thesis resides with the copyright holder(s) of those works.

I also give permission for the digital version of my thesis to be made available on the web, via the University's digital research repository, the Library Search and also through web search engines, unless permission has been granted by the University to restrict access for a period of time.

Signed: Van Dac Ho Date: 23/09/2020

Acknowledgements

Firstly, I would like to sincerely thank my supervisors; Professor Dusan Losic and Associate Professor (Alex) Ching-Tai Ng, for their supervision, guidance and patience with my research. Without their support, this thesis would not be possible.

I am grateful to all my friends and the staff of the School of Civil, Environmental and Mining Engineering for their inspirations and advice that helped me overcome difficult times during my research.

I also thank Jon Ayoub, Adam Ryntjes, Dale Hodson, Gary Bowman for providing technical assistance in performing many experimental tasks.

I must thank The University of Adelaide for providing me with the scholarship to undertake this research. I also thank the ARC Research Hub and First Graphene Ltd for their support and funding.

Last but not least, I am grateful to my parents; Dai Ho and Thi Thuy Huong Nguyen, my wife; Thi My Nhat Phan, and my daughter; My Anh Ho, who supplied me with unwavering encouragement and motivation that helped me so much throughout this special and remarkable journey.

List of Publications

Journals papers – Published, Accepted for Publication, Submitted for Publication, In preparation

(1) **Ho, V. D.,** Ng, C. T., Coghlan, C. J., Goodwin, A., Mc Guckin, C., Ozbakkaloglu, T., & Losic, D. (2020). Electrochemically produced graphene with ultra large particles enhances mechanical properties of Portland cement mortar. *Construction and Building Materials*, *234*, 117403. (Published)

(2) **Ho, V. D.,** Ng, C. T., Ozbakkaloglu, T., Goodwin, A., Mc Guckin, C., Karunagaran, R. U., & Losic, D. Influence of pristine graphene particle sizes on physicochemical, microstructural and mechanical properties of Portland cement mortars. *Construction and Building Materials*. (Published)

(3) **Ho, V. D.,** Ng, C. T., Ozbakkaloglu, T., Karunagaran, R. U., Farivar, F., Goodwin, A., Mc Guckin, C., Ho, V. D., & Losic, D. Investigating the reinforcing mechanism and optimized dosage of pristine graphene for enhancing mechanical strengths of cementitious composites. (In preparation)

(4) **Ho, V. D.,** Gholampour, A., Losic, D., & Ozbakkaloglu, T. Influence of graphene oxide on the properties of ambient-cured alkali-activated binder mortars prepared with natural sand and lead smelter slag. (In preparation)

Contributing papers

(5) Gholampour, A., **Ho, V. D.,** & Ozbakkaloglu, T. (2019). Ambient-cured geopolymer mortars prepared with waste-based sands: Mechanical and durability-related properties and microstructure. *Composites Part B: Engineering*, *160*, 519-534. (Published)

CHAPTER 1: INTRODUCTION AND GENERAL OVERVIEW

1. Research background

1.1. Ordinary Portland cement and some of its limitations

Ordinary Portland cement (OPC) is a complex product manufactured from the combination of limestone and clay that is heated up to a high temperature at about 1450^0C. It is one of the most commonly used cementitious materials in building construction worldwide due to its outstanding properties, such as high compressive strength, low cost, and global availability. However, the process to create OPC is considered to be one of the major contributors to greenhouse gases leading to a high impact on climate change [1, 2]. It contributes approximately 7% of the carbon dioxide (CO_2) emissions into the atmosphere globally. Therefore, it has attracted significant research interests in recent years to reduce the amount of CO_2 emissions associated with OPC production. In addition, OPC suffers from low tensile strength, flexural strength, brittleness, and resistance to crack propagation and corrosive environment (e.g. sulfate ion, chloride ion). These cause durability problems and costly maintenance for construction products [3-5]. As a result, several approaches were explored by researchers to address these drawbacks, such as improving cement plant efficiency [1], using supplementary materials [6-8], and alternative binders [9]. In these approaches, there have been intensive studies with many significant publications in recent decades on using **supplementary materials and alternative binders to either improve the properties of cementitious composites or replace OPC in the composites** [1, 7-10].

1.2. A general overview of using supplementary materials (additives) to address the drawbacks of OPC

OPC binder consists of four main components, i.e. tricalcium silicate (C_3S), dicalcium silicate (C_2S), tricalcium aluminate (C_3A), tetracalcium ferroaluminate (C_4AF), and a small amount of gypsum. These components react with water to create bonds in the cement matrix via the

hydration cement process. The products of this chemical reaction process include calcium silicate hydrate (CSH), Portlandite (CH), and ettringite (Aft). Among them, CSH gels are the main part of cement paste contributing to mechanical strengths of cementitious composites [11, 12]. Therefore, in order to improve the properties of cementitious composites, most studies have focused on enhancing the properties of CSH gels (or cement paste). For better visualization of the cement matrix, the multiscale nature of cement-based composites is shown in Fig. 1 [13].

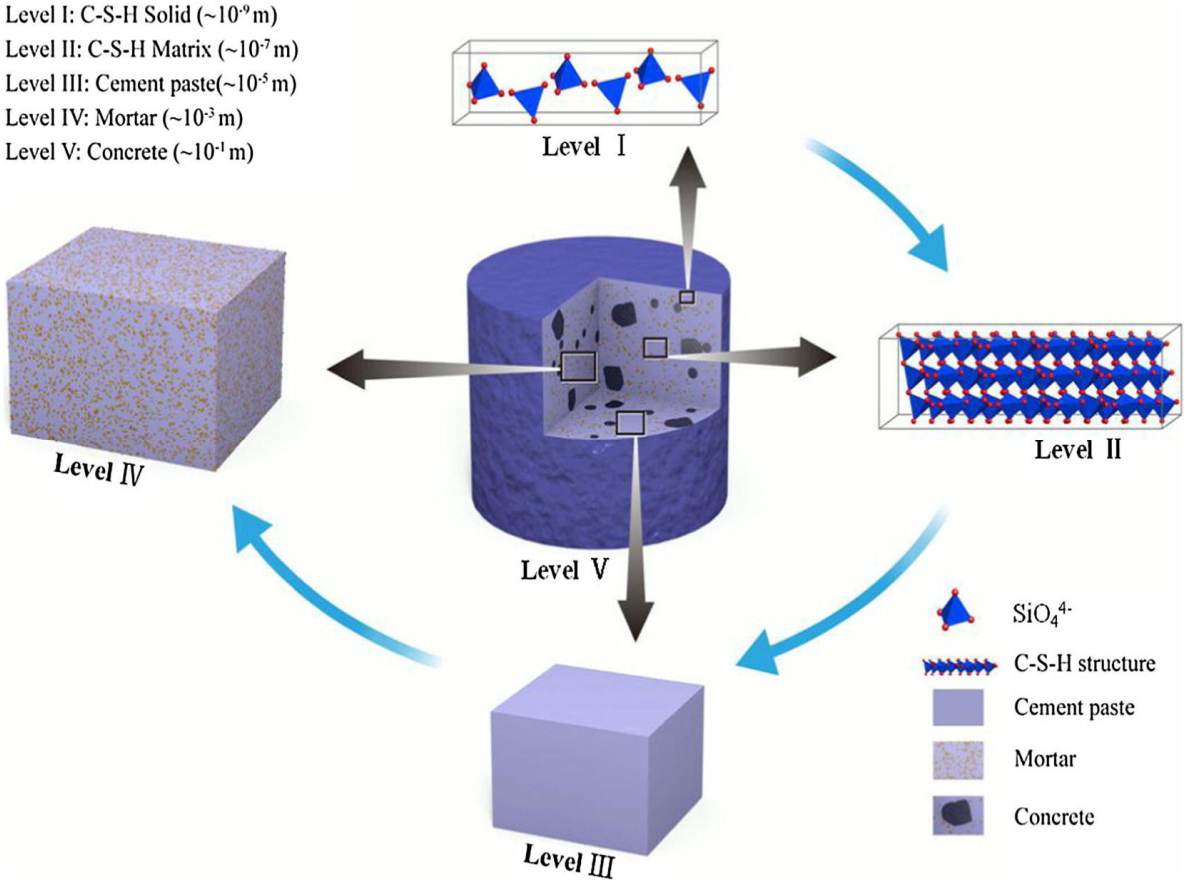

Fig. 1. Overview of the multiscale nature of cement-based composites [13]

Several methods have been used to improve the cement matrix by using supplementary materials (additives) from macroscale (e.g. fibers) to nanoscale (e.g. nano-silica). The sections below highlight some presentative studies of these methods and their limitations:

1.2.1. Fibrous-based reinforcement methods

Researchers have studied various types of fibers from synthetic fibers to natural fibers, such as steel fibers [14], glass fibers [15], polypropylene fibers [16] or coir [17], to reinforce the structural performance of cement-based composites. Steel fibers are commonly used in cement-based composites due to their outstanding mechanical properties and availability. Felekoğlu et al. [18] reported that adding steel fibers at 2% by volume fraction into the design mix could enhance the 28-day flexural strength of cement-based mortar by 40%, whereas there was no significant influence of steel fibers on compressive strengths. Song and Hwang [19] studied the effect of different volume fractions of steel fibers on the mechanical properties of high-strength concrete. They revealed that while the compressive strength of the fiber-reinforced concrete is improved by 15.3% at 1.5% volume fraction, the splitting tensile strength of the fiber-reinforced concrete increases with the volume fraction and enhanced by 98.3% at 2% volume fraction. Although the incorporation of steel fibers into cementitious composites showed advantages in improving their mechanical properties, one of the concerns of using steel fibers materials in cementitious composites is corrosion, which affects the durability and performance of structures [20, 21]. Other fibrous materials, such as glass fibers, polypropylene fibers, are non-renewable resources, expensive and one-dimensional materials. Therefore, they both cause environmental problems and have drawbacks in the structure of the interface of fibers and cement matrix, which impacts mechanical and durability properties of cementitious composites [22].

1.2.2. Nanomaterials additives-based reinforcement methods

The use of nanomaterials to reinforce cement-based composites is a promising method to refine the structure of CSH gels and cement matrix. Different studies have incorporated a variety of nanomaterials, such as nano-silica [23], nano-alumina [24], nano-titanium [25], nano-ferric oxide [26], and nano kaolin [27], to improve microstructures at the nanoscale and enhance the performance of cementitious composites. Among them, nano-silica has attracted significant

interests in the research field of cement-based composite materials because it not only provides seeding and filling effects like other nanomaterials, but also chemically react with the cement matrix to create silicate chain [28]. This results in a good performance in the properties of cementitious composites. Li et al. [26] investigated the effect of the different dosages of nano-silica (i.e. 3%, 5%, and 10% by weight of cement binder) on 7- and 28-day compressive strengths of cement paste. They showed that incorporating 3%, 5%, and 10% nano-silica into cement paste could enhance 7-day & 28-day compressive strengths by 6%, 20%, and 20% & 14%, 17%, and 26%, respectively. According to Ref. [29], the addition of 0.25% nano-silica to cement-based mortars could enhance 28-day compressive and flexural strengths of the mortars by 4.1% and 18%, respectively. Qing et al. [23] demonstrated that 28- and 60-day compressive strengths of cement paste prepared with 5% nano-silica could enhance by 25% and 15%, respectively. Another study performed by Li et al. [30] showed that incorporation 1% nano-silica into the cement-based concrete could improve its compressive strength, flexural strength, and abrasion resistance at 28 days about 12.3, 4.2, and 157%, respectively. Although nano-silica presents beneficial effects on enhancing the performance of cementitious composites, it also has some disadvantages limiting its applications as construction materials, such as high cost, inconsistent results among studies, negative effects on setting time of composites, and only available in certain countries. Moreover, like nano-silica, other nanomaterials are low aspect ratios. This leads to a lack of ability to arrest microcracks derived from nano-cracks, resulting in the less efficiency of their enhancement [31].

1.2.3. Carbon materials-based reinforcement methods

1.2.3.1 Carbon nanofibers and carbon nanotubes additives (one-dimension materials)

Carbon-based nanomaterials, which primarily consist of carbon atoms with low density and high aspect ratio, have been attracted significant research interests to combine them with construction materials. As a result, the number of studies that combined carbon-based

nanomaterials and cementitious composites, such as carbon nanofibers [32, 33], carbon nanotubes [34, 35] to enhance their performances, has considerably increased recently. Gdoutos et al. [36] investigated the effect of carbon nanofibers on flexural strength and fracture toughness of cement-based mortars. The study showed that the addition of 0.1% carbon nanofibers could increase 28-day flexural strength and fracture toughness of the mortar by 105.9% and 128.6%, respectively. As reported in Ref. [33], incorporating 0.2% carbon nanofibers into cement paste could enhance 28- and 56-day compressive strength about 30.2% and 13.8%, respectively. Xu et al. [35] investigated the effects of multi-walled carbon nanotubes on the mechanical and microstructure properties of cement paste. The study revealed that the addition of 0.1% multi-walled carbon nanotubes could increase 7-day and 28-day compressive strengths by 22% and 15%, respectively. According to Ref. [34], Portland cement pastes containing 0.12% multi-walled carbon nanotubes could enhance a 28-day flexural toughness index by 31.6% and decrease 28-day porosity by 20.9% compared with the control mix. Carriço et al. [37] studied the influence of carbon nanotubes of 0.05% and 0.1% on compressive strength and durability properties (i.e. water absorption, chloride penetration resistance, carbonation resistance) of cement-based concrete prepared with different water and cement ratios. The study showed that the addition of 0.05-0.1% carbon nanotubes increases 28-day compressive strength and durability properties of the concrete up to 21% and 25%, respectively. The mix containing the dosage of 0.1% has better enhancement rate than that of 0.05%. Although carbon nanofibers and carbon nanotubes can enhance mechanical and durability properties of cement-based composites, there have been some challenges and disadvantages in terms of the application of cement-based construction materials, such as costly materials [38], the formation of agglomeration due to strong van der Waals forces that leads to the influence on a combination of them and the cement matrix [31, 39, 40], a lack of interfacial areas between these nano materials and the cement matrix that reduces their reinforcing efficiency [31, 41].

1.2.3.2 Graphene-based additives (two-dimension materials)

From the above analyses, it is clear that the use of nanoparticles (zero dimension), carbon nanofibers and carbon nanotubes (one dimension) in cement-based composites is unable to enhance their performances efficiently due to the low aspect ratio of zero-dimension materials and the lack of interfacial area between one-dimension materials and the cement matrix. Graphene, a -two-dimensional material with a single layer sheet of sp^2 bonded carbon atoms, was discovered in 2004 [42]. This two-dimension material has shown great potential for applying in a variety of research fields due to its outstanding properties, e.g. high mechanical properties, large specific surface areas and aspect ratios, and high conductivity [43-48]. The graphene derivatives that have been commonly studied in civil engineering are graphene oxide (GO), reduced graphene oxide (rGO), and pristine graphene (PRG), which was also named as graphene nanoplatelets in other studies. There are different methods to produce these graphene materials. GO, which consists of a high level of oxygen-functional groups (i.e. hydroxyl, epoxide, carboxyl, and carbonyl), can be produced by Hummer or modified Hummer's methods [49, 50]. RGO, which composes of a lower level of these oxygen-functional groups, can be produced by thermal or chemical processes [51, 52]. PRG, which consists of several layers of sp^2 bonded carbon atoms, can be produced by thermal, mechanical, or electrochemical processes [45, 53-55]. Their chemical representation is shown in Fig. 2 [56, 57]. The research of incorporating these materials into cement-based composites is generally described in the sub-sections below.

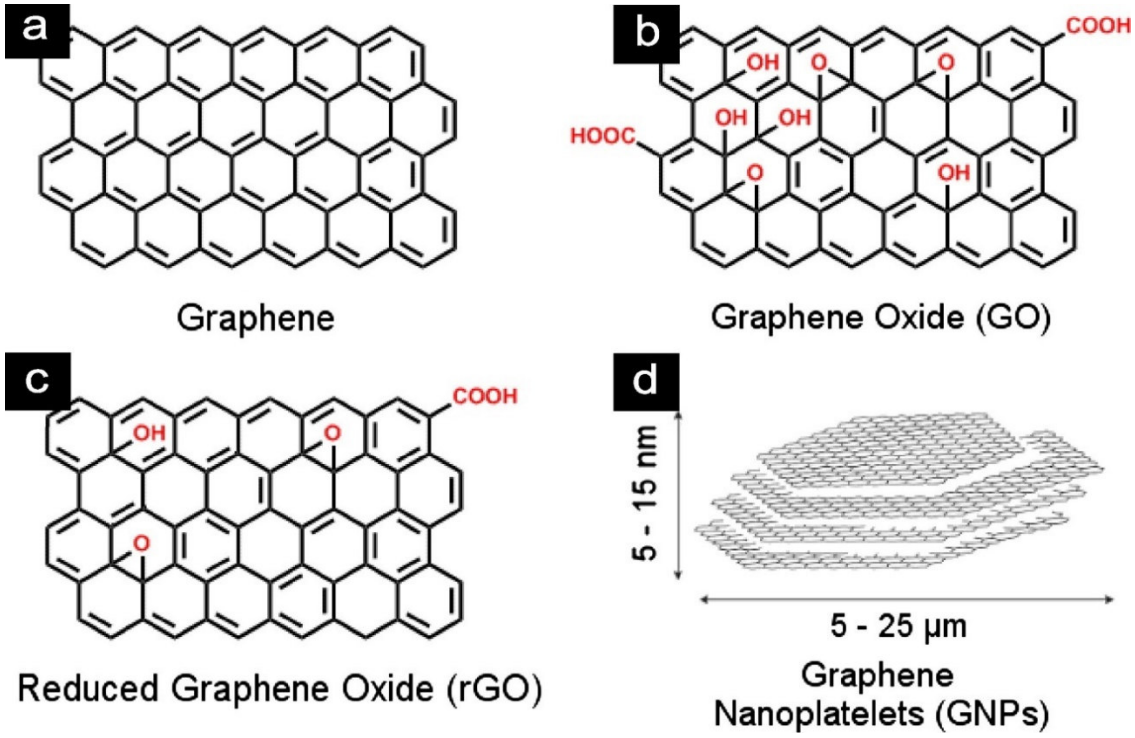

Fig. 2. Chemical representation of graphene and its derivatives: (a) graphene, (b) graphene oxide, (c) reduced graphene oxide, (d) common sizes of graphene nanoplatelets [56, 57].

1.2.3.2.1 Graphene oxide and reduced graphene oxide additives

GO with a high level of the abundance of oxygen-functional groups is highly dispersive in water, and thus, it has attracted significant attention in using GO to improve the properties of cement composites in the literature [13, 57, 58]. One of the pioneer studies on the effect of GO on microstructure and mechanical properties of cementitious composites was investigated by Lv et al. [12]. The study showed that the addition of 0.03% GO to cement-based mortars could not only improve 28-day compressive, tensile, and flexural strengths by 38.9%, 78.6%, and 60.7%, respectively, but also regulate the microstructures of the mortars. Wang et al. [59] found that using 0.05% GO in cement pastes increase compressive and flexural strength at 28 days, of 40.4% and 90.5%, respectively. Lv et al. [60] reported that 0.06% GO could enhance the compressive strength of the cement paste by 58.5% after 28 days, while the flexural strength could improve by 67.1% after 28 days with 0.04% GO concentration. Mohammed et al. [61] presented that the cement mortar with 0.03% GO additive could increase 30% compressive strength at 28 days. The effects of different GO dosages and sizes on microstructures of cement

mortars were also studied by Sharma and Kothiyal [62]. The study showed that the properties of cement mortars strongly depend on the dosages and sizes of GO. The mix with a smaller GO size (i.e. 100nm) improves compressive strength by 86% at 1% GO concentration. This improvement is more than that of using the larger GO size (i.e. 900nm) at the same dosage, which only improves 63%. The reinforcing mechanism of GO on mechanical properties of cementitious composites is attributed to the considerable effect of oxygen-functional groups of GO on the cement matrix. Several studies reported that the reinforcing mechanism of mechanical strengths of GO-cement based composites are mainly governed by chemical reactions between hydroxyl and carboxyl groups of GO and the mediating Ca^{2+} ions from calcium silicate hydrate of cementitious gels (Fig. 3). This results in a space network structure in the cement matrix that enhances the load transfer efficiency in cementitious composites [31, 63].

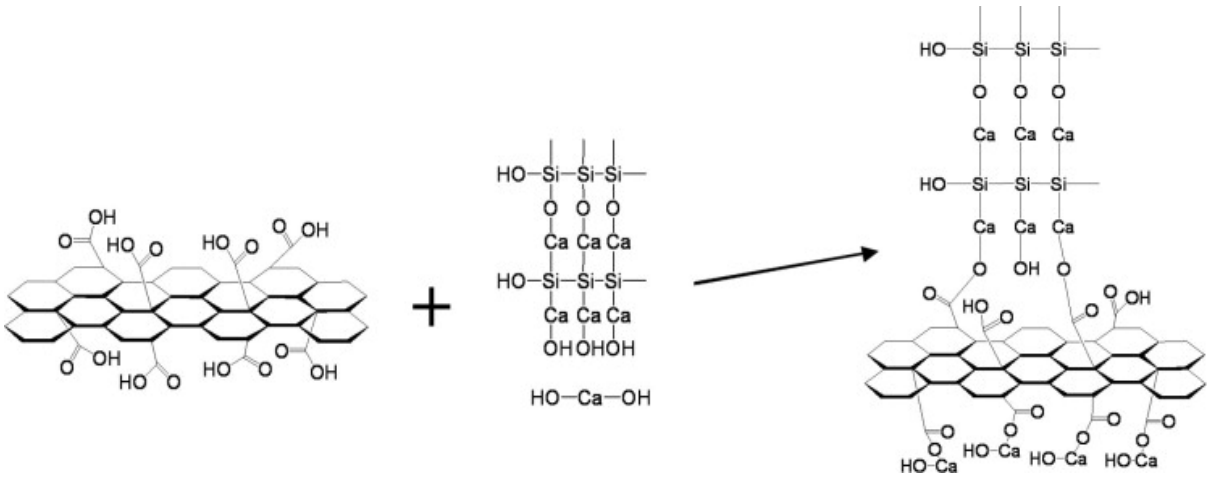

Fig.3. Outline the schematic reaction between GO and hydration products [31].

There have been few studies investigating the influence of rGO on the properties of cementitious composites. Murugan et al. [64] revealed that the addition of 0.02% rGO to cement paste could not only enhance 28-day compressive and flexural strengths of the paste about 22% and 23% respectively but also refine voids and capillary pores in the cement paste. The effect of different dosages of rGO on the properties of cement paste was investigated by Qureshi and

Panesar [65]. The study showed that 0.06% rGO could improve the compressive and flexural strengths of the cement paste at 28 days by 14.9% and 33.7%, respectively. The influence of different sizes of rGO on the mechanical properties of cement-based mortars was also revealed in the study of Kiamahalleh et al. [66]. The results showed that the mix containing 0.1% rGO with the smallest size of exhibited 91% and 52.5% higher 28-day compressive and tensile strength than the plain, respectively. Although GO and rGO materials have shown beneficial effects on mechanical and durability properties of cementitious composites, they still have some limitations that need to be addressed before applying them as constructional materials. The first limitation is that there is a wide range of optimum dosages of GO (i.e. from 0.01% to 1%) for enhancing the properties of cement-based composites presented in the literature [13, 57, 58], which causes the difficulty for practical applications. Secondly, the current methods to produce these materials are costly and cause negative environmental impacts due to producing toxic emissions [67]. The other limitation is that GO and rGO are materials with a high level of defects and less crystalline and weak mechanical properties than PRG [68, 69], resulting in the effects on their interactions with the cement matrix.

1.2.3.2.2 Pristine graphene additives

PRG materials have low levels of defects, stronger crystalline and mechanical properties and can be produced by an environmentally sustainable process in high quality at industrial scales, which are outlined in Figs. 4 and 5, with much lower costs than GO and rGO. Therefore, the application of PRG in cementitious composites is expected to be more beneficial for improving structural performances of cement-based materials. Besides, the limitation in water dispersion of PRG sheets (PRGs) has been addressed in recent studies by using superplasticizer and ultrasonication methods [70, 71]. As a result, the number of studies on combining PRG and cementitious composites has increased recently. It has been shown in the literature that a small amount of PRG has great potential to enhance the strength of PRG-cement composites [71-74]. Wang et al. [71] investigated the different compressive strengths of cement mortars between

the control mix and the mix containing 0.05% PRG. The study reported that compressive and flexural strengths at 7 days of the mortar with 0.05% PRG were improved by 8% and 24%, respectively. As reported in Ref. [72], the compressive strength of cement mortar could improve by 19.9% after 28 days by adding 0.1% PRG. A recent study of PRG-cement mortars with different PRG concentrations (i.e. 0%, 0.05%, 0.1%, 0.5% and 1% by weight of cement) showed that the cement-based mortar with 0.05% PRG additive could improve 28-day compressive strength and flexural strengths at 28 days by 8.3% and 15.6%, respectively. However, the strengths start decreasing when the PRG dosages were increased to exceed 0.05% due to the agglomeration of PRGs [74]. Baomin and Shuang [73] investigated the use of four different PRG dosages (i.e. 0%, 0.03, 0.06, and 0.09%) in cement paste and reported that the optimal PRG dosage of 0.06% could increase the compressive and flexural strength of the cement paste at 28 days by 11% and 27.8%, respectively. Another study with four different PRG concentrations (i.e. 0%, 2.5%, 5.0%, and 7.5%) showed that the incorporation of PRG into cement mortars could considerably decrease water penetration depth whereas there were insignificant effects of PRG on compressive and flexural strengths of cement mortars, which was due to the agglomeration of PRG coming from the high PRG dosages rate used [75].

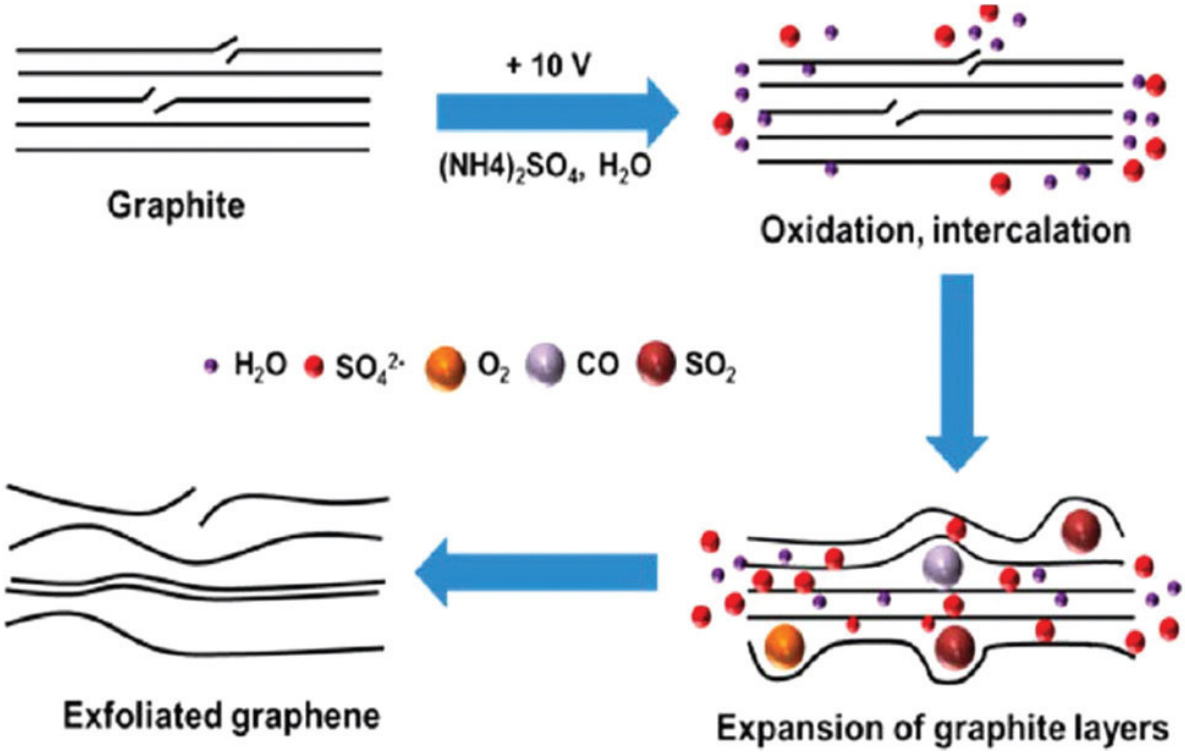

Fig. 4. Electrochemical production of graphene: a new generation of graphene materials [54, 55].

Fig. 5. Photos of production facilities of PRG materials manufactured at the industrial scale by an electrochemical process at First Graphene Ltd in Perth, Australia (https://firstgraphene.net/).

Although these studies presented the dependence of the properties of PRG-cement mortars on PRG dosages, the characteristics of the mechanism behind this dependence have not been well understood. In addition to the dosage of PRG, several parameters of PRGs, such as particle sizes, number of layers, and level of defects, can affect the performance of PRG-cement based composites. As reported in Refs. [76-78], these parameters have a significant influence on mechanical properties of polymer composites. However, there were very limited studies on the effects of these parameters on mechanical properties of PRG-cement based composites. Moreover, unlike GO and rGO, PRG materials have very few oxygen-functional groups. Therefore, the reinforcing mechanism of PRG for enhancing the properties of cementitious composites is different and has not been revealed in the literature [13, 57, 71, 74]. To date, research on the effects of PRG additives on the durability properties of PRG-cement composites has not been sufficiently studied, although the durability properties are important to service life, maintenance costs, and practical applications of the construction structures. Besides, the existing studies only investigated the effects of graphene materials on the short-term mechanical properties (e.g. 7-, 14-, or 28-day curing ages) of cementitious composites and no studies have been done to investigate the effect of dosages and sizes of graphene materials on the long-term mechanical properties (e.g. curing ages of 3 months, 6 months, 9 months or over) of cementitious composites. Together with the dosages and sizes of PRG, the effects of design mixes of water and cement ratios can be an important factor. It affects enhancement rates of the properties of PRG-cement based composites because it has an impact on the strengths of cementitious gels, resulting in the influence on a combination of PRGs and cementitious gels. These have not been investigated in the literature. This PhD project will address these aforementioned research gaps.

1.3. A general overview of using alternative binders to replace OPC binder

As mentioned in Section 1.1, the OPC binder has a high impact on climate change [1, 2]. Therefore, researchers have investigated some new materials that can partially or fully replace

OPC. Among them, alkali-activated binders have been identified as one of the most promising materials. Geopolymers are one of alkali-activated binders that have the gels formed by the geopolymerization process, which are chemical reactions between materials with high aluminosilicate constituents, such as fly ash, and alkali activators. Researchers have also explored the properties of geopolymer-based materials (e.g. [79-85]). As reported in the literature, geopolymer-based materials exhibit highly desirable mechanical and durability properties that are comparable to or better than those of their OPC-based counterparts [86-89]. However, geopolymer-based composites develop low strengths under ambient curing conditions and must be cured at high temperatures (e.g. 60^0C, 90^0C) for 24 hours to reach normal strengths at an early age (e.g. 7 days, 28 days). These curing conditions can only be performed in manufacturing companies, resulting in difficulties in applying geopolymers in construction sites. To overcome this limitation, researchers have investigated combining fly ash (FA) with materials that have a high calcium oxide content, such as ground granulated blast furnace slag (GGBS), which was named as FA/GGBS alkali-activated binder (AAB) composites, in order to significantly improve their mechanical properties at the early stage [90-93]. Although alkali-activated binder based composites can develop high compressive strengths, they still exhibit brittle behaviour as well as low toughness, low flexural, and tensile strength similar to OPC-based composites [94]. Researchers have explored the use of different additives to reinforce alkali-activated binders, such as carbon fibers [95] or carbon nanotubes [89]. However, these one-dimensional materials still have limited interfacial connections in the gel matrix, resulting in reducing their reinforcing efficiency as discussed above [31, 41, 96].

Therefore, two-dimensional materials, such as GO have been considered as a promising additive to better enhance the properties of alkali-activated binder based composites. The use of GO in alkali-activated binder based composites is due to its better dispersion in the alkaline activator. However, very few studies have focused on the combination of graphene materials and alkali-activated binder based composites. Yan et al. [97] studied the influence of different

GO dosages on mechanical properties and microstructures of geopolymer pastes cured at 60 °C in 7 days. They showed that the mixes with 0.3% and 0.5% of GO could increase the flexural strength and fracture toughness of geopolymer pastes by 45.5% and 61.5%, respectively. Saafi et al. [94] reported that 0.35% GO could increase the flexural strength, Young's modulus, and flexural toughness of geopolymer pastes cured at 60 °C for 24 h by 134%, 376%, and 56%, respectively. These two studies have only investigated the effects of GO on the properties of geopolymer pastes. However, it is difficult to apply geopolymer composites in construction sites due to their heat-cured conditions that are challenging in practical sites. Therefore, the combination of GO and AAB based composites is more practical for building. To date, no research has investigated in the influence of GO additives on mechanical and durability properties of ambient-cured AAB mortars containing natural sand (NS). Moreover, it is also necessary to find materials to alter NS due to its over-exploitation. Natural sand is the most commonly used fine aggregate used in infrastructure; therefore, the over-exploitation of NS has been warned by scientists because this is leading to harmful environmental consequences on the ecosystem [98, 99]. Lead smelter slag (LSS) is an abundant waste material that is currently considered as a promising solution to alter NS in construction materials [100, 101]. As reported in Ref. [102], the worldwide generation of the lead slag was approximately 3.9 million tons in 2009, and each ton generated 100 to 350 kg of LSS, only 15% of which was recycled. Therefore, there is significant potential for LSS to alter NS in composite materials for achieving resource sustainability in the construction industry while reducing the environmental impact of this abundant waste product. To date, no research has studied the effect of GO additives on mechanical and durability properties of ambient-cured AAB mortars prepared with LSS. These aforementioned research gaps are also investigated in my study.

2. Research gaps

As discussed in the previous sections, the combination of graphene materials and composite materials (i.e. cementitious composites and alkali-activated binder composites) has attracted

significant attention in recent years. It can address the drawbacks of Portland cement binders and natural sand by using supplementary materials and alternative binders to either improve the properties of cementitious composites or replace OPC and NS in the composites. Although existing studies demonstrated the benefits of using pristine graphene additive in Portland cement composites and graphene oxide additive in alkali-activated binder composites, there are still many limitations that need to be investigated in order to have a better understanding of the interaction and mechanism of their combinations. The fundamental and practical aspects to deal with the limitations in this research field are shown below:

✓ **Fundamental aspects**

- Understanding the interaction and mechanism of PRG materials on improving the mechanical properties of cement-based composites.
- Understanding the effect of PRG materials on the mechanical and durability properties of cement-based composites cured in short-term and long-term periods.
- Understanding the effect of different design mixes on the enhancement of PRG materials for mechanical and durability properties of cement-based composites.
- Understanding the interaction and mechanism of GO materials on enhancing the mechanical and durability properties of alkali-activated binder based composites prepared with natural sand and lead smelter slag sand.

✓ **Practical aspects**

- Influence of different dosages of PRG on physicochemical, microstructural, and mechanical properties of cement-based mortars.
- Influence of different sizes of PRG on physicochemical, microstructural, and mechanical properties of cement-based mortars.
- Influence of physical properties of PRG on the reinforcing mechanism and optimized dosage for enhancing mechanical properties of cement-based mortars.
- Influence of different PRG dosages, sizes, and design mixes on physicochemical, microstructural, mechanical, and durability properties of cement-based mortars cured at short-term and long-term ages.

- Influence of different dosages of GO on microstructural, mechanical, and durability properties of alkali-activated binder based mortars prepared with NS and LSS sand.

Hence, this thesis is designed to not only address these research gaps but also contribute to developing the next-generation of construction materials with graphene additives. The outcomes of this study can address the current drawbacks of cementitious composites and create green construction materials by reducing the negative environmental impact of using Portland cement and natural sand resources.

3. Research aims and objectives

The research performed during this PhD project has the aims and objectives outlined below:

3.1. Aim 1: To study the effect of the dosages of an ultra-large PRG size on enhancing mechanical properties of PRG-cement mortars. **(Journal Paper 1)**

- ✓ **Objectives 1:** investigating the effect of different concentrations of an ultra-large PRG size influence on compressive and tensile strengths of Portland cement mortars.
- ✓ **Objectives 2:** analysing physicochemical and microstructural properties of ultra-large PRG-cement based mortars to gain a better understanding of the dosage dependence on mechanical strengths of the mortars.

3.2. Aim 2: To explore the influence of different PRG particle sizes on enhancement rates of compressive and tensile strengths of ordinary Portland cement mortars. **(Journal Paper 2)**

- ✓ **Objectives 1:** investigating the influence of particle sizes of PRG sheets on compressive and tensile strengths of Portland cement mortars; and the benefits of using PRG as the additives to reduce the environmental impact of Portland cement.
- ✓ **Objectives 2:** analysing physicochemical and microstructure properties of cement-based mortars containing different PRG particle sizes to improve understanding of the reasons behind their different enhancement rates.

3.3. Aim 3: To investigate the influence of physical properties of PRG on the reinforcing mechanism and optimized dosage for enhancing mechanical properties of cement-based mortars. **(Journal Paper 3)**

- ✓ **Objectives 1:** studying the main factors that influence the interaction between PRG and cementitious gels and evaluate the optimal dosage range of PRG in for PRG-cement mortars.
- ✓ **Objectives 2:** analysing physicochemical, microstructural and mechanical properties of PRG-cement mortars to confirm the main influence factor; and revealing the proposed reinforcing mechanism and optimized dosage of PRG for enhancing mechanical properties of PRG-cement based mortars.

3.4. Aim 4: To explore the effect of different PRG dosages and design mixes on physicochemical, microstructural, mechanical, and durability properties of Portland cement-based mortars cured at short-term and long-term ages.

- ✓ **Objectives 1:** investigating the influence of different dosages of PRG and design mixes on mechanical and durability properties of Portland cement-based mortars cured in short-term and long-term periods.
- ✓ **Objectives 2:** analysing physicochemical and microstructural properties of PRG-cement based mortars to improve the understanding of the dosage dependence of mechanical and durability properties of Portland cement-based mortars cured in short-term and long-term periods.

3.5. Aim 5: To explore the effect of different PRG sizes and design mixes on physicochemical, microstructural, mechanical, and durability properties of Portland cement-based mortars cured at short-term and long-term ages.

- ✓ **Objectives 1:** investigating the influence of different PRG sizes and design mixes on short-term and long-term mechanical and durability properties of Portland cement-based mortars.

- ✓ **Objectives 2:** analysing physicochemical and microstructural properties of PRG-cement based mortars to improve understanding of the impact of PRG sizes and design mixes on mechanical and durability properties of Portland cement-based mortars cured at short-term and long-term periods.

3.6. Aim 6: To explore the effect of GO on mechanical, durability, and microstructural properties of FA/GGBS alkali-activated binder (AAB) mortars prepared with natural sand (NS) and lead smelter slag sand (LSS); and contributing to developing green construction materials by using waste-based materials to replace both cement binder and natural sand. **(Journal Paper 4)**

- ✓ **Objectives 1:** investigating the influence of the addition of GO to AAB on compressive and tensile strengths, water absorption, and drying shrinkage of AAB mortars prepared with NS and LSS.

- ✓ **Objectives 2:** analysing the microstructures of GO-AAB based mortars prepared with NS and LSS to gain understanding of the interaction mechanism of GO and AAB based mortars containing NS and LSS.

4. Thesis structure

This thesis has been presented as a combination of journal publications, which were published, accepted for publication, submitted, and unsubmitted to peer-review journals, and chapters which are prepared as a conventional thesis. It consists of eight chapters, and the overview of the contents are shown below:

- ✓ **Chapter 1:** presents the research background and general overview of the existing studies on using supplementary materials and alternative binders to overcome drawbacks of OPC by either improve the properties of cementitious composites or replace the OPC binder. The benefits of graphene materials in cementitious and alkali-activated binder based composites have been presented and analysed, which

has been followed by the research gaps, the aims and objectives, thesis structure, significance of the proposed study.

- ✓ **Chapter 2:** presents the results of the study on the effects of the dosages of an ultra-large PRG size on enhancing mechanical properties of PRG-cement mortars. All the contents of this chapter are shown in journal paper 1 “Electrochemically produced graphene with ultra-large particles enhances mechanical properties of Portland cement mortars”.

- ✓ **Chapter 3:** presents the results of the study on exploring how different particle sizes of PRG influence on enhancement rates of compressive and tensile strengths of Portland cement mortars. The contents of this chapter are presented in journal paper 2 “Influence of pristine graphene particle sizes on physicochemical, microstructural and mechanical properties of Portland cement mortars”.

- ✓ **Chapter 4:** reveals the results of the study on the influence of physical properties of PRG on the reinforcing mechanism and optimized dosage for enhancing mechanical properties of Portland cement-based mortars. All the contents of this chapter are shown in journal paper 3 “Investigating the reinforcing mechanism and optimized dosage of pristine graphene for enhancing mechanical strengths of cementitious composites”.

- ✓ **Chapter 5:** presents the results of the study on investigating the effects of different PRG dosages and design mixes on physicochemical, microstructural, mechanical, and durability properties of Portland cement-based mortars cured at short-term and long-term ages.

- ✓ **Chapter 6:** presents the results of the study on exploring the influence of different PRG sizes and design mixes on physicochemical, microstructural, mechanical, and

durability properties of Portland cement-based mortars cured at short-term and long-term ages.

- ✓ **Chapter 7:** shows the results of the study on investigating the influence of GO on mechanical, durability, and microstructural properties of FA/GGBS alkali-activated binder mortars prepared with natural sand and lead smelter slag sand. The contents of this chapter are shown in journal paper 4 "Influence of graphene oxide on the properties of ambient-cured alkali-activated binder mortars prepared with natural sand and lead smelter slag".
- ✓ **Chapter 8:** summarizes the outcomes of this study and also provides recommendations for further research toward the development of next-generation construction materials with graphene additives.

5. Significance of the proposed research

As discussed and analyzed in the previous sections (Research Background, Research Gaps, Research Aims and Objectives), cementitious materials are currently an indispensable part of the construction industry. Ordinary Portland cement, which is the main binder of cementitious composites, is commonly used in the building construction worldwide. However, the process to create OPC has a high impact on climate change due to its high carbon dioxide emissions. Besides, OPC suffers from low tensile strength, flexural strength, brittleness, and resisting crack propagation and a corrosive environment. These lead to durability problems and costly maintenance and the longevity of construction products. Moreover, natural sand, which is the most commonly used fine aggregate in infrastructure, is being over-exploitation. The over-exploitation of NS has been warned by scientists because this is leading to harmful environmental consequences on the ecosystem. Therefore, it is imperative to find measures to overcome these drawbacks by using supplementary materials, alternative binders and waste-

based sands to either improve the properties of cementitious composites or replace OPC binder and NS in the composite materials.

Researchers have utilized the outstanding properties of graphene materials and abundant waste products to study how a combination of graphene materials and composite materials can address the drawbacks of OPC and NS. Although existing studies have demonstrated the benefits of using pristine graphene in cementitious composites and graphene oxide in alkali-activated binder based composites, they still have many limitations that need to be studied profoundly to provide a better understanding on the main factors impacting on the interaction and mechanism of these graphene additives in these composite materials cured at different ages.

As a result, this thesis will comprehensively and systematically investigate the influence of different parameters of PRG on physicochemical, microstructural, mechanical and durability properties of cement-based mortars together with the proposed reinforcing mechanism and optimized dosage of PRG for enhancing their mechanical strengths. The thesis will also provide comprehensive results of the combination of GO and alkali-activated binder based composites prepared with NS and LSS sand. The outcomes of this study show the great potential for incorporating either PRG into cementitious composites or GO into alkali-activated binder based composites prepared with NS and LSS to address their drawbacks and replace OPC binders and NS. The promising results of this thesis contribute to the development of next-generation construction materials with graphene additives, which not only have better mechanical and durability properties but also reduce harmful environmental consequences of using OPC and NS on the climate change and ecosystem.

REFERENCES

[1] P. Van den Heede, N. De Belie, Environmental impact and life cycle assessment (LCA) of traditional and 'green'concretes: literature review and theoretical calculations, Cement and Concrete Composites 34(4) (2012) 431-442.

[2] P.K. Mehta, H. Meryman, Tools for reducing carbon emissions due to cement consumption, Structure 1(1) (2009) 11-15.

[3] M.S. Choi, S.-T. Kang, B.Y. Lee, K.-T. Koh, G.-S. Ryu, Improvement in Predicting the Post-Cracking Tensile Behavior of Ultra-High Performance Cementitious Composites Based on Fiber Orientation Distribution, Materials 9(10) (2016) 829.

[4] R.V. Sagar, B.R. Prasad, S.S. Kumar, An experimental study on cracking evolution in concrete and cement mortar by the b-value analysis of acoustic emission technique, Cement and Concrete Research 42(8) (2012) 1094-1104.

[5] H.F. Taylor, Cement chemistry, Thomas Telford1997.

[6] B. Lothenbach, K. Scrivener, R. Hooton, Supplementary cementitious materials, Cement and concrete research 41(12) (2011) 1244-1256.

[7] A. Anandamurthy, V. Guna, M. Ilangovan, N. Reddy, A review of fibrous reinforcements of concrete, Journal of Reinforced Plastics and Composites 36(7) (2017) 519-552.

[8] M.M. Norhasri, M. Hamidah, A.M. Fadzil, Applications of using nano material in concrete: A review, Construction and Building Materials 133 (2017) 91-97.

[9] C. Shi, B. Qu, J.L. Provis, Recent progress in low-carbon binders, Cement and Concrete Research 122 (2019) 227-250.

[10] C. Shi, A.F. Jiménez, A. Palomo, New cements for the 21st century: The pursuit of an alternative to Portland cement, Cement and concrete research 41(7) (2011) 750-763.

[11] A.N. Junior, M.S. Lemos, R.D. Toledo Filho, E.d.M.R. Fairbairn, J. Dweck, Early stages hydration of high initial strength Portland cement, Journal of thermal analysis and calorimetry 113(2) (2013) 659-665.

[12] S. Lv, Y. Ma, C. Qiu, T. Sun, J. Liu, Q. Zhou, Effect of graphene oxide nanosheets of microstructure and mechanical properties of cement composites, Construction and building materials 49 (2013) 121-127.

[13] H. Yang, H. Cui, W. Tang, Z. Li, N. Han, F. Xing, A critical review on research progress of graphene/cement based composites, Composites Part A: Applied Science and Manufacturing 102 (2017) 273-296.

[14] R. Olivito, F. Zuccarello, An experimental study on the tensile strength of steel fiber reinforced concrete, Composites Part B: Engineering 41(3) (2010) 246-255.

[15] M.A. Adam, M. Said, A.A. Mahmoud, A.S. Shanour, Analytical and experimental flexural behavior of concrete beams reinforced with glass fiber reinforced polymers bars, Construction and Building Materials 84 (2015) 354-366.

[16] H.-b. Zhu, M.-z. Yan, P.-m. Wang, C. Li, Y.-j. Cheng, Mechanical performance of concrete combined with a novel high strength organic fiber, Construction and Building Materials 78 (2015) 289-294.

[17] L. Yan, N. Chouw, Experimental study of flax FRP tube encased coir fibre reinforced concrete composite column, Construction and Building Materials 40 (2013) 1118-1127.

[18] B. Felekoğlu, S. Türkel, Y. Altuntaş, Effects of steel fiber reinforcement on surface wear resistance of self-compacting repair mortars, Cement and Concrete Composites 29(5) (2007) 391-396.

[19] P. Song, S. Hwang, Mechanical properties of high-strength steel fiber-reinforced concrete, Construction and Building Materials 18(9) (2004) 669-673.

[20] J.-L. Granju, S.U. Balouch, Corrosion of steel fibre reinforced concrete from the cracks, Cement and Concrete Research 35(3) (2005) 572-577.

[21] C. Frazão, A. Camões, J. Barros, D. Gonçalves, Durability of steel fiber reinforced self-compacting concrete, Construction and Building Materials 80 (2015) 155-166.

[22] S. Mukhopadhyay, S. Khatana, A review on the use of fibers in reinforced cementitious concrete, Journal of Industrial Textiles 45(2) (2015) 239-264.

[23] Y. Qing, Z. Zenan, K. Deyu, C. Rongshen, Influence of nano-SiO2 addition on properties of hardened cement paste as compared with silica fume, Construction and building materials 21(3) (2007) 539-545.

[24] S. Barbhuiya, S. Mukherjee, H. Nikraz, Effects of nano-Al2O3 on early-age microstructural properties of cement paste, Construction and Building Materials 52 (2014) 189-193.

[25] P. Maravelaki-Kalaitzaki, Z. Agioutantis, E. Lionakis, M. Stavroulaki, V. Perdikatsis, Physico-chemical and mechanical characterization of hydraulic mortars containing nano-titania for restoration applications, Cement and Concrete Composites 36 (2013) 33-41.

[26] H. Li, H.-g. Xiao, J. Yuan, J. Ou, Microstructure of cement mortar with nano-particles, Composites Part B: Engineering 35(2) (2004) 185-189.

[27] B. Sabir, S. Wild, J. Bai, Metakaolin and calcined clays as pozzolans for concrete: a review, Cement and concrete composites 23(6) (2001) 441-454.

[28] S. Papatzani, Effect of nanosilica and montmorillonite nanoclay particles on cement hydration and microstructure, Materials Science and Technology 32(2) (2016) 138-153.

[29] K. Sobolev, I. Flores, L. Torres-Martinez, P. Valdez, E. Zarazua, E. Cuellar, Engineering of SiO 2 nanoparticles for optimal performance in nano cement-based materials, Nanotechnology in construction 3, Springer2009, pp. 139-148.

[30] H. Li, M.-h. Zhang, J.-p. Ou, Abrasion resistance of concrete containing nano-particles for pavement, Wear 260(11-12) (2006) 1262-1266.

[31] Z. Pan, L. He, L. Qiu, A.H. Korayem, G. Li, J.W. Zhu, F. Collins, D. Li, W.H. Duan, M.C. Wang, Mechanical properties and microstructure of a graphene oxide–cement composite, Cement and Concrete Composites 58 (2015) 140-147.

[32] H. Wang, X. Gao, R. Wang, The influence of rheological parameters of cement paste on the dispersion of carbon nanofibers and self-sensing performance, Construction and Building Materials 134 (2017) 673-683.

[33] S. Barbhuiya, P. Chow, Nanoscaled mechanical properties of cement composites reinforced with carbon nanofibers, Materials 10(6) (2017) 662.

[34] B. Wang, Y. Han, S. Liu, Effect of highly dispersed carbon nanotubes on the flexural toughness of cement-based composites, Construction and Building Materials 46 (2013) 8-12.

[35] S. Xu, J. Liu, Q. Li, Mechanical properties and microstructure of multi-walled carbon nanotube-reinforced cement paste, Construction and Building Materials 76 (2015) 16-23.

[36] E.E. Gdoutos, M.S. Konsta-Gdoutos, P.A. Danoglidis, Portland cement mortar nanocomposites at low carbon nanotube and carbon nanofiber content: A fracture mechanics experimental study, Cement and Concrete Composites 70 (2016) 110-118.

[37] A. Carriço, J. Bogas, A. Hawreen, M. Guedes, Durability of multi-walled carbon nanotube reinforced concrete, Construction and Building Materials 164 (2018) 121-133.

[38] C.H. See, A.T. Harris, A review of carbon nanotube synthesis via fluidized-bed chemical vapor deposition, Industrial & engineering chemistry research 46(4) (2007) 997-1012.

[39] S. Musso, J.-M. Tulliani, G. Ferro, A. Tagliaferro, Influence of carbon nanotubes structure on the mechanical behavior of cement composites, Composites Science and Technology 69(11-12) (2009) 1985-1990.

[40] S. Parveen, S. Rana, R. Fangueiro, A review on nanomaterial dispersion, microstructure, and mechanical properties of carbon nanotube and nanofiber reinforced cementitious composites, Journal of Nanomaterials 2013 (2013).

[41] M.A. Rafiee, W. Lu, A.V. Thomas, A. Zandiatashbar, J. Rafiee, J.M. Tour, N.A. Koratkar, Graphene nanoribbon composites, ACS nano 4(12) (2010) 7415-7420.

[42] K.S. Novoselov, A.K. Geim, S.V. Morozov, D. Jiang, Y. Zhang, S.V. Dubonos, I.V. Grigorieva, A.A. Firsov, Electric field effect in atomically thin carbon films, science 306(5696) (2004) 666-669.

[43] B. Han, S. Sun, S. Ding, L. Zhang, X. Yu, J. Ou, Review of nanocarbon-engineered multifunctional cementitious composites, Composites Part A: Applied Science and Manufacturing 70 (2015) 69-81.

[44] A.K. Geim, K.S. Novoselov, The rise of graphene, Nature materials 6(3) (2007) 183-191.

[45] C. Soldano, A. Mahmood, E. Dujardin, Production, properties and potential of graphene, Carbon 48(8) (2010) 2127-2150.

[46] C. Lee, X. Wei, J.W. Kysar, J. Hone, Measurement of the elastic properties and intrinsic strength of monolayer graphene, science 321(5887) (2008) 385-388.

[47] B. Marinho, M. Ghislandi, E. Tkalya, C.E. Koning, G. de With, Electrical conductivity of compacts of graphene, multi-wall carbon nanotubes, carbon black, and graphite powder, Powder Technology 221 (2012) 351-358.

[48] A. Tiwari, M. Syväjärvi, Graphene materials: fundamentals and emerging applications, John Wiley & Sons2015.

[49] W.S. Hummers Jr, R.E. Offeman, Preparation of graphitic oxide, Journal of the american chemical society 80(6) (1958) 1339-1339.

[50] D.C. Marcano, D.V. Kosynkin, J.M. Berlin, A. Sinitskii, Z. Sun, A.S. Slesarev, L.B. Alemany, W. Lu, J.M. Tour, Correction to improved synthesis of graphene oxide, ACS nano 12(2) (2018) 2078-2078.

[51] S. Stankovich, D.A. Dikin, R.D. Piner, K.A. Kohlhaas, A. Kleinhammes, Y. Jia, Y. Wu, S.T. Nguyen, R.S. Ruoff, Synthesis of graphene-based nanosheets via chemical reduction of exfoliated graphite oxide, carbon 45(7) (2007) 1558-1565.

[52] H. Wang, J.T. Robinson, X. Li, H. Dai, Solvothermal reduction of chemically exfoliated graphene sheets, Journal of the American Chemical Society 131(29) (2009) 9910-9911.

[53] L. Rodríguez-Pérez, M.Á. Herranz, N. Martín, The chemistry of pristine graphene, Chemical Communications 49(36) (2013) 3721-3735.

[54] K. Parvez, Z.-S. Wu, R. Li, X. Liu, R. Graf, X. Feng, K. Mullen, Exfoliation of graphite into graphene in aqueous solutions of inorganic salts, Journal of the American Chemical Society 136(16) (2014) 6083-6091.

[55] S. Yang, M.R. Lohe, K. Müllen, X. Feng, New-generation graphene from electrochemical approaches: production and applications, Advanced materials 28(29) (2016) 6213-6221.

[56] B. Vinayan, Heteroatom-doped graphene-based hybrid materials for hydrogen energy conversion, recent advances in graphene research, InTech (2016) 177-194.

[57] E. Shamsaei, F.B. de Souza, X. Yao, E. Benhelal, A. Akbari, W. Duan, Graphene-based nanosheets for stronger and more durable concrete: A review, Construction and Building Materials 183 (2018) 642-660.

[58] L. Zhao, X. Guo, L. Song, Y. Song, G. Dai, J. Liu, An intensive review on the role of graphene oxide in cement-based materials, Construction and Building Materials 241 (2020) 117939.

[59] Q. Wang, J. Wang, C.-x. Lu, B.-w. Liu, K. Zhang, C.-z. Li, Influence of graphene oxide additions on the microstructure and mechanical strength of cement, New Carbon Materials 30(4) (2015) 349-356.

[60] S. Lv, S. Ting, J. Liu, Q. Zhou, Use of graphene oxide nanosheets to regulate the microstructure of hardened cement paste to increase its strength and toughness, CrystEngComm 16(36) (2014) 8508-8516.

[61] A. Mohammed, J. Sanjayan, W. Duan, A. Nazari, Graphene Oxide Impact on Hardened Cement Expressed in Enhanced Freeze–Thaw Resistance, Journal of Materials in Civil Engineering 28(9) (2016) 04016072.

[62] S. Sharma, N. Kothiyal, Influence of graphene oxide as dispersed phase in cement mortar matrix in defining the crystal patterns of cement hydrates and its effect on mechanical, microstructural and crystallization properties, RSC Advances 5(65) (2015) 52642-52657.

[63] D. Hou, Z. Lu, X. Li, H. Ma, Z. Li, Reactive molecular dynamics and experimental study of graphene-cement composites: Structure, dynamics and reinforcement mechanisms, Carbon 115 (2017) 188-208.

[64] M. Murugan, M. Santhanam, S.S. Gupta, T. Pradeep, S.P. Shah, Influence of 2D rGO nanosheets on the properties of OPC paste, Cement and Concrete Composites 70 (2016) 48-59.

[65] T.S. Qureshi, D.K. Panesar, Impact of graphene oxide and highly reduced graphene oxide on cement based composites, Construction and Building Materials 206 (2019) 71-83.

[66] M.V. Kiamahalleh, A. Gholampour, D.N.H. Tran, T. Ozbakkaloglu, D. Losic, Physiochemical and mechanical properties of reduced graphene oxide–cement mortar composites: Effect of reduced graphene oxide particle size, Construction and Building Materials 250 (2020) 118832.

[67] L. Serrano-Luján, S. Víctor-Román, C. Toledo, O. Sanahuja-Parejo, A.E. Mansour, J. Abad, A. Amassian, A.M. Benito, W.K. Maser, A. Urbina, Environmental impact of the production of graphene oxide and reduced graphene oxide, SN Applied Sciences 1(2) (2019) 179.

[68] S. Chuah, Z. Pan, J.G. Sanjayan, C.M. Wang, W.H. Duan, Nano reinforced cement and concrete composites and new perspective from graphene oxide, Construction and Building Materials 73 (2014) 113-124.

[69] Y. Zhu, S. Murali, W. Cai, X. Li, J.W. Suk, J.R. Potts, R.S. Ruoff, Graphene and graphene oxide: synthesis, properties, and applications, Advanced materials 22(35) (2010) 3906-3924.

[70] Z. Metaxa, Polycarboxylate based superplasticizers as dispersant agents for exfoliated graphene nanoplatelets reinforcing cement based materials, J. Eng. Sci. Tech. Rev 8 (2015) 1-5.

[71] B. Wang, R. Jiang, Z. Wu, Investigation of the mechanical properties and microstructure of graphene nanoplatelet-cement composite, Nanomaterials 6(11) (2016) 200.

[72] T. Tong, Z. Fan, Q. Liu, S. Wang, S. Tan, Q. Yu, Investigation of the effects of graphene and graphene oxide nanoplatelets on the micro-and macro-properties of cementitious materials, Construction and Building Materials 106 (2016) 102-114.

[73] W. Baomin, D. Shuang, Effect and mechanism of graphene nanoplatelets on hydration reaction, mechanical properties and microstructure of cement composites, Construction and Building Materials 228 (2019) 116720.

[74] J. Tao, X. Wang, Z. Wang, Q. Zeng, Graphene nanoplatelets as an effective additive to tune the microstructures and piezoresistive properties of cement-based composites, Construction and Building Materials 209 (2019) 665-678.

[75] H. Du, S. Dai Pang, Enhancement of barrier properties of cement mortar with graphene nanoplatelet, Cement and Concrete Research 76 (2015) 10-19.

[76] P. Xu, J. Loomis, R.D. Bradshaw, B. Panchapakesan, Load transfer and mechanical properties of chemically reduced graphene reinforcements in polymer composites, Nanotechnology 23(50) (2012) 505713.

[77] S. Chatterjee, F. Nafezarefi, N. Tai, L. Schlagenhauf, F. Nüesch, B. Chu, Size and synergy effects of nanofiller hybrids including graphene nanoplatelets and carbon nanotubes in mechanical properties of epoxy composites, Carbon 50(15) (2012) 5380-5386.

[78] M. Shtein, R. Nadiv, M. Buzaglo, K. Kahil, O. Regev, Thermally conductive graphene-polymer composites: size, percolation, and synergy effects, Chemistry of Materials 27(6) (2015) 2100-2106.

[79] M.Z.N. Khan, Y. Hao, H. Hao, F.U.A. Shaikh, Experimental evaluation of quasi-static and dynamic compressive properties of ambient-cured high-strength plain and fiber reinforced geopolymer composites, Construction and Building Materials 166 (2018) 482-499.

[80] H.Y. Zhang, V. Kodur, B. Wu, L. Cao, F. Wang, Thermal behavior and mechanical properties of geopolymer mortar after exposure to elevated temperatures, Construction and Building Materials 109 (2016) 17-24.

[81] A. Islam, U.J. Alengaram, M.Z. Jumaat, I.I. Bashar, The development of compressive strength of ground granulated blast furnace slag-palm oil fuel ash-fly ash based geopolymer mortar, Materials & Design 56 (2014) 833-841.

[82] G. Görhan, G. Kürklü, The influence of the NaOH solution on the properties of the fly ash-based geopolymer mortar cured at different temperatures, Composites part b: engineering 58 (2014) 371-377.

[83] J. Temuujin, A. van Riessen, K. MacKenzie, Preparation and characterisation of fly ash based geopolymer mortars, Construction and Building Materials 24(10) (2010) 1906-1910.

[84] P. Chindaprasirt, T. Chareerat, S. Hatanaka, T. Cao, High-strength geopolymer using fine high-calcium fly ash, Journal of Materials in Civil Engineering 23(3) (2010) 264-270.

[85] A. Sathonsaowaphak, P. Chindaprasirt, K. Pimraksa, Workability and strength of lignite bottom ash geopolymer mortar, Journal of Hazardous Materials 168(1) (2009) 44-50.

[86] F. Colangelo, G. Roviello, L. Ricciotti, C. Ferone, R. Cioffi, Preparation and characterization of new geopolymer-epoxy resin hybrid mortars, Materials 6(7) (2013) 2989-3006.

[87] P. Duxson, A. Fernández-Jiménez, J.L. Provis, G.C. Lukey, A. Palomo, J.S. van Deventer, Geopolymer technology: the current state of the art, Journal of materials science 42(9) (2007) 2917-2933.

[88] J. Davidovits, Geopolymer chemistry and applications, Geopolymer Institute2008.

[89] M. Saafi, K. Andrew, P.L. Tang, D. McGhon, S. Taylor, M. Rahman, S. Yang, X. Zhou, Multifunctional properties of carbon nanotube/fly ash geopolymeric nanocomposites, Construction and Building Materials 49 (2013) 46-55.

[90] A. Gholampour, V.D. Ho, T. Ozbakkaloglu, Ambient-cured geopolymer mortars prepared with waste-based sands: Mechanical and durability-related properties and microstructure, Composites Part B: Engineering 160 (2019) 519-534.

[91] J.G. Jawahar, G. Mounika, STRENGTH PROPERTIES OF FLY ASH AND GGBS BASED GEO POLYMER CONCRETE, Asian Journal of Civil Engineering (BHRC) 17(1) (2016) 127-135.

[92] A. Wardhono, D.W. Law, A. Strano, The strength of alkali-activated slag/fly ash mortar blends at ambient temperature, Procedia Engineering 125 (2015) 650-656.

[93] P.S. Deb, P. Nath, P.K. Sarker, The effects of ground granulated blast-furnace slag blending with fly ash and activator content on the workability and strength properties of geopolymer concrete cured at ambient temperature, Materials & Design (1980-2015) 62 (2014) 32-39.

[94] M. Saafi, L. Tang, J. Fung, M. Rahman, J. Liggat, Enhanced properties of graphene/fly ash geopolymeric composite cement, Cement and Concrete Research 67 (2015) 292-299.

[95] T. Lin, D. Jia, P. He, M. Wang, D. Liang, Effects of fiber length on mechanical properties and fracture behavior of short carbon fiber reinforced geopolymer matrix composites, Materials Science and Engineering: A 497(1-2) (2008) 181-185.

[96] A. Cwirzen, K. Habermehl-Cwirzen, A. Nasibulin, E. Kaupinen, P. Mudimela, V. Penttala, SEM/AFM studies of cementitious binder modified by MWCNT and nano-sized Fe needles, Materials Characterization 60(7) (2009) 735-740.

[97] S. Yan, P. He, D. Jia, Z. Yang, X. Duan, S. Wang, Y. Zhou, Effect of reduced graphene oxide content on the microstructure and mechanical properties of graphene–geopolymer nanocomposites, Ceramics International 42(1) (2016) 752-758.

[98] A.C. Sankh, P.M. Biradar, S. Naghathan, M.B. Ishwargol, Recent trends in replacement of natural sand with different alternatives, Proceedings of the International Conference on Advances in Engineering and Technology, 2014, pp. 59-66.

[99] J.-P. Bravard, M. Goichot, S. Gaillot, Geography of sand and gravel mining in the Lower Mekong River. First survey and impact assessment, EchoGéo (26) (2013).

[100] B. Tripathi, A. Misra, S. Chaudhary, Strength and abrasion characteristics of ISF slag concrete, Journal of Materials in Civil Engineering 25(11) (2013) 1611-1618.

[101] C. Atzeni, L. Massidda, U. Sanna, Use of granulated slag from lead and zinc processing in concrete technology, Cement and Concrete Research 26(9) (1996) 1381-1388.

[102] M. Ogundiran, H. Nugteren, G. Witkamp, Immobilisation of lead smelting slag within spent aluminate—fly ash based geopolymers, Journal of hazardous materials 248 (2013) 29-36.

CHAPTER 2:

DEMONSTRATION OF THE EFFECT OF AN ULTRA-LARGE SIZE OF PRISTINE GRAPHENE ON ENHANCING MECHANICAL PROPERTIES OF PORTLAND CEMENT MORTARS

THE AIM AND OBJECTIVE OF THIS CHAPTER:

Aim: This chapter aims to study the effect of the dosages of PRG with an ultra-large size on enhancing mechanical properties of PRG-cement mortars.

Objectives 1: investigating the effect of different concentrations of PRG with an ultra-large size influence on compressive and tensile strengths of Portland cement mortars.

Objectives 2: analysing physicochemical and microstructural properties of ultra-large PRG-cement based mortars to gain a better understanding of the dosage dependence on mechanical strengths of the mortars.

Statement of Authorship

Title of Paper	Electrochemically produced pristine graphene with ultra large particles enhances mechanical properties of Portland cement mortar
Publication Status	☑ Published ☐ Accepted for Publication ☐ Submitted for Publication ☐ Unpublished and Unsubmitted work written in manuscript style
Publication Details	Ho, V. D., Ng, C. T., Coghlan, C. J., Goodwin, A., Mc Guckin, C., Ozbakkaloglu, T., & Losic, D. (2020). Electrochemically produced graphene with ultra large particles enhances mechanical properties of Portland cement mortar. Construction and Building Materials, 234, 117403.

Principal Author

Name of Principal Author (Candidate)	Van Dac Ho		
Contribution to the Paper	Literature review, preparing and doing experiments, assessment and analysis of test results, and preparation of the manuscript.		
Overall percentage (%)	85		
Certification:	This paper reports on original research I conducted during the period of my Higher Degree by Research candidature and is not subject to any obligations or contractual agreements with a third party that would constrain its inclusion in this thesis. I am the primary author of this paper.		
Signature		Date	10/12/2019

Co-Author Contributions

By signing the Statement of Authorship, each author certifies that:

i. the candidate's stated contribution to the publication is accurate (as detailed above);

ii. permission is granted for the candidate in include the publication in the thesis; and

iii. the sum of all co-author contributions is equal to 100% less the candidate's stated contribution.

Name of Co-Author	Dusan Losic		
Contribution to the Paper	Research supervision, review and revisions of the manuscript.		
Signature		Date	11/04/2020

Name of Co-Author	Ching-Tai Ng		
Contribution to the Paper	Research supervision, review and revisions of the manuscript.		
Signature		Date	10/12/2019

Name of Co-Author	Togay Ozbakkaloglu		
Contribution to the Paper	Review of the manuscript.		
Signature		Date	20/01/2020

Name of Co-Author	Campbell J.Coghlan		
Contribution to the Paper	Review of the manuscript.		
Signature		Date	11/12/2019

Name of Co-Author	Andy Goodwin		
Contribution to the Paper	Review of the manuscript.		
Signature		Date	26/12/2019

Name of Co-Author	Craig Mc Guckin		
Contribution to the Paper	Review of the manuscript.		
Signature		Date	23/01/2020

Journal paper 1 (Published)

Electrochemically produced graphene with ultra large particles enhances mechanical properties of Portland cement mortars

Van Dac Ho[1,2,3], Ching-Tai Ng[1], Campbell J. Coghlan[2.3], Andy Goodwin[4], Craig Mc Guckin[4], Togay Ozbakkaloglu[1], Dusan Losic*[2,3]

[1]School of Civil, Environmental and Mining Engineering, The University of Adelaide, South Australia, 5005, Australia

[2]School of Chemical Engineering, The University of Adelaide, South Australia, 5005 Australia

[3]ARC Research Hub for Graphene Enabled Industry Transformation, The University of Adelaide, South Australia, 5005 Australia

[4] First Graphene Ltd, Suite 3, 9 Hampden Road, Nedlands WA 6009, Australia

*Corresponding authors: dusan.losic@adelaide.edu.au

ABSTRACT

The effects of the dosages (0.01%, 0.03%, 0.05%, 0.07%, 0.1%, and 0.3% by weight of cement binder) of an ultra-large size (56±12 μm) of pristine graphene (PRG) industrially manufactured by electrochemical process on compressive and tensile strengths of cement mortars are presented. To have a better understanding of the reinforcement mechanism of PRG-cementitious gels, the physicochemical and microstructure analyses were performed. The results show that the addition of PRG to cement mortars improves their mechanical properties, with characteristic concentration dependence. The mortar mix with 0.07% PRG is identified as the optimal concentration, which provides 34.3% and 26.9% improvement in compressive and tensile strength at 28 days, respectively. This enhancement is attributed to the improvement of the hydration degree of cement paste, resulting in more Calcium Silicate Hydrate gel production. This also comes from the reinforcement of the adhesion bond that was created from friction forces between PRG sheets and cement gels, resulting in strengthening cement matrix composites and impeding crack propagations in the structure. However, with the further increases in PRG contents (i.e. 0.1 %, 0.3 %), the enhancement of mechanical properties of mortars is limited due to the impact of the van der Waals force on the sedimentation of PRG suspension, leading to the poor dispersion of the prepared PRG suspension. These results suggest that industrially produced pristine graphene by an electrochemical process is a promising additive for improving performances of construction materials.

Keywords: Pristine graphene; Cementitious composites; Compressive strengths; Tensile strengths; Hydration process; Microstructures.

1. Introduction

Cementitious materials are one of the most commonly used materials in the construction industry due to their high compressive strength. However, they suffer from poor tensile strength, flexural strength, fracture toughness and brittleness giving rise to durability issues [1, 2]. To overcome these issues, cement materials are augmented through the use of specific additives, reduction of water and cement ratios, and reinforcement materials such as steel, carbon and plastic fibers [3].

Recently, cementitious material development has focused on the incorporation of nanomaterials to not only enhance the mechanical properties but also retard the propagation of cracks to generate a more durable composite [4]. These studies revealed two critical mechanisms [5], which affect the strength of cementitious materials in incorporating nanoparticles, such as nano-SiO_2 [6], nano-TiO_2 [7] and nano-$CaCO_3$ [8], into the cement matrix. The first is the high specific surface area of nanoparticles, which accelerates the progression of cement hydration and creates more Calcium Silicate Hydrate (CSH) gels. The second mechanism comes from the small particle size property, which allows them to act as a filler. This grants the material with a denser microstructure. However, nanoparticles with low aspect ratios lack competence in arresting the propagation of cracks from the nanoscale cracks, they are thus unable to enhance the reinforcement efficiency [9].

In addition to inorganic nanomaterials, carbon-based materials, such as nanofibers and nanotubes, have been investigated in cementitious composites as additives and demonstrated they can improve the mechanical properties [10, 11]. However, these carbon materials showed some limitations to generate a full bonding with cementitious materials due to a lack of interfacial areas between them [12].

Graphene, a recently discovered two-dimensional (2D) carbon material has many outstanding properties such as high electrical and thermal conductivity, high-temperature stability, high mechanical properties, and ultra-large specific surface areas and high aspect ratio. Graphene is widely recognized to be an ideal additive to enhance performances of cementitious materials [13, 14]. There are several different forms of graphene materials such as graphene oxide (GO), reduced graphene oxide (rGO), pristine graphene (PRG), doped graphene, and functionalized graphene that have different functionality and properties. The pristine graphene produced by a direct exfoliation process from graphite using electrochemical methods has different properties compared with rGO, showing less defects, better crystallinity and conductivity. GO is an oxygenated derivate of graphene prepared by acid oxidation of graphite and is water-compatible and highly dispersible. This is one of the reasons why GO was preferentially explored as an additive for improving mechanical performances of cementitious composites. Wang, et al. [15] demonstrated that including 0.05% of GO in cement pastes can increase 40.4% and 90.5% in compressive and flexural strength at 28 days, respectively. This was confirmed by Lv, et al. [16]. They reported that GO can enhance strength and toughness properties of cement composites. Their results show that the compressive strength of cement paste with 0.06% GO is increased by 58.5% after 28 days, while the flexural strength is improved by 67.1% after 28 days with the mix used 0.04% GO concentration. Sharma and Kothiyal [17] reported that the compressive strength of the cement mortar with 0.1% GO additive is increased by 86.3% after 28 days. Recently few studies revealed the influence of different oxygen functional groups from GO on the phase composition and intermolecular interaction of cementitious materials to help early-age hydration characteristics of the composites [18, 19]. Nevertheless, GO material has some limitations that could impact its performance in cementitious composites. It is less crystalline with a high level of defects and has mechanical properties that are considerably lower than those compared to PRG or rGO. Therefore, the application of PRG and rGO in

cementitious composites is expected to be more beneficial for improving structural performances of cement-based materials [18, 19].

Graphene materials, such as rGO and PRG, are highly hydrophobic and less dispersible in water compared to GO. This is the reason for being less attractive to be incorporated into cement composites to improve cement performances regardless of their better mechanical properties [20, 21]. Recent studies proved that the rGO and PRG dispersion in aqueous solution can be improved by a combination of surfactants and ultrasonication methods and could significantly enhance mechanical properties of cement materials [20, 22]. For example, Wang, et al. [20] found that the addition of 0.05% PRG in cement mortar can improve compressive strength and flexural strength at 7 days, by 8% and 24%, respectively. Tong, et al. [23] showed that the compressive strength of cement mortar is improved by 19.9% after 28 days when adding 0.1% PRG by weight of cement. However, these studies have only focused on investigating the changes in mechanical properties of cementitious composites between the control mortar and the mix with a certain PRG content (e.g. 0.05 or 0.1 %) but limited details about properties of used graphene materials [24]. In 2015, Du and Dai Pang [25] studied the properties of cement mortars with four different PRG dosages (i.e. 0%, 2.5%, 5.0% and 7.5% by weight of cement, with PRG size 8 μm), and showed that the addition of PRG can significantly decrease water penetration depth. However, their study indicates there are insignificant effects of PRG on compressive and flexural strengths of cement mortars. This is attributed to the high rate of PRG dosages used, resulting in the agglomeration of PRG sheets and forming multi-layers PRG sheets, which resulted in the hindrance to the interaction between PRG and cement matrix. A recent study of PRG-cement mortars with different PRG concentrations (i.e. 0%, 0.05%, 0.1%, 0.5% and 1% by weight of cement, with PRG size 5-10 μm) done by Tao, et al. [26] confirmed that cement mortar with 0.05% PRG additive can improve compressive strength and flexural strength at 28 days, by about 8.3% and 15.6%, respectively, but the strengths start decreasing when the PRG dosages are increased to exceed 0.05% owing to the agglomeration of PRG.

Although these studies present the dependence of the properties of PRG-cement mortars on PRG dosages, the characteristics of the mechanism behind this dependence are not well understood. Compared to the proposed reinforcement mechanism of GO in cement composites, this is attributed to the strong interfacial adhesion between carboxyl, hydroxyl groups and cement matrix [27], which indicates that smaller size GO often shows a better enhancement rate in mechanical properties of cement composites than larger size GO as smaller size GO has more of these functional groups [17, 24]. Unlike GO, graphene sheets of PRG materials have very few of oxygen groups located at the edges, where different mechanisms are involved with the friction adhesion forces between PRG sheets and cement matrix. Thus, the larger size of single PRG structure is proposed to have the better enhancement to the cement matrix. To date, no studies have been done to investigate the influence of the ultra-large size of PRG on mechanical properties of cement-based mortars. While graphene materials are slowly moving into industrial space with many graphene manufacturers around the world that are able to produce their large quantities, there is still a lack of studies using industrially manufactured graphene to improve performances of cementitious.

To address these research gaps, the aim of this study is to investigate the use of industrially manufactured PRG produced by an electrochemical process with focuses on studying the effects of the ultra-large size of PRG (i.e. 56 μm) and their dosages (i.e. from 0% to 0.3% by weight of cement binder) on the physicochemical and mechanical properties of PRG-cement mortars. Our hypothesis is that very large sheets of graphene with the size of several tens of micron will significantly improve the mechanical properties of cement. Most of the previous studies were based on PRG prepared in research laboratories with variable quality and less reproducible structural and mechanical characteristics. In this work, it is the first time to use industrially produced PRG manufactured by an electrochemical process that has recently been established by First Graphene Ltd in Perth, Australia, with the capacity of 100 t/year. To better understand the mechanism behind the positive effects of ultra-large PRG particles with different dosages

on cement mortars, a series of microanalyses were completed using X-ray diffraction analysis (XRD), Thermogravimetric analysis (TGA), Fourier transform infrared spectroscopy (FTIR), Scanning electron microscopy (SEM), and Ultraviolet–visible spectrophotometer (UV–vis). Industrial production of graphene has dramatically reduced the cost of producing graphene in large quantities, allowing it to be incorporated into industrial-scale materials, such as concrete. Hence, the promising results from this study will provide an attractive avenue to practical applications of graphene-based materials for a broad range of construction materials to enhance their mechanical and durability properties.

2. Experimental Methods

2.1. Materials

The PRG with the physical properties shown in Table 1 were provided by First Graphene Ltd (Australia) from their industrial production plant. Ordinary Portland Cement (OPC), which is general purpose cement according to Australian Standard AS 3972-2010 [28], with the chemical composition shown in Table 2 were used as the binder of mortar mixes. Natural sand with a 2.36-mm maximum particle size was used as the fine aggregate, and its particle size distribution is presented in Table 3. MasterGlenium SKY 8100, which is the second generation polycarboxylic ether polymer superplasticizer in compliance with Australian Standard AS 1478.1-2000 [29], was used in all mortar mixes as a surfactant to increase the dispersion of PRG in aqueous solution and workability of mortars. The properties of the superplasticizer are shown in Table 4.

Table 1. Physical properties of pristine graphene supplied by First Graphene Ltd.

ID	Average particle size (μm)	Thickness (nm)	Purity (%)	Bulk density (g/cm^3)
PRG-70	56±12	1-3	98.3	0.1

Table 2. Chemical composition of Ordinary Portland Cement (OPC).

Compounds	OPC (%)
CaO	63.28
SiO_2	19.95
Al_2O_3	4.79
Fe_2O_3	3.14
MgO	2.03
Na_2O	0.29
K_2O	0.4
SO_3	2.69
P_2O_5	0.04

Table 3. Particle size distribution of natural sand.

Mesh size (mm)	2.36	1.18	0.6	0.15	0.075
Cumulative passing (%)	96.7	84.6	62.2	4.5	0.4

Table 4. Properties of superplasticizer (MasterGlenium SKY 8100).

pH	Boiling temperature (^oC)	Density at 20 ^oC (kg/dm^3)	Flash point (^oC)	Vapour pressure at 20 ^oC (hPa)	Solid content (mass, %)
6.4	≥ 100	1.06	> 100	23	30.7

2.2. Preparation of PRG suspension

The aqueous solution for mortar mixes, including water, PRG and superplasticizer, was prepared following the steps: (i) MasterGlenium SKY 8100 was mixed and stirred in water within 2 minutes; (ii) PRG was then added and stirred for 2 minutes; (iii) the solution was then

sonicated by Ultrasonicator UIP1000hdT for 30 minutes to create the aqueous solution for the mortar mixes.

2.3. Preparation of PRG-cement mortar composites

A total of seven unique mixes of PRG-cement based mortars were prepared. Their detailed mix proportions are described in Table 5. As shown in the table, there are seven concentrations of PRG used, i.e. 0 % (as the plain mortar), 0.01, 0.03, 0.05, 0.07, 0.1 and 0.3% by weight of cement binder. These seven concentrations were designed based on a comprehensive literature review, which focused on investigating the effects of graphene's derivative (e.g. GO, rGO, PRG) on properties of cementitious materials [19, 30].

To prepare the mortar mixes, the procedures described below were adopted to improve the uniform of the cement matrix: natural sand and OPC were mixed together for four minutes, and then the aqueous solution (preparation procedures as described in Section 2.2) was gradually added to the mortars and continued mixing together within five minutes, which contained one minute to check and stir the mixes. All samples after mounting were vibrated for one minute to eliminate the entrapped air in samples during mounting. All specimens were demounted after 24 hours cured at room temperature and covered with wet fabric sheets to prevent the loss of moisture. They continued to be cured in a fog room under the ambient temperature of 23 ± 2 $^{\circ}$C until the testing days (i.e. at 7 days and 28 days).

The labels of the PRG-cement based mortar mixes shown in Table 5 are designed as follows: the PRG letter is used to refer to pristine graphene in the mixes. The number after the PRG letter stands for the proportion of PRG calculated by the weight of Portland cement in the mixes. To illustrate, PRG0 and PRG0.07 are the mortar mixes prepared with 0% (i.e. the control mix) and 0.07 % PRG by the weight of cement, respectively.

Table 5. Mix proportions of the cement mortar composites.

Mix	Pristine Graphene (%)*	Water/cement ratio	Cement (kg/m^3)	Water (kg/m^3)	Pristine Graphene (kg/m^3)	Sand (kg/m^3)	Superplasticizer (kg/m^3)
PRG0	0	0.485	527	256	0.0	1448	1.4
PRG0.01	0.01	0.485	527	256	0.1	1448	1.4
PRG0.03	0.03	0.485	527	256	0.2	1448	1.4
PRG0.05	0.05	0.485	527	256	0.3	1448	1.4
PRG0.07	0.07	0.485	527	256	0.4	1448	1.4
PRG0.1	0.1	0.485	527	256	0.5	1448	1.4
PRG0.3	0.3	0.485	527	256	1.6	1448	1.4

* The percentage of pristine graphene based on weight of cement binder.

2.4. Characterization of microstructural tests

2.4.1. Scanning electron microscopy and particle size measurements

SEM was obtained by using the FEI Quanta 450, which analyzes and provides high-resolution images of surface topography. The SEM analysis was conducted at 28 days, and SEM specimens were cut from the samples of PRG-cement mortars at 28-day mechanical tests with the dimensions of about $5 \times 5 \times 5$ mm to analyze their surface morphologies and microstructures. All these specimens were dried and then coated by a 5 nm-thick platinum layer to enhance the quality of SEM images. Particle size measurement of PRG dispersions was measured in triplicate by a Nanosight NS300 (Malvern Instruments) coupled with a green laser (532 nm) using the O-ring top-plate sample chamber configuration. The pre-installed Nanoparticle Tracking Analysis (NTA) software version 3.3 took into account the Brownian motion trajectory of the particles to measure its size.

2.4.2. X-ray diffraction analysis

XRD was conducted by using the Rigaku MiniFlex 600 X-Ray diffractometer to find the mineralogical characteristics (i.e. the crystalline phases) of materials (i.e. OPC, natural sand, PRG, and hydration products of PRG-cement mortars). The XRD was worked at conditions 40 kV and 15 mA, $2\theta = 5°–80°$ at 0.02° step size. The XRD specimens were collected from

remnant pieces of PRG-cement mortars at 28-day compression tests, and then, they were dried in the oven for one day, then ground, and sieved into fine powders (i.e., < 10 μm) for analysis.

2.4.3. Thermogravimetric analysis

TGA was performed by using the TGA Q500 instrument to investigate the effects of PRG on the hydration process of cement composites at 7 and 28 days. About 20 mg of the powder (i.e. < 10 μm) of mortar mixes was heated from room temperature to 900 °C with the heating rate of 10 °C per minute under the nitrogen atmosphere condition. The outcomes of the TGA analysis are able to identify the contents of evaporable water (i.e. free water covers outer surfaces of cement composites) and non-evaporable water (i.e. the water content bound by products (e.g. portlandite, calcium silicate hydrate gels) of the cement hydration process). Based on the proportion of the weight loss of testing samples, the hydration degree of cement pastes of the control and PRG-cement samples was calculated (the details are discussed later in Section 3.4.2).

2.4.4. Fourier transform infrared spectroscopy

FTIR was performed by using the Nicolet 6700 to determine specific functional groups and their intensities in samples, including PRG, cement, sand, powder cementitious materials at 28 days. The infrared spectrum was obtained by using the support of the spectrum analysis software, which shows spectrums in transmission mode with the range of frequency in wavenumber from 400 cm^{-1} to 4000 cm^{-1}.

2.4.5. Ultraviolet-visible spectrophotometer

UV–vis was obtained by using Shimadzu UV-1601 to investigate the dispersion of PRG aqueous solution, varying with the time between two methods: 30 min sonicated by Ultrasonication UIP 1000hdT (Hielscher, Germany) and without sonication. The percentage of

the transmittance of PRG aqueous solution determined by UV–vis varies with time is used to provide a quantitative analysis of the dispersity or sedimentation of the solution.

2.5. Flowability test and mechanical property tests

The flow test of fresh mortars was performed immediately after mixed mortars, according to ASTM C1437 [31]. The dimensions of the truncated cone mold are top diameter 70mm, height 50mm, and bottom diameter 100mm. The truncated cone mold was filled with fresh mortars by layers and tamped by a tamper to ensure uniform filling of the mold, then the mold was raised vertically, and the mean horizontal spreads of fresh mortars were recorded. This test was conducted to investigate the flowability of PRG-cement mortar mixes. For hardened cement composites, the compressive strength was determined at 7 and 28 days by carrying out compressive tests. A typical 50 mm cube was used according to the ASTM standard C109/C109M-07 [32]. The direct tensile test with a dog-bone shaped sample was also conducted at 7 days and 28 days in accordance with the ASTM standard C307-03 [33]. These tests were performed to identify the effect of PRG concentrations on mechanical properties of PRG-cement based mortars. The compressive and tensile strengths were determined from the averaged values of three nominally identical specimens for each mix proportion.

3. Results and Discussion

3.1. Characterization of industrial manufactured pristine graphene (PRG) materials

The morphology and physical properties of industrially produced PRG material used in this study are summarized in Fig. 1 and Table 1, which show their morphology, particle size and crystallinity. The graphene particle has irregular shaped structures and the average particle size of the graphene sheets is 56 ± 12 μm and a carbon content of >98.3%. From Fig. 1(c), the XRD pattern shows the crystalline phase of PRG at the scattering angle $2\theta = 26.64°$. The interplanar spacing between layers (i.e. d-spacing) calculated based on the Bragg's Law is 0.334 nm, which

is the same as the interplanar spacing of Graphite [24, 34], showing a high quality of PRG used in the study.

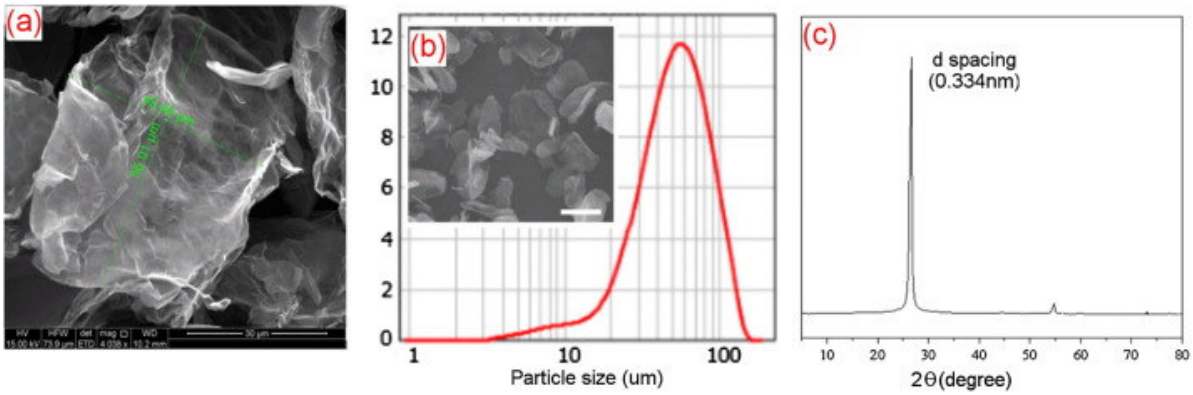

Fig. 1. (a) High resolution SEM images showing the size of single PRG particle and b) Low resolution SEM image (bar scale 50u m) and PRG particle size distribution (C) XRD pattern of PGR material.

The observations of the sedimentation of PRG in aqueous solution with times between 30 min sonicated and without sonicated at the same 0.03% PRG content based on the percentage of transmittance of these solutions from UV–vis analysis are shown in Fig. 2. It is important to note that a solution with a lower percentage of the transmittance with time presents for better dispersion of PRG aqueous solution with time. As shown in Fig. 2(a), without a sonication, the transmittance is high at the early stage about 30%, and continues rising remarkably with time about 70% and 90% after 4 h and 24 h, respectively. In Fig. 2(b), 30 min sonicated, the transmittance values are low and rise very slowly with time compared to no sonication, which is about 0.5%, 2.5%, and 25% after sonication, 4 h, and 24 h respectively. From the photos in Fig. 2(c) and (d), we can note that the suspension of PRG aqueous solution without a sonication shows a clear variation of sedimentation following the time whereas it is hard to observe the change of the sedimentation of the one with 30 min sonicated. The results from UV–vis and observed photos indicate that the PRG aqueous solution is much more stable and well dispersed with the sonication method than without sonication, especially within 4 h after

the sonication, which is important to be able to create mixes with high quality because of the effects of initial setting time characteristic of OPC on cementitious composites [35].

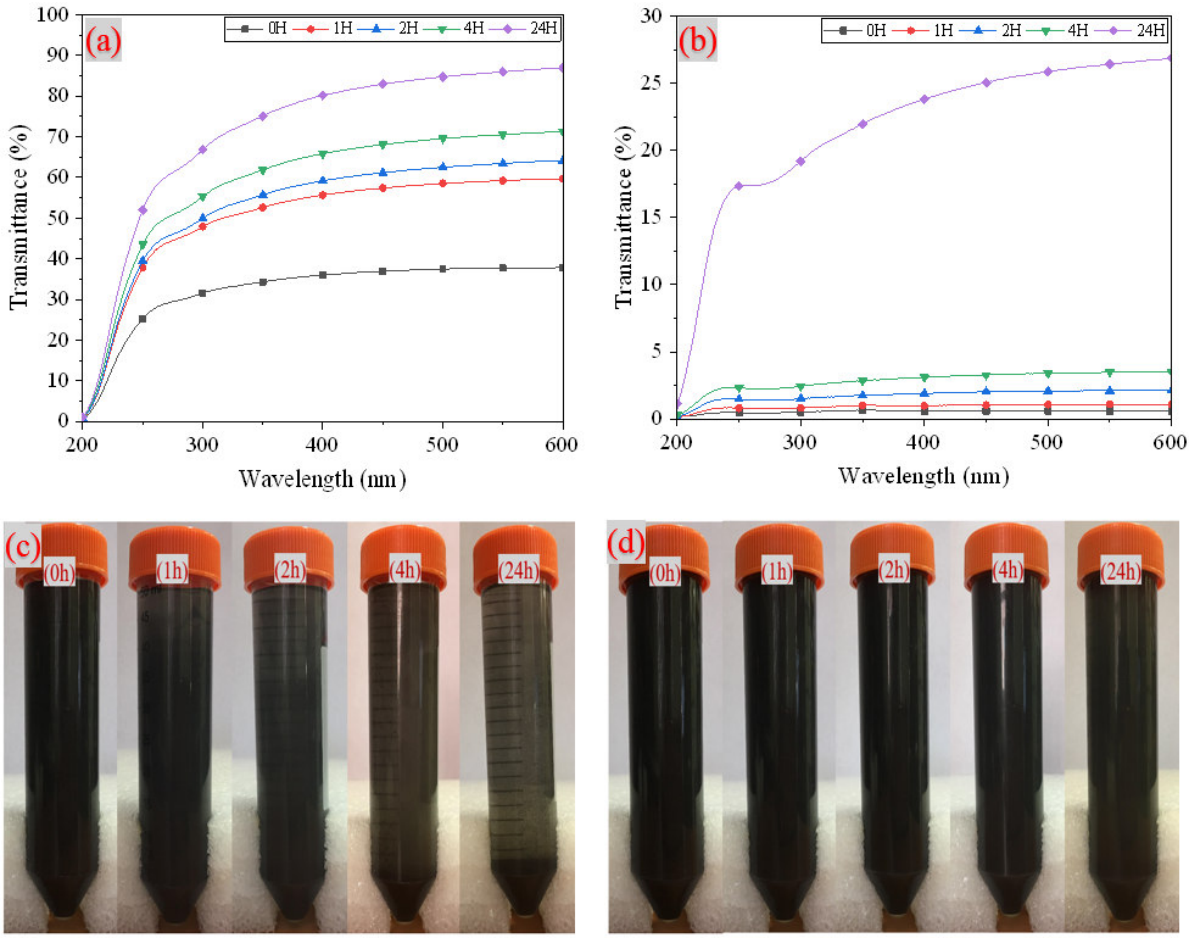

Fig. 2. Variation of transmittance of pristine graphene suspension at 0.03% PRG with time from UV-Vis test: (a) without sonication, and (b) 30 minutes sonication. Photographs of PRG aqueous suspension after 0 h, 1 hour, 2 hours, 4 hours, and 24 hours: (c) without sonication, and (d) 30 minutes sonication.

3.2. Effects of PRG on the flowability of PRG-cement mortar composites

Fig. 3 presents the flowability of the mortar mixes with different concentrations of PRG. As shown in the figure, the flowability of the mortars reduces with an increase in the PRG contents, and the mean value of the flowability of the control mix is 135 mm, which is 22.7% higher compared to the mix with the addition of 0.3% PRG (mean value of the flowability is 110 mm). The decrease of the flowability of the mixes with the rise in the PRG contents is attributed to

the large specific surface area of PRG, resulting in more amount of water required to lubricate their surface sheets, which is in agreement with the previous research studies on the effects of nanomaterials (e.g. GO, nano-SiO2, PRG) on the flowability of the cement matrix [19, 20].

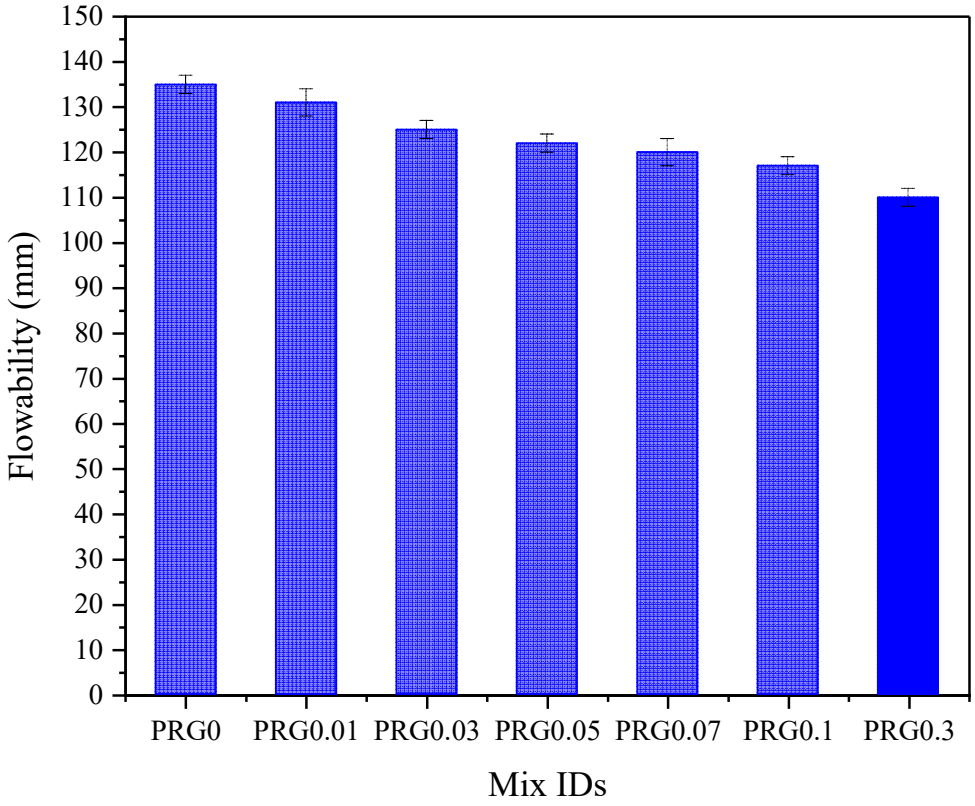

Fig. 3. Flowability test results of fresh mortars with different PRG contents.

3.3. Effects of PRG on mechanical properties of PRG-cement mortar composites

The 7 and 28 days compressive test results of the control mix and the mixes with different PRG concentrations, and their enhancement strengths compared to the control mortar are shown in Fig. 4. It can be seen that the addition of PRG to the mortar mixes results in an increase in the compressive strength of the cementitious composites for both 7 and 28 days compressive test results. The optimal concentration of PRG is at 0.07% PRG, which is 50.0 MPa and 56.3 MPa at 7 and 28 days, respectively. Compared to these tests with the control mix at the same test days, which is 36.5 MPa and 42 MPa, the results show that the strength is enhanced about 36.8% at 7 days and 34.3% at 28 days, respectively. The trend of the compressive

strengths of the mortars at 7 and 28 days decreases when the PRG contents beyond the optimum value (i.e. 0.07% PRG). The graph in Fig. 4(b) shows that the compressive test results at 7 days of the PRG-cement mortar mixes with the PRG concentrations under the optimum value have lower enhancement strength rates than those at 28 days. Whereas the trend is upside-down for the mixes with the PRG contents beyond 0.07% PRG.

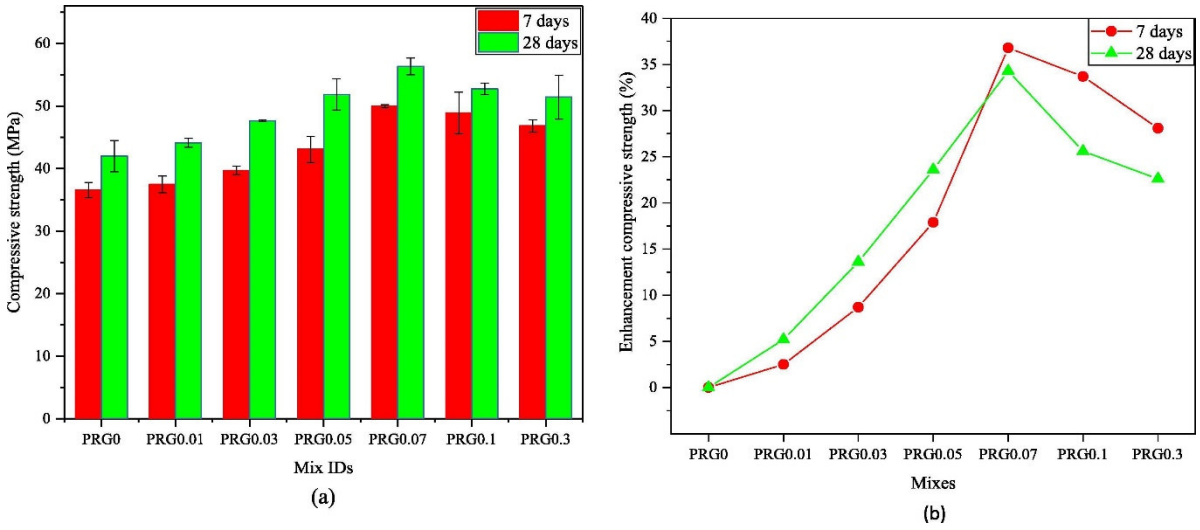

Fig. 4. (a) Compressive strength and (b) enhancement compressive strength of PRG-cement mortars with different proportions of PRG at 7 and 28 days.

Fig. 5 describes the 7 and 28 days tensile test results of the different mortar mixes, and their enhancement strengths compared to the control mix. As shown in the figure, the tensile strength of the PRG-cement mortars increases with an increase in the PRG concentrations at all curing ages. It is evident from Fig. 5 that the optimal concentration of PRG is at 0.07% PRG, which is 3.9 MPa at 7 days and 4.6 MPa at 28 days, compared to these testing days of the control mix, which is 3.1 MPa and 3.6 MPa, respectively. This enhancement in tensile strengths equates to about 25.3% at 7 days and 26.7% at 28 days. Fig. 5(a) also shows that the tensile strength of the PRG-cement mortars starts dropping when the PRG contents beyond 0.07% PRG. From Fig. 5(b), the enhancement strength rates of the tensile test results at 7 days of the PRG-cement mortar mixes are higher than those at 28 days, except for the mixes PRG0.01 and PRG0.07.

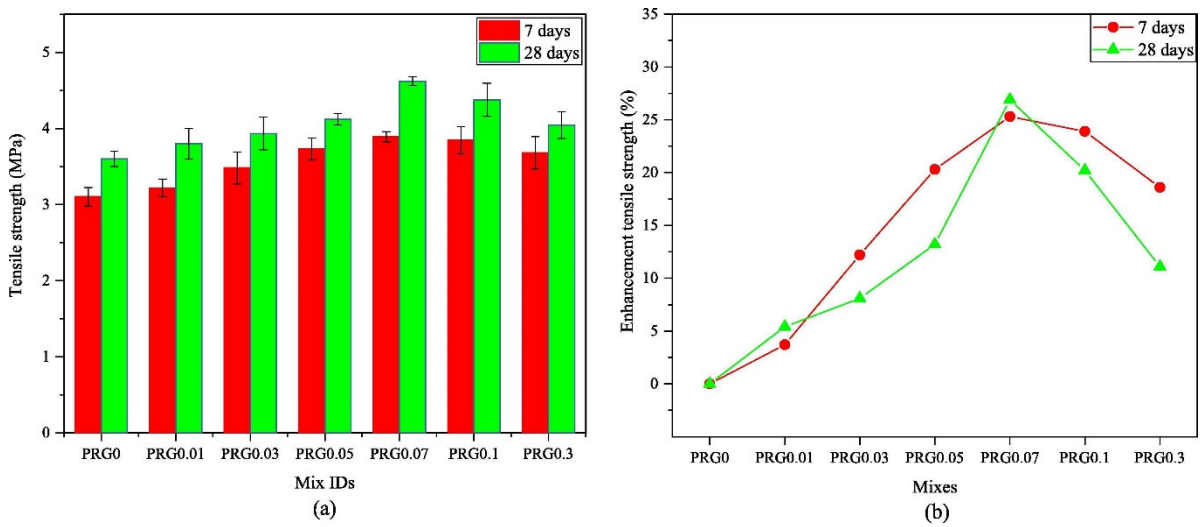

Fig. 5. (a) Tensile strength and (b) enhancement tensile strength of PRG-cement mortars with different proportions of PRG at 7 and 28 days.

The observed improvement in the compressive and tensile strengths of the PRG-cement mortar composites with the highest strength at the PRG0.07 mix, which will be discussed in more details in Section 3.4, could be explained by the following reasons: (i) the enhanced cement gel of the cement matrix composite owing to: (1) the improvement of the hydration degree of cement pastes due to the high specific surface area of PRG sheets, resulting in better spreading water to cement particles, which is similar with the observation of previous studies on mechanical properties of GO and cementitious composites [9, 30]; (2) the closer of cement particles in the cement matrix caused by the van der Waals forces between PRG sheets, resulting in an enhancement of strengths of cement gels [30, 36]; (ii) the improvement of bonding gels comes from the improved interfacial friction and interconnecting behavior between the crystals of the hydration products in cement gels, which was created from a part of the covalent bonds between some COOH groups in PRG and cement gels (this is similar to other studies observed in a combination of carbon nanotube and GO and Portland cement [9, 37]), and most from friction forces between the areas of PRG sheets and cement gels (this was reported in previous research by using the molecular dynamics simulation method [38, 39]), resulting in being able to enhance the stress distribution and impeding the propagation of cracks from nanoscale to

microscale and macroscale in the cement matrix [19, 20]. Nevertheless, the mixes with the high PRG concentrations, which are beyond the optimum value, i.e. PRG0.1 and PRG0.3, lead to poor dispersion resulting in the re-stacking of PRG sheets due to the effect of the van der Waals force. This is attributed to the creation of multi-layers PRG sheets with a thicker thickness that results in poor interfacial friction and interconnecting behaviour, and thus, reduces the compressive and tensile strengths. This is in line with previous findings on GO and cement composites [19, 40].

The axial compressive stress and strain relationship of the mortar mixes with different PRG concentrations at 28 days is shown in Fig. 6. The curves show that for a given PRG concentration, the compressive strength increases with an increase in the PRG content, and reaches the highest strength with the PRG0.07 mix, and then, starts decreasing in strengths when the PRG contents beyond this optimal value. It is important to note that the stress-strain curves can also show the estimated elastic modulus of materials, deduced from the ratio between stress and strain which are taken at about 40 % of the ultimate compressive strength. Therefore, from Fig. 6, it is possible to conclude that the elastic modulus of the PRG-cement based mortars is higher than the plain mortar, and the mix with a higher compressive strength often presents a higher elastic modulus. This trend is consistent with the widespread relationship between compressive strength and elastic modulus in solid materials as shown in other research or standards [19, 41].

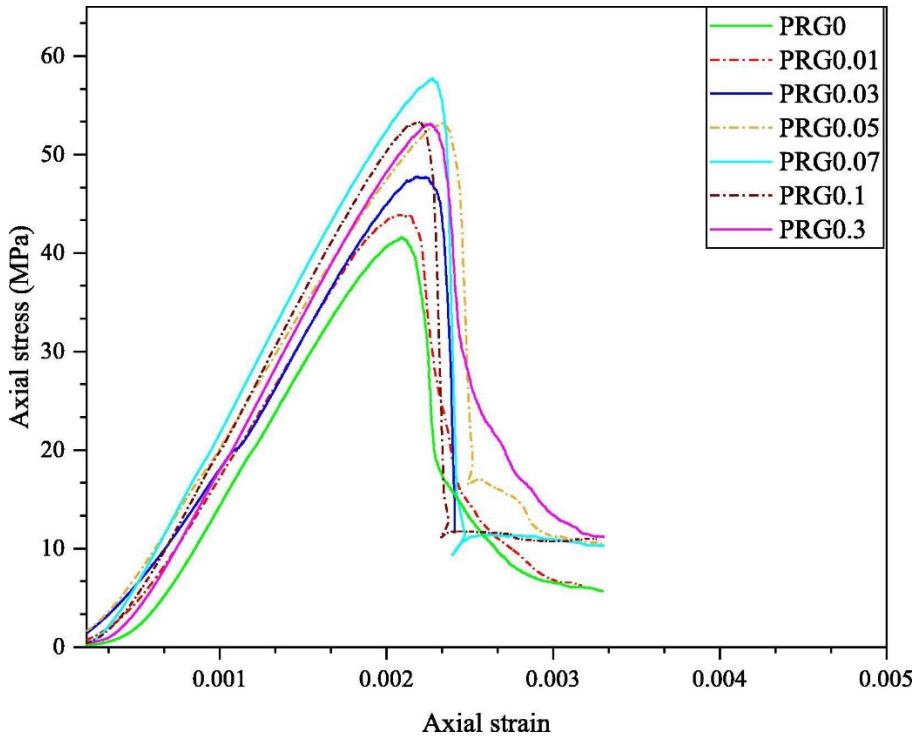

Fig. 6. The axial stress and axial strain relationship of mortar mixes with different PRG contents at 28-day compressive testing.

3.4. Microstructure and characterization of PRG-cement mortar composites

The influence of the PRG concentrations on the mechanical properties of cement mortar composites at microscale was evaluated using microstructural tests: XRD, TGA, FTIR, and SEM. These tests were designed and conducted by four different contents of PRG as follows: 0 (the control mix), 0.03% (as shown the transparently effective effect of PRG), 0.07% (the optimum PRG content based on the experimental results from mechanical tests), 0.3% (the maximum PRG content).

3.4.1. XRD analysis

The XRD patterns of OPC, sand, and PRG-cement mortar mixes are shown in Fig. 7. As shown in Fig. 7(a), the peaks detected in the XRD pattern for the natural sand are at positions: from 21.2°, 26.7°, 36.7°, etc. to 77.9°, which indicates crystalline phases of quartz in natural sand [42, 43]. Fig. 7(a) also shows that the peaks of diffraction spectra for OPC powder identified

the following main phases: (i) Alite ($3CaO.SiO_2$, C_3S) at positions: from 29.5°, 32.3°, etc. to 62.4°; (ii) Belite ($2CaO.SiO_2$, C_2S) at positions: 30.2°, and 32.7°; (iii) Tricalcium aluminate ($3CaO.Al_2O_3$, C_3A) at 23.1° and 32.3°; (iv) Tetracalcium aluminateferrite ($4CaO.Al_2O_3.Fe_2O_3$, C_4AF) at 12.3°; and Gypsum ($CaO.SO_3.2H_2O$) at 11.8°. It is also notable from the figure that C_3S shows the major content in the OPC powder, followed by C_2S, C_3A, C_4AF, and Gypsum, respectively. These identified phases and characteristics are in agreement with previous studies on the OPC components and its hydration process using the XRD analysis [44, 45].

In cementitious composites, the main products of the hydrated cement paste are portlandite ($Ca(OH)_2$, CH) and calcium silicate hydrate (CSH), which contribute to mechanical properties of cementitious composites, and part of ettringite. The brief hydration reaction process can be seen in Eqs. (1), (2) in Section 3.4.2. The XRD patterns of the mortar mixes with different PRG concentrations, i.e. PRG0, PRG0.03, PRG0.07, PRG0.3, are shown in Figure 7(b). Although they have similar types of hydrated productions, their contents are different, resulting in different mechanical strengths (as discussed before in Section 3.3). It is important to note that CSH gels often stay at the amorphous phases, the XRD analysis is thus limited to identify CSH phases [20, 45]. However, the content of CSH gels can be estimated based on the amount of CH (as shown in Eq. (1) in Section 3.4.2), and the amount of the un-hydrated cement (e.g. alite) [24, 45, 46]. The degree of the hydration process of cement mortars can be estimated by the amount of the crystalline phases of CH in XRD analysis results. In order to make the equal percentage of natural sand existed in each sample of each mix, the major peak of natural sand at the position 26.7° of each mix was standardized to have equal intensity in all spectra of all the mixes [17, 46].

Fig. 7(b)-(c) show that the detected peaks at the scattering angles of 18.2°, 34.2°, and 47.1° correspond with CH phases [44, 46]. Fig. 7(c) shows that the intensities of these peaks for portlandite in the mixes having PRG (i.e. PRG0.03, PRG0.07, and PRG0.3) are higher than the

control mix (i.e. PRG0), and are augmented with the increase of the PRG contents. It reaches the highest value at the PRG0.07 mix, and then decreases when the PRG concentration beyond 0.07% (i.e. PRG0.3). This suggests that the mixes containing PRG contents have higher degrees of the hydration of cement pastes than the control (as will be also validated by TGA, FTIR results), which is consistent with the studies on graphene and cementitious composites in literature [20, 46].

Moreover, the major peaks of un-hydrated alite (2θ = 29.5°, 32.3°) in these mixes detailed in Fig. 7(c) show that the control mix has the highest intensity of the amount of un-hydrated alite than the others, which is followed by PRG0.03, PRG0.3, and PRG0.07, respectively. This shows that PRG can accelerate the degree of the hydration of cement pastes and create more CSH gels in cementitious materials [17, 45, 46]. In summary, the XRD analysis results are in agreement with the growth trend of the mechanical strengths of PRG-cement mortar composites discussed previously in Section 3.3.

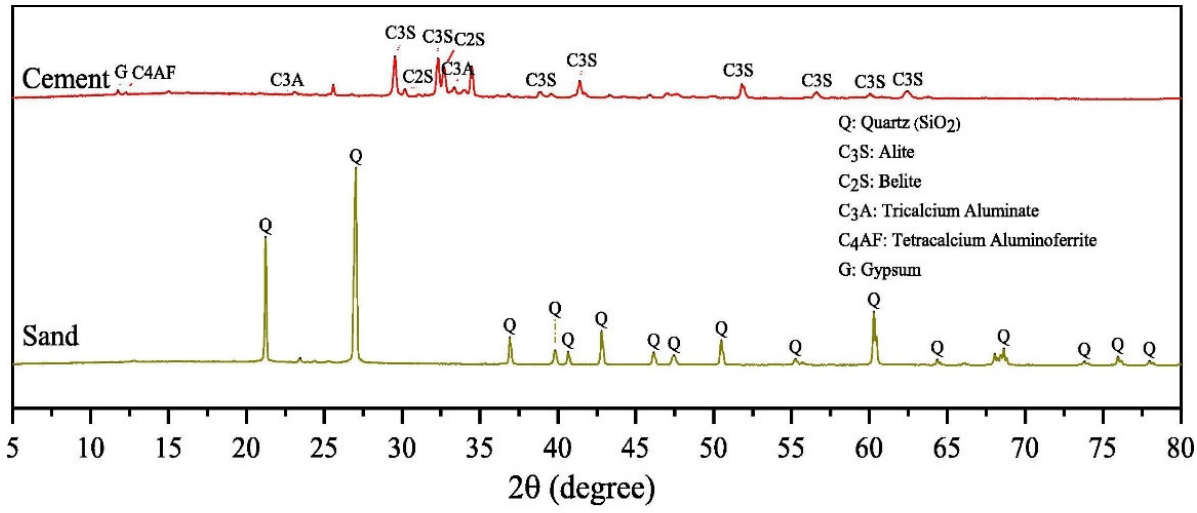

(a)

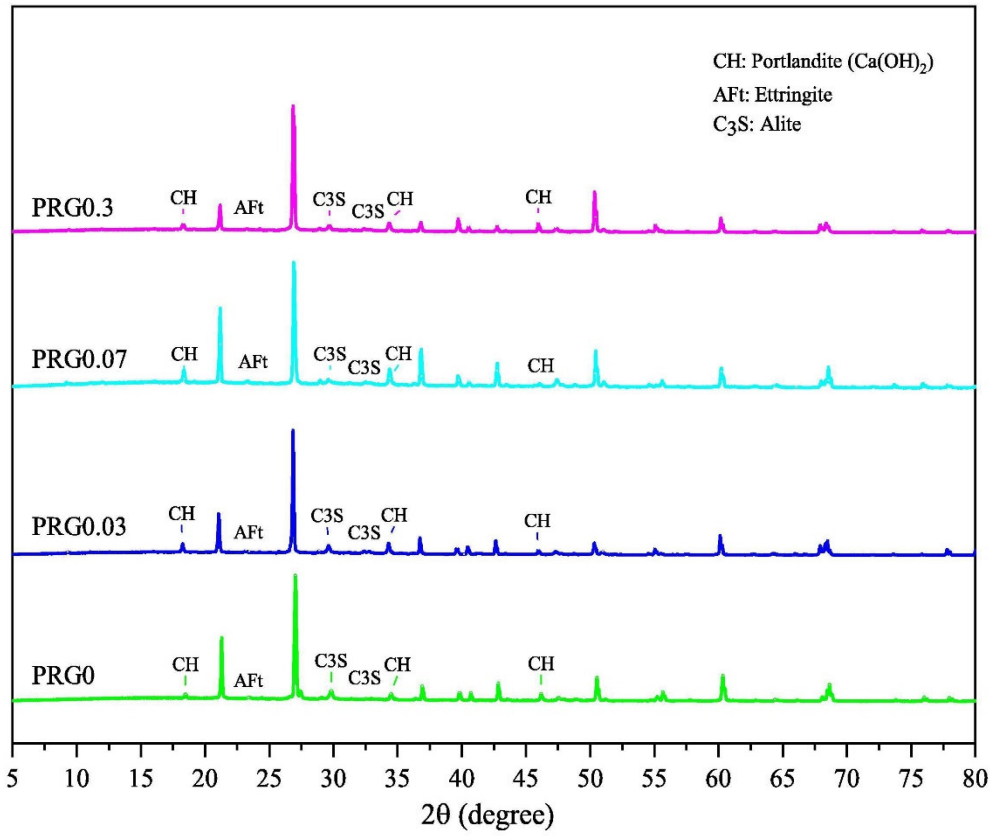

(b)

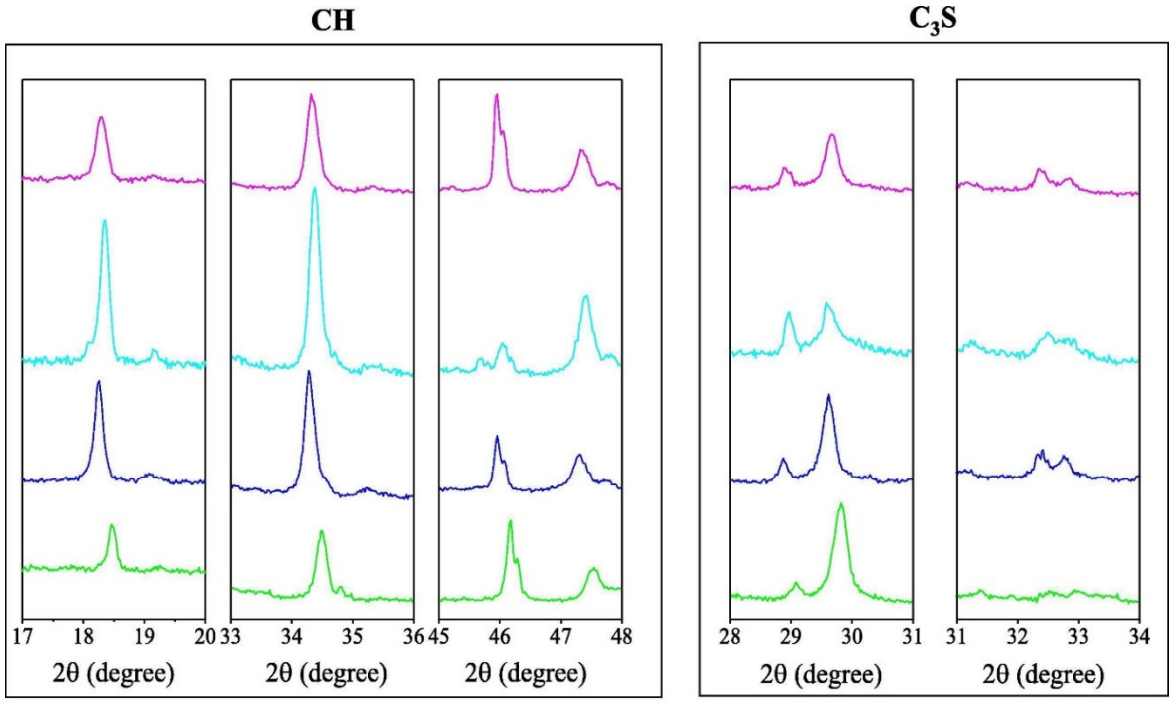

Summary of intensity of peaks

ID	PRG0	PRG0.03	PRG0.07	PRG0.3
CH	5390	8037	11848	8908
C_3S	3848	3770	3456	3616

(c)

Fig. 7. Powder XRD patterns of: (a) natural sand and original Portland cement; (b) PRG-cement composites with different PRG contents (i.e. 0%, 0.03%, 0.07%, and 0.3%) at 28 days; (c) insets of portlandite and tricalcium silicate details of different PRG-cement composites at 28 days.

3.4.2. TGA analysis

TGA is another well-known method used to analyze the hydration degree of cementitious composites, which is based on the content of portlandite and non-evaporable water calculated from samples [47, 48]. According to previous studies on cementitious composites [24, 49], the brief chemical reactions of the hydration performance of OPC and the decomposition reactions of its hydration products summarized below can provide a better understanding to identify different phases in TGA analysis results.

$$(C_3S, C_2S) + H_2O \rightarrow CH + CSH \quad (1)$$

$$(C_3A, C_4AF) + \text{Gypsum } (CaO.SO_3.2H_2O) + H_2O \rightarrow \text{AFt} + \text{AFm (monosulphoaluminate)} \quad (2)$$

$$(CSH) \rightarrow C_3S + H_2O \quad (3)$$

$$Ca(OH)_2 \rightarrow CaO + H_2O \quad (4)$$

$$CaCO_3 \rightarrow CO_2 + H_2O \quad (5)$$

$$Ca(OH)_2 + CO_2 \rightarrow CaCO_3 + H_2O \quad (6)$$

Fig. 8(a), (b) shows the TGA analysis results of cement composites at 7 and 28 days of curing age, respectively. As shown in Fig. 8(b), from the derivative weight change cures, it can be divided into four main loss mass phases: (i) the mass loss below 145 °C is referred to as evaporable water and part of bound water [50, 51]; (ii) the mass loss in the range from 145 °C to 200 °C is attributed to CSH gels (Eq. (3)) [20, 48]; (iii) from 350 °C to 500 °C is related to the decomposition of portlandite (Eq. (4)) [47, 52]; (iv) the mass loss in the range of 600-700 °C is referred to the composition of $CaCO_3$ (Eq. (5)) [48, 49]. The non-evaporable water and portlandite contents can be estimated by the following equations [47, 48]:

$$M_{non\text{-}water} = M_{145\,°C} - M_{900\,°C} \quad (\%) \qquad (7)$$

$$M_{CH} = \frac{74}{18} * ML_{CH} + \frac{74}{44} * ML_{CaCO3} \ (\%) \qquad (8)$$

where: (i) $M_{145\,°C}$, $M_{900\,°C}$, and $M_{non\text{-}water}$ present for the mass loss of sample at 145 °C, 900 °C, and non-evaporable water in percentage, respectively. (ii) ML_{CH} and ML_{CaCO3}, present for the mass loss in percentage due to the decomposition of portlandite and $CaCO_3$ phases, respectively; M_{CH} stands for the content of portlandite in percentage, $\frac{74}{18}$ and $\frac{74}{44}$ stand for factors that showed the ratios of molecular weight of water in the decomposition phases of portlandite and $CaCO_3$ (as referred to Eqs. (4) to (6)).

Based on Eqs. (7) and (8), the amount of portlandite and non-evaporable water of samples at 7 and 28 days are shown in Fig. 8(a)-(b). The contents of portlandite and non-evaporable water increase with an increase in the curing ages, i.e. 7 and 28 days, in all the samples, regardless of the PRG concentrations in the mixes, which is in line with other studies on cementitious composites [19, 48]. The PRG mixes show higher percentages of portlandite and non-evaporable water than those of the control at all curing times. In addition, it is evident from the figures that these proportions increase with an increase in the PRG contents. The highest proportion is achieved in the PRG0.07 mix, and then decreased when using beyond this PRG concentration (i.e. PRG0.3), which is consistent with the observed results in the mechanical strengths and XRD analysis (as discussed before in Sections 3.3 and 3.4.1). In summary, from the TGA analysis results, the PRG can accelerate the hydration degree of cementitious composites, which is in agreement with the previous finding in graphene and cement matrix composites [19, 20, 47].

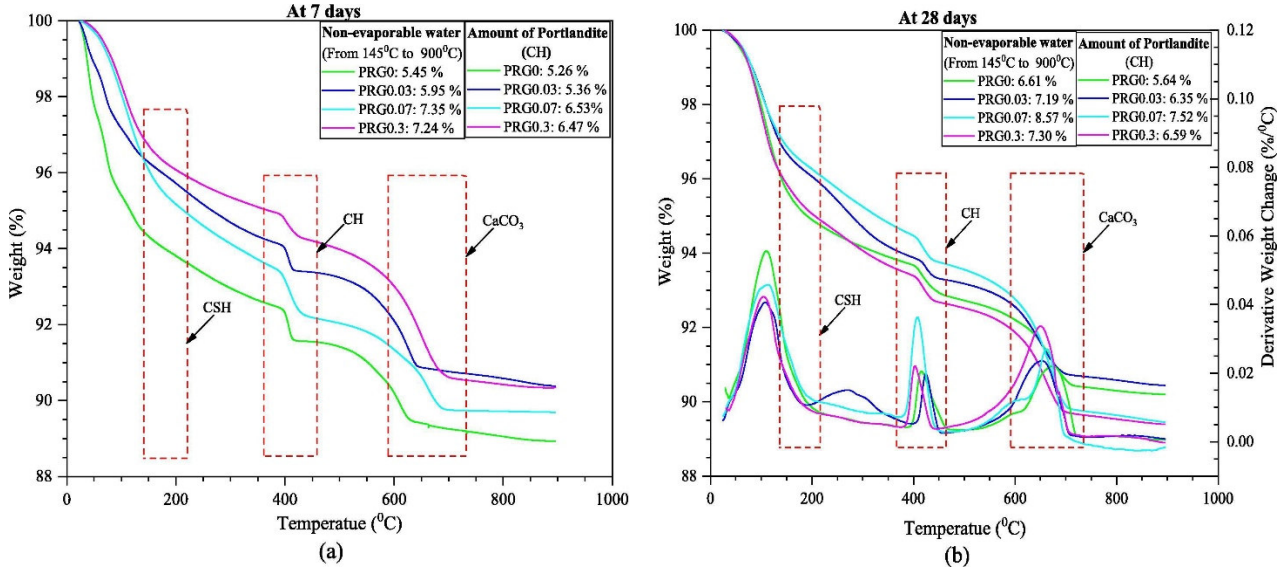

Fig. 8. TGA cures show the weight loss as variation of temperature of PRG-cement composites with different PRG contents (i.e. 0%, 0.03%, 0.07%, and 0.3%) at different days: (a) 7 days; (b) 28 days.

3.4.3. FTIR analysis

The FTIR spectra of natural sand, OPC, and PRG are shown in Fig. 9(a). The major bands observed for natural sand are: the asymmetrical bending vibration of Si-O-Si at about 470 cm^{-1}; the band at about 520 cm^{-1} attributed to the asymmetrical bending vibration of Si-O-Al; the symmetrical bending variation of Si-O observed at about 692 cm^{-1} presents the crystalline form of quartz in natural sand; the band from 750 to 810 cm^{-1} is attributed to the symmetrical stretching variation of Si-O; and the asymmetrical stretching variation from about 950 to 1100 $cm^{-1}$for Si-O. All observed bands for natural sand from FTIR analysis results are in agreement with previous studies on natural sand using infrared spectrum [53, 54].

For OPC, the bands at about 450 cm^{-1} and 525 cm^{-1}correspond to out-of-plane and in-plane bending vibrations of Si-O bonds and stretching vibration from about 800 cm^{-1} to 1000 $cm^{-1}$with peaks at about 879 and 935 cm^{-1} correspond to Si-O bonds within the SiO_4 groups. These bands are attributed to C_3S and C_2S main constituents in OPC [55-57]; the Al-O bending vibration at about 720 cm^{-1} is belong to AlO_4 groups in C_3A composition in OPC [55, 56]; two

bending vibrations at about 600 and 650 cm^{-1} and the stretching band from about 1050 to 1150 cm^{-1} correspond to the S-O bonds within SO_4 tetrahedral groups, belong to the gypsum constituent in OPC [56, 57]; the stretching variation from 1370 cm^{-1} to 1520 cm^{-1} is attributed to $(CO_3)^{2-}$ in OPC [57].

The major bands of PRG showed the stretching vibrations: from about 1000 cm^{-1} to about 1240 cm^{-1}, which represents the appearance of alkoxy groups (C-O); about from 1300 cm^{-1} to 1600 cm^{-1} corresponds to aromatic double carbon groups (C=C); about 1700 cm^{-1} and from 2500 cm^{-1} to 3600 cm^{-1} refers to the carboxyl (C=O) and hydroxyl (O-H) groups, respectively. This shows that the existing of carboxylic acid groups (i.e. COOH) in PRG is in agreement with other studies on graphene composites [58, 59].

Fig. 9(b), (c) shows the FTIR spectra of the plain mix and PRG-cement mixes at 28 days of curing age. The group bands in the ranges of 400-550 cm^{-1} and 800-1200 cm^{-1} represent Si-O bonds in the CSH gels [55, 60]. A broad band from 2800 to 3600 cm^{-1} attributed to O-H groups in water molecules belongs to CSH gels in the mixes [55, 56, 60]. The narrow vibration in the range of about 3500-3600 cm^{-1} corresponds to O-H bonds in CH (portlandite) [55], and C-O bonds in $(CO_3)^{2-}$ groups observed in a range of 1350-1550 cm^{-1} [56, 60]. From Fig. 9(b), (c), it is evident that the intensities of spectra represented for CSH gels (i.e. Si-O, H-O-H), CH (i.e. O-H), and $CaCO_3$ (i.e. $(CO_3)^{2-}$) in PRG-cement mixes (i.e. PRG0.03, PRG0.07, PRG0.3) are stronger than those of the control mix (PRG0). This is attributed to higher hydration degrees in PRG-cement pastes, which results in the enhancement of mechanical properties of the PRG mixes. This is consistent with mechanical properties, XRD, TGA results discussed before, and in agreement with previous studies on graphene in cementitious composites [56, 58, 60]. Moreover, at a given PRG concentration, the intensity of the spectrum of PRG0.07 shows the strongest band, followed by PRG0.3 and PRG0.03 respectively. This is consistent with the trend

curves of the mortar mixes in compressive and tensile strengths as discussed earlier in Section 3.3.

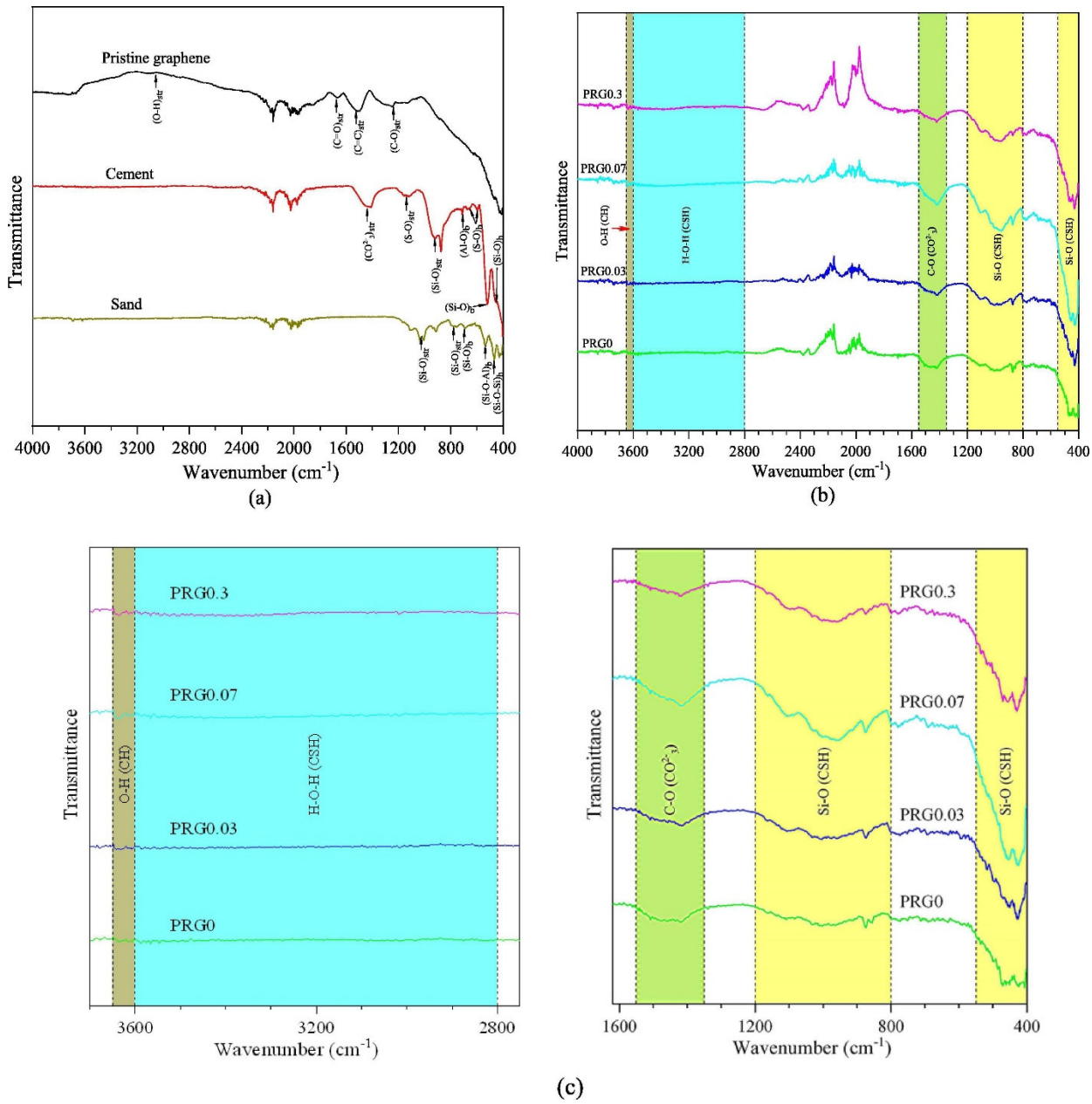

Fig. 9. FTIR spectra of: (a) PRG, OPC and NS; (b, c) PRG-cement composite mixes with different PRG contents (i.e. 0%, 0.03%, 0.07%, and 0.3%) and their insets at 28 days.

3.4.4. SEM cross-sectional analysis

The SEM images of cracking patterns of the mortar mixes, i.e. PRG0, PRG0.03, PRG0.07, and PRG0.3, at 28 days at 50 µm and 30 µm magnification are shown in Fig. 10. The density and

width of micro-cracks lead to a reduction in bonding, interconnecting, and interfacial friction properties of cementitious composites as shown in these SEM images. The control mix (Fig. 10(a), (b)) shows a higher degree of cracks both in the density and size and the lower compactness of the microstructure than those in PRG0.03, PRG0.07, and PRG0.3, as shown in Fig. 10(c)–(h), resulting in the lower strengths of the control mix than the others. Thus, the PRG-cement based mortars with better microstructures have the efficient capacity in crack bridging, crack branching and stress distribution, and also impeding crack propagations in structures, which leads to significant enhancement of compressive and tensile strengths. This is consistent with the results discussed in previous sections and also in agreement with the observations of other studies on graphene and cement materials [17, 19, 20, 47].

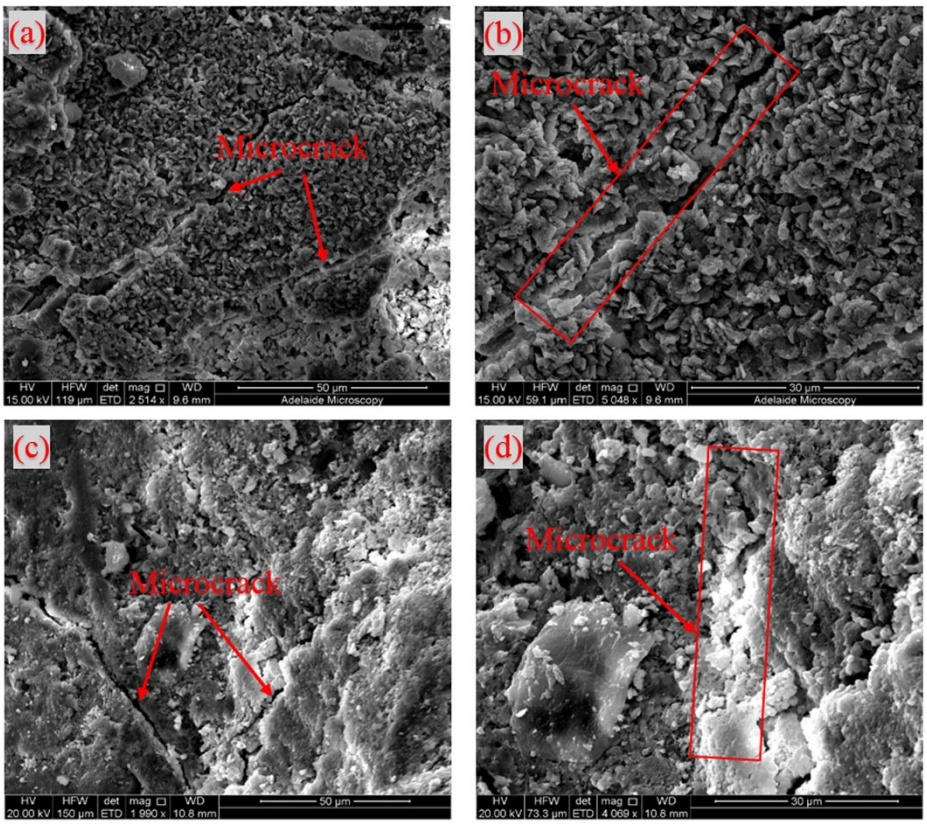

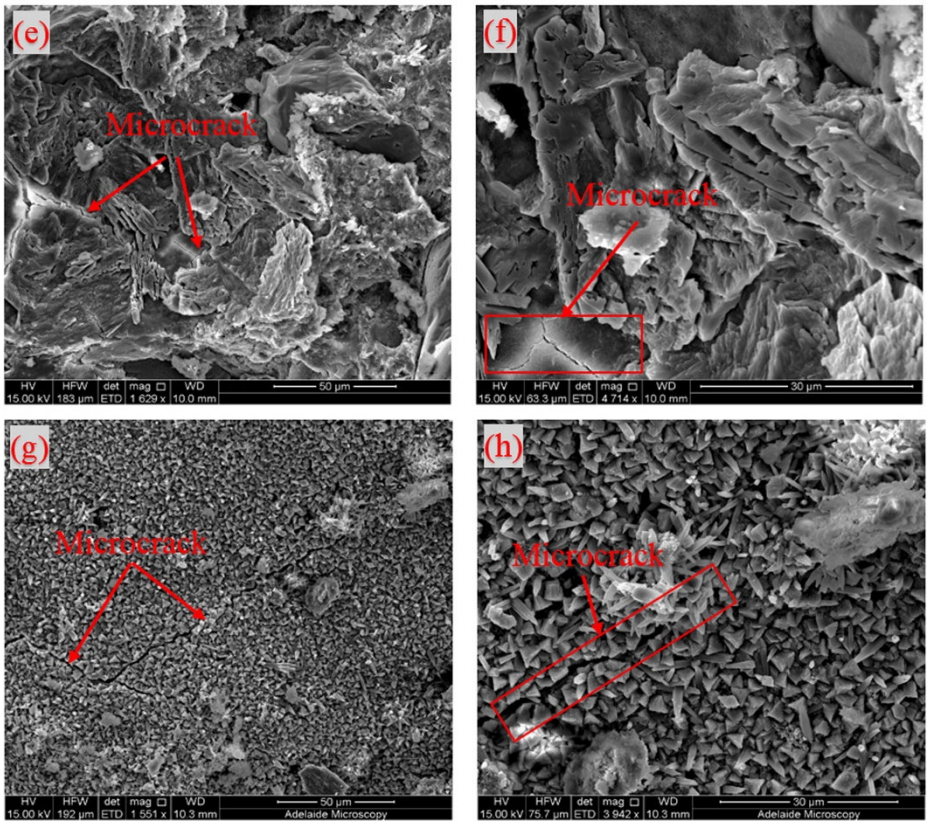

Fig. 10. SEM images of cracking patterns at 50 µm and 30 µm magnification of PRG-cement mortar mixes with different PRG contents (i.e. 0%, 0.03%, 0.07%, and 0.3%) at 28 days: (a, b) PRG0; (c, d) PRG0.03; (e, f) PRG0.07; (g, h) PRG0.3.

Fig. 11 shows the high magnification at 10 µm and 5 µm of SEM images of the mortar mixes with different PRG concentrations, i.e. 0%, 0.03%, 0.07%, and 0.3%, at 28-day curing age. The SEM images show four main compositions of the microstructures of the samples: CSH gels have tetrahedral and polyhedral shapes; CH has hexagonal shapes; Aft has needle-rod shapes; and pores intercalate between crystals [16, 17, 24]. It can be observed that they have similar types of the compositions in microstructures while the density and distribution of these components in each sample are different. For PRG0 shown in Fig. 11(a), (b), it not only shows fewer contents and smaller sizes of CSH and CH crystals, but also consists of significant numbers of pores in its microstructure. This leads to smaller mechanical strengths than those of the PRG-cement mixes (as consistent with the results discussed in the previous sections).

By the addition of the 0.03%, 0.07%, and 0.3% PRG content (Fig. 11(c)–(h)), there are apparent changes in their microstructures with larger sizes and enhanced densities of crystals, also more compactness. The best observation in the change of the microstructure can be seen in PRG0.07 (Fig. 11(e), (f)), which is the densest, and followed by PRG0.3 (Fig. 11(g), (h)) and PRG0.03 (Fig. 11(c), (d)). This is because PRG0.07 not only shows the highest degree of the cement hydration, which was discussed earlier in XRD, TGA, and FTIR results, but also comes from the mechanical adhesive friction forces between PRG sheets and cement gels, resulting in the strong interconnection across the compositions of cement matrix composites.

When PRG concentration is increased up to 0.3%, it leads to poor dispersion. The agglomeration of PRG sheets occurs due to the effect of the van der Waals force. This creates multi-layers PRG sheets with thicker thickness, and hence, it prevents PRG sheets to contribute to improve the degree of the cement hydration process and to interact with the crystals compositions of cement gels. This leads to the reduction in mechanical strengths, which is in line with the results discussed in the previous sections and previous studies on a combination of graphene and cementitious composites [19].

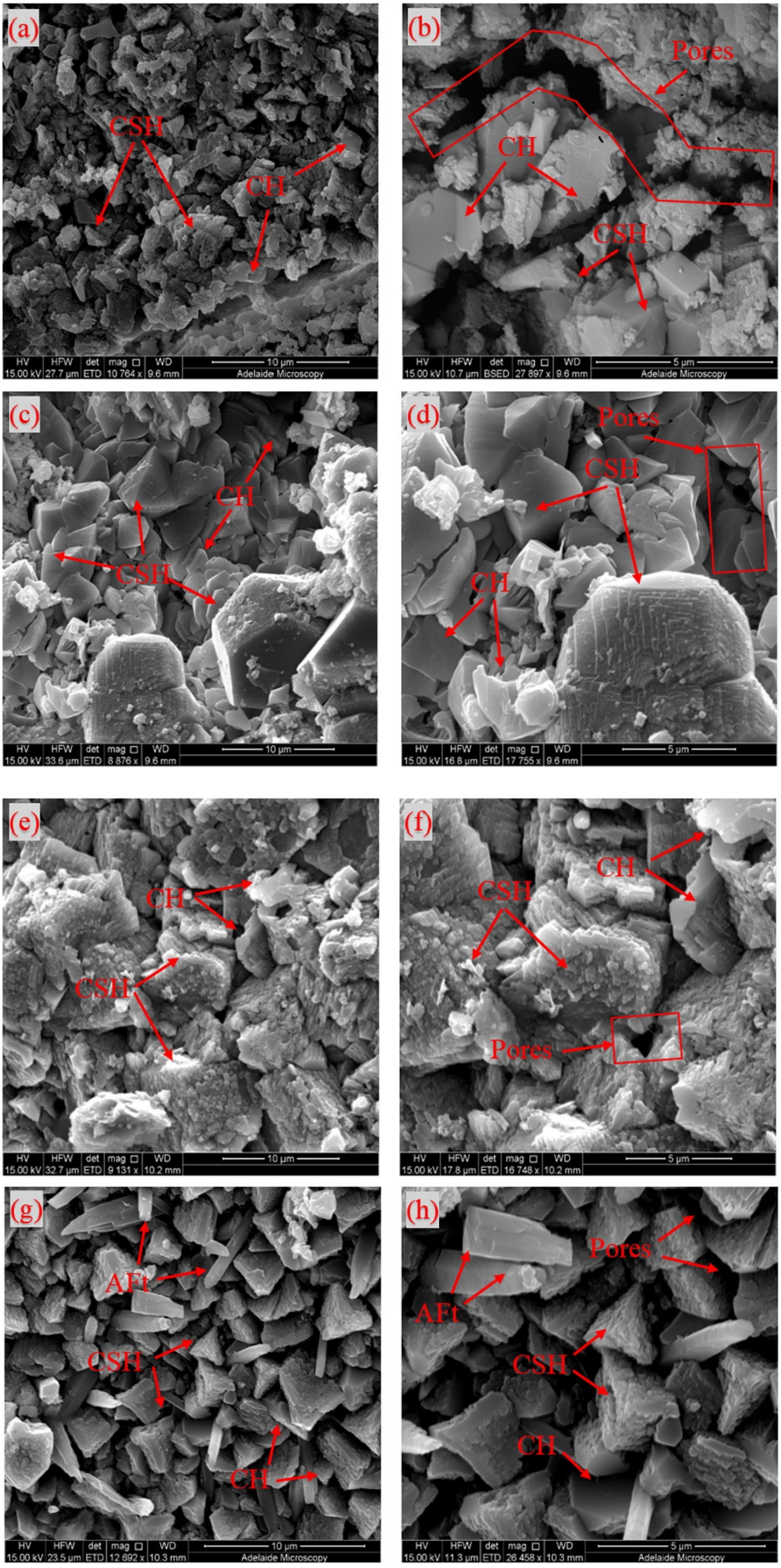
(a)
CSH
CH
HV 15.00 kV | HFW 27.7 µm | det ETD | mag 10 764 x | WD 9.6 mm | 10 µm | Adelaide Microscopy
(b)
Pores
CH
CSH
HV 15.00 kV | HFW 10.7 µm | det BSED | mag 27 897 x | WD 9.6 mm | 5 µm | Adelaide Microscopy
(c)
CH
CSH
HV 15.00 kV | HFW 33.6 µm | det ETD | mag 8 876 x | WD 9.6 mm | 10 µm
(d)
Pores
CSH
CH
HV 15.00 kV | HFW 16.8 µm | det ETD | mag 17 755 x | WD 9.6 mm | 5 µm
(e)
CH
CSH
HV 15.00 kV | HFW 32.7 µm | det ETD | mag 9 131 x | WD 10.2 mm | 10 µm
(f)
CH
CSH
Pores
HV 15.00 kV | HFW 17.8 µm | det ETD | mag 16 748 x | WD 10.2 mm | 5 µm
(g)
AFt
CSH
CH
HV 15.00 kV | HFW 23.5 µm | det ETD | mag 12 892 x | WD 10.3 mm | 10 µm | Adelaide Microscopy
(h)
Pores
AFt
CSH
CH
HV 15.00 kV | HFW 11.3 µm | det ETD | mag 26 458 x | WD 10.3 mm | 5 µm | Adelaide Microscopy

Fig. 11. High magnification at 10 μm and 5 μm of SEM images of PRG-cement mortar mixes with different PRG contents (i.e. 0%, 0.03%, 0.07%, and 0.3%) at 28 days: (a, b) PRG0; (c, d) PRG0.03; (e, f) PRG0.07; (g, h) PRG0.3.

4. Conclusions

The results of the investigation on the effects of different concentrations of industrially produced PRG by electrochemical exfoliation of graphite on the physicochemical and mechanical properties of PRG-cement mortar composites have been presented. The following key conclusions have been drawn based on the results and discussions in the study:

- The first study of the ultra-large size of PRG particles in the average of 56 ± 12 μm produced by this industrial process has been confirmed that there is a significant enhancement of the ultra-large PRG size to mechanical properties of cementitious composites, compared to all previous studies using graphene based materials.
- It has been shown that the addition of PRG to cement mortars can improve their mechanical properties and the level of improvement depends on PRG contents. The 0.07% PRG mix has been identified as the optimal PRG concentration in this study, which provides 34.3% and 26.9% enhancement of compressive and tensile strengths at 28 days, respectively.
- PRG has improved the microstructure of the cement matrix, which comes from the rise in the hydration degree of cement pastes and the adhesive friction forces between PRG sheets and cement gels, and has also impeded crack propagations in the structures.
- The mixes with the PRG contents, which are higher of the optimal value (i.e. 0.07%), lead to poor dispersion resulting in the agglomeration of PRG sheets. This limits the improvement of mechanical strengths.

- The results from XRD, TGA, FTIR, and SEM analyses have shown that there is a strong relationship between mechanical results and bonding gels, densities and arrangements of the crystals in the microstructures.

The results and findings from this study have suggested a promising capability of industrially manufactured PRG using electrochemical process due to their unique properties to be used as a next-generation of additives in cementitious composites. This could improve the properties of building materials, such as mechanical, durability, conductivity, and shielding properties. We are currently in the process of investigating the effects of the different contents, sizes and types of PRG on these properties, and the findings will be presented in separate studies.

Declaration of Competing Interest

The authors declare that they have no known competing for financial interests or personal relationships that could have appeared to influence the work reported in this paper.

Acknowledgements

This work is supported and funded by the ARC Research Hub for Graphene Enabled Industry Transformation (Grant IH150100003) and First Graphene Ltd. The authors also thank the Schools of Civil, Environmental and Mining Engineering and Chemical Engineering and Advanced Materials at the University of Adelaide for supporting this work. The authors also acknowledge Adam Ryntjes as the technical support in the experimental works.

REFERENCES

[1] M.S. Choi, S.-T. Kang, B.Y. Lee, K.-T. Koh, G.-S. Ryu, Improvement in Predicting the Post-Cracking Tensile Behavior of Ultra-High Performance Cementitious Composites Based on Fiber Orientation Distribution, Materials 9(10) (2016) 829.

[2] R.V. Sagar, B.R. Prasad, S.S. Kumar, An experimental study on cracking evolution in concrete and cement mortar by the b-value analysis of acoustic emission technique, Cement and Concrete Research 42(8) (2012) 1094-1104.

[3] H. Du, H.J. Gao, S. Dai Pang, Improvement in concrete resistance against water and chloride ingress by adding graphene nanoplatelet, Cement and Concrete Research 83 (2016) 114-123.

[4] M.S. Konsta-Gdoutos, Z.S. Metaxa, S.P. Shah, Multi-scale mechanical and fracture characteristics and early-age strain capacity of high performance carbon nanotube/cement nanocomposites, Cement and Concrete Composites 32(2) (2010) 110-115.

[5] F. Sanchez, K. Sobolev, Nanotechnology in concrete–a review, Construction and building materials 24(11) (2010) 2060-2071.

[6] T. Ji, Preliminary study on the water permeability and microstructure of concrete incorporating nano-SiO 2, Cement and Concrete Research 35(10) (2005) 1943-1947.

[7] L. Senff, D. Tobaldi, S. Lucas, D. Hotza, V. Ferreira, J. Labrincha, Formulation of mortars with nano-SiO 2 and nano-TiO 2 for degradation of pollutants in buildings, Composites Part B: Engineering 44(1) (2013) 40-47.

[8] W. Li, Z. Huang, T. Zu, C. Shi, W.H. Duan, S.P. Shah, Influence of nanolimestone on the hydration, mechanical strength, and autogenous shrinkage of ultrahigh-performance concrete, Journal of Materials in Civil Engineering 28(1) (2015) 04015068.

[9] Z. Pan, L. He, L. Qiu, A.H. Korayem, G. Li, J.W. Zhu, F. Collins, D. Li, W.H. Duan, M.C. Wang, Mechanical properties and microstructure of a graphene oxide–cement composite, Cement and Concrete Composites 58 (2015) 140-147.

[10] B.M. Tyson, R.K. Abu Al-Rub, A. Yazdanbakhsh, Z. Grasley, Carbon nanotubes and carbon nanofibers for enhancing the mechanical properties of nanocomposite cementitious materials, Journal of Materials in Civil Engineering 23(7) (2011) 1028-1035.

[11] M.S. Konsta-Gdoutos, C.A. Aza, Self sensing carbon nanotube (CNT) and nanofiber (CNF) cementitious composites for real time damage assessment in smart structures, Cement and Concrete Composites 53 (2014) 162-169.

[12] M.A. Rafiee, W. Lu, A.V. Thomas, A. Zandiatashbar, J. Rafiee, J.M. Tour, N.A. Koratkar, Graphene nanoribbon composites, ACS nano 4(12) (2010) 7415-7420.

[13] S. Lv, L. Deng, W. Yang, Q. Zhou, Y. Cui, Fabrication of polycarboxylate/graphene oxide nanosheet composites by copolymerization for reinforcing and toughening cement composites, Cement and Concrete Composites 66 (2016) 1-9.

[14] B. Han, S. Sun, S. Ding, L. Zhang, X. Yu, J. Ou, Review of nanocarbon-engineered multifunctional cementitious composites, Composites Part A: Applied Science and Manufacturing 70 (2015) 69-81.

[15] Q. Wang, J. Wang, C.-x. Lu, B.-w. Liu, K. Zhang, C.-z. Li, Influence of graphene oxide additions on the microstructure and mechanical strength of cement, New Carbon Materials 30(4) (2015) 349-356.

[16] S. Lv, S. Ting, J. Liu, Q. Zhou, Use of graphene oxide nanosheets to regulate the microstructure of hardened cement paste to increase its strength and toughness, CrystEngComm 16(36) (2014) 8508-8516.

[17] S. Sharma, N. Kothiyal, Influence of graphene oxide as dispersed phase in cement mortar matrix in defining the crystal patterns of cement hydrates and its effect on mechanical, microstructural and crystallization properties, RSC Advances 5(65) (2015) 52642-52657.

[18] S. Lv, J. Liu, T. Sun, Y. Ma, Q. Zhou, Effect of GO nanosheets on shapes of cement hydration crystals and their formation process, Construction and Building Materials 64 (2014) 231-239.

[19] A. Gholampour, M.V. Kiamahalleh, D.N. Tran, T. Ozbakkaloglu, D. Losic, Revealing the dependence of the physiochemical and mechanical properties of cement composites on graphene oxide concentration, RSC Advances 7(87) (2017) 55148-55156.

[20] B. Wang, R. Jiang, Z. Wu, Investigation of the mechanical properties and microstructure of graphene nanoplatelet-cement composite, Nanomaterials 6(11) (2016) 200.

[21] K. Chu, W.-s. Li, H. Dong, Role of graphene waviness on the thermal conductivity of graphene composites, Applied Physics A 111(1) (2013) 221-225.

[22] Z. Metaxa, Polycarboxylate based superplasticizers as dispersant agents for exfoliated graphene nanoplatelets reinforcing cement based materials, J. Eng. Sci. Tech. Rev 8 (2015) 1-5.

[23] T. Tong, Z. Fan, Q. Liu, S. Wang, S. Tan, Q. Yu, Investigation of the effects of graphene and graphene oxide nanoplatelets on the micro-and macro-properties of cementitious materials, Construction and Building Materials 106 (2016) 102-114.

[24] S. Lv, Y. Ma, C. Qiu, T. Sun, J. Liu, Q. Zhou, Effect of graphene oxide nanosheets of microstructure and mechanical properties of cement composites, Construction and building materials 49 (2013) 121-127.

[25] H. Du, S. Dai Pang, Enhancement of barrier properties of cement mortar with graphene nanoplatelet, Cement and Concrete Research 76 (2015) 10-19.

[26] J. Tao, X. Wang, Z. Wang, Q. Zeng, Graphene nanoplatelets as an effective additive to tune the microstructures and piezoresistive properties of cement-based composites, Construction and Building Materials 209 (2019) 665-678.

[27] E. Shamsaei, F.B. de Souza, X. Yao, E. Benhelal, A. Akbari, W. Duan, Graphene-based nanosheets for stronger and more durable concrete: A review, Construction and Building Materials 183 (2018) 642-660.

[28] AS3972, General purpose and blended cements, Standard, Standard Australia, Australian Standard, 2010.

[29] AS1478.1, Chemical admixtures for concrete, mortar and grout - Admixtures for concrete, Australian Standard, 2000.

[30] H. Yang, H. Cui, W. Tang, Z. Li, N. Han, F. Xing, A critical review on research progress of graphene/cement based composites, Composites Part A: Applied Science and Manufacturing 102 (2017) 273-296.

[31] ASTM-C1437, Standard Test Method for Flow of Hydraulic Cement Mortar, Standard, ASTM, 2015.

[32] ASTM-C109/C109M-07, Standard test method for compressive strength of hydraulic

cement mortars, ASTM International: USA 2008, 2008.

[33] ASTM-C307-03, Standard Test Method for Tensile Strength of Chemical-Resistant Mortar, Grouts, and Monolithic Surfacings Monolithic Surfacings, ASTM International, 2012.

[34] N. Kothiyal, S. Sharma, S. Mahajan, S. Sethi, Characterization of reactive graphene oxide synthesized from ball–milled graphite: its enhanced reinforcing effects on cement nanocomposites, Journal of adhesion science and Technology 30(9) (2016) 915-933.

[35] H. Du, S. Dai Pang, Dispersion and stability of graphene nanoplatelet in water and its influence on cement composites, Construction and Building Materials 167 (2018) 403-413.

[36] M. Wang, R. Wang, H. Yao, Z. Wang, S. Zheng, Adsorption characteristics of graphene oxide nanosheets on cement, RSC Advances 6(68) (2016) 63365-63372.

[37] Z. Lu, D. Hou, L. Meng, G. Sun, C. Lu, Z. Li, Mechanism of cement paste reinforced by graphene oxide/carbon nanotubes composites with enhanced mechanical properties, RSC Advances 5(122) (2015) 100598-100605.

[38] D. Hou, Z. Lu, X. Li, H. Ma, Z. Li, Reactive molecular dynamics and experimental study of graphene-cement composites: Structure, dynamics and reinforcement mechanisms, Carbon 115 (2017) 188-208.

[39] S.J. Chen, C.Y. Li, Q. Wang, W.H. Duan, Reinforcing mechanism of graphene at atomic level: Friction, crack surface adhesion and 2D geometry, Carbon 114 (2017) 557-565.

[40] C. Lu, Z. Lu, Z. Li, C.K. Leung, Effect of graphene oxide on the mechanical behavior of strain hardening cementitious composites, Construction and Building Materials 120 (2016) 457-464.

[41] B. Code, ACI 318-11 Building Code Requirements for Structural Concrete and Commentary, American Concrete Institute, Retrieved 8 (2012).

[42] B. Bahoria, D. Parbat, P. Nagarnaik, XRD Analysis of Natural sand, Quarry dust, waste plastic (ldpe) to be used as a fine aggregate in concrete, Materials Today: Proceedings 5(1) (2018) 1432-1438.

[43] M. Zainuri, Synthesis of SiO2 nanopowders containing quartz and cristobalite phases from silica sands, Materials Science-Poland 33(1) (2015) 47-55.

[44] J. Elena, M.D. Lucia, X-RAY Diffraction Study of hydration Processes in the Portland Cement, JAESVol 1 14.

[45] R. Jadhav, N. Debnath, Computation of X-ray powder diffractograms of cement components and its application to phase analysis and hydration performance of OPC cement, Bulletin of Materials Science 34(5) (2011) 1137-1150.

[46] S. Sharma, N. Kothiyal, Comparative effects of pristine and ball-milled graphene oxide on physico-chemical characteristics of cement mortar nanocomposites, Construction and Building Materials 115 (2016) 256-268.

[47] L. Zhao, X. Guo, C. Ge, Q. Li, L. Guo, X. Shu, J. Liu, Investigation of the effectiveness of PC@ GO on the reinforcement for cement composites, Construction and Building Materials 113 (2016) 470-478.

[48] L. Zhao, X. Guo, Y. Liu, C. Ge, L. Guo, X. Shu, J. Liu, Synergistic effects of silica nanoparticles/polycarboxylate superplasticizer modified graphene oxide on mechanical behavior and hydration process of cement composites, RSC Advances 7(27) (2017) 16688-16702.

[49] F.G.S. Silva, R.A.F. Junior, J.S. da Silva, K.W. Pinto, H.M.C. Andrade, J. Dweck, J.P. Gonçalves, Hydration of the equilibrium catalyst (Ecat) calcium hydroxide system, Journal of Thermal Analysis and Calorimetry 120(2) (2015) 1089-1098.

[50] V.S. Ramachandran, J.J. Beaudoin, Handbook of analytical techniques in concrete science and technology: principles, techniques and applications, Elsevier2000.

[51] P. Mounanga, A. Khelidj, A. Loukili, V. Baroghel-Bouny, Predicting Ca (OH) 2 content and chemical shrinkage of hydrating cement pastes using analytical approach, Cement and Concrete Research 34(2) (2004) 255-265.

[52] W. Wongkeo, P. Thongsanitgarn, P. Chindaprasirt, A. Chaipanich, Thermogravimetry of ternary cement blends, Journal of thermal analysis and calorimetry 113(3) (2013) 1079-1090.

[53] J. Hlavay, K. Jonas, S. Elek, J. Inczedy, Characterization of the particle size and the crystallinity of certain minerals by ir spectrophotometry and other instrumental methods: II, Investigations on quartz and feldspar, Clays and Clay Minerals 26(2) (1978) 139-43.

[54] G. Anbalagan, A. Prabakaran, S. Gunasekaran, Spectroscopic characterization of Indian standard sand, Journal of applied spectroscopy 77(1) (2010) 86-94.

[55] M. Horgnies, J. Chen, C. Bouillon, Overview about the use of Fourier transform infrared spectroscopy to study cementitious materials, WIT Trans. Eng. Sci 77 (2013) 251-262.

[56] L. Fernández Carrasco, D. Torrens Martín, L. Morales, S. Martínez Ramírez, Infrared spectroscopy in the analysis of building and construction materials, InTech2012.

[57] P.A. Bhat, N. Debnath, Theoretical and experimental study of structures and properties of cement paste: The nanostructural aspects of C–S–H, Journal of Physics and Chemistry of Solids 72(8) (2011) 920-933.

[58] A. Gholampour, M. Valizadeh Kiamahalleh, D.N. Tran, T. Ozbakkaloglu, D. Losic, From Graphene Oxide to Reduced Graphene Oxide: Impact on the Physiochemical and Mechanical Properties of Graphene–Cement Composites, ACS applied materials & interfaces 9(49) (2017) 43275-43286.

[59] R. Gao, N. Hu, Z. Yang, Q. Zhu, J. Chai, Y. Su, L. Zhang, Y. Zhang, like graphene-Ag composite films with enhanced mechanical and electrical properties, Nanoscale research letters 8(1) (2013) 32.

[60] P. Yu, R.J. Kirkpatrick, B. Poe, P.F. McMillan, X. Cong, Structure of calcium silicate hydrate (C-S-H): Near-, mid-, and far-infrared spectroscopy, Journal of the American Ceramic Society 82(3) (1999) 742-748.

CHAPTER 3:

DEMONSTRATION OF THE INFLUENCE OF THE DIFFERENT PARTICLE SIZES OF PRISTINE GRAPHENE ON ENHANCING MECHANICAL PROPERTIES OF PORTLAND CEMENT MORTARS

THE AIM AND OBJECTIVE OF THIS CHAPTER:

Aim: This chapter aims to explore the influence of different PRG particle sizes on enhancement rates of compressive and tensile strengths of ordinary Portland cement mortars.

Objectives 1: investigating the influence of particle sizes of PRG sheets on compressive and tensile strengths of Portland cement mortars; and the benefits of using PRG as the additives to reduce the environmental impact of Portland cement.

Objectives 2: analysing physicochemical and microstructure properties of cement-based mortars containing different PRG particle sizes to improve understanding of the reasons behind their different enhancement rates.

Statement of Authorship

Title of Paper	Influence of pristine graphene particle sizes on physicochemical, microstructural and mechanical properties of Portland cement mortars
Publication Status	☑ Published ☐ Accepted for Publication ☐ Submitted for Publication ☐ Unpublished and Unsubmitted work written in manuscript style
Publication Details	Ho, V. D., Ng, C. T., Ozbakkaloglu, T., Goodwin, A., Mc Guckin, C., Karunagaran, R. U., & Losic, D. Influence of pristine graphene particle sizes on physicochemical, microstructural and mechanical properties of Portland cement mortars. *Construction and Building Materials.* (Accepted for Publication)

Principal Author

Name of Principal Author (Candidate)	Van Dac Ho		
Contribution to the Paper	Literature review, preparing and doing experiments, assessment and analysis of test results, and preparation of the manuscript.		
Overall percentage (%)	85		
Certification:	This paper reports on original research I conducted during the period of my Higher Degree by Research candidature and is not subject to any obligations or contractual agreements with a third party that would constrain its inclusion in this thesis. I am the primary author of this paper.		
Signature		Date	18/03/2020

Co-Author Contributions

By signing the Statement of Authorship, each author certifies that:

i. the candidate's stated contribution to the publication is accurate (as detailed above);

ii. permission is granted for the candidate in include the publication in the thesis; and

iii. the sum of all co-author contributions is equal to 100% less the candidate's stated contribution.

Name of Co-Author	Dusan Losic		
Contribution to the Paper	Research supervision, review and revisions of the manuscript.		
Signature		Date	10/05/2020

Name of Co-Author	Ching-Tai Ng		
Contribution to the Paper	Research supervision, review and revisions of the manuscript.		
Signature		Date	25/04/2020

Name of Co-Author	Togay Ozbakkaloglu		
Contribution to the Paper	Review of the manuscript.		
Signature		Date	11/04/2020

Name of Co-Author	Ramesh U. Karunagaran		
Contribution to the Paper	Review of the manuscript.		
Signature		Date	20/03/2020

Name of Co-Author	Andy Goodwin		
Contribution to the Paper	Review of the manuscript.		
Signature		Date	22/03/2020

Name of Co-Author	Craig Mc Guckin		
Contribution to the Paper	Review of the manuscript.		
Signature		Date	23/03/2020

Journal paper 2 (Published)

Influence of pristine graphene particle sizes on physicochemical, microstructural and mechanical properties of Portland cement mortars

Van Dac Ho[1,2,3], Ching-Tai Ng[1], Togay Ozbakkaloglu[4], Andy Goodwin[5], Craig McGuckin[5] Ramesh U. Karunagaran[2,3], Dusan Losic*[2,3]

[1]School of Civil, Environmental and Mining Engineering, The University of Adelaide, South Australia, 5005, Australia

[2]School of Chemical Engineering, The University of Adelaide, South Australia, 5005 Australia

[3]ARC Research Hub for Graphene Enabled Industry Transformation, The University of Adelaide, South Australia, 5005 Australia

[4] Ingram School of Engineering, Texas State University, United States

[5] First Graphene Ltd, Suite 3, 9 Hampden Road, Nedlands WA 6009, Australia

*Corresponding authors: dusan.losic@adelaide.edu.au

ABSTRACT

This paper aims to study the effect of the size of pristine graphene (PRG) particles on the compressive and tensile strengths of cement-based mortars and to gain better understandings of the mechanism behind the enhancement of these properties. PRG industrially manufactured by the electrochemical process with a variety of particle sizes including 5μm, 43μm, 56μm, and 73μm was used at the optimal dosage of 0.07% by weight of cement binder. The results indicate that mechanical strengths of cement mortars at 7 and 28 days considerably depend on the size of PRG. The mixes with size 56μm and 73μm show significant influence on both compressive and tensile strengths of cement mortars, which increase approximately 34.3% and 30.1% at 28-day compressive strengths, and 26.9% and 38.6% at 28-day tensile strengths, respectively. On the other hand, the mix with size 43μm of PRG addition exhibits a significant increase only in tensile strength, and there are no significant effects on either compressive strengths or tensile strengths of the mix containing 5μm particles. The observed enhancement in the mechanical properties of cement mortars by large PRG sizes is attributed to the improvement of cement hydration level, the reduction of cement particles' distance in cement gels because of the effect of van der Waals forces between PRG sheets, and the most important from the mechanical adhesion forces between PRG sheets and cement gels. The results from this study indicate that PRG is not only a promising additive in practical application for building materials to improve the current drawbacks of cement composites, but also a feasible option to support the reduction of cement mass used in cement composites, which could reduce the CO_2 footprint and amount of CO_2 emission into the atmosphere.

Keywords: Pristine graphene; Cement mortar; Mechanical properties; Acceleration; Microstructure.

1. Introduction

The most commonly used materials in the construction industry are cementitious composites. Although they are strong in compressive strength, they are weak in tensile and corrosive properties [1]. Researchers have proposed different approaches to improve their properties such as plastic and carbon fibers [2, 3], nanoparticles [4], carbon nanofibers and nanotubes [5, 6]. However, these additives are unable to effectively improve properties of cementitious composites due to limitations in bonding and arresting microcracks [5-7]. Moreover, the core component of cementitious composites, which is Portland cement, is also one of the factors contributing to a major amount of carbon dioxide (CO_2) into the atmosphere that causes greenhouse gases. Global Portland cement production is estimated at 4 billion tons per year which the largest man-made material in the world [8-10]. It was reported that one ton of Portland cement production could release about one ton of carbon dioxide [11, 12], which accounts for about 7% of CO_2 release globally [8, 9, 11, 13]. Therefore, developing approaches and new additives to improve the properties of cement composites and reduce the amount of cement consumption in order to decrease CO2 emission have attracted significant research interests. Improving only 1-2% in the reduction of CO2 release by enhancing properties of cement composites could make a significant contribution to climate change.

To address these problems, several measures were explored by researchers such as improving cement plant efficiency or using supplementary materials [4, 14, 15]. There have been intense studies in using supplementary materials to enhance properties of cement composites and reduce the mass of cement consumption with many publications in recent decades, including using fly ash, ground granulated blast furnace slag, nanoparticles or graphene materials [4, 16-20]. Among them, graphene and its derivatives (i.e. graphene oxide (GO), reduced graphene oxide (rGO) and pristine graphene (PRG), as two-dimensional materials, have shown the great potential for improving properties of cementitious materials owing to their outstanding

properties of high mechanical and conductivity properties, large specific surface areas and aspect ratios [16, 18, 21, 22]. These studies showed graphene additives could significantly enhance key properties of cement composites such as compressive and tensile strengths, chloride penetration, and electrical conductivity [16, 18]. It is important to note that there are significant differences in structural, chemical, mechanical and electrical properties of these graphene materials. While GO materials which are often oxidized from graphite are well known, the difference between graphene nanoplatelets produced from rGO and PRG materials has not been well described in research papers because both are termed as graphene nanoplatelets or flakes. PRG made by an electrochemical process from graphite materials preserves its original pristine structure. Thus, it has different properties compared with graphene nanoplatelets produced from rGO sheets that are also produced from graphite materials in different methods treated by harsh acids and oxidants to make GO and followed by a thermal or chemical process, which cause a significant level of defects and less crystallinity in the properties of graphene nanoplatelets.

For GO studies, Li et al. [23] showed that incorporating of 0.04% GO into cement paste produced a 14% improvement in its compressive strength at 28 days, and there was no positive effect on its compressive strengths when the incorporation of GO below 0.03%. Another study performed by Wang et al. [24] reported that cement paste and cement mortar with 0.05% GO additive showed the highest enhancement rates in their compressive and flexural strengths, which could increase by 40.4% & 90.5% and 24.4% & 70.5% in compressive & flexural strengths of cement paste and cement mortar at 28 days, respectively. Although a significant process has been made in studying the effects of GO additives on properties of cement composites, the mechanism between GO and cement composites in the strength improvement has not been studied in-depth [18]. Few studies have recently explored the influence of oxygen functional groups from GO on the mechanism of the intermolecular interaction between GO sheets and the cementitious matrix, resulting in the improvement in the properties of cement

composites [16, 25, 26]. Besides, the effects of different GO dosages and sizes on microstructures of cement mortars were also revealed in the study performed by Sharma and Kothiyal [27]. They showed that the mix with a smaller GO size (i.e. 100nm) improved compressive strength by 86% at 1% GO concentration. This improvement was more than that of using the larger GO size (i.e. 900 nm) at the same dosage, which was improved by 63% only. This enhancement was explained by the effects of a larger level of oxygen-functional groups (e.g. carboxyl, hydroxyl) of GO with the smaller size compared to those with the larger size, resulting in stronger chemical adhesion forces between them and cement gels in the cement matrix [16, 28].

In the case of PRG additives, recent studies on a combination of PRG and cement composites have shown great potential in strength improvement in PRG-cement composites [16, 18]. These studies were mainly focused on the effects of dosages with limited numbers of studies revealing the influence of other parameters such as the sizes, number of layers, functional groups and the mechanism of the strength improvement of cement composites. In the study performed by Wang et al. [29], which only compared compressive strengths of cement mortars between the control and the mix with 0.05% PRG, compressive and flexural strengths at 7 days of the mortar with 0.05% PRG was respectively improved by 8% and 24%. Another study with four different PRG concentrations (i.e. 0%, 2.5%, 5.0%, and 7.5%) performed by Du and Dai Pang [30] showed that the incorporation of PRG into cement mortars could considerably decrease water penetration depth whereas there were insignificant effects of PRG on compressive and flexural strengths of cement mortars, which was due to the agglomeration of PRG coming from the high PRG dosages rate used. In 2019, Tao et al. [31] combined cement mortars with five different PRG dosages (i.e. 0%, 0.05%, 0.1%, 0.5%, and 1%) and revealed that 0.05% PRG additive was the optimal dosage and could respectively improve compressive and flexural strengths of the mortar at 28 days by 8.3% and 15.6%, however, the strengths started decreasing when PRG dosages over 0.05% owing to the agglomeration of PRG.

Even though these studies show a strong dependence of the properties of cement composites on PRG dosages, the mechanisms of this dosage dependence have not been clearly explained. Additionally, unlike GO, rGO and PRG sheets (PRGs) have very few oxygen-functional groups that indicate a different mechanism to enhance the cement matrix, which is likely based on friction adhesion forces between PRGs and cementitious gels [32]. Also, all the studies on PRG-cement composites from the literature have used PRGs with the average size varying from 5µm to 25µm [16, 18, 29, 31], with no study has been exploring how an ultra-large size influences on strength improvement in PRG-cement composites, together with revealing its enhancement mechanism. Our previous study [32] was the first study investigating the effects of dosages using the ultra-large PRG size (56um) on mechanical, microstructural and physicochemical properties of cement-based mortars. The study showed that at the optimal concentration (0.07% PRG), compressive and tensile strengths at 28 days of the mortar mix with PRG size 56um could enhance 34.3% and 26.9%, respectively. The study also revealed that the strengthening mechanism of cement mortars with the ultra-large PRG size was mostly due to friction adhesion forces between PRGs and cementitious gels. Compared with GO materials that have high levels of defects, high costs and environmental impact in production, and weaker mechanical properties [33, 34], PRG materials have low levels of defects, stronger crystalline and mechanical properties and can be produced by an environmentally sustainable process in high quality at industrial scales with much lower costs. Therefore, PRG materials are expected to be more acceptable to be applied for building and infrastructure materials. This is a strong motivation to have more studies on the effects of other parameters of PRGs on properties of cementitious composites.

To address the above-mentioned research gaps, this study aims to explore the effects of different PRG sizes, which was industrially manufactured by an electrochemical process, on compressive and tensile strengths of cement mortars. The objectives of the study not only consider a range of PRG sizes including 5 µm, 43 µm, 56 µm, and 73 µm on these properties, but also evaluate

their effects on physicochemical and microstructural properties of the mortars. The outcomes of this study will provide better understandings of the strengthening mechanism of compressive and tensile strengths of cement mortars, which is still lacking in the case of research of PRG-cement composites. The results of this study will contribute to future studies on using PRGs as additives in cement composites to enhance the performance of construction materials. The reduced mass of Portland cement in the binder of cement composites as a result of strength improvement due to the addition of PRGs will result in a reduction of the environmental impact of Portland cement products thanks to reduced CO_2 emission.

Table 1. Physical properties of different PRG sizes supplied by First Graphene Ltd.

ID	Particle Size-d50 (μm)	Thickness (nm)	Purity (%)	Poured bulk density (g/cm3)
Size 5μm	5	1-3	~98	~ 0.11
Size 43μm	43	1-3	~98	~ 0.13
Size 56μm	56	1-3	~98	~ 0.12
Size 73μm	73	1-3	~98	~ 0.12

Table 2. Typical chemical properties of general purpose cement.

Compounds	OPC (%)
CaO	63.28
SiO_2	19.95
Al_2O_3	4.79
Fe_2O_3	3.14
MgO	2.03
Na_2O	0.29
K_2O	0.4
SO_3	2.69
P_2O_5	0.04

2. Experimental programs

2.1. Materials

The physical properties of four different PRG sizes provided by First Graphene Ltd in Perth, Australia are shown in Table 1. From the table, it is important to note that although they are different in sizes, the other properties are similar. General purpose cement provided by Adelaide Brighton Cement LTD and complied with Australian Standard AS 3972-2010 [35] was used as the binder of mortar mixes and its typical chemical properties are shown in Table 2. Natural sand with 2.36-mm maximum particle sizes was used as fine-aggregate of mortar mixes. MasterGlenium SKY 8100 complied with Australian Standard AS 1478.1-2000 [36] was used as the superplasticizer to improve the dispersion of PRGs in water.

Table 3. Designed mixes of cementitious composites.

Mix	Pristine Graphene (%)*	Graphene size (µm)	Cement (kg/m3)	Water (kg/m3)	Pristine Graphene (kg/m3)	Sand (kg/m3)	Superplasticizer (kg/m3)
Control			527	255.6	0.000	1448	1.4
Size 5µm	0.07	5	527	255.6	0.369	1448	1.4
Size 43µm	0.07	43	527	255.6	0.369	1448	1.4
Size 56µm	0.07	56	527	255.6	0.369	1448	1.4
Size 73µm	0.07	73	527	255.6	0.369	1448	1.4

* The percentage of pristine graphene based on weight of cement binder.

2.2. Specimens

In this study, we designed the mixes with different PRG sizes at the optimal dosage (0.07% PRG), which is based on our previous study [32] on the effects of PRG concentrations on mechanical properties of cement mortars, to investigate the effects of different PRG sizes on mechanical, physicochemical, and microstructural properties of cement mortars. The details of the designed mixes of cementitious composites are shown in Table 3. As shown in the table, the four different PRG sizes considered in this study are a small size 5µm, a large size 46µm, and two ultra-large sizes 56µm and 73µm. Prior to the mixing of the mortars, the aqueous

solutions including water, superplasticizer and PRG were sonicated for 30 minutes by using Ultrasonication UIP1000hdT. Then, these solutions were gradually added for 5 minutes to natural sand and binder, which were mixed for four minutes. All samples were vibrated for one minute after mounting to mitigate entrapped air during the mounting process. After that, they were covered with wet fabrics and plastic sheets to prevent moisture loss and were demounted after 24 hours cured at room temperature. After that, all the samples continued to be cured in a fog room until testing days.

2.3. Test methods

Compressive and tensile strengths were tested at 7 and 28 days to investigate the influence of different PRG sizes on cement mortars. For compression, 50×50×50 mm^3 cubes complied with ASTM C109/C109M-07 [37] were used. Dog-bone shaped samples, according to ASTM C307-03 [38], were used for tensile tests. The values of each designed mix at testing days were calculated by averaging values obtained from three nominal identical samples of each mix. Scanning electron microscopy (SEM) were obtained by using the FEI Quanta 450 to analyze PRG sizes and surface morphologies of the mortars. X-ray diffraction (XRD) was performed by using the Rigaku MiniFlex 600 X-Ray diffractometer to find the mineralogical characteristics of cement hydration products of the mortars and PRGs. Fourier transform infrared spectroscopy (FTIR) was conducted using the Nicolet 6700 to determine specific functional groups of PRG-cement based mortars. Raman spectra and particle size distribution (PSD) were respectively performed by using the HORIBA LabRAM HR Evolution and Mastersizer 2000 - Malvern to test the number of layers and particle sizes of PRGs. Analysis of variance (ANOVA) method was also used to evaluate how significant effects of different PRG sizes on compressive and tensile strengths of PRG-cement based mortars.

3. Results and Discussion

3.1. Characteristics of PRGs

Fig. 1 shows typical SEM images and related PSD graphs of four PRG samples used for this study. As shown in the figure, their average particle sizes determined from SEM and PSD data are 5±2µm (Fig. 1(a)), 43±8µm (Fig. 1(b)), 56±12µm (Fig. 1(c)) and 73±13µm (Fig. 1(d)), and the PRG structures show wrinkled and irregular shapes with few layer thicknesses. Their XRD patterns presented in Fig. 2(a) show the typical peaks of these PRGs at the position 26.64°, resulting in their d-spacing between layers is 0.334nm that can contribute to a few layers of PRGs [28, 39]. Fig. 2(b) shows the Raman spectra of different PRG sizes. As shown in the figure, the relative intensity ratios of $I_D/I_{D'}$ and I_{2D}/I_G of all the PRG samples are respectively below 3.5 and 1. These mean that these PRG samples don't have basal plane defects [40] and contain mostly several layers (from four layers) [41], showing the high quality of PRGs used in this study and being consistent with their average thickness and other properties provided by the provider.

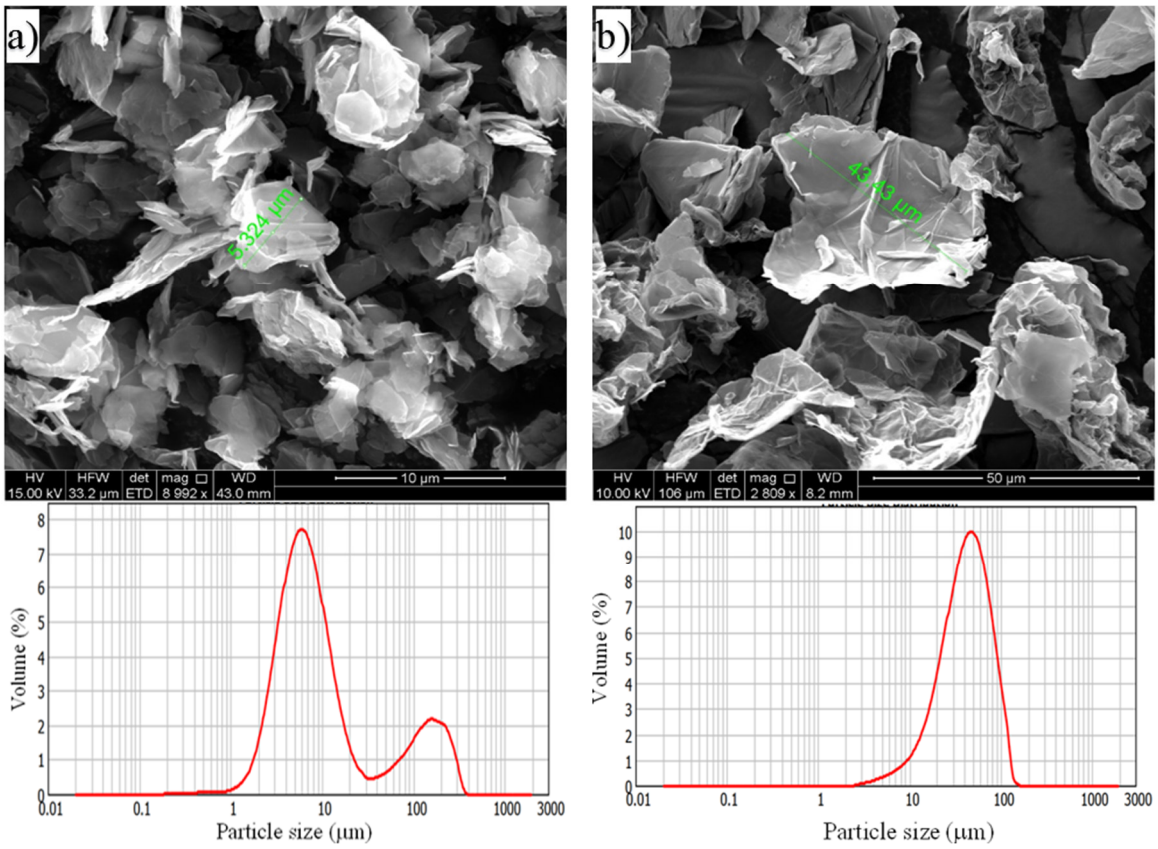

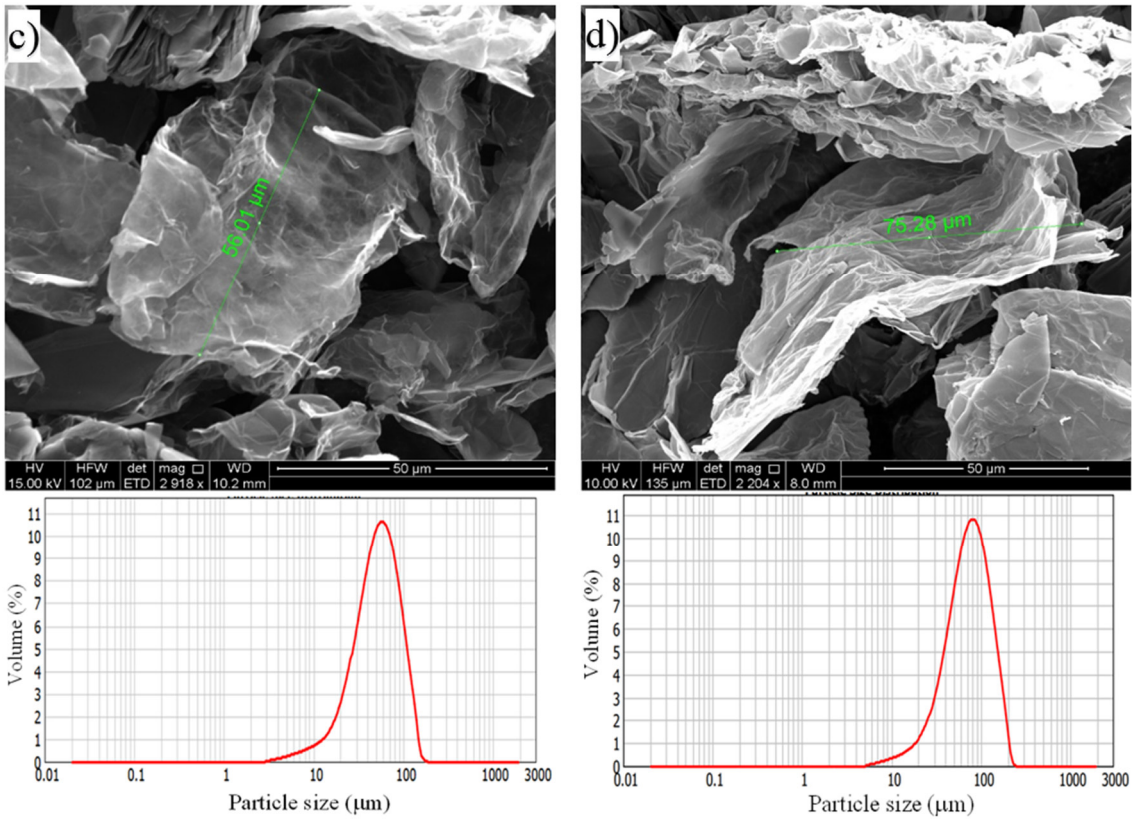

Fig. 1. SEM images and particle size distribution of PRG: (a) size 5µm, (b) size 43µm, (c) size 56µm, (d) size 73µm.

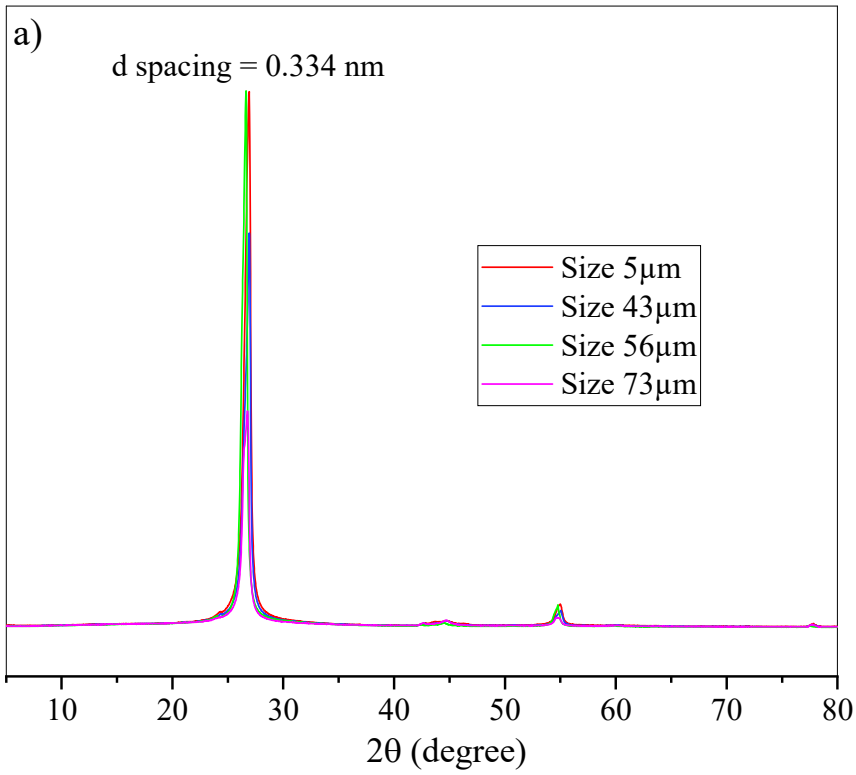

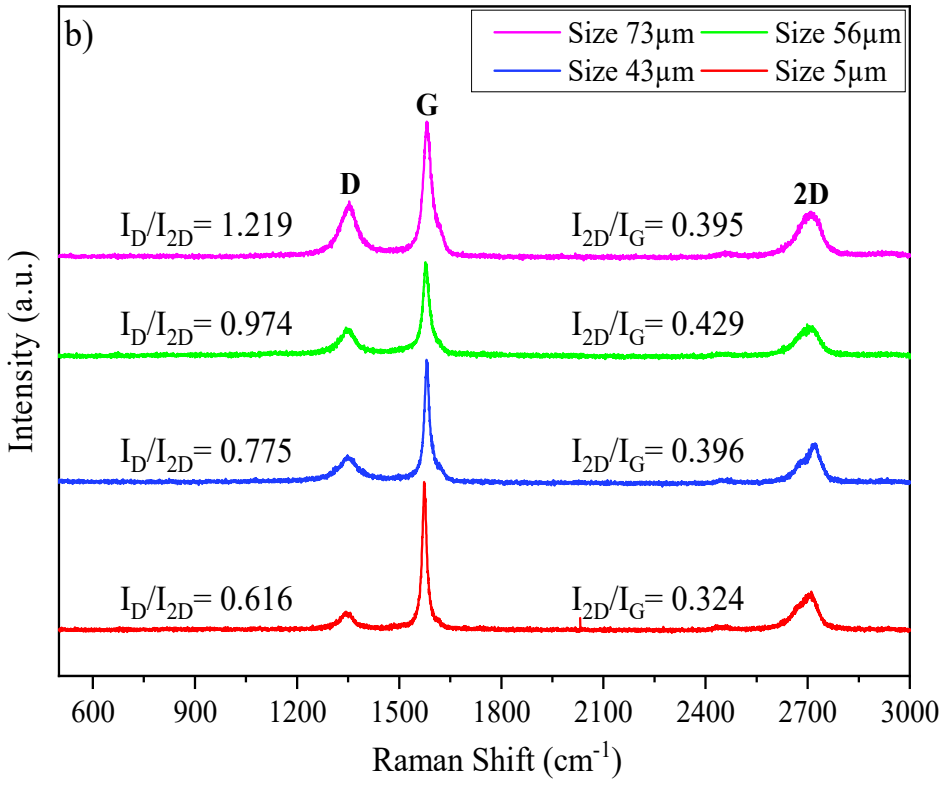

Fig. 2. (a) XRD patterns and (b) Raman spectra of different PRG sizes.

3.2. Mechanical properties of PRG-cement based mortars

Compressive strengths and their enhancement rates at 7 and 28 days of the mortars with different PRG sizes are shown in Fig. 3. As shown in Fig. 3(a) and (b), the addition of PRGs has a positive effect on compressive strengths of the mortars at 7 and 28 days regardless of PRG sizes. The mix with size 56μm shows the highest compressive strength at 7 days and 28 days (49.96 MPa and 56.33 MPa respectively), which increase approximately 36.8% and 34.3%, respectively, in comparison with the control mix that is 36.53 MPa and 41.96 MPa. A similar trend is observed in size 73μm, which rises approximately 24.3% and 30.1% at 7 days and 28 days, respectively. However, the mixes with size 5μm and 43μm present low enhancement rates in compressive strengths of cement based mortars at both testing days, which are respectively approximately 0.5% and 4.5% for size 5μm, and 7% and 7.7% for size 43μm. Therefore, it is concluded that the ultra-large sizes (56μm and 73μm) have a stronger influence on compressive strengths of cementitious composites than those of the small size and large size (5μm and 43μm), which will be discussed in Section 3.3.

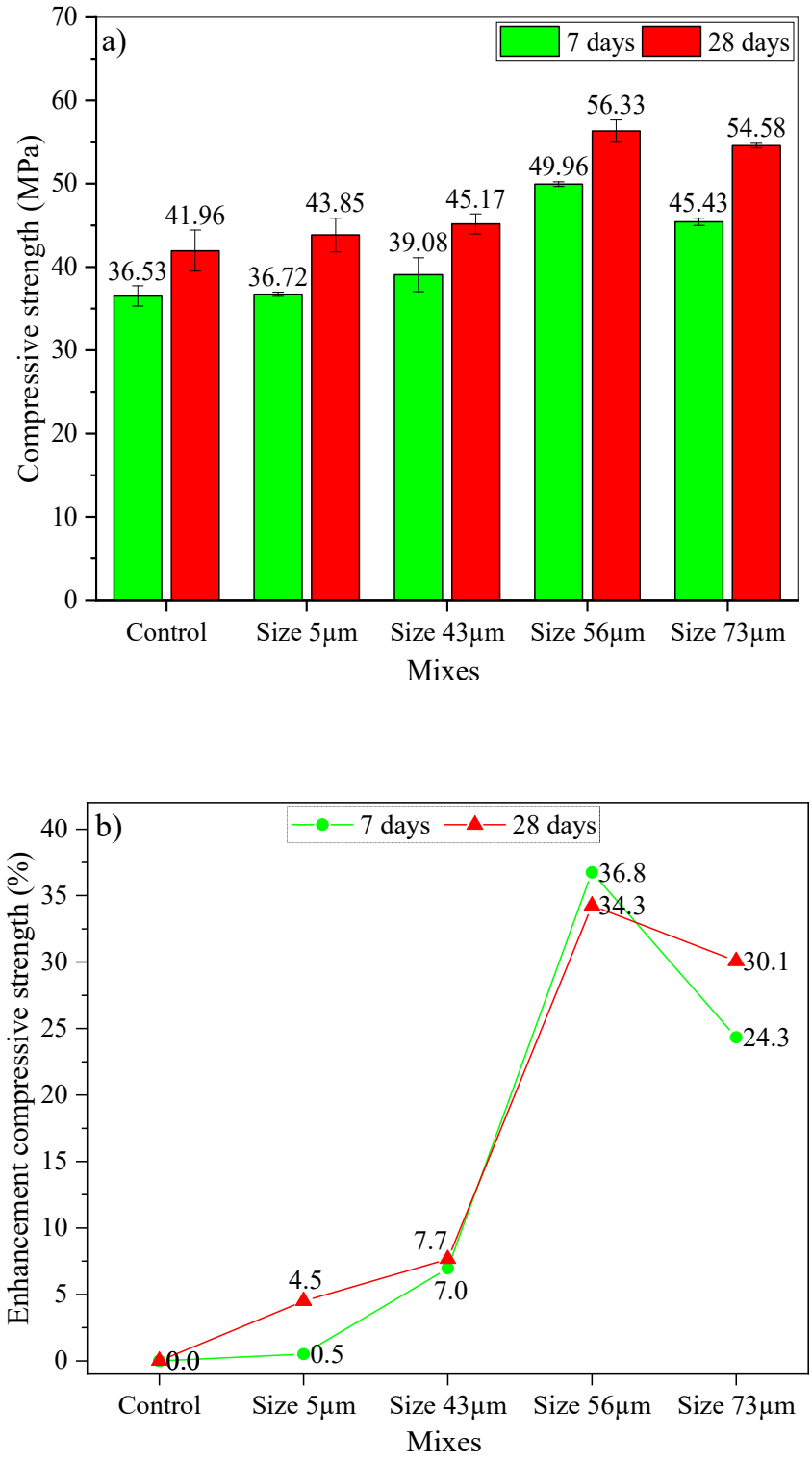

Fig. 3. (a) Compressive strength and (b) enhancement compressive strength at 7 and 28 days of different PRG sizes.

Fig. 4 presents tensile strengths and their enhancement rates at 7 days and 28 days of the mortars with different PRG sizes. Fig. 4(a), (b) shows that tensile strengths of the PRG-cement mortars of different PRG sizes at both testing days increase with the addition of PRG, and their

enhancement strength rates depend on the sizes of PRGs. The size 73µm mix shows the highest values in direct tensile strengths at 7 days (4.14 MPa) and 28 days (5.05 MPa), which enhance approximately 33.5% and 38.6%, respectively, compared to the control mix (3.1 MPa at 7 days and 3.67 MPa at 28 days). The size 43µm and 56µm mixes show similar enhancement rates in tensile strengths of the mortar mixes at 7 and 28 days, which respectively increase approximately 25% and 26.3% for size 43µm, and 25.3% and 26.9% for size 56µm. In contrast, the mix with size 5µm presents the lowest enhancement in tensile strengths at both testing days, which are approximately 10.1% at 7 days and 3.1% at 28 days. In summary, it is evident from the results that the large size (43µm) and ultra-large sizes (56µm and 73µm) shows significant enhancement on tensile strengths of the cement mortars whereas the small size (5µm) presents less enhancement on tensile strengths of cementitious composites, which will be further discussed in Section 3.3.

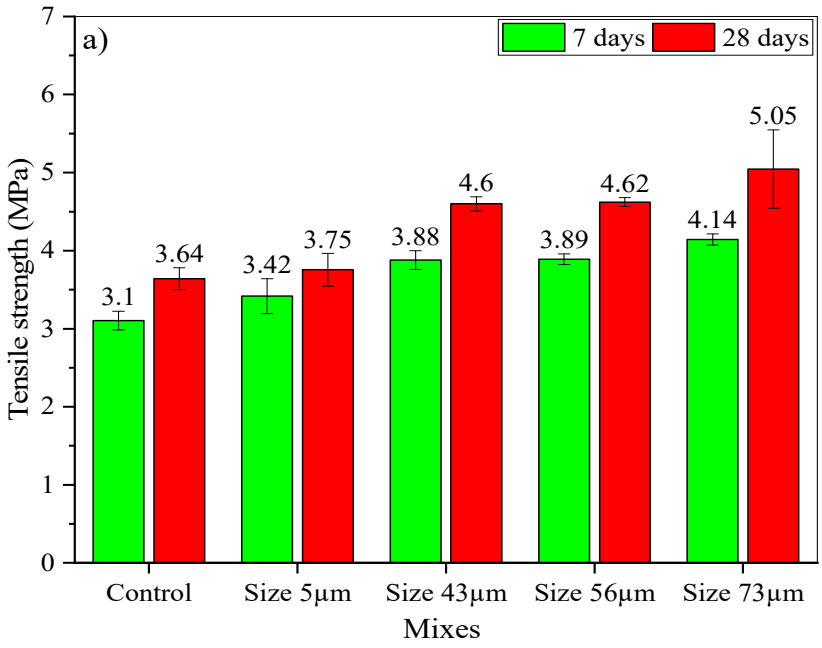

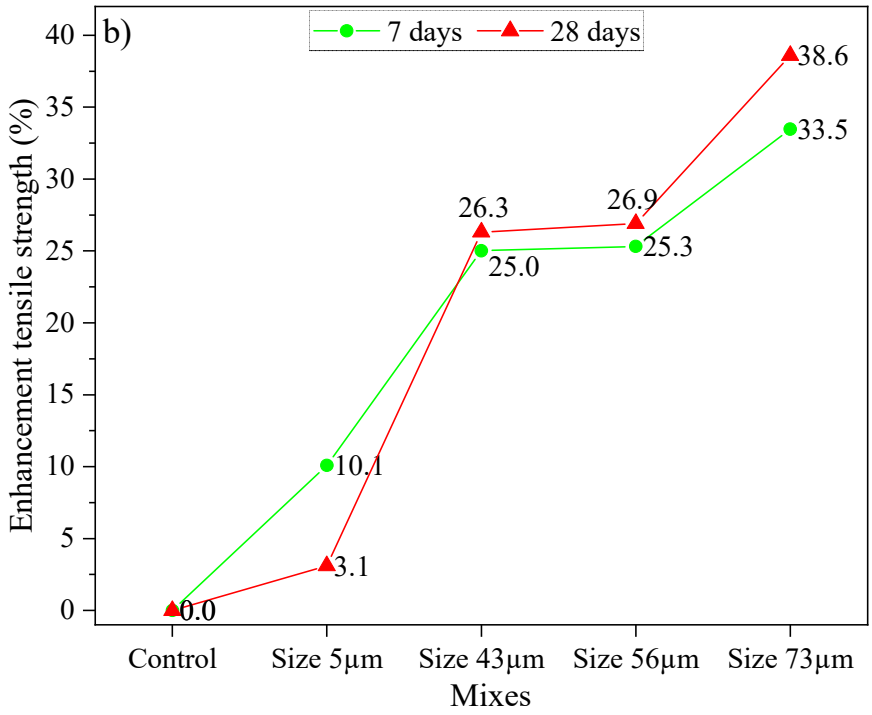

Fig. 4. (a) Tensile strength and (b) enhancement tensile strength at 7 and 28 days of different PRG sizes.

3.3. Physicochemical, microstructural and ANOVA analyses of PRG-cement mortars with different sizes of PRGs

3.3.1 XRD, FTIR and SEM characterizations

The XRD patterns of the mortars with different sizes of PRGs at 28 days are shown in Fig. 5(a). It is important to note that these XRD spectra were standardized to the equal intensity at the major peak of natural sand of 26.7° for making the equal percentage of existing sand in all the samples [32, 42]. Also, only main crystalline phases that relate to the cement hydration process were marked in XRD patterns to avoid a distraction from the analysis (most of the remaining peaks, such as 21.2°, 36.7°, or 77.9°, indicate crystalline phases of quartz [32]). As shown in Fig. 5(a), all the samples have similar spectrum patterns, showing similar main crystalline phases confirmed including cement hydration products (i.e. Portlandite and Ettringite) and un-hydrated cement (i.e. Alite). This means the addition of PRGs into cementitious composites does not create any new crystalline phases in the cement matrix. Moreover, the main cement

hydration product in cementitious composites is calcium silicate hydrate (CSH) gels could not recognize in these spectra because CSH gels often exist at amorphous phases in a cement matrix and it is thus hard to identify with XRD test [29, 43]. However, CSH contents can be inferred from the contents of portlandite and alite phases [32, 42]. It can also be seen from the figure that the portlandite phases in the mixes with size 43µm, 56µm and 73µm show higher intensities than the others. This observation, together with the fewer contents of alite in these mixes (size 43µm, 56µm and 73µm) compared with those in the other mixes (control and size 5µm), can result in higher degrees of the hydration of cement pastes in these mixes than the control and size 5µm mixes [32, 42]. This could account for the better enhancement in compressive and tensile strengths of the large size and ultra-large sizes than the others due to higher CSH gels created, as discussed above in Section 3.2. Moreover, it can also be seen in Fig.5(a) that although the mix with size 5µm has the higher peak intensity of un-hydrated alite phases than the control, it still has a higher peak intensity of portlandite than the control. This could be because the mix with size 5µm had a higher amount of belite hydrated in the cement hydration process than the control (i.e. (alite, belite) + H_2O $\rightarrow$ portlandite + CSH [28, 32]), contributing to a higher peak intensity of portlandite of this mix at the short-term mechanical strengths.

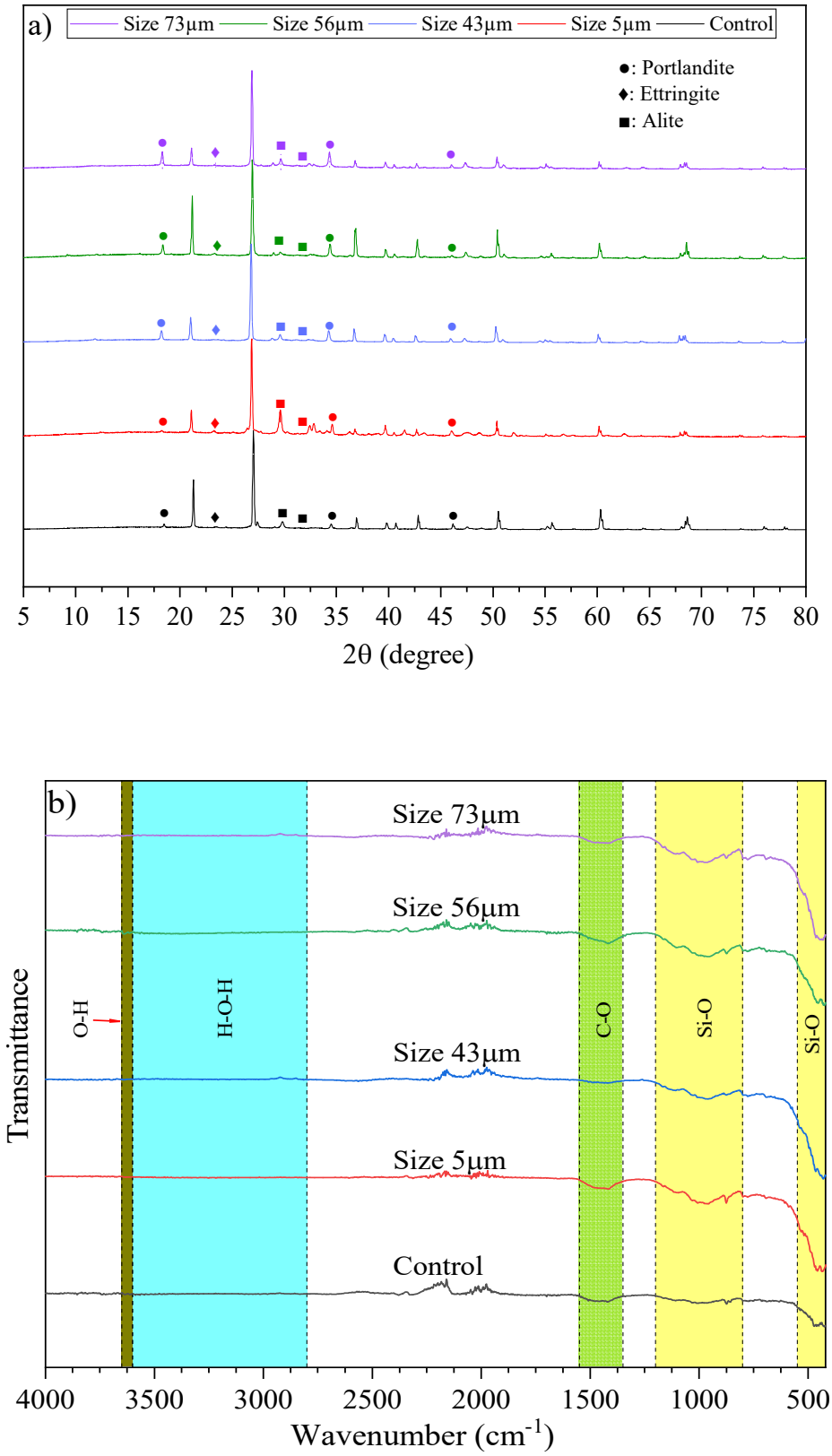

Fig. 5. (a) XRD and (b) FTIR of PRG-cement mortars with different PRG sizes at 28 days.

Fig. 5(b) shows the FTIR patterns of the mixes with different PRG sizes at 28 days. As shown in the figure, all the samples have similar spectra with some functional groups determined in

the range of the band from 400 cm^{-1} to 4000 cm^{-1}, showing that there are no new distinguishing groups observed in all the samples, which are consistent with the results of XRD discussed above and the previous research [44]. From the figure, some functional groups are observed in these samples including Si-O bonds in CSH gels, which are in the ranges of 400-550 cm^{-1} and 800-1200 cm^{-1} [45, 46], and O-H bond in CSH gels and portlandite, which are in the range of 2800-3600 cm^{-1} [46, 47] and 3600-3650 cm^{-1} [45, 48]. C-O bond in $(CO_3)^{2-}$ groups are observed in a range of 1350-1550 cm^{-1} [46, 47], which indicates the appearance of $CaCO_3$ in these samples due to the chemical reaction between cement products and carbon dioxide during the curing and testing period (it can also observed on the surface of cement hydration products in Fig. 6(j) [32, 49, 50]). Although all the spectra show the same functional groups, it is evident from the figure that the intensities of functional groups belonging to CSH gels in the mixes with PRGs are higher than the control. This could be attributed to higher hydration degrees of cement binder in the mortars with PRGs additive, resulting in the improvement in compressive and tensile strengths of these mixes as discussed above in Section 3.2.

SEM images of microstructures of the mortars with different sizes of PRGs at 28 days are shown in Fig. 6. It is evident from the figure that although these samples show similar components in their SEM images, they are different from how these components are distributed and compacted. In particular, the control mix and size 5µm mix not only show less compact in the microstructure, which is large sizes in microcracks and less dense in the interfacial transition zones (ITZ) (Fig. 6(a) and (c)), but also present smaller sizes of crystal components and larger contents of pores distributed in the cement matrix (Fig. 6(b) and (d)) than the others (Fig. 6(e)-(j)). It can also be seen from the figure that the mixes with size 56µm (Fig. 6(g), (h)) and 73µm (Fig. 6(i), (j)) show the most compact in the cement matrix of the mortars, followed by the size 43µm mix (Fig. 6(e), (f)). This is attributed to the higher cement hydration degree and a stronger connection between PRGs and cement gels in the cement matrix of these mixes than the others,

resulting in their stronger enhancement rates in compression and tension [29, 32, 51] as discussed in Section 3.2.

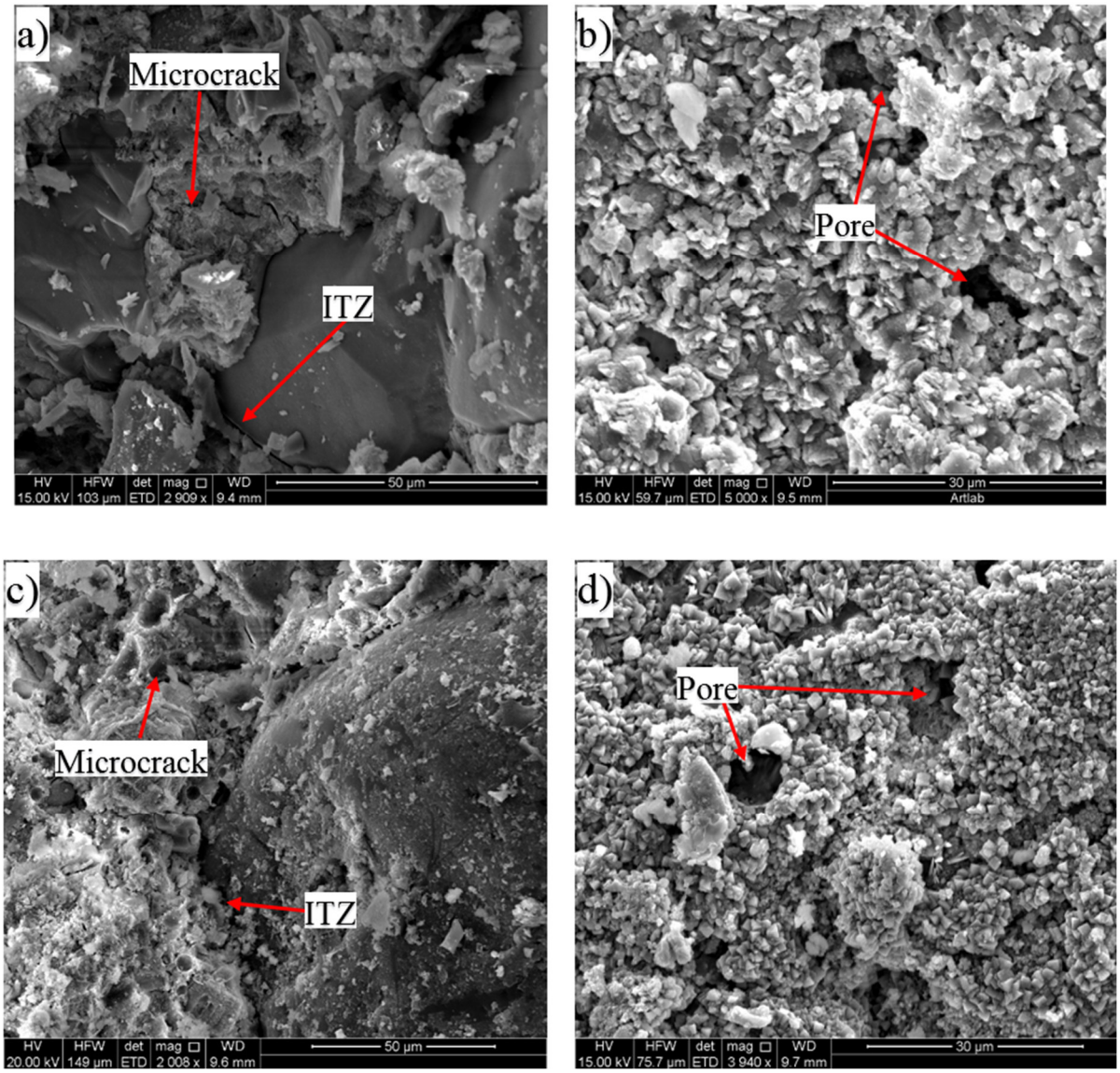

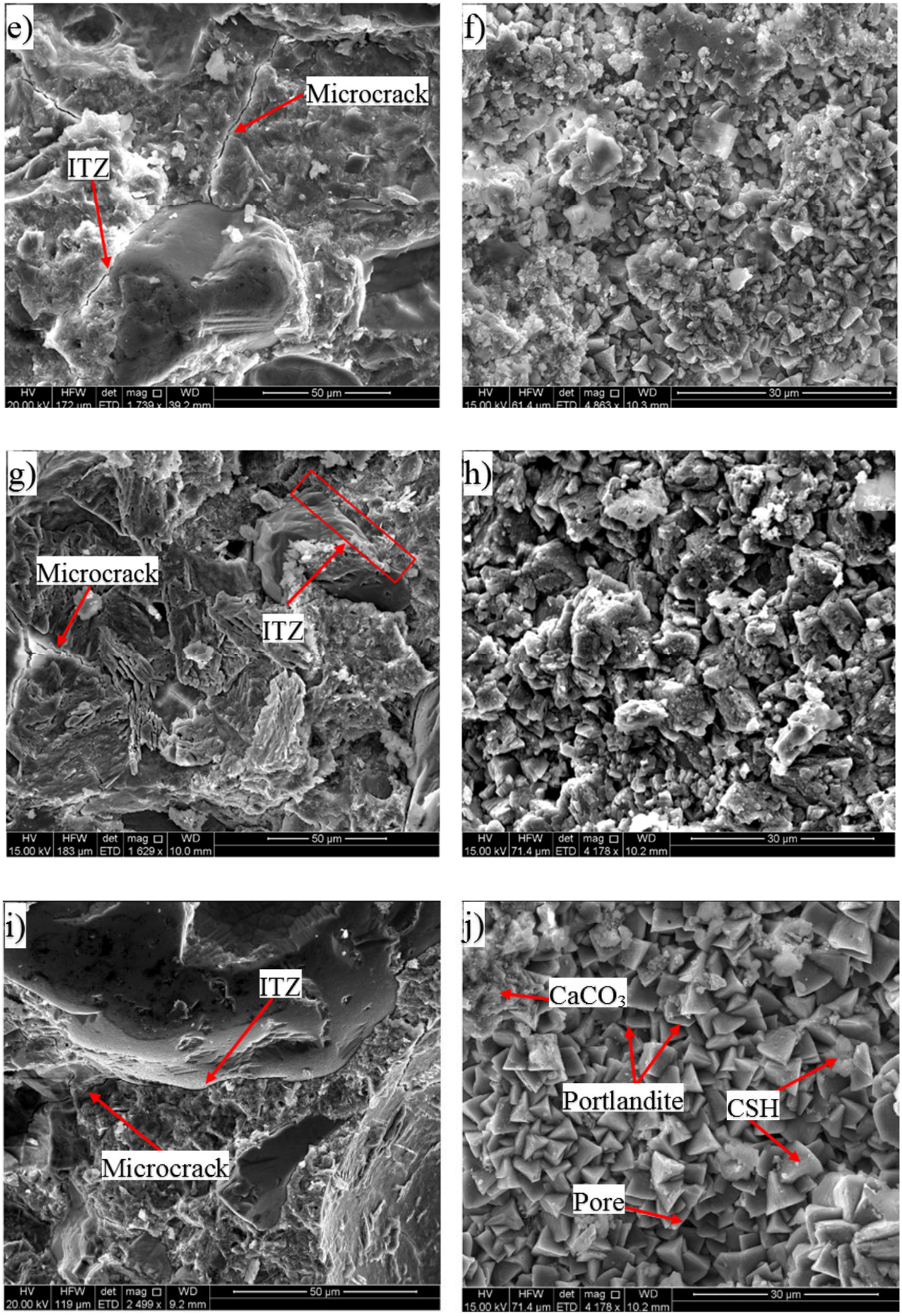

Fig. 6. SEM images of PRG-cement mortars with different PRG sizes at 28 days: (a, b) control, (c, d) size 5µm, (e, f) size 43µm, (g, h) size 56µm, (i, j) size 73µm.

From the above observations and analyses, it can be concluded that physicochemical, microstructural and mechanical properties of cement-based mortars are strongly dependent on the sizes of PRGs additives. The benefits of PRG additives in the cement matrix could come from the combination of the following reasons: (1) a part of the enhancement in the cement hydration process due to the better spreading water of PRGs in a cement matrix, and the reduction of distances between cement particles in cement gels because of the effect of van der Waals forces between PRGs [18, 32, 51]; (2) most of the mechanical adhesion forces created from the friction forces between surfaces of PRGs and cement gels [32], suggesting that PRGs with larger sizes will have stronger friction adhesion forces due to having larger surface areas to connect with cement gels (e.g. 5µm×5µm (25µm^2), 73µm×73µm (5329µm^2)), resulting in their better enhancement rates in mechanical strengths of cement composites as discussed in Section 3.2. This type of friction forces between PRGs and cement gels was also identified by previous research in simulation studies using molecular dynamics simulation methods [52, 53]. Therefore, PRGs can reinforce cement gels in cementitious composites, integrating PRGs into cement gels to create PRG-cementitious gels in the cement matrix, resulting in the improvement of microstructures of the PRG-cement mortars and contributing to a better capacity in stress-distribution and propagation of cracks of these PRG-cement mixes.

3.3.2 ANOVA analysis to evaluate the benefit of different sizes of PRGs on compressive and tensile strengths of cement mortars

The ANOVA analysis by applying the Dunnett method is used to determine whether the enhancement of different sizes of PRGs on compressive and tensile strengths of cement mortars is statistically significant or not. This analysis method is based on the null hypothesis theory with a significant level of 0.05 to assess how significant differences between the mortar mixes, which is detailed in previous studies [54, 55]. The results of the ANOVA analyses for compressive strengths at 7 days and 28 days of the different mixes are shown in Table 4. As can be seen from the table, only the ultra-large sizes mixes (size 56µm and 73µm) are significant

improvements in compressive strengths at both testing days compared to the others (their P-values < 0.05). Moreover, while the size 56µm mix shows the most benefit at the 7 days test because it shows significant difference even with the size 73µm (i.e. P-value=0.009), there is no significant difference between them at 28 days (i.e. P-value=0.186).

Table 4. Assessment of effects of different PRG sizes on compressive strengths of PRG-cement mortars at 7 days and 28 days using ANOVA tests.

Difference of levels	7-day compression			28-day compression		
	Difference of means	T-Value	Adjusted P-Value	Difference of means	T-Value	Adjusted P-Value
Size 5µm - Control	0.19	0.21	0.998	1.89	1.41	0.464
Size 43µm - Control	2.55	2.88	0.051	3.22	2.40	0.111
Size 56µm - Control	13.43	15.21	0.000	14.37	10.72	0.000
Size 73µm - Control	8.90	10.07	0.000	12.62	9.42	0.000
Size 56µm - Size 43µm	10.88	11.05	0.000	11.16	12.96	0.000
Size 73µm - Size 43µm	6.35	6.44	0.002	9.41	10.93	0.000
Size 73µm - Size 56µm	-4.53	-4.6	0.009	-1.75	-2.03	0.186

Table 5 presents the results of the ANOVA tests at 7 days and 28 days for tensile strengths of the different mortars. It is evident from the table that the mixes with size 43µm, 56µm and 73µm show significant benefit in tensile strengths at both testing days compared with the control. In addition, the size 73µm mix presents the strongest effect at the age of 7 days compared to size 43µm (i.e. P-value=0.026) and size 56µm (i.e. P-value=0.03), whereas there are no significant differences between these PRG sizes on tensile strengths at 28-day.

Table 5. Assessment of effects of different PRG sizes on tensile strengths of PRG-cement mortars at 7 days and 28 days using ANOVA tests.

Difference of levels	7-day tension			28-day tension		
	Difference of means	T-Value	Adjusted P-Value	Difference of means	T-Value	Adjusted P-Value
Size 5µm - Control	0.31	2.88	0.051	0.11	0.54	0.949
Size 43µm - Control	0.78	7.15	0.000	0.96	4.62	0.003
Size 56µm - Control	0.79	7.24	0.000	0.98	4.72	0.003
Size 73µm - Control	1.04	9.57	0.000	1.41	6.77	0.000
Size 56µm - Size 43µm	0.01	0.13	0.990	0.02	0.09	0.996
Size 73µm - Size 43µm	0.26	3.62	0.026	0.45	1.86	0.230
Size 73µm - Size 56µm	0.25	3.49	0.030	0.43	1.77	0.256

In summary, it is evident from all the above analyses that compressive and tensile strengths of cement based mortars at 7 days and 28 days strongly depend on the sizes of PRG additives. While the small size (5µm) does not show any significant influence on compressive and tensile strengths of the cement mortars at both testing days, the large size (43µm) only shows a significant influence on tensile strengths at both testing days. In contrast, the ultra-large sizes (56µm and 73µm) show a significant influence on both compression and tension at all the testing days. This confirms the strong benefit of the ultra-large sizes on the mechanical properties of cementitious composites.

3.3.3 Prediction the benefit of PRG additive to reduce the amount of Portland cement used in building materials

As mentioned in the Introduction Section, the use of Portland cement accounts for about 7% of CO_2 emission into the atmosphere globally, causing greenhouse gases. Thus, it is important to find methods to reduce the amount of cement used in building materials without impacting on requirements of their designed strengths. In this case, PRG appears as a promising additive for building materials to reduce the amount of Portland cement used globally. From the previous sections, it can be concluded that the addition of PRGs to cement mortars can enhance their

mechanical strengths. The ultra-large sizes (56µm and 73µm) show the significant improvement in both compressive and tensile strengths at all the testing days.

As discussed in Section 3.2, the size 56µm mix can enhance the 28-day compressive and tensile strengths of the mortar up to 56.33 MPa (↑34.3%) and 4.62 MPa (↑26.9%) compared to the control mix 41.96 MPa and 3.67 MPa, respectively. In practice, we often use the compressive strength at 28 days as the most important parameter to design for new constructions. As shown in Table 3, the mass of Portland cement in 1 m^3 of cement mortars for the current design mixes is 527 kg, and the compressive strength at 28 days of the control mix is 41.96 MPa. Based on compressive strengths of cement pastes and water/cement ratio of mortars, we can predict compressive strengths of cement mortars and one of the precise design-oriented models for predicting was proposed by Kargari et al. [56], which considers different formulas for different cement paste classes. In this study, we used the cement paste with 45 MPa at 28-day compressive strength. According to Kargari et al. [56], the formula used to predict compressive strengths of cement mortars with cement paste class 42.5 MPa is shown below:

$$f'_{c28} = 25.32(1/(W/C)-0.443); \quad (1)$$

where W/C means water and cement ratios. The water and cement ratio we used in this study is 0.485. According to the formula above, the compressive strength of the cement mortar is 40.1 MPa, which is only a 2.31% error compared to the experimental result (41.96 MPa). If we simply assume that the required compressive strength for designing building construction is 56.33 MPa. From Equation (1), the requirement of water and cement ratio for the cement mortar calculated is 0.375. Thus, the mass of Portland cement for the practical design mix with the above water and cement ratio (0.375) is 610 kg. This means if we use 369 gram PRG size 56µm as the additive for 1 m^3 cement mortar with 0.485 water/cement ratio, we can reduce about 83 kg (↓15.75%) Portland cement for the required compressive strength at 0.375 water/cement ratio. As reported in Refs. [8-10], it takes approximately 4 billion tons of cement production in

the world yearly, and thus, PRG additive can support to reduce the mass of cement production down to 3.37 billion tons, which can decrease approximately 1.1% of the CO_2 emission caused by cement production every year. This will be a significant contribution to mitigate greenhouse gases, which accounts for the global warming gases and climate change. However, this contribution should consider that some impact on CO_2 and environmental footprint coming from the graphene manufacturing process. The production of PRG materials used in this paper is industrially manufactured using the electrochemical process by First Graphene Ltd that has several advantages providing significantly lower footprints compared with other PRG materials used chemical oxidation/reduction-based manufacturing processes [57]. Firstly, this process utilizes the world's highest purity vein graphite with a carbon content greater than 98% of total graphitic carbon which is used directly without a further process that excludes extensive graphite processing footprint (gridding, flotation). Secondly, the electrochemically produced process of PRG from this graphite is a single-step process that is a closed-loop, therefore, all electrolytes are recovered and reused. Due to the extremely high carbon content of the graphite used in the system, the kWh per each kilogram of produced PRG materials is extremely low with a very high conversion from graphite to graphene approaching 100% conversion. It is also important to note that although the dispersion of PRG solutions has been improved with the addition of superplasticizers and showed good consistent results, the hydrophobicity of PRG materials can result in the non-uniform distribution of PRG in the cement matrix. Therefore, it is also important to develop better methods by using additional additives or advanced mixing methods to create composites with better uniform distribution.

4. Conclusions

The effects of different sizes of PRGs on physicochemical, microstructural and mechanical properties of cement-based mortars have been presented and evaluated in this study. Based on the results and discussion above, the following conclusions have been drawn:

- The addition of PRGs additive to cement-based mortars enhances their compressive and tensile strengths at 7 days and 28 days. The enhancement accounts for the improvement of compactness of mortars, which is due to the increase in cement hydration degrees, the reduction of distances between cement particles, and the most important part from mechanical adhesion forces between PRGs and cement gels.
- Compressive and tensile strengths of the cement mortars considerably depend on the sizes of PRGs additive. While the small size (5μm) presents no significant effect on both mechanical tests, the large size (43μm) only shows a significant influence on tensile strengths. The ultra-large sizes (56μm and 73μm) have shown the most prominent benefit to compressive and tensile strengths at both testing days.
- The results from XRD, FTIR, and SEM analyses show that compressive and tensile strengths PRG-cement mortars have a close relationship with their physicochemical and microstructure properties. The higher mechanical strengths they are, the better microstructures they have.
- The use of PRGs in cement composites as an additive can support to reduce the mass of cement production, and thus decrease the amount of the CO_2 emission into the atmosphere caused by cement production, contributing to mitigating the global warming gases and climate change yearly.

The results from the study confirm the prominent benefit of the ultra-large sizes on mechanical properties of cementitious composites. This provides the potential to apply ultra-large PRG sizes to cementitious composites as additives to not only enhance both compressive and tensile strengths but also contribute to alleviating the global warming gases. The study also contributes to providing a fast track in studying PRG and cement composites to investigate the influence of PRGs on other properties of cementitious composites, such as permeability, toughness, shrinkage, or corrosion; therefore, the application of this promising additive in practice for building materials could complete soon.

Declaration of Competing Interest

The authors declare that they have no known competing for financial interests or personal relationships that could have appeared to influence the work reported in this paper.

Acknowledgements

This work is supported and funded by the ARC Research Hub for Graphene Enabled Industry Transformation (IH 1500003) and First Graphene Ltd (Perth, Australia). The authors also thank the Schools of Civil, Environmental and Mining Engineering and School of Chemical Engineering at the University of Adelaide for supporting this work. The authors also acknowledge Adam Ryntjes and Dale Hodson as the technical support in the experimental works.

REFERENCES

[1] H.F. Taylor, Cement chemistry, Thomas Telford1997.

[2] D. Chung, Comparison of submicron-diameter carbon filaments and conventional carbon fibers as fillers in composite materials, Carbon 39(8) (2001) 1119-1125.

[3] E.T. Dawood, M. Ramli, High strength characteristics of cement mortar reinforced with hybrid fibres, Construction and Building Materials 25(5) (2011) 2240-2247.

[4] P. Stynoski, P. Mondal, C. Marsh, Effects of silica additives on fracture properties of carbon nanotube and carbon fiber reinforced Portland cement mortar, Cement and Concrete Composites 55 (2015) 232-240.

[5] A. Cwirzen, K. Habermehl-Cwirzen, A. Nasibulin, E. Kaupinen, P. Mudimela, V. Penttala, SEM/AFM studies of cementitious binder modified by MWCNT and nano-sized Fe needles, Materials Characterization 60(7) (2009) 735-740.

[6] B.M. Tyson, R.K. Abu Al-Rub, A. Yazdanbakhsh, Z. Grasley, Carbon nanotubes and carbon nanofibers for enhancing the mechanical properties of nanocomposite cementitious materials, Journal of Materials in Civil Engineering 23(7) (2011) 1028-1035.

[7] M.S. Konsta-Gdoutos, C.A. Aza, Self sensing carbon nanotube (CNT) and nanofiber (CNF) cementitious composites for real time damage assessment in smart structures, Cement and Concrete Composites 53 (2014) 162-169.

[8] K. Rashid, S. Farooq, A. Mahmood, S. Iftikhar, A. Ahmad, Moving towards resource conservation by automated prioritization of concrete mix design, Construction and Building Materials 236 (2020) 117586.

[9] R. Maddalena, J.J. Roberts, A. Hamilton, Can Portland cement be replaced by low-carbon alternative materials? A study on the thermal properties and carbon emissions of innovative cements, Journal of Cleaner Production 186 (2018) 933-942.

[10] M. Schneider, M. Romer, M. Tschudin, H. Bolio, Sustainable cement production—present and future, Cement and concrete research 41(7) (2011) 642-650.

[11] G.L. Golewski, Generalized fracture toughness and compressive strength of sustainable concrete including low calcium fly ash, Materials 10(12) (2017) 1393.

[12] P.K. Mehta, H. Meryman, Tools for reducing carbon emissions due to cement consumption, Structure 1(1) (2009) 11-15.

[13] A. Gholampour, V.D. Ho, T. Ozbakkaloglu, Ambient-cured geopolymer mortars prepared with waste-based sands: Mechanical and durability-related properties and microstructure, Composites Part B: Engineering 160 (2019) 519-534.

[14] P. Van den Heede, N. De Belie, Environmental impact and life cycle assessment (LCA) of traditional and ‘green’concretes: literature review and theoretical calculations, Cement and Concrete Composites 34(4) (2012) 431-442.

[15] B. Lothenbach, K. Scrivener, R. Hooton, Supplementary cementitious materials, Cement and concrete research 41(12) (2011) 1244-1256.

[16] E. Shamsaei, F.B. de Souza, X. Yao, E. Benhelal, A. Akbari, W. Duan, Graphene-based nanosheets for stronger and more durable concrete: A review, Construction and Building Materials 183 (2018) 642-660.

[17] T.H.Y. Nguyen, K. Tsuchiya, D. Atarashi, Microstructure and composition of fly ash and ground granulated blast furnace slag cement pastes in 42-month cured samples, Construction and Building Materials 191 (2018) 114-124.

[18] H. Yang, H. Cui, W. Tang, Z. Li, N. Han, F. Xing, A critical review on research progress of graphene/cement based composites, Composites Part A: Applied Science and Manufacturing 102 (2017) 273-296.

[19] O. Karahan, Transport properties of high volume fly ash or slag concrete exposed to high temperature, Construction and Building Materials 152 (2017) 898-906.

[20] A. Gholampour, T. Ozbakkaloglu, Performance of Sustainable Concretes Containing Very High Volume Class-F Fly Ash and Ground Granulated Blast Furnace Slag, Journal of Cleaner Production (2017).

[21] B. Han, S. Sun, S. Ding, L. Zhang, X. Yu, J. Ou, Review of nanocarbon-engineered multifunctional cementitious composites, Composites Part A: Applied Science and Manufacturing 70 (2015) 69-81.

[22] A.K. Geim, K.S. Novoselov, The rise of graphene, Nature materials 6(3) (2007) 183-191.

[23] X. Li, Y.M. Liu, W.G. Li, C.Y. Li, J.G. Sanjayan, W.H. Duan, Z. Li, Effects of graphene oxide agglomerates on workability, hydration, microstructure and compressive strength of cement paste, Construction and Building Materials 145 (2017) 402-410.

[24] Q. Wang, J. Wang, C.-x. Lu, B.-w. Liu, K. Zhang, C.-z. Li, Influence of graphene oxide additions on the microstructure and mechanical strength of cement, New Carbon Materials 30(4) (2015) 349-356.

[25] S. Lv, J. Liu, T. Sun, Y. Ma, Q. Zhou, Effect of GO nanosheets on shapes of cement hydration crystals and their formation process, Construction and Building Materials 64 (2014) 231-239.

[26] A. Gholampour, M.V. Kiamahalleh, D.N. Tran, T. Ozbakkaloglu, D. Losic, Revealing the dependence of the physiochemical and mechanical properties of cement composites on graphene oxide concentration, RSC Advances 7(87) (2017) 55148-55156.

[27] S. Sharma, N. Kothiyal, Influence of graphene oxide as dispersed phase in cement mortar matrix in defining the crystal patterns of cement hydrates and its effect on mechanical, microstructural and crystallization properties, RSC Advances 5(65) (2015) 52642-52657.

[28] S. Lv, Y. Ma, C. Qiu, T. Sun, J. Liu, Q. Zhou, Effect of graphene oxide nanosheets of microstructure and mechanical properties of cement composites, Construction and building materials 49 (2013) 121-127.

[29] B. Wang, R. Jiang, Z. Wu, Investigation of the mechanical properties and microstructure of graphene nanoplatelet-cement composite, Nanomaterials 6(11) (2016) 200.

[30] H. Du, S. Dai Pang, Enhancement of barrier properties of cement mortar with graphene nanoplatelet, Cement and Concrete Research 76 (2015) 10-19.

[31] J. Tao, X. Wang, Z. Wang, Q. Zeng, Graphene nanoplatelets as an effective additive to tune the microstructures and piezoresistive properties of cement-based composites, Construction and Building Materials 209 (2019) 665-678.

[32] V.D. Ho, C.-T. Ng, C.J. Coghlan, A. Goodwin, C. Mc Guckin, T. Ozbakkaloglu, D. Losic, Electrochemically produced graphene with ultra large particles enhances mechanical properties of Portland cement mortar, Construction and Building Materials 234 (2020) 117403.

[33] S. Chuah, Z. Pan, J.G. Sanjayan, C.M. Wang, W.H. Duan, Nano reinforced cement and concrete composites and new perspective from graphene oxide, Construction and Building Materials 73 (2014) 113-124.

[34] Y. Zhu, S. Murali, W. Cai, X. Li, J.W. Suk, J.R. Potts, R.S. Ruoff, Graphene and graphene oxide: synthesis, properties, and applications, Advanced materials 22(35) (2010) 3906-3924.

[35] AS3972, General purpose and blended cements, Standard, Standard Australia, Australian Standard, 2010.

[36] AS1478.1, Chemical admixtures for concrete, mortar and grout - Admixtures for concrete, Australian Standard, 2000.

[37] ASTM-C109/C109M-07, Standard test method for compressive strength of hydraulic

cement mortars, ASTM International: USA 2008, 2008.

[38] ASTM-C307-03, Standard Test Method for Tensile Strength of Chemical-Resistant Mortar, Grouts, and Monolithic Surfacings Monolithic Surfacings, ASTM International, 2012.

[39] T.T. Mai, C.N. Ha Thuc, H.H. Thuc, Preparation of graphene nano-layer by chemical graphitization of graphite oxide from exfoliation and preliminary reduction, Fullerenes, Nanotubes and Carbon Nanostructures 23(8) (2015) 742-749.

[40] A. Eckmann, A. Felten, A. Mishchenko, L. Britnell, R. Krupke, K.S. Novoselov, C. Casiraghi, Probing the nature of defects in graphene by Raman spectroscopy, Nano letters 12(8) (2012) 3925-3930.

[41] Y. Shen, A.C. Lua, A facile method for the large-scale continuous synthesis of graphene sheets using a novel catalyst, Scientific reports 3(1) (2013) 1-6.

[42] S. Sharma, N. Kothiyal, Comparative effects of pristine and ball-milled graphene oxide on physico-chemical characteristics of cement mortar nanocomposites, Construction and Building Materials 115 (2016) 256-268.

[43] R. Jadhav, N. Debnath, Computation of X-ray powder diffractograms of cement components and its application to phase analysis and hydration performance of OPC cement, Bulletin of Materials Science 34(5) (2011) 1137-1150.

[44] J. Wang, J. Tao, L. Li, C. Zhou, Q. Zeng, Thinner fillers, coarser pores? A comparative study of the pore structure alterations of cement composites by graphene oxides and graphene nanoplatelets, Composites Part A: Applied Science and Manufacturing 130 (2020) 105750.

[45] M. Horgnies, J. Chen, C. Bouillon, Overview about the use of Fourier transform infrared spectroscopy to study cementitious materials, WIT Trans. Eng. Sci 77 (2013) 251-262.

[46] P. Yu, R.J. Kirkpatrick, B. Poe, P.F. McMillan, X. Cong, Structure of calcium silicate hydrate (C-S-H): Near-, mid-, and far-infrared spectroscopy, Journal of the American Ceramic Society 82(3) (1999) 742-748.

[47] L. Fernández Carrasco, D. Torrens Martín, L. Morales, S. Martínez Ramírez, Infrared spectroscopy in the analysis of building and construction materials, InTech2012.

[48] S. Ghosh, S. Handoo, Infrared and Raman spectral studies in cement and concrete, Cement and Concrete Research 10(6) (1980) 771-782.

[49] J. Jiang, Q. Zheng, D. Hou, Y. Yan, H. Chen, W. She, S. Wu, D. Guo, W. Sun, Calcite crystallization in the cement system: morphological diversity, growth mechanism and shape evolution, Physical Chemistry Chemical Physics 20(20) (2018) 14174-14181.

[50] S. Lv, H. Hu, J. Zhang, X. Luo, Y. Lei, L. Sun, Fabrication of GO/cement composites by incorporation of few-layered GO nanosheets and characterization of their crystal/chemical structure and properties, Nanomaterials 7(12) (2017) 457.

[51] Z. Pan, L. He, L. Qiu, A.H. Korayem, G. Li, J.W. Zhu, F. Collins, D. Li, W.H. Duan, M.C. Wang, Mechanical properties and microstructure of a graphene oxide–cement composite, Cement and Concrete Composites 58 (2015) 140-147.

[52] S.J. Chen, C.Y. Li, Q. Wang, W.H. Duan, Reinforcing mechanism of graphene at atomic level: Friction, crack surface adhesion and 2D geometry, Carbon 114 (2017) 557-565.

[53] D. Hou, Z. Lu, X. Li, H. Ma, Z. Li, Reactive molecular dynamics and experimental study of graphene-cement composites: Structure, dynamics and reinforcement mechanisms, Carbon 115 (2017) 188-208.

[54] V. Bewick, L. Cheek, J. Ball, Statistics review 9: one-way analysis of variance, Critical care 8(2) (2004) 130.

[55] C.W. Dunnett, A multiple comparison procedure for comparing several treatments with a control, Journal of the American Statistical Association 50(272) (1955) 1096-1121.

[56] A. Kargari, H. Eskandari-Naddaf, R. Kazemi, Effect of cement strength class on the generalization of Abrams' law, Structural Concrete 20(1) (2019) 493-505.

[57] R. Arvidsson, D. Kushnir, B.r.A. Sandén, S. Molander, Prospective life cycle assessment of graphene production by ultrasonication and chemical reduction, Environmental science & technology 48(8) (2014) 4529-4536.

CHAPTER 4:

INVESTIGATING THE REINFORCING MECHANISM AND OPTIMIZED DOSAGE OF PRISTINE GRAPHENE FOR ENHANCING MECHANICAL STRENGTHS OF CEMENTITIOUS COMPOSITES

THE AIM AND OBJECTIVE OF THIS CHAPTER:

Aim: This chapter aims to investigate the influence of physical properties of PRG on the reinforcing mechanism and optimized dosage for enhancing mechanical properties of cement-based mortars.

Objectives 1: studying the main factors that influence the interaction between PRG and cementitious gels and evaluate the optimal dosage range of PRG in for PRG-cement mortars.

Objectives 2: analysing physicochemical, microstructural and mechanical properties of PRG-cement mortars to confirm the main influence factor; and revealing the proposed reinforcing mechanism and optimized dosage of PRG for enhancing mechanical properties of PRG-cement based mortars.

Statement of Authorship

Title of Paper	Investigating the reinforcing mechanism and optimized dosage of pristine graphene for enhancing mechanical strengths of cementitious composites
Publication Status	☐ Published ☐ Accepted for Publication ☐ Submitted for Publication ☑ Unpublished and Unsubmitted work written in manuscript style
Publication Details	Ho, V. D., Ng, C. T., Ozbakkaloglu, T., Karunagaran, R. U., Farivar, F., Goodwin, A., Mc Guckin, C., Ho, V. D., & Losic, D. Investigating the reinforcing mechanism and optimized dosage of pristine graphene for enhancing mechanical strengths of cementitious composites.

Principal Author

Name of Principal Author (Candidate)	Van Dac Ho		
Contribution to the Paper	Literature review, preparing and doing experiments, assessment and analysis of test results, and preparation of the manuscript.		
Overall percentage (%)	85		
Certification:	This paper reports on original research I conducted during the period of my Higher Degree by Research candidature and is not subject to any obligations or contractual agreements with a third party that would constrain its inclusion in this thesis. I am the primary author of this paper.		
Signature		Date	18/05/2020

Co-Author Contributions

By signing the Statement of Authorship, each author certifies that:

i. the candidate's stated contribution to the publication is accurate (as detailed above);

ii. permission is granted for the candidate in include the publication in the thesis; and

iii. the sum of all co-author contributions is equal to 100% less the candidate's stated contribution.

Name of Co-Author	Dusan Losic		
Contribution to the Paper	Research supervision, review and revisions of the manuscript.		
Signature		Date	25/05/2020

Name of Co-Author	Ching-Tai Ng		
Contribution to the Paper	Research supervision, review and revisions of the manuscript.		
Signature		Date	10/05/2020

Name of Co-Author	Togay Ozbakkaloglu		
Contribution to the Paper	Review of the manuscript.		
Signature		Date	04/04/2020

Name of Co-Author	Ramesh U. Karunagaran		
Contribution to the Paper	Review of the manuscript.		
Signature		Date	20/03/2020

Name of Co-Author	Van Duong Ho		
Contribution to the Paper	Aid in developing Section 3.		
Signature		Date	15/03/2020

Name of Co-Author	Andy Goodwin		
Contribution to the Paper	Review of the manuscript.		
Signature		Date	22/03/2020

Name of Co-Author	Craig Mc Guckin		
Contribution to the Paper	Review of the manuscript.		
Signature		Date	23/03/2020

Name of Co-Author	Farzan Farivar		
Contribution to the Paper	Aid in Raman tests.		
Signature		Date	13/04/2020

Journal paper 3 (In preparation)

Investigating the reinforcing mechanism and optimized dosage of pristine graphene for enhancing mechanical strengths of cementitious composites

Van Dac Ho[1,2,3], Ching-Tai Ng[1]*, Togay Ozbakkaloglu[4], Ramesh U. Karunagaran[2.3], Farzaneh Farivar[2.3], Andy Goodwin[5], Craig Mc Guckin[5], Van Duong Ho[6], Dusan Losic*[2,3]

[1]School of Civil, Environmental and Mining Engineering, The University of Adelaide, South Australia, 5005, Australia

[2]School of Chemical Engineering, The University of Adelaide, South Australia, 5005 Australia

[3]ARC Research Hub for Graphene Enabled Industry Transformation, The University of Adelaide, South Australia, 5005 Australia

[4] Ingram School of Engineering, Texas State University, United States

[5] First Graphene Ltd, Suite 3, 9 Hampden Road, Nedlands WA 6009, Australia

[6] University of Architecture Ho Chi Minh City

*Corresponding authors:

alex.ng@adelaide.edu.au (Ching-Tai Ng)

dusan.losic@adelaide.edu.au (Dusan Losic)

ABSTRACT

The proposed reinforcing mechanism and optimized dosage of pristine graphene (PRG) for enhancing mechanical, physicochemical and microstructural properties of cementitious mortar composites are presented. Five concentrations of PRG and two particle sizes are explored in this study. The results confirmed that the strength of the mortars depends on the dosage of PRG. The PRG sizes have a significant influence on the enhancement rate of mechanical strengths of the mortars, whereas they do not have a significant influence on the optimized PRG dosage for mechanical strengths. The PRG dosage of 0.07% is identified as the optimized content of PRG for enhancing mechanical strengths. The reinforcing mechanism of PRG for cement-based composites is mostly attributed to adhesion friction forces between PRG sheets and cementitious gels, which highly depends on the surface area of PRG sheets. The larger surface area of PRG sheets has a larger friction area associated with cementitious gels.

Keywords: Pristine graphene; Cement mortars; Mechanical properties; Reinforcing mechanism; Microstructure.

1. Introduction

Cementitious composites are the most common construction materials because of their low cost, availability, and high strength in compression. Nevertheless, cementitious composites are weak in tensile strength, and poor in resisting crack propagation and corrosive environment, e.g. sulfate ion, chloride ion [1, 2]. To improve these drawbacks, studies showed benefits of using reinforcement such as steel, carbon or plastic fibers [3, 4] to impede the propagation of microcracks, or additives with nanomaterials such as SiO_2 and TiO_2 [5, 6], carbon nanofibers and carbon nanotubes [7-9] to accelerate the cement hydration process and create materials with denser microstructures [10-13]. However, these supplementary materials are zero or one-dimensional materials with limited performance in bonding and arresting cracks at the nanoscale, and unable to efficiently enhance the reinforcement [7-9, 14].

Recently studies have shown that two-dimensional materials such as graphene derivatives have a good potential for enhancing performances of cement composites due to their outstanding properties, e.g. high mechanical properties, high conductivity, and large aspect ratios [15, 16]. The applications of different forms of graphene materials with different properties (e.g. graphene oxide (GO), reduced graphene oxide (rGO), and pristine graphene (PRG)) in cementitious composites have been explored in the literature [17-19]. GO was the most attractive graphene material due to its favorable functional groups on the surface (i.e. hydroxyl, epoxide, carboxyl, and carbonyl), which provides higher reactivity with cement and high dispersion in water. Many studies reported that the addition of GO into cement composites could significantly improve their mechanical properties [17-19]. Kang et al. [20] reported that incorporating GO into cement-based mortars improved 28-day compressive and flexural strength by approximately 32% (at 0.05% GO) and 20% (at 0.1% GO). Zhao et al. [21] showed that incorporating 0.022% GO into cement mortars produced a 34.1% and 30.4% improvement in 28-day compressive and flexural strength, respectively. The effects of different GO dosages

and sizes on microstructures of cement-based mortars were also reported in the literature [22, 23]. Lv et al. [23] showed that as the size of GO decreased from 430nm to 72nm, the enhancement rates of 28-day compressive and flexural strengths could be increased from 29.5% and 30.7% to 38.2% and 51.9%, respectively.

The reinforcing mechanism of GO on mechanical properties of cementitious composites is attributed to the considerable effect of oxygen-functional groups (i.e. carboxyl, hydroxyl) of GO on the cement matrix. This shows that smaller sizes of GO will have more oxygen-functional groups than larger sizes of GO, which leads to stronger adhesion forces between the functional groups and cementitious gels. Based on GO research, several studies reported the reinforcing mechanism of mechanical strengths of GO-cement based composites which were mainly governed by chemical reactions between hydroxyl and carboxyl groups of GO and the mediating Ca^{2+} ions from calcium silicate hydrate of cementitious gels. This results in a space network structure in the cement matrix that supports the load transfer efficiency in cementitious composites [14, 24]. Compared with GO, PRG is a remarkably different graphene material with a very limited level of oxygen groups, higher crystallinity, lower defects, and significantly stronger mechanical properties [25, 26]. Therefore, it has attracted significant research interests in using the PRG in cementitious composites [17, 18, 27-30]. The limitation in water dispersion of PRG sheets (PRGs) has been addressed in recent studies by using superplasticizer and ultrasonication methods [27, 30, 31]. It has been shown that a small amount of PRG has great potential to enhance the strength of PRG-cement composites [27-30, 32]. Wang et al. [30] reported that 0.05% of PRG could enhance 7 & 28-day flexural compressive strengths of cement-based mortars by 23.5% & 16.8% and 7.5% & 1.3%, respectively. Besides, the influence of different dosages of PRG on mechanical strengths of cement-based mortars has been reported in recent studies [27, 28, 32]. Baomin and Shuang [32] investigated the use of four different dosages of PRG in cement paste and reported that the optimal PRG dosage of 0.06% could increase compressive and flexural strength of the cement paste at 28 days by 11%

and 27.8%, respectively. Tao et al. [28] studied a combination of cement-based mortars and five dosages of PRG. The results showed that the mortar with PRG of 0.05% could enhance 28-day compressive strength about 8.3% and 28-day flexural strength about 15.6%. However, when the dosages of PRG over 0.05%, the strengths started reducing because of the agglomerations of PRGs. In our previous work, we performed a comprehensive investigation of the dosage dependence of PRG-cement based mortars using seven dosages of pristine graphene [27]. The study showed that at the optimal dosage of 0.07% PRG, compressive and tensile strengths at 7 & 28 days of the mortar mix containing PRG could significantly enhance by 36.8% & 34.3% and 25.3% & 26.9%, respectively.

These studies only showed the influence of the dosages of pristine graphene on the properties of cementitious composites. The reinforcing mechanism of pristine graphene on mechanical strengths of cement mortars has not been well understood. In addition to the dosage of PRG, there are several parameters of PRGs, such as particle sizes, number of layers, and level of defects, can affect the performance of PRG-cement based composites. As reported in Refs. [33-35], these parameters have a significant influence on mechanical properties of polymer composites. However, there were very limited studies on the effects of these parameters on mechanical strengths of PRG and cementitious composites. To date, only few studies have applied molecular dynamics simulation methods to investigate the interaction between PRGs and cementitious gels at the atomic level [36, 37]. The outcomes of these studies showed that the pull-out behavior of PRG in cementitious gels was governed by interfacial interaction and crack surface adhesion forces of PRG-cementitious gels. Although these studies provided the initial knowledge of the incorporation of pristine graphene into cementitious gels, there is still a lack of experimental confirmation on the reinforcing mechanism of PRGs in cementitious composites.

On the other hand, studies on GO-cement showed a wide range of optimum dosages of GO (i.e. from 0.01% to 1%) for improving the strengths of the composites [17-19], which is one of the bottlenecks in practical applications. The dosage dependence of mechanical properties of cementitious composites prepared with pristine graphene on the dosages of PRG showed a much better convergence in the optimal PRG dosage range (i.e. from 0.05% to 0.07%) even though they differed from mix designs and PRG materials used [27, 28, 32]. These studies showed great potential for applying a small amount of PRG additives in construction materials to improve their mechanical strengths and other properties. However, very limited studies have been done to explore the consistency of these optimum PRG dosages used in cement composites which can support future studies on designing tests for investigating other properties of cement-based materials by graphene additives. Moreover, PRG materials have better crystalline structures with low levels of defects and mechanical properties than GO. They are now produced at industrial scales with high quality and lower costs. Therefore, it is expected that industrially produced PRG materials will be more acceptable additives for improving the properties of construction materials

This study aims at providing an in-depth investigation of the aforementioned issues with a focus on revealing the reinforcing mechanism and optimized dosage of industrially manufactured PRG materials for enhancing the strengths of cement based mortars. The impact of the dosage of pristine graphene with two different particle sizes on mechanical and microstructural properties of cementitious mortar composites are explored, compared, and presented in this research. From the findings and comprehensive analyses of this study, we provide new inputs toward a better knowledge in the proposed reinforcing mechanism and optimized dosage of pristine graphene on the strength of cementitious mortars. This paper not only provides a better knowledge of incorporating PRG into cementitious composites, but they also show the great potential for low-cost industrially produced PRG materials for addressing current drawbacks of cementitious materials.

2. Experimental Methods

2.1. Materials

PRG materials manufactured by First Graphene Ltd in Perth, Australia, were used in this study (Table 1). It is important to note that these PRG materials were produced by an electrochemical process, which is a unique manufacturing process using electrochemistry to exfoliate PRGs with a few layers, large particle sizes and low defects from graphite that are not achievable by other methods (e.g. thermal or chemical methods from rGO). The binder was ordinary Portland Cement (OPC) with general purpose and the chemical composition (Table 2) complied with the Australian Standard AS 3972-2010 [38]. Natural sand was used as the fine-aggregate for all mortar mixes, which had a 2.36-mm maximum particle size. Table 3 presents the properties of the superplasticizer, named MasterGlenium SKY 8100, which was complied with the Australian Standard AS 1478.1-2000 [39].

Table 1. Physical properties of PRGs used in this study.

ID	Average particle size (μm)	Thickness (nm)	Purity (%)	Poured bulk density (g/cm3)
S1	56 ± 12	1-3	98.3	~ 0.12
S2	23 ± 10	1-3	98.3	~ 0.11

Table 2. Chemical properties of Portland cement.

Compounds	OPC (%)
CaO	63.28
SiO_2	19.95
Al_2O_3	4.79
Fe_2O_3	3.14
MgO	2.03
Na_2O	0.29
K_2O	0.4
SO_3	2.69
P_2O_5	0.04

Table 3. Properties of superplasticizer.

pH	Boiling temperature (°C)	Density at 20 °C (kg/dm^3)	Flash point (°C)	Vapour pressure at 20 °C (hPa)	Solid content (mass, %)
6.4	≥ 100	1.06	> 100	23	30.7

2.2. Preparation of the mortar composites

The design mixes are given in Table 4. As shown in the table, a total of 9 unique mortar mixes were performed, including five different concentrations and two different sizes of PRG, i.e. 0 %, 0.05%, 0.07%, 0.1% and 0.3% mixes and average PRG diameters of 56µm (S1) and 23µm (S2). Table 4 shows the labels used for the mixes. S1 and S2 refer to PRG with an average size of 56µm and 23µm, respectively. The number after that indicates the PRG dosage in each mix, which is calculated by the weight of the binder. For example, S1-0.05 indicates the PRG-cement based mortar prepared with a PRG size 56µm and a PRG content of 0.05%.

The procedures described below were applied to prepare PRG-cement based mortars. The aqueous solution was first prepared, and it consisted of water, superplasticizer and pristine graphene. Sonication was then carried out using Ultrasonication UIP1000hdT for 30 minutes. After that, the sonicated aqueous solution was gradually added into dry mixings, which included OPC and natural sand mixed within four minutes, for five minutes. A vibration table was used to vibrate these specimens for one minute to remove the entrapped air, then covered by wet fabrics to contain the moisture loss, and demolded after 24 hours of curing at room temperature. After that, they were cured in a fog room with a temperature of 23 ± 2 °C until the testing ages.

Table 4. The design mixes of the mortars.

Mix	PRG* (%)	PRG size (µm)	Water/cement ratio	Cement (kg/m^3)	Water (kg/m^3)	PRG (kg/m3)	Sand (kg/m3)	Superplasticizer (kg/m3)
Plain	-	-	0.485	527	255.6	0.0	1448	1.4
S1-0.05	0.05	56	0.485	527	255.6	0.3	1448	1.4
S1-0.07	0.07	56	0.485	527	255.6	0.4	1448	1.4
S1-0.1	0.1	56	0.485	527	255.6	0.5	1448	1.4
S1-0.3	0.3	56	0.485	527	255.6	1.6	1448	1.4
S2-0.05	0.05	23	0.485	527	255.6	0.3	1448	1.4
S2-0.07	0.07	23	0.485	527	255.6	0.4	1448	1.4
S2-0.1	0.1	23	0.485	527	255.6	0.5	1448	1.4
S2-0.3	0.3	23	0.485	527	255.6	1.6	1448	1.4

* The percentage of PRG based on cement weight.

2.3. Test methods

Mechanical strengths (compression and tension) of cementitious composites were determined at 7 and 28 days according to ASTM standards C109/C109M-07 [40] and C307-03 [41], respectively. These tests were performed to study the effects of dosage and size of PRG on the mechanical properties of cementitious mortar composites. The mechanical strengths of each design mix were determined by calculating the average values of three samples. The analysis

of variance method was also used to assess the statistically significant difference in mechanical strengths of the mortars containing PRG in the optimum dosage range.

Scanning electron microscopy (SEM) and energy-dispersive X-ray spectroscopy (EDX) were obtained by using FEI Quanta 450 to analyze surface morphologies and elemental compositions of materials. The particle size distribution was performed by using the Mastersizer 2000-Malvern to analyze the particle size of PRGs used in this study. The Rigaku MiniFlex 600 X-Ray diffractometer was used for X-ray diffraction (XRD) analyses to find the mineralogical characteristics of hydration products of cementitious composites and the distances between layers in pristine graphene sheets. The XRD was carried out at conditions 40 kV and 15 mA, $2\theta = 5°–80°$ at 0.02° step size. Thermogravimetric analysis (TGA) of PRG samples was conducted with Mettler Toledo TGA/DSC 2 (the heating rate at 10°C/min under air atmosphere with a flow rate of 60 ml/min). Raman spectroscopy (LabRAM HR Evolution, Horiba Jvon Yvon Technology, Japan) with a 532 nm laser (mpc3000) as the excitation source in the range of 500-3500 cm^{-1} was utilized to study the vibrational characteristics of carbon materials. All spectra were collected at an integration time of 10s for 3 accumulations using a 100× objective lens with a spot size of 100µm. Raman map was performed for a 20µm×20µm area with 2µm steps and Raman spectrum of overall 121 points were collected for each sample. Nicolet 6700 was used for Fourier transform infrared spectroscopy (FTIR) analyses to identify functional groups of materials.

3. Results and Discussion

3.1. Characteristics of pristine graphene sheets

The physical properties and morphology of industrially manufactured PRG with two different graphene sheets particle sizes used in the study are characterized and summarized in Table 1 and Fig. 1, respectively. The irregular shapes of PRGs were observed in SEM images as shown in Fig. 1. These SEM images and particle size distributions shown in Fig. 1(a) and (b) present

a considerable difference in the particle size of 56µm (S1) and 23µm (S2), respectively. Table 1 also shows that the physical properties of these two PRGs are similar and only different in particle sizes.

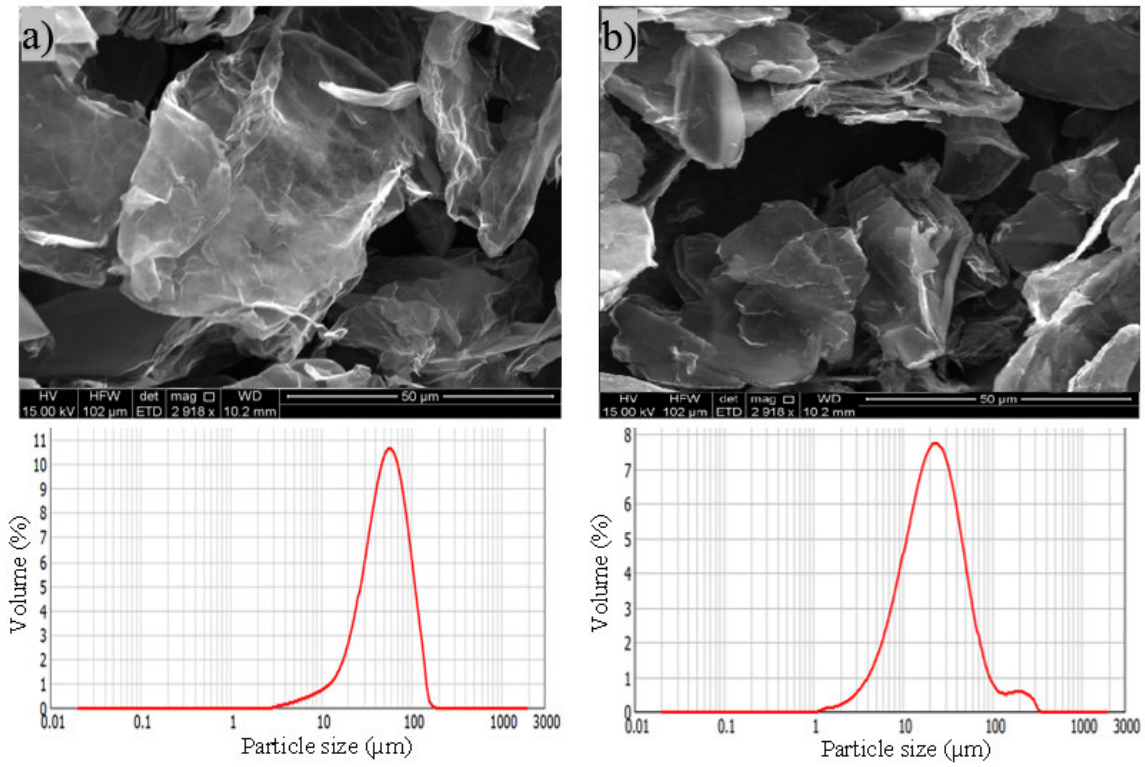

Fig. 1. SEM images and particle size distribution of PRG: (a) size 56µm (S1), (b) size 23µm (S2).

Fig. 2(a)-(c) presents the Raman spectra and Raman I_D/I_G map of both PRG samples. The Raman peak at the 2D band can be used to indicate the number of layers in the graphene samples based on the frequency shift and the shape of the 2D peak. It can be seen in Fig. 2(a) that a narrow and symmetric 2D band at 2709 cm^{-1} is observed in these PRG samples which are different from graphite materials that have a broad and asymmetric 2D peak located at 2719 cm^{-1}. Besides, their relative intensity ratios I_D/I_D, and I_{2D}/I_G shown in Fig. 2(a) are respectively 1.58 & 1.59 and 0.39 & 0.32, which are below 3.5 and 1. Moreover, the distribution histogram plots of relative intensity ratios I_D/I_G of both PRG sizes obtained from the mapping study are mostly below 0.4-0.6 (Fig. 2(b), (c)). These combined results confirm that both PRG samples

are high-quality products with low defects, and they mostly consist of few-layer sheets of graphene [42-45], which are critical for their optimized performance in cement-based composites.

Fig. 2(d) presents XRD graphs showing typical peaks for both PRG samples at position 2θ = 26.64°. Based on the Bragg's Law, the d-spacing between layers of both PRGs was 0.334 nm, the same as the properties of graphite materials [46, 47]. This shows that the high crystalline structure and quality of pristine graphene materials in this investigation. FTIR spectra in Fig. 2(e) show the major characteristic bands for both PRG sizes at: 1000 cm^{-1} to 1240 cm^{-1} is attributed to C-O groups; 1700 cm^{-1}, and from 2500 cm^{-1} to 3300 cm^{-1} are referred to C=O stretching and O-H stretching. These functional groups present the existence of carboxylic acids (i.e. COOH) in both PRGs, which are likely in limited numbers at the edge of PRG structure. The stretching vibration from 1300 cm^{-1} to 1600 cm^{-1} corresponds to C=C groups. These are consistent with FTIR results on pristine graphene materials in the literature, which shows minor oxygen groups at edges of their structures [48, 49]. Fig. 2(f) shows a typical TGA-DTG graph of PRG samples. The figure shows the maximum thermal decomposition peak of both PRG samples is about 700^0C which is different from GO, rGO [48, 50, 51], presenting the high quality of PRG materials used in this study.

It is important to note that, in this study, two industrially produced PRG samples with the same manufacturing process were used, which are high-quality products, have similar physicochemical properties, and their main difference is particle sizes. Therefore, the influence of other parameters of PRG materials (e.g. level of defects, and number of layers) on mechanical strengths of cement-based mortars is negligible, and the main influence parameter of PRG materials on the different mechanical results of the mortars containing two PRG samples in this study accounts for the difference in PRG sizes.

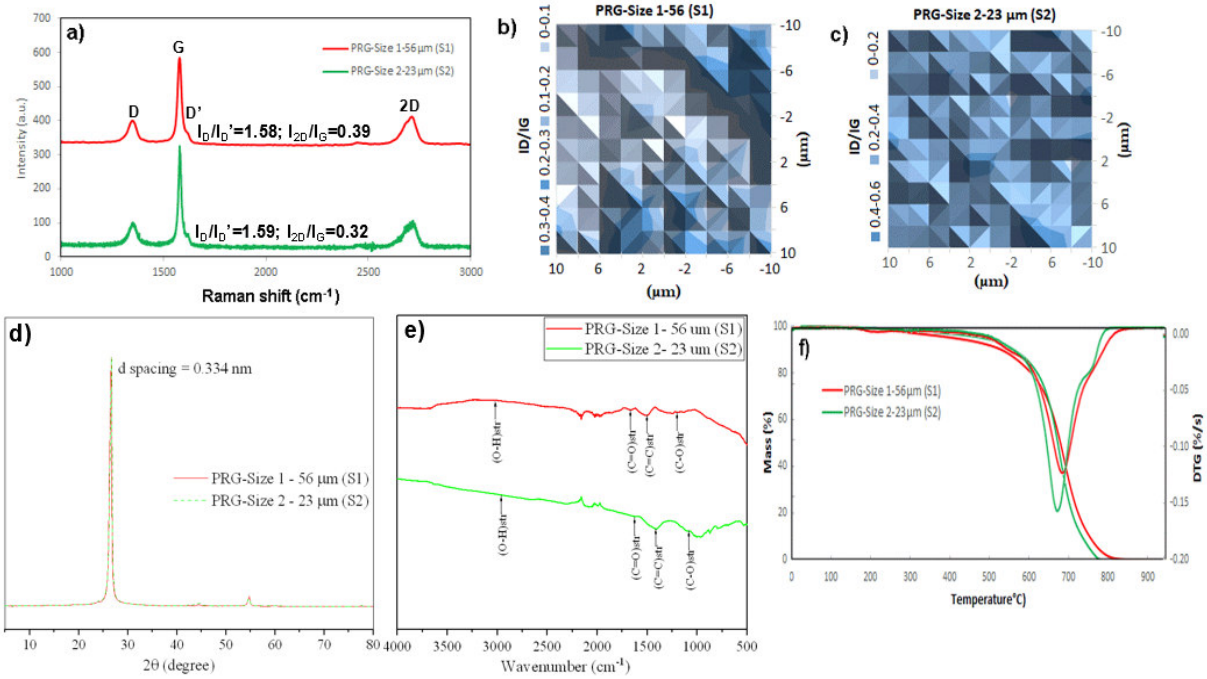

Fig. 2. Characterization of two PRG samples: (a) Raman spectra, (b-c) I_D/I_G peak ratio mappings, (d) XRD patterns, (e) FTIR spectra, (f) TGA/DTG graphs.

3.2. Mechanical properties of mortar mixes

Fig. 3 shows the compressive strengths and strength enhancements of cement-based mortars with different PRG dosages and sizes at 7 and 28 days. As shown in Fig. 3(a)-(c), the addition of PRG to cementitious composites increases the 7-day and 28-day compressive strengths of the mortars. The mixes containing larger PRG size S1 and smaller PRG size S2 have the optimal PRG dosage at 0.07% and 0.1%, respectively. When PRG is used beyond the optimal dosage, the compressive strengths of the mortars in both PRG sizes start decreasing. As shown in the figure, at the optimal dosage of 0.07% PRG, the 7-day and 28-day compressive strengths of the mix containing larger PRG size S1 (i.e. S1-0.07) are approximately 50 MPa and 56.3 MPa, respectively. These are 36.8% and 34.3% higher than the corresponding strengths of the plain mortar (36.5 MPa and 42 MPa, respectively). For the mortar containing smaller PRG size S2 at the optimal dosage of 0.1%, the 7-day and 28-day compressive strengths are 40.4 MPa and 48.6

MPa, respectively, which represent only a 10.6% and 15.7% respective increase compared to the plain mortar.

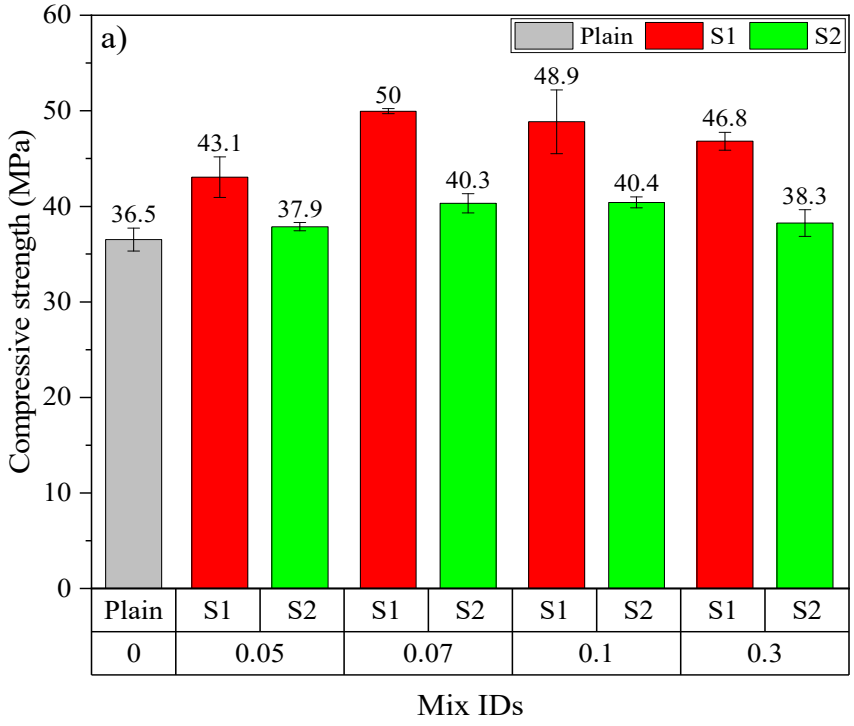

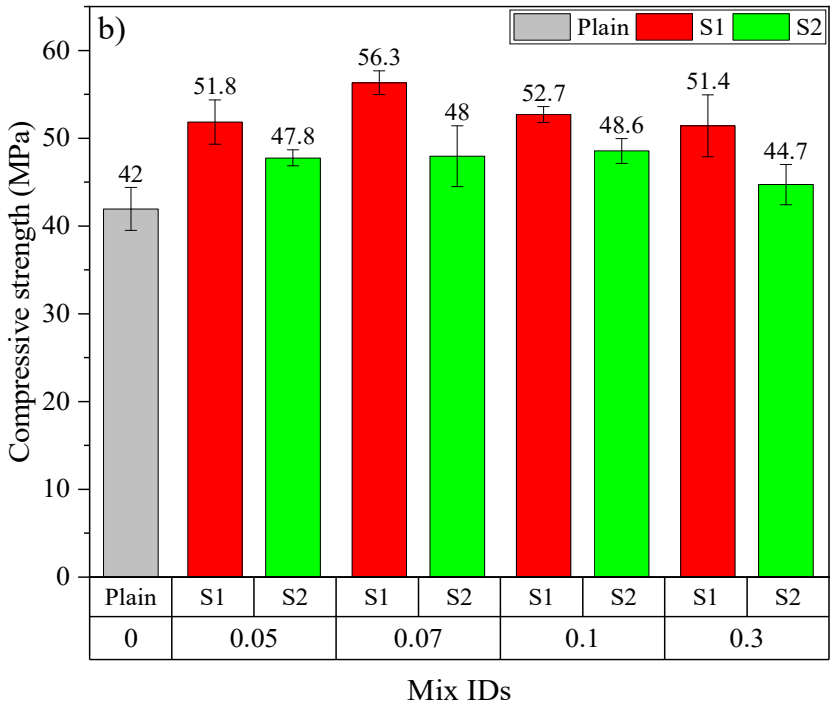

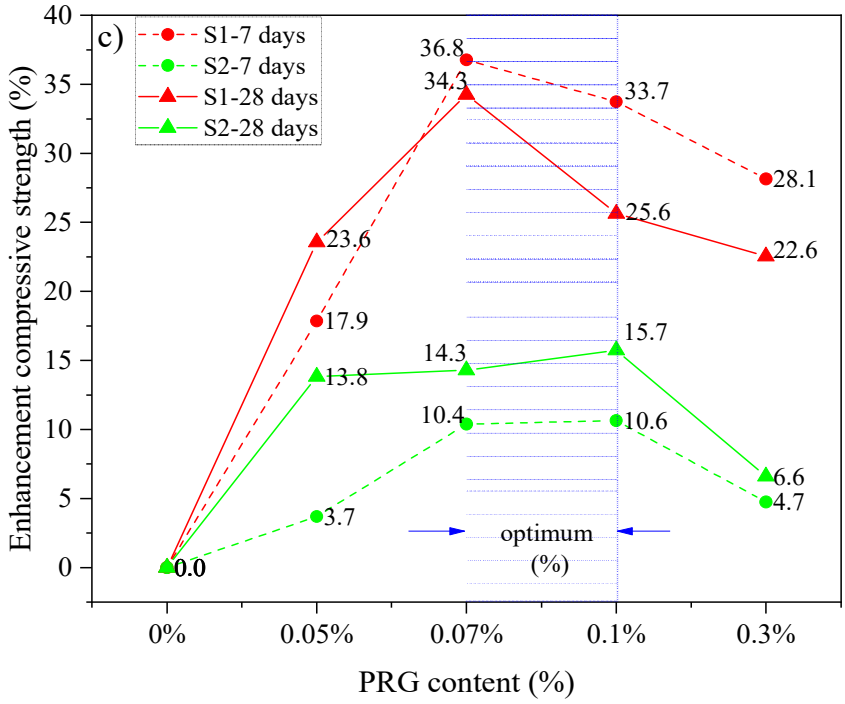

Fig. 3. Compressive strength at: (a) 7 days, (b) 28 days; (c) enhancement compressive strength at 7 and 28 days of different PRG-cement based mortars.

The tensile strengths and strength enhancements of cementitious mortar composites with the different dosage and size of pristine graphene at 7 and 28 days are shown in Fig. 4. From Fig. 4(a)-(c), it can be seen that incorporating PRG into cementitious composites increases the 7-day and 28-day tensile strengths of the mortars. The trend in tensile strengths is similar to that in compressive strengths for both PRG samples at both ages. As shown in the figure, at the optimal dosage of 0.07% PRG, the 7-day and 28-day tensile strengths of the mix containing larger PRG size S1 are 3.89 MPa and 4.62 MPa, respectively, which respectively improve approximately 25.3% and 26.9% compared with the plain mortar at these testing days (3.10 MPa and 3.64 MPa). However, for the mix containing smaller PRG size S2 at the optimal dosage of 0.1% PRG, the 7-day and 28-day tensile strengths are 3.84 MPa and 4.19 MPa, respectively, which represent a 23.7% and 15.2% respective increase compared to the plain mortar.

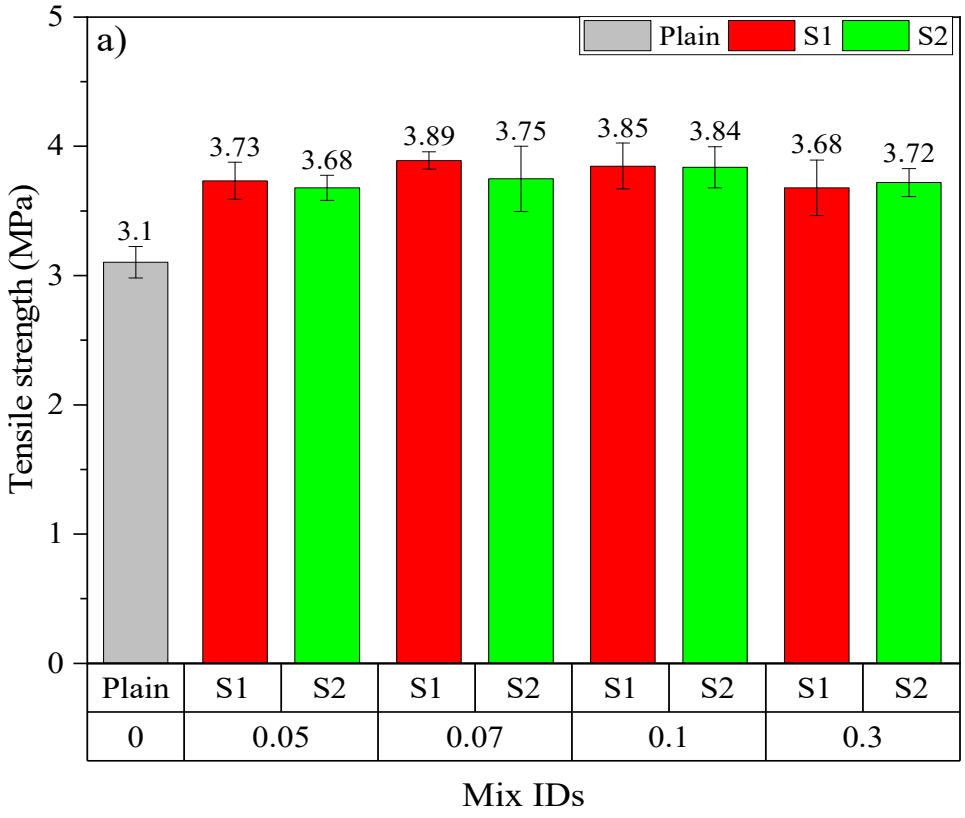
a)
Plain
S1
S2
Tensile strength (MPa)
0
1
2
3
4
5
3.1
3.73
3.68
3.89
3.75
3.85
3.84
3.68
3.72
Plain
S1
S2
S1
S2
S1
S2
S1
S2
0
0.05
0.07
0.1
0.3
Mix IDs

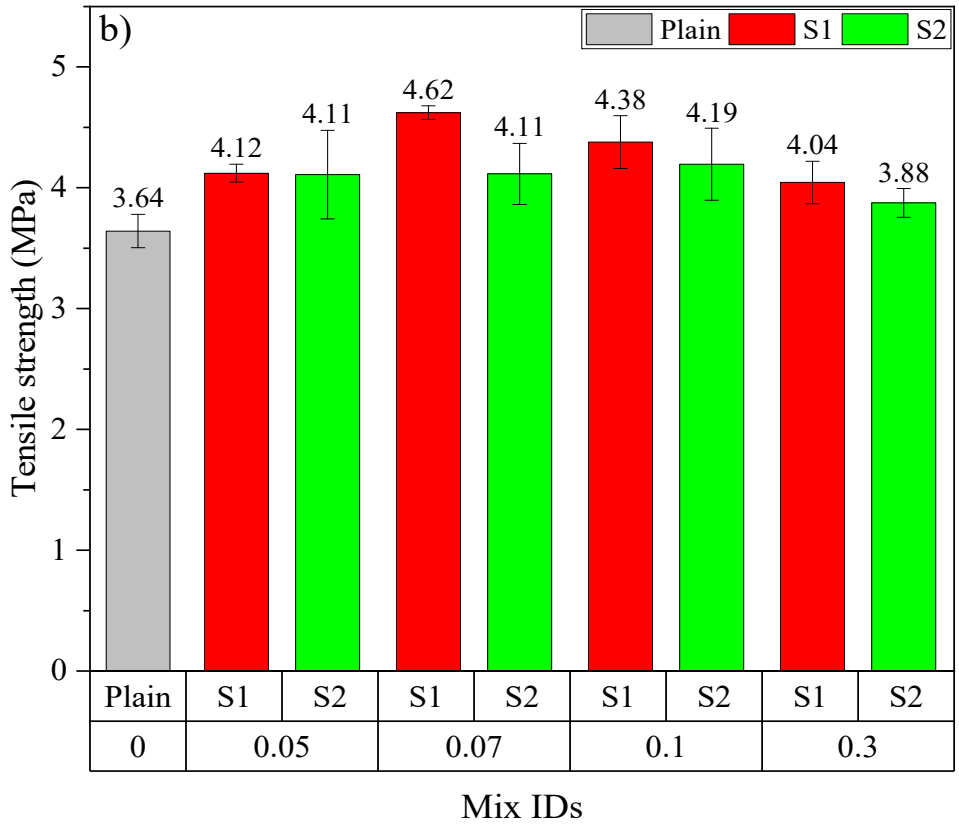
b)
Plain
S1
S2
Tensile strength (MPa)
0
1
2
3
4
5
3.64
4.12
4.11
4.62
4.11
4.38
4.19
4.04
3.88
Plain
S1
S2
S1
S2
S1
S2
S1
S2
0
0.05
0.07
0.1
0.3
Mix IDs

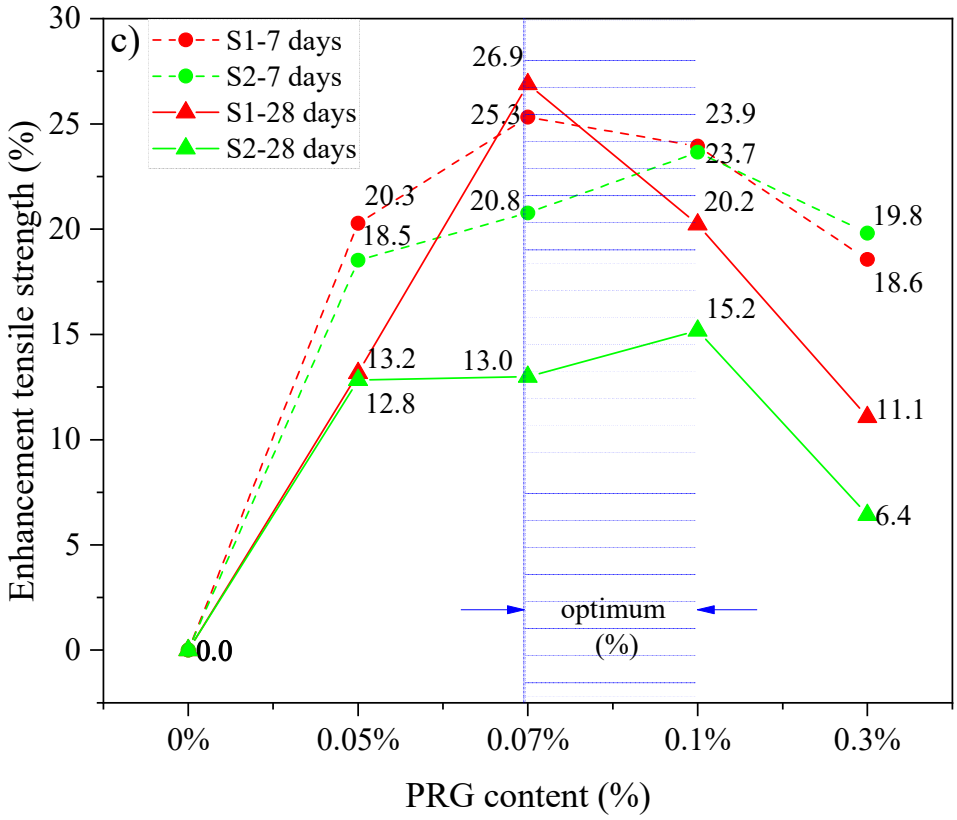

Fig. 4. Tensile strength at: (a) 7 days, (b) 28 days; (c) enhancement tensile strength at 7 and 28 days of different PRG-cement based mortars.

The reduction in enhancement rates of mechanical strengths of the mortars when using PRG beyond the optimal dosage can stem from the poor dispersion of PRG suspension due to the van der Waals forces between PRGs. This leads to the agglomeration of PRGs and the formation of multi-layers PRGs, resulting in the hindrance to the enhancement of PRGs to the hydration process, as well as their interaction with cementitious gels [27,48,52].

Figs. 3(c) and 4(c) show the optimal PRG range for both compression and tension at 7-day and 28-day ages of PRG-cement based mortars. Both pristine graphene samples are in a relatively low dosage range of from 0.07% to 0.1%, and the strength improvement rates are between 10.4% and 36.8%. The variance test was performed to assess if the difference in the strength of mortars containing PRG in the optimal range (i.e. 0.07% and 0.1%) to be statistically significant. To do this, the variance analysis based on the theory of the null hypothesis with the significant level of 0.05 was tested (the details of this method can be seen in Refs. [53,54]). The

results of the analysis of variance test are shown in Table 5. It is evident from the table that the difference between S1-0.07 and S1-0.1 at 28-day compressive strength is statistically significant (i.e. P-value=0.018<0.05). However, there are no statistically significant differences in tensile and compressive strengths at curing ages of 7 and 28 days of the other mixes between 0.07% and 0.1% (i.e. P-values>0.05). Moreover, for the PRG dosage of 0.07%, the enhancement rates of 7-day & 28-day compressive strengths and tensile strengths of the mix containing larger PRG size S1 are approximately 3.5 & 2.4 times and 1.2 & 2.1 times more than those of the mix containing smaller PRG size S2, respectively. From those analytic results, it can be concluded that the PRG sizes have a significant effect on the enhancement rates of mechanical strengths of the mortars, whereas they do not have a significant influence on the optimized PRG dosage for mechanical strengths of the mortars. Therefore, the pristine graphene dosage of 0.07% is identified as the optimized content of PRG for enhancing the strength of cementitious mortar composites for both sizes. The reinforcing mechanism of pristine graphene on the strengths of the mortars will be discussed in detail in Sections 3.3 and 3.4.

Table 5. Analysis of variance tests for evaluating the difference in 7-day and 28-day mechanical strengths of the mortars containing PRG in the optimal dosage range (0.07% PRG and 0.1% PRG).

Difference of levels	Difference of means	T-Value	Adjusted P-Value	Evaluate significant differences
S1-0.07 - S1-0.1 (7-day compression)	1.110	0.57	0.596	No
S1-0.07 - S1-0.1 (7-day tension)	0.043	0.39	0.716	No
S1-0.07 - S1-0.1 (28-day compression)	3.615	3.85	0.018	Yes
S1-0.07 - S1-0.1 (28-day tension)	0.243	1.86	0.136	No
S2-0.1 - S2-0.07 (7-day compression)	0.092	0.14	0.897	No
S2-0.1 - S2-0.07 (7-day tension)	0.090	0.52	0.630	No
S2-0.1 - S2-0.07 (28-day compression)	0.610	0.28	0.793	No
S2-0.1 - S2-0.07 (7-day tension)	0.080	0.35	0.742	No

3.3. Physicochemical and microstructural characterizations of mortar mixes

Complementary XRD, FTIR, and SEM-EDX characterizations were performed to examine the influence of the different dosage and size of pristine graphene on the physicochemical and microstructure characteristics of the composites. The three different PRG concentrations were selected for analysis. They are 0%, 0.07% and 0.3%, which represent the plain mix, the mix with the optimized, and highest considered PRG dosage, respectively. However, XRD and FTIR analysis of smaller PRG size S2 were only presented at 0.07% PRG content for the comparison purpose.

3.3.1. XRD and FTIR characterizations

There are four main components of the OPC binder, i.e. tricalcium silicate or alite (C_3S), dicalcium silicate (C_2S), tricalcium aluminate (C_3A), tetracalcium ferroaluminate (C_4AF), and a small amount of gypsum. The hydration products of the cement matrix resulting from chemical reactions between these components and water [55, 56] can be described by the following equation:

(C_3S, C_2S, C_3A, C_4AF) + Gypsum + H_2O → Calcium silicate hydrate (CSH) + Portlandite (CH) + Sulphoaluminates (most ettringite (Aft) + part of monosulphoaluminate) (1)

Fig. 5 presents XRD patterns of different mortar mixes (i.e. the plain, S1-0.07, S2-0.07, S1-0.3) at 28 days of curing age. As shown in Eq. (1), the production of the Portland cement hydration process consists of CSH gels, CH and Aft. Among them, CSH gels are the main part contributing to mechanical strengths of cementitious composites. Therefore, samples with a larger amount of CSH gels can have better strength properties in composites. In XRD analysis, although there are some difficulties in identifying CSH phases that are often as amorphous phases [22,57,58], the content of CSH gels and the hydration degree of the binder can be estimated by the content of portlandite and un-hydrated cement particles (e.g. C_3S, C_2S))

[57,58]. The XRD spectra of all samples were standardized at the peak of 26.7° to ensure the amount of natural sand in specimens equal, [22,58,59].

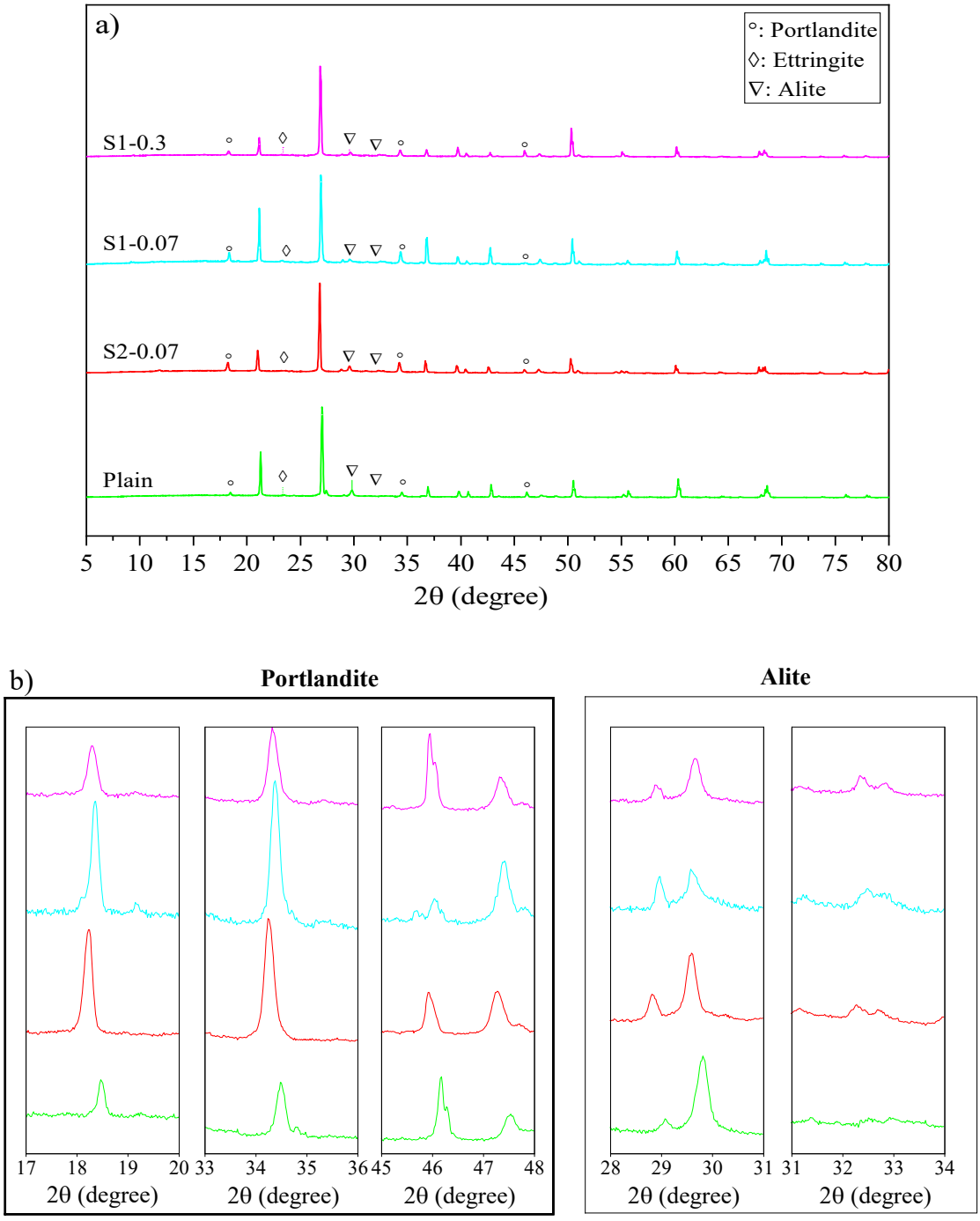

Fig. 5. XRD patterns of: (a) different PRG-cement based mortars at 28 days, (b) portlandite and alite detailed from Fig. 5(a). (PRG-cement mortar with size S2 only presented at 0.07% PRG concentration for the comparison purpose).

It can be seen in Fig. 5(a) that although the samples containing pristine graphene show similar spectra with the plain mortar, they have different intensities, which might cause differences in their mechanical properties. From Fig. 5(a) and (b), the peaks of portlandite phases can be identified at 18.2°, 34.2° and 47.1° [58,60]; and the intensities of these peaks are different from each mix. The highest value is observed at S1-0.07, followed by S1-0.3, S2-0.07, and the plain. This reveals that the hydration degree of cement paste of the mixes containing PRG is higher than that of the plain mix, which is consistent with previous research on PRG-cement composites [30,58]. In addition, the figures also show that the scattering angles at 29.5° and 32.3° of un-hydrated alite [57,60] of these mixes have different intensities, which is the highest in the plain mix and followed by the PRG-cement samples. This can be attributed to the beneficial effect of PRG on the cement hydration process, which might lead to the creation of more CSH gels in the cement matrix [22,57,58]. This is in agreement with the observed trends of the mechanical results of the mixes analyzed in Section 3.2.

The FTIR spectra of the different mixes (i.e. the plain, S1-0.07, S2-0.07, S1-0.3) at the 28-day testing are shown in Fig. 6. The figure shows that the spectrum of these samples is similar. This means no new specific groups observed when adding PRG. The group bands ranged 400-550 cm^{-1} and 800-1200 cm^{-1} are attributed to Si-O bonds in the CSH gels [61,62]. The band ranged from 2800 to 3600 cm^{-1} represents O-H groups in H_2O belonging to CSH gels [61-63]. The narrow band in the range of about 3600-3650 cm^{-1} is attributed to portlandite, i.e. O-H bonds [61,64]. The band of 1350-1550 cm^{-1} is attributed to C-O bonds in calcium carbonate [62,63]. Fig. 6 also shows that although these mixes have similar spectra, the spectral intensities representing CSH gels and portlandite in these mixes are different. This indicates that the mortars with pristine graphene materials have stronger intensities than the plain mix and the strongest intensity can be observed in the S1-0.07 mix. This may be due to the higher cement hydration degree in the mixes containing pristine graphene, leading to the enhancement in

mechanical strengths of those mixes compared with the plain. This is in agreement with the results of mechanical strengths, and XRD shown above.

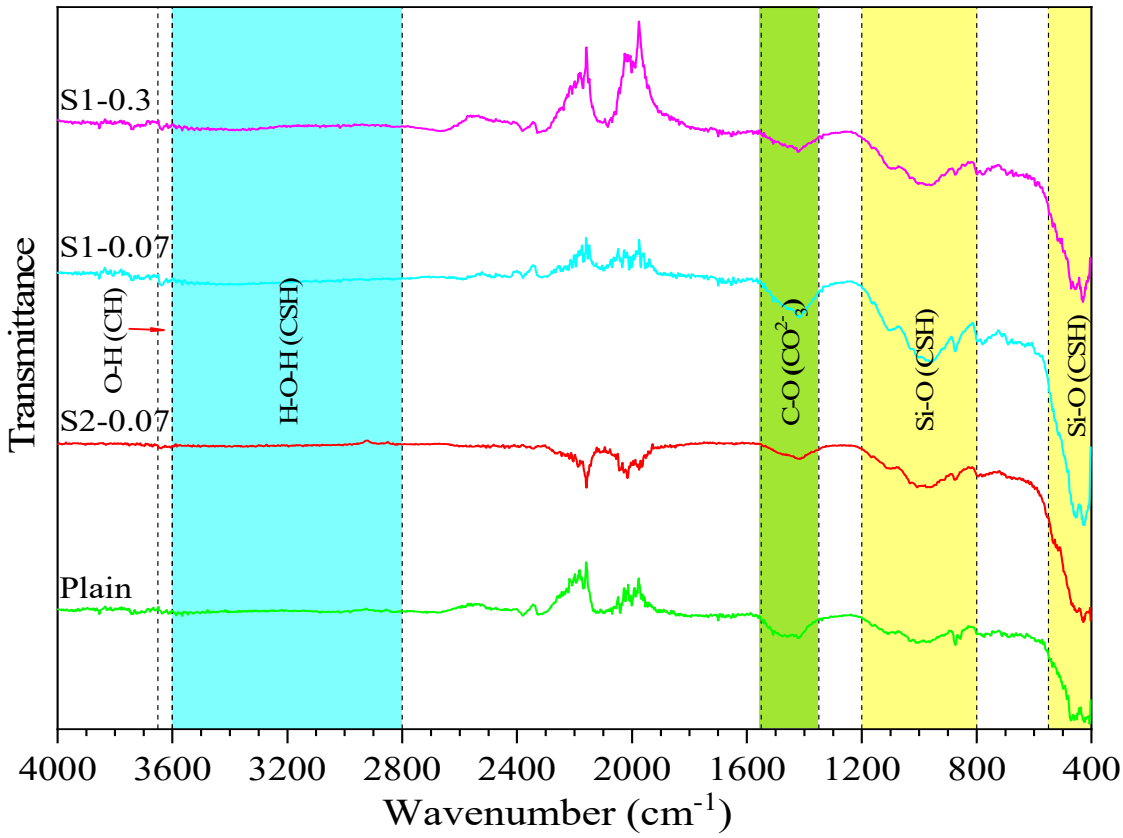

Fig. 6. FTIR of different PRG-cement based mortars at 28 days. (PRG-cement mortar with size S2 only presented at 0.07% PRG concentration for the comparison purpose).

3.3.2. SEM characterizations

Fig. 7(a)-(j) shows a series of SEM images of observed microcrack patterns and crystals in different PRG-cement based mortars at the 28-day testing, i.e. the plain mortar, S1-0.07, S2-0.07, S1-0.3, and S2-0.3. As shown in the figure, although these mixes have similar components in their structures (e.g. CSH, CH, Aft and pores), the distribution and compaction of these components at the microscale are different. The plain mix (Fig. 7(a), (b)) exhibits higher content of pores and density of microcracks in its microstructure compared to the other mixes. This explains the reason for the lower strengths of the plain mix than those of the mixes prepared

with pristine graphene. It can be seen in Fig. 7(c)-(j) that, for a given PRG size, the mixes prepared with the larger PRG size (S1) exhibit better microstructure patterns than those with the smaller PRG size (S2). The crystal content and compactness of the PRG-cement samples are also altered by different PRG dosages for both PRG sizes, which shows the densest microstructure at 0.07% PRG content and followed by 0.3%. As shown in Fig. 7(c)-(f) (i.e. at the optimized dosage of 0.07% PRG), the SEM images of the mix containing the larger PRG size (Fig. 7(c)-(d)) are not only more compact in microstructure but it also has denser interfacial transition zones (ITZ) between cementitious gels and fine aggregates than that of the mix containing the smaller PRG size (Fig. 7(e)-(f)). This can contribute to more efficient stress distribution and better inhibition of crack propagation in the structure of the S1 series, resulting in improvements in their mechanical properties [14,22,30], and this will be discussed further in Section 3.4.

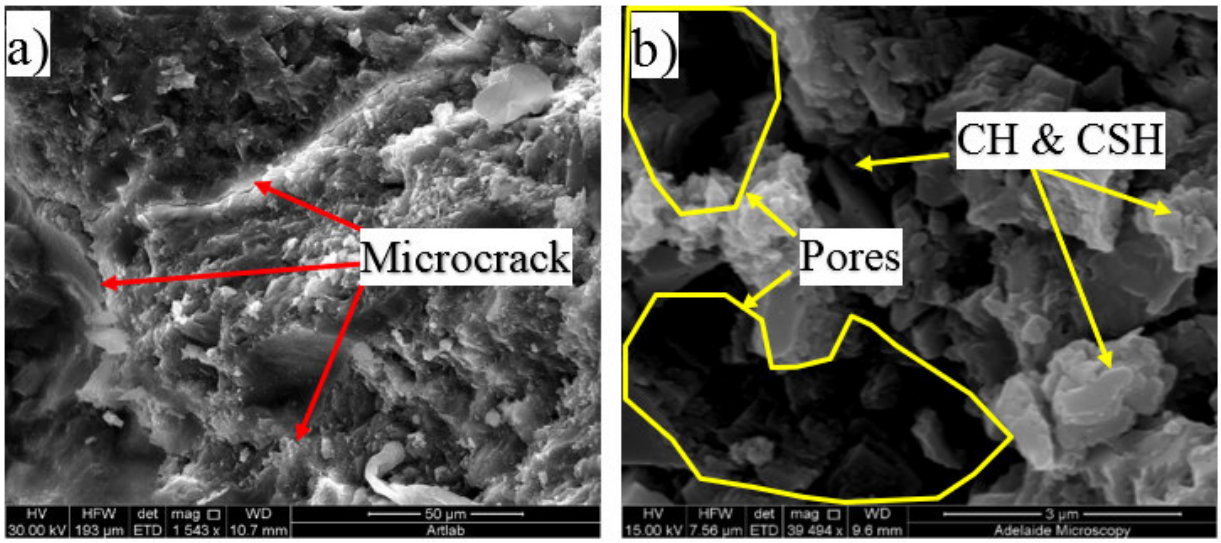

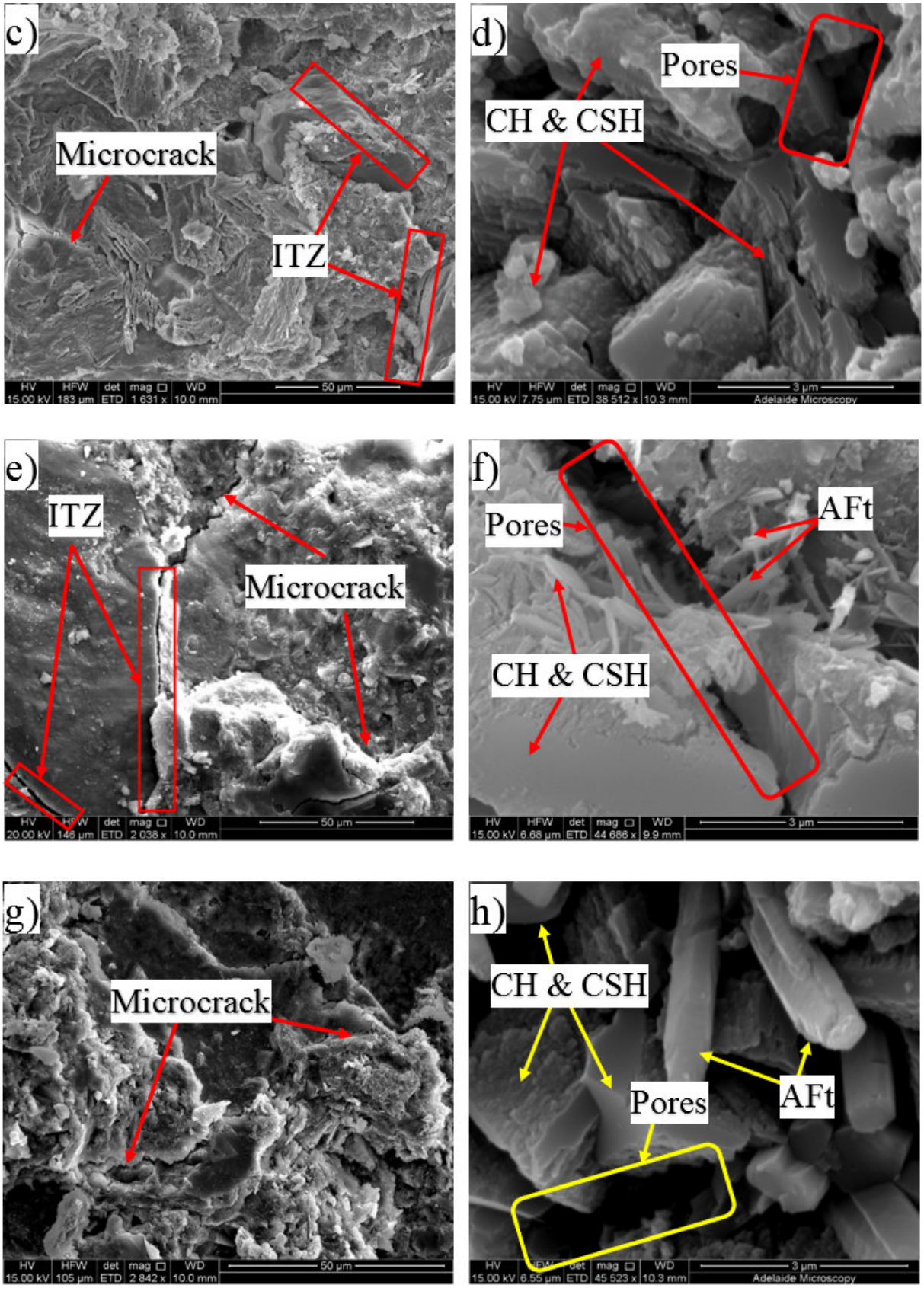
c)
Microcrack
ITZ
d)
Pores
CH & CSH
e)
ITZ
Microcrack
f)
Pores
AFt
CH & CSH
g)
Microcrack
h)
CH & CSH
Pores
AFt

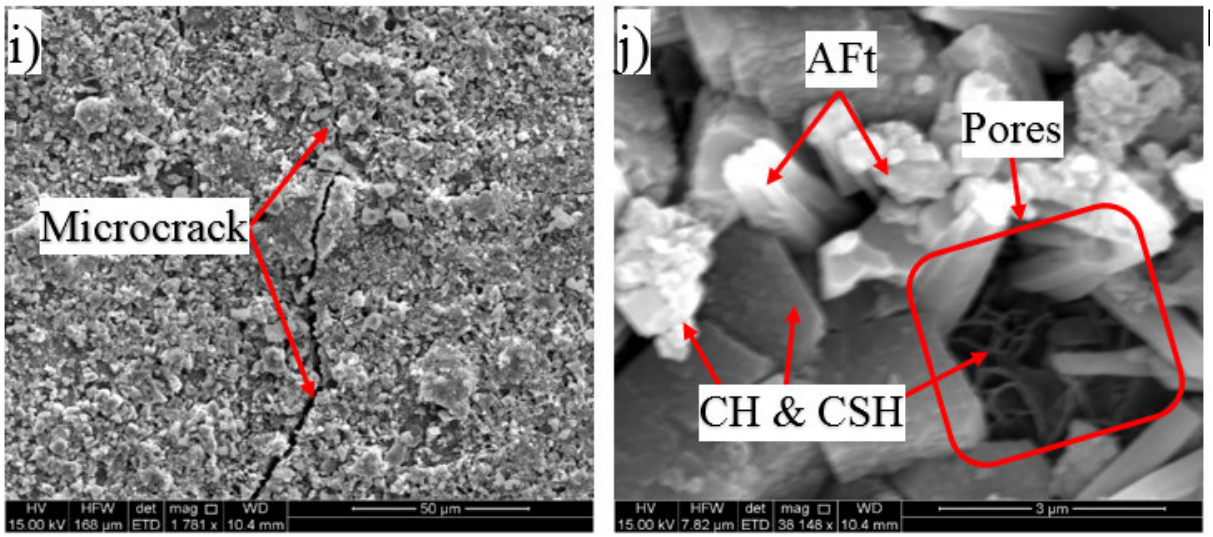

Fig. 7. SEM images of different PRG-cement based mortars at 28 days: (a, b) Plain (control), (c, d) S1-0.07, (e, f) S2-0.07, (g, h) S1-0.3 and (i, j) S2-0.3. (for each mix, 50µm and 3µm magnification corresponds to the former and latter figure respectively)

3.4. The reinforcing mechanism of PRG for enhancing mechanical properties of cement based composites

The strengths of traditional cementitious composites depend on the strengths of Portland cementitious gels, which are formed by the chemical reaction between cement powder and water. The most important product of the cement hydration process is CSH gels, which contribute most of the strength of Portland cementitious gels [2, 65]. Similar to traditional cement mortar, the strengths of PRG and cementitious mortar composites are governed by PRG-cementitious gels, which are created by the interaction between PRG structure and Portland cementitious gels (CSH gels). Fig. 8 outlines a general illustration of the proposed mechanism showing the interaction of PRG and CSH structures as a key parameter for the enhancement of PRG-cementitious gels in PRG-cement based mortars. As mentioned in the Introduction (Section 1), for GO-cement based composites, the reinforcing mechanism of their mechanical properties was proposed as a result of chemical reactions between the oxygen-functional groups of GO and the mediating Ca^{2+} ions from cementitious gels. However, the level of these oxygen-

functional groups at the edge of the PRG structure is very limited, and hence, their contribution to strength enhancement of PRG-cementitious gels is less significant. Moreover, as discussed in Section 3.1, both PRG samples have the same manufacturing process, high-quality products and similar physicochemical properties, and are only different in particle sizes. Consequently, the main factor to reinforce the strength of PRG-cementitious gels must be related to the interaction between basal planes of PRGs and CSH gels, which depend on surface areas of PRGs. This means PRGs with larger particle sizes will have larger basal plane areas to interact with CSH gels around. This leads to a stronger connection between them in cement matrix. This finding is significantly supported by the considerable difference in mechanical results of PRG-cement based mortars between the larger PRG size 56µm (S1) and smaller PRG size 23µm (S2) as discussed in Section 3.2.

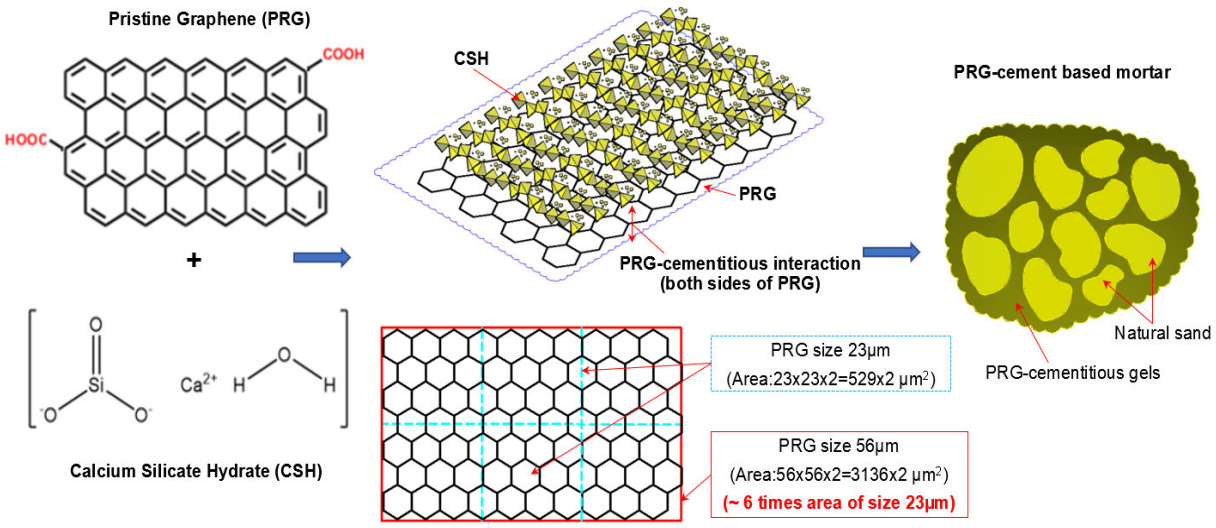

Fig. 8. The outline of the proposed mechanism for the formation and enhancement of cementitious gels by PRGs.

The increase in mechanical strengths of PRG-cement mortars can be explained (which is also supported by the findings presented in next paragraphs): (1) part from the improvement of cementitious gels due to the closer distance between the particles of the cement binder caused by van der Waals forces between PRGs [17]; (2) the most important part to reinforce PRG-

cementitious gels is proposed to be contributed by the adhesion friction forces between surface areas of PRGs and CSH gels: these adhesion friction forces are a combination of crack surface adhesion forces (which was created by atoms near crack surfaces during the pull-out process [37]), and friction forces between surface areas of PRGs and CSH gels, which depend on particle sizes of PRGs that will increase with an increase in graphene size. This was also demonstrated in the study conducted by Chen et al. [37] using molecular dynamic (MD) simulation to investigate the interaction mechanism of PRGs (with low surface roughness properties) and CSH gels. The benefit of PRG sizes to enhance PRG-cementitious gels is clearly supported by the experimental results of this study. At the optimized dosage of 0.07%, 28-day compressive and tensile strengths of the larger PRG size S1 mix are 2.4 and 2.1 times higher than those of the smaller PRG size S2 mix, respectively. This is because the larger PRG size has larger contact surface areas, which contribute to a better adhesion friction force compared with the smaller PRG size. It is also noted that both PRG samples have similar thicknesses and densities (Table 1), so there is no significant difference in their specific surface areas (i.e. unit with m2/g) at the same dosage. However, they are significantly different from the contact surface area of each of PRGs with CSH gels (i.e. the area of the large PRG size 56μm (S1) is approximately 6 times as equal as that of smaller the PRG size 23μm (S2), as shown in Fig. 8).

The investigation of the interface of PRGs and cementitious gels and the propagation of microcracks in the cement matrix was performed and the results are presented in Fig. 9(a)-(i). As can be seen in Fig.9(a)-(f), the EDX results indicate that the carbon contents of spectrums 1, 2, and 3 are dominant and much higher than the other spectrums nearby (i.e. spectrums 4 and 5). This confirms the cement matrix containing a combination of PRGs and cementitious gels. Fig. 9(g) depicts the detailed outline of the reinforcing mechanism and crack propagation in the cement matrix due to PRG additives. The figure also shows that the combination of PRGs and CSH gels can enhance cementitious gels around PRGs and create interlocked PRG-cementitious gels in a space network structure, resulting in the effectiveness of stress

distribution. Fig. 9(g), (h) also presents that PRGs can increase the path of crack developments through crack bridging, crack branching, and crack deflection. This contributes to the benefit of the reduction of crack widths in structures. As a result, it can be said that PRGs with the larger size can create larger interaction areas with CSH gels, and hence, leading to larger strengthened areas. This is more beneficial for their interlocks in the cement matrix compared to the smaller size. This finding is consistent with the important role of PRG sizes on adhesion friction forces of PRG-cementitious gels as discussed before in the previous paragraph.

Moreover, as discussed in Section 3.2, the enhancement strength rates of the mortars start decreasing when PRG is used over the optimum dosage due to the agglomeration of PRGs in cement matrix, which can also be explained from the SEM images in Fig. 9(g). From the figure, we can figure out that when the agglomeration of PRGs happens, it means many layers of PRGs will stack together and form multi-layers PRGs. As a result, the adhesion friction forces between PRGs and cementitious gels in the cement matrix are diminished due to the effects of weak van der Walls bonds among multi-layers PRGs. This causes the debonding and displacement between those PRGs during sustaining external loads. Based on the SEM images and the above analyses, the crack paths of PRG-cement based composites under external loads are outlined in Fig. 9(i). The outcomes of these findings have provided a better knowledge of the reinforcing mechanism of PRGs on the strengths of cementitious composites prepared with PRG additive through enhancing the PRG-cementitious gels, load-transfer mechanism, and crack paths of the composites.

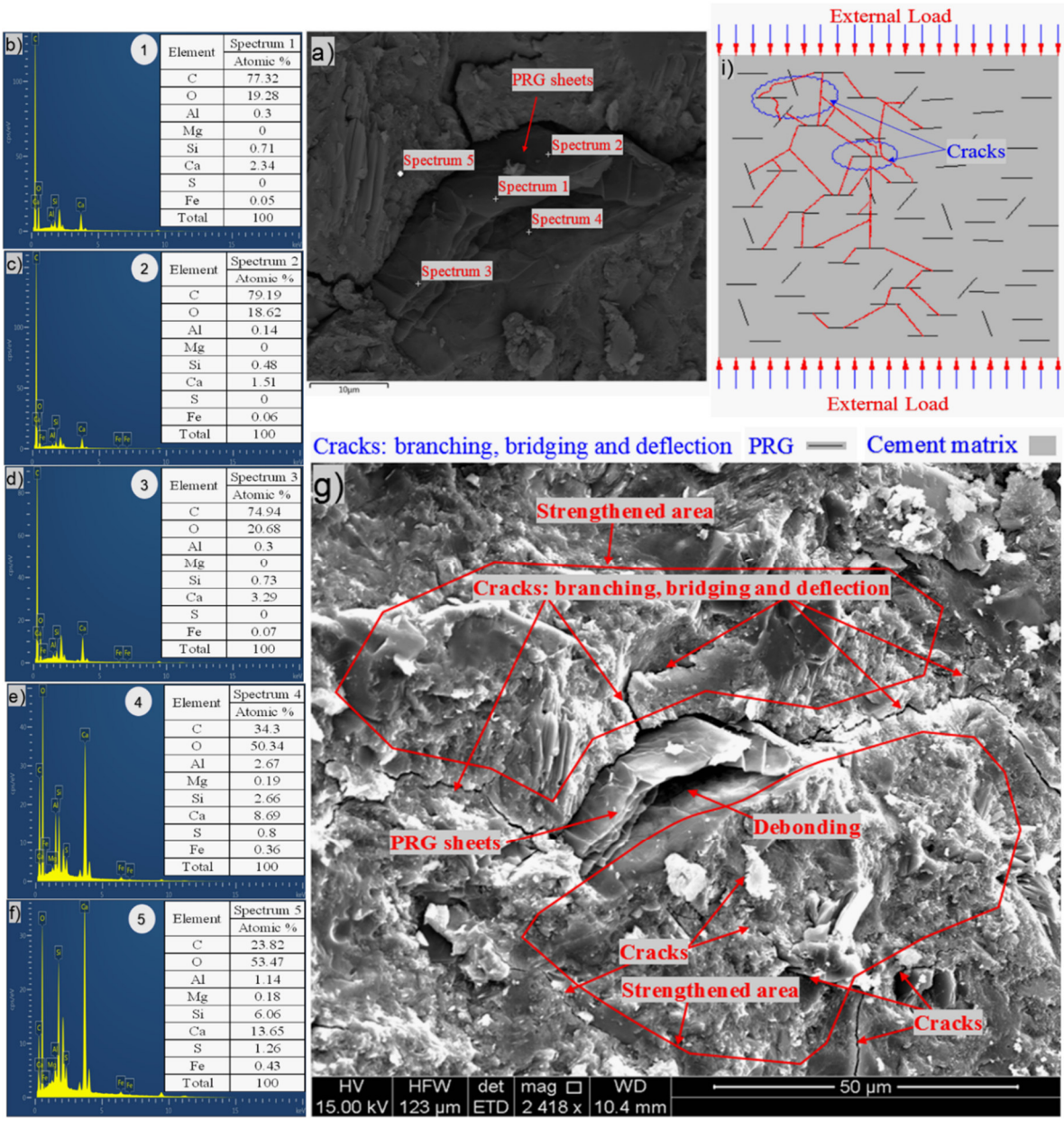
b)
1
Element
Spectrum 1
Atomic %
C 77.32
O 19.28
Al 0.3
Mg 0
Si 0.71
Ca 2.34
S 0
Fe 0.05
Total 100
c)
2
Element
Spectrum 2
Atomic %
C 79.19
O 18.62
Al 0.14
Mg 0
Si 0.48
Ca 1.51
S 0
Fe 0.06
Total 100
d)
3
Element
Spectrum 3
Atomic %
C 74.94
O 20.68
Al 0.3
Mg 0
Si 0.73
Ca 3.29
S 0
Fe 0.07
Total 100
e)
4
Element
Spectrum 4
Atomic %
C 34.3
O 50.34
Al 2.67
Mg 0.19
Si 2.66
Ca 8.69
S 0.8
Fe 0.36
Total 100
f)
5
Element
Spectrum 5
Atomic %
C 23.82
O 53.47
Al 1.14
Mg 0.18
Si 6.06
Ca 13.65
S 1.26
Fe 0.43
Total 100
a)
PRG sheets
Spectrum 5
Spectrum 2
Spectrum 1
Spectrum 4
Spectrum 3
10μm
i)
External Load
Cracks
External Load
Cracks: branching, bridging and deflection
PRG
Cement matrix
g)
Strengthened area
Cracks: branching, bridging and deflection
Debonding
PRG sheets
Cracks
Strengthened area
Cracks
HV
15.00 kV
HFW
123 μm
det
ETD
mag
2 418 x
WD
10.4 mm
50 μm

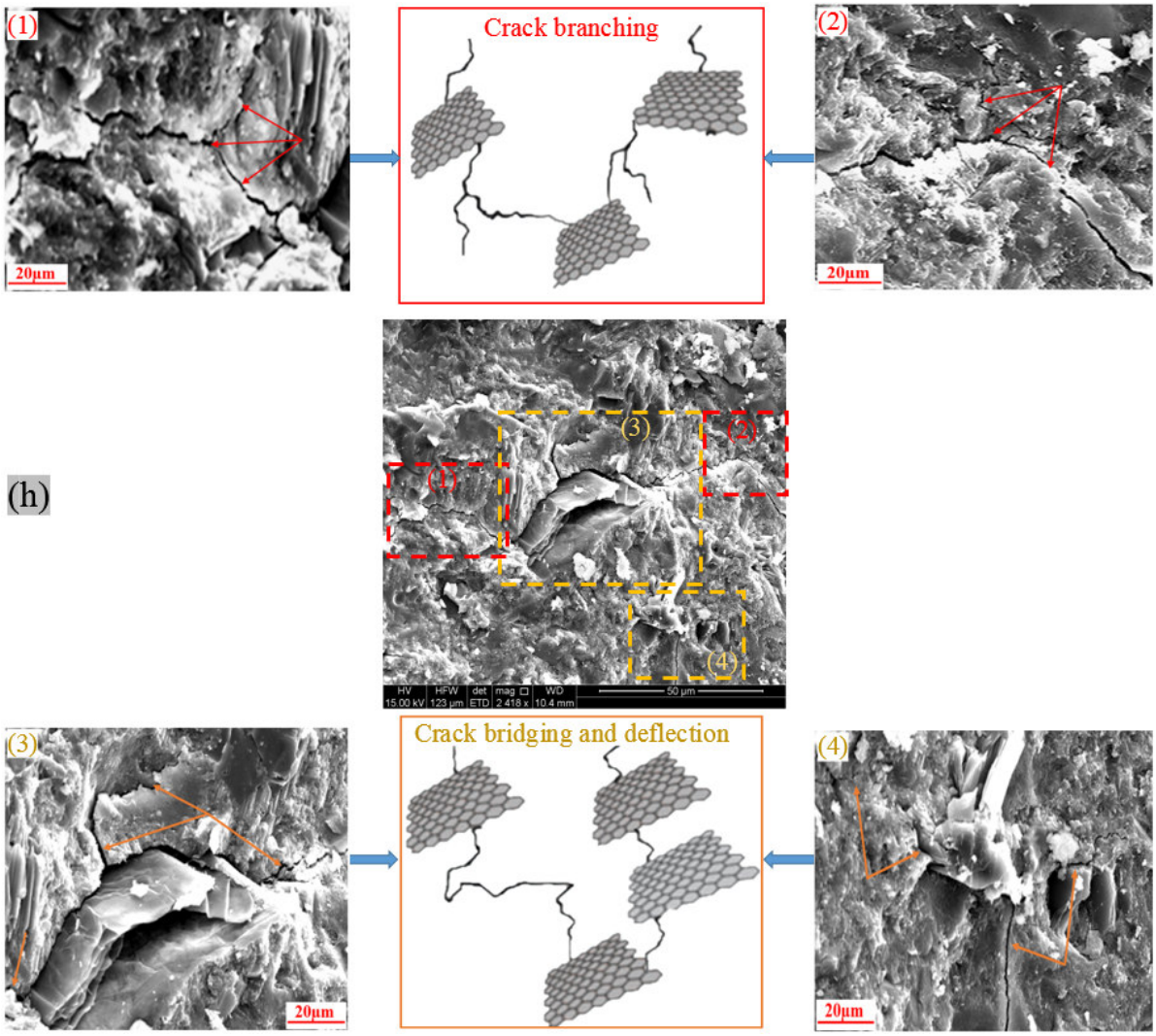

Fig. 9. (a-f) Energy dispersive X-ray results confirm the combination of PRGs and cement gels in the cement matrix; (g) the detailed outlines of the supporting of PRGs to enhance properties of cementitious gels when sustaining external loads; (h) some details of the propagation of cracks in the cement matrix; (i) the outline of crack paths of PRG-cement based composites under external loads.

4. Conclusions

This study has presented the proposed reinforcing mechanism and optimized dosage of pristine graphene additives for improving the mechanical strengths of cementitious mortar composites. The main findings of this study can be drawn below:

- The strengths of the mortars are dependent on the PRG dosage and size. The PRG sizes (as changed from 23μm (S2) to 56μm (S1)) have a significant effect on the enhancement rates of mechanical strengths of the mortars, whereas they do not have a significant influence on the optimized PRG dosage for mechanical strengths of the mortars. The PRG dosage of 0.07% is identified as the optimized concentration of PRG for enhancing mechanical strengths of cement-based mortars.
- At the optimized dosage of 0.07%, the enhancement rates of the compressive strengths and tensile strengths at 7 and 28 days of the mix containing larger PRG size S1 are approximately 3.5 and 2.4 times, and 1.2 and 2.1 times more than those of the mix with smaller PRG size S2, respectively. The mortars show less improvement in strengths when PRG is used over the optimal dosages. This is due to van der Waals forces between PRGs, resulting in the agglomeration of PRGs and the formation of multi-layers PRGs, resulting in the hindrance to the enhancement of PRGs to the hydration process.
- The reinforcing mechanism of PRG on the strengths of cementitious composites is mostly attributed to the adhesion friction forces between pristine graphene sheets and cementitious gels. This can enhance cementitious gels around PRGs and create interlocked PRG-cementitious gels in a space network structure, resulting in the effectiveness of stress distribution. As a result, the mixes containing the larger PRG size (S1) have higher strength improvements than those containing the smaller PRG size (S2). This is because the larger PRG size has larger interaction areas with CSH gels, leading to larger strengthened areas that will be more beneficial for their interlock in the cement matrix compared to the smaller size.
- The results from microstructural analyses have indicated that there is a close correlation between the strengths of PRG-cement based mortars and their microstructures. This shows that the mixes with higher strengths often have better microstructure patterns.

The results of this study have not only provided a better understanding of incorporating PRG into cementitious composites, but they have also shown the great potential for low-cost industrially produced PRG materials for improving the performance of cement-based construction materials. The study has also provided a valuable orientation in studying PRG-cement based composites so that future studies on other properties of pristine graphene and cementitious composites can be performed with less time and effort and fewer costs.

Conflict of interest

The authors state no conflict of interest.

Acknowledgements

This work is supported and funded by the ARC Research Hub for Graphene Enabled Industry Transformation (IH 1500003) and First Graphene Ltd (Perth, Australia). The authors also thank the Schools of Civil, Environmental and Mining Engineering and School of Chemical Engineering at the University of Adelaide for supporting this work. The authors also acknowledge Adam Ryntjes and Dale Hodson as the technical support in experimental works.

REFERENCES

[1] R.V. Sagar, B.R. Prasad, S.S. Kumar, An experimental study on cracking evolution in concrete and cement mortar by the b-value analysis of acoustic emission technique, Cement and Concrete Research 42(8) (2012) 1094-1104.

[2] H.F. Taylor, Cement chemistry, Thomas Telford1997.

[3] D. Chung, Comparison of submicron-diameter carbon filaments and conventional carbon fibers as fillers in composite materials, Carbon 39(8) (2001) 1119-1125.

[4] E.T. Dawood, M. Ramli, High strength characteristics of cement mortar reinforced with hybrid fibres, Construction and Building Materials 25(5) (2011) 2240-2247.

[5] M.S. Konsta-Gdoutos, Z.S. Metaxa, S.P. Shah, Multi-scale mechanical and fracture characteristics and early-age strain capacity of high performance carbon nanotube/cement nanocomposites, Cement and Concrete Composites 32(2) (2010) 110-115.

[6] P. Stynoski, P. Mondal, C. Marsh, Effects of silica additives on fracture properties of carbon nanotube and carbon fiber reinforced Portland cement mortar, Cement and Concrete Composites 55 (2015) 232-240.

[7] A. Cwirzen, K. Habermehl-Cwirzen, A. Nasibulin, E. Kaupinen, P. Mudimela, V. Penttala, SEM/AFM studies of cementitious binder modified by MWCNT and nano-sized Fe needles, Materials Characterization 60(7) (2009) 735-740.

[8] B.M. Tyson, R.K. Abu Al-Rub, A. Yazdanbakhsh, Z. Grasley, Carbon nanotubes and carbon nanofibers for enhancing the mechanical properties of nanocomposite cementitious materials, Journal of Materials in Civil Engineering 23(7) (2011) 1028-1035.

[9] M.S. Konsta-Gdoutos, C.A. Aza, Self sensing carbon nanotube (CNT) and nanofiber (CNF) cementitious composites for real time damage assessment in smart structures, Cement and Concrete Composites 53 (2014) 162-169.

[10] H. Li, H.-g. Xiao, J. Yuan, J. Ou, Microstructure of cement mortar with nano-particles, Composites Part B: Engineering 35(2) (2004) 185-189.

[11] T. Ji, Preliminary study on the water permeability and microstructure of concrete incorporating nano-SiO 2, Cement and Concrete Research 35(10) (2005) 1943-1947.

[12] F. Sanchez, K. Sobolev, Nanotechnology in concrete–a review, Construction and building materials 24(11) (2010) 2060-2071.

[13] L. Senff, D. Tobaldi, S. Lucas, D. Hotza, V. Ferreira, J. Labrincha, Formulation of mortars with nano-SiO 2 and nano-TiO 2 for degradation of pollutants in buildings, Composites Part B: Engineering 44(1) (2013) 40-47.

[14] Z. Pan, L. He, L. Qiu, A.H. Korayem, G. Li, J.W. Zhu, F. Collins, D. Li, W.H. Duan, M.C. Wang, Mechanical properties and microstructure of a graphene oxide–cement composite, Cement and Concrete Composites 58 (2015) 140-147.

[15] B. Han, S. Sun, S. Ding, L. Zhang, X. Yu, J. Ou, Review of nanocarbon-engineered multifunctional cementitious composites, Composites Part A: Applied Science and Manufacturing 70 (2015) 69-81.

[16] A.K. Geim, K.S. Novoselov, The rise of graphene, Nature materials 6(3) (2007) 183-191.

[17] H. Yang, H. Cui, W. Tang, Z. Li, N. Han, F. Xing, A critical review on research progress of graphene/cement based composites, Composites Part A: Applied Science and Manufacturing 102 (2017) 273-296.

[18] E. Shamsaei, F.B. de Souza, X. Yao, E. Benhelal, A. Akbari, W. Duan, Graphene-based nanosheets for stronger and more durable concrete: A review, Construction and Building Materials 183 (2018) 642-660.

[19] L. Zhao, X. Guo, L. Song, Y. Song, G. Dai, J. Liu, An intensive review on the role of graphene oxide in cement-based materials, Construction and Building Materials 241 (2020) 117939.

[20] D. Kang, K.S. Seo, H. Lee, W. Chung, Experimental study on mechanical strength of GO-cement composites, Construction and Building Materials 131 (2017) 303-308.

[21] L. Zhao, X. Guo, C. Ge, Q. Li, L. Guo, X. Shu, J. Liu, Mechanical behavior and toughening mechanism of polycarboxylate superplasticizer modified graphene oxide reinforced cement composites, Composites Part B: Engineering 113 (2017) 308-316.

[22] S. Sharma, N. Kothiyal, Influence of graphene oxide as dispersed phase in cement mortar matrix in defining the crystal patterns of cement hydrates and its effect on mechanical, microstructural and crystallization properties, RSC Advances 5(65) (2015) 52642-52657.

[23] S. Lv, J. Liu, T. Sun, Y. Ma, Q. Zhou, Effect of GO nanosheets on shapes of cement hydration crystals and their formation process, Construction and Building Materials 64 (2014) 231-239.

[24] D. Hou, Z. Lu, X. Li, H. Ma, Z. Li, Reactive molecular dynamics and experimental study of graphene-cement composites: Structure, dynamics and reinforcement mechanisms, Carbon 115 (2017) 188-208.

[25] Y. Zhu, S. Murali, W. Cai, X. Li, J.W. Suk, J.R. Potts, R.S. Ruoff, Graphene and graphene oxide: synthesis, properties, and applications, Advanced materials 22(35) (2010) 3906-3924.

[26] S. Chuah, Z. Pan, J.G. Sanjayan, C.M. Wang, W.H. Duan, Nano reinforced cement and concrete composites and new perspective from graphene oxide, Construction and Building Materials 73 (2014) 113-124.

[27] V.D. Ho, C.T. Ng, C.J. Coghlan, A. Goodwin, C. Mc Guckin, T. Ozbakkaloglu, D. Losic, Electrochemically produced graphene with ultra large particles enhances mechanical properties of Portland cement mortar, Construction and Building Materials 234 (2020).

[28] J. Tao, X. Wang, Z. Wang, Q. Zeng, Graphene nanoplatelets as an effective additive to tune the microstructures and piezoresistive properties of cement-based composites, Construction and Building Materials 209 (2019) 665-678.

[29] T. Tong, Z. Fan, Q. Liu, S. Wang, S. Tan, Q. Yu, Investigation of the effects of graphene and graphene oxide nanoplatelets on the micro-and macro-properties of cementitious materials, Construction and Building Materials 106 (2016) 102-114.

[30] B. Wang, R. Jiang, Z. Wu, Investigation of the mechanical properties and microstructure of graphene nanoplatelet-cement composite, Nanomaterials 6(11) (2016) 200.

[31] Z. Metaxa, Polycarboxylate based superplasticizers as dispersant agents for exfoliated graphene nanoplatelets reinforcing cement based materials, J. Eng. Sci. Tech. Rev 8 (2015) 1-5.

[32] W. Baomin, D. Shuang, Effect and mechanism of graphene nanoplatelets on hydration reaction, mechanical properties and microstructure of cement composites, Construction and Building Materials 228 (2019) 116720.

[33] P. Xu, J. Loomis, R.D. Bradshaw, B. Panchapakesan, Load transfer and mechanical properties of chemically reduced graphene reinforcements in polymer composites, Nanotechnology 23(50) (2012) 505713.

[34] S. Chatterjee, F. Nafezarefi, N. Tai, L. Schlagenhauf, F. Nüesch, B. Chu, Size and synergy effects of nanofiller hybrids including graphene nanoplatelets and carbon nanotubes in mechanical properties of epoxy composites, Carbon 50(15) (2012) 5380-5386.

[35] M. Shtein, R. Nadiv, M. Buzaglo, K. Kahil, O. Regev, Thermally conductive graphene-polymer composites: size, percolation, and synergy effects, Chemistry of Materials 27(6) (2015) 2100-2106.

[36] F. Sanchez, L. Zhang, Molecular dynamics modeling of the interface between surface functionalized graphitic structures and calcium–silicate–hydrate: interaction energies, structure, and dynamics, Journal of colloid and interface science 323(2) (2008) 349-358.

[37] S.J. Chen, C.Y. Li, Q. Wang, W.H. Duan, Reinforcing mechanism of graphene at atomic level: Friction, crack surface adhesion and 2D geometry, Carbon 114 (2017) 557-565.

[38] AS3972, General purpose and blended cements, Standard, Standard Australia, Australian Standard, 2010.

[39] AS1478.1, Chemical admixtures for concrete, mortar and grout - Admixtures for concrete, Australian Standard, 2000.

[40] ASTM-C109/C109M-07, Standard test method for compressive strength of hydraulic

cement mortars, ASTM International: USA 2008, 2008.

[41] ASTM-C307-03, Standard Test Method for Tensile Strength of Chemical-Resistant Mortar, Grouts, and Monolithic Surfacings Monolithic Surfacings, ASTM International, 2012.

[42] A. Eckmann, A. Felten, A. Mishchenko, L. Britnell, R. Krupke, K.S. Novoselov, C. Casiraghi, Probing the nature of defects in graphene by Raman spectroscopy, Nano letters 12(8) (2012) 3925-3930.

[43] X. Liu, X. Wang, G. Licht, S. Licht, Transformation of the greenhouse gas carbon dioxide to graphene, Journal of CO2 Utilization 36 (2020) 288-294.

[44] Y. Shen, A.C. Lua, A facile method for the large-scale continuous synthesis of graphene sheets using a novel catalyst, Scientific reports 3(1) (2013) 1-6.

[45] A.C. Ferrari, J. Meyer, V. Scardaci, C. Casiraghi, M. Lazzeri, F. Mauri, S. Piscanec, D. Jiang, K. Novoselov, S. Roth, Raman spectrum of graphene and graphene layers, Physical review letters 97(18) (2006) 187401.

[46] N. Kothiyal, S. Sharma, S. Mahajan, S. Sethi, Characterization of reactive graphene oxide synthesized from ball–milled graphite: its enhanced reinforcing effects on cement nanocomposites, Journal of adhesion science and Technology 30(9) (2016) 915-933.

[47] T.T. Mai, C.N. Ha Thuc, H.H. Thuc, Preparation of graphene nano-layer by chemical graphitization of graphite oxide from exfoliation and preliminary reduction, Fullerenes, Nanotubes and Carbon Nanostructures 23(8) (2015) 742-749.

[48] A. Gholampour, M. Valizadeh Kiamahalleh, D.N. Tran, T. Ozbakkaloglu, D. Losic, From Graphene Oxide to Reduced Graphene Oxide: Impact on the Physiochemical and Mechanical Properties of Graphene–Cement Composites, ACS applied materials & interfaces 9(49) (2017) 43275-43286.

[49] M. Hu, K. Hui, K. Hui, Role of graphene in MnO2/graphene composite for catalytic ozonation of gaseous toluene, Chemical Engineering Journal 254 (2014) 237-244.

[50] Y. He, N. Zhang, F. Wu, F. Xu, Y. Liu, J. Gao, Graphene oxide foams and their excellent adsorption ability for acetone gas, Materials Research Bulletin 48(9) (2013) 3553-3558.

[51] Y. Devrim, A. Albostan, Graphene-supported platinum catalyst-based membrane electrode assembly for PEM fuel cell, Journal of Electronic Materials 45(8) (2016) 3900-3907.

[52] A. Gholampour, M.V. Kiamahalleh, D.N. Tran, T. Ozbakkaloglu, D. Losic, Revealing the dependence of the physiochemical and mechanical properties of cement composites on graphene oxide concentration, RSC Advances 7(87) (2017) 55148-55156.

[53] V. Bewick, L. Cheek, J. Ball, Statistics review 9: one-way analysis of variance, Critical care 8(2) (2004) 130.

[54] C.W. Dunnett, A multiple comparison procedure for comparing several treatments with a control, Journal of the American Statistical Association 50(272) (1955) 1096-1121.

[55] A.N. Junior, M.S. Lemos, R.D. Toledo Filho, E.d.M.R. Fairbairn, J. Dweck, Early stages hydration of high initial strength Portland cement, Journal of thermal analysis and calorimetry 113(2) (2013) 659-665.

[56] S. Lv, Y. Ma, C. Qiu, T. Sun, J. Liu, Q. Zhou, Effect of graphene oxide nanosheets of microstructure and mechanical properties of cement composites, Construction and building materials 49 (2013) 121-127.

[57] R. Jadhav, N. Debnath, Computation of X-ray powder diffractograms of cement components and its application to phase analysis and hydration performance of OPC cement, Bulletin of Materials Science 34(5) (2011) 1137-1150.

[58] S. Sharma, N. Kothiyal, Comparative effects of pristine and ball-milled graphene oxide on physico-chemical characteristics of cement mortar nanocomposites, Construction and Building Materials 115 (2016) 256-268.

[59] F. Rendell, R. Jauberthie, M. Grantham, Deteriorated concrete: Inspection and physicochemical analysis, Thomas Telford2002.

[60] J. Elena, M.D. Lucia, X-RAY Diffraction Study of hydration Processes in the Portland Cement, JAESVol 1 14.

[61] M. Horgnies, J. Chen, C. Bouillon, Overview about the use of Fourier transform infrared spectroscopy to study cementitious materials, WIT Trans. Eng. Sci 77 (2013) 251-262.

[62] P. Yu, R.J. Kirkpatrick, B. Poe, P.F. McMillan, X. Cong, Structure of calcium silicate hydrate (C-S-H): Near-, mid-, and far-infrared spectroscopy, Journal of the American Ceramic Society 82(3) (1999) 742-748.

[63] L. Fernández Carrasco, D. Torrens Martín, L. Morales, S. Martínez Ramírez, Infrared spectroscopy in the analysis of building and construction materials, InTech2012.

[64] S. Ghosh, S. Handoo, Infrared and Raman spectral studies in cement and concrete, Cement and Concrete Research 10(6) (1980) 771-782.

[65] P.A. Bhat, N. Debnath, Theoretical and experimental study of structures and properties of cement paste: The nanostructural aspects of C–S–H, Journal of Physics and Chemistry of Solids 72(8) (2011) 920-933.

CHAPTER 5:

STUDYING THE INFLUENCE OF DIFFERENT PRISTINE GRAPHENE DOSAGES AND DESIGN MIXES ON ENHANCING MECHANICAL AND DURABILITY PROPERTIES OF PORTLAND CEMENT MORTARS CURED AT DIFFERENT CURING AGES

THE AIM AND OBJECTIVE OF THIS CHAPTER:

Aim: This chapter aims to explore the effect of different PRG dosages and design mixes on physicochemical, microstructural, mechanical, and durability properties of Portland cement-based mortars cured at short-term and long-term ages.

Objectives 1: investigating the influence of different dosages of PRG and design mixes on mechanical and durability properties of Portland cement-based mortars cured in short-term and long-term periods.

Objectives 2: analysing physicochemical and microstructural properties of PRG-cement based mortars to improve the understanding of the dosage dependence of mechanical and durability properties of Portland cement-based mortars cured in short-term and long-term periods.

Influence of pristine graphene dosages on short-term and long-term mechanical and durability properties of Portland cement mortars

1. Introduction

Graphene, a two-dimensional carbon material discovered in 2004, has shown a significant interest in applying in various types of materials such as metal, polymer, and ceramic. The graphene derivatives, such as graphene oxide (GO), reduced graphene oxide, and pristine graphene (PRG), have recently presented great potential for incorporating into cement-based composites to reinforce their properties. This is due to the excellent properties of graphene materials that have high mechanical and conductivity properties, large aspect ratios and specific surface areas [1-4]. Most research studies have shown that the addition of graphene into cementitious composites could improve their compressive and tensile strengths, and the reinforcement rate of the composites depends on the dosages of graphene used in design mixes [1, 2]. According to Refs. [5, 6], 0.04% GO could enhance the 28-day compressive and tensile strength of cement paste by 14% and 67% respectively, whereas there was no significant influence of GO on compressive strengths of cement pastes when GO dosages were below 0.03%. Lv et al. [7] reported that incorporation of 0.06% GO into the cement mortar increased its compressive and flexural strengths at 28 days by 29.5% and 30.7%, respectively. Another study performed by Zhao et al. [8] revealed that 28-day compressive and flexural strength of the cement-based mortar could enhance by 22.6% and 24.6% respectively when using 0.022% GO additive.

Like GO, research studies on a combination of PRG and cement-based materials have recently shown great potential for enhancing mechanical strengths of PRG-cement composites [1, 2, 9-12]. Wang et al. [9] performed an experimental study to compare compressive strengths of cement-based mortars between the control and the mix containing 0.05% PRG. The study showed that 7-day compressive and flexural strengths of the mortar with 0.05% PRG were

respectively improved by 8% and 24%. Du and Dai Pang [11] studied effects of PRG on properties of cement mortars with four different PRG dosages and showed that PRG additive could significantly decrease water penetration depth, whereas there were no significant effects of PRG on compressive and flexural strengths of cement mortars, which was attributed to the agglomeration of PRG sheets (PRGs) coming from the use of high PRG dosages. Another study performed by Tao et al. [10] with five different PRG dosages added to cement mortars reported that the PRG-cement mortar at 0.05% dosage could improve 28-day compressive and flexural strengths of the mortar by 8.3% and 15.6% respectively; however, the strengths started decreasing when PRG dosages over 0.05% because of the agglomeration of PRG. The effects of the agglomeration of PRG due to its overdose on properties of cement mortars were also reported in Ref. [13]**.** This study experimented with seven different dosages of an ultra-large particle size of PRGs produced by an industrially electrochemical process, and the results showed that 0.07% PRG was identified as the optimal concentration. The mix at this dosage could improve 28-day compressive and tensile strengths by 34.3% and 26.9%, respectively. The study also revealed that the enhancement of PRG-cementitious composites is attributed to the reinforcement of adhesion friction forces between PRGs and cement gels. However, with the further increases in PRG dosages, the enhancement of those properties of mortars was limited due to the impact of the van der Waals force on the sedimentation of PRG suspension.

The effects of PRG on other properties of cementitious composites were also reported in some limited studies. In particular, Du et al. [14] reported that concrete containing 1.5% PRG could reduce its water penetration depth and chloride diffusion by 80%, which is attributed to the increase in tortuosity and pore refinement. Du et al. [15] also revealed that an increase in PRG dosages could significantly reduce the electrical resistance of cement mortars and its electrical conductivity became insensitive to moisture contents when PRGs dosages used over 3.6% by volume of mortars [16]. To date, research on the effects of PRG additives on durability properties of PRG-cement composites has not been sufficiently studied although the durability

properties are important to service life, maintenance costs, and practical applications of the construction structures. In addition, the existing studies only investigate the effects of graphene materials on the short-term mechanical properties (e.g. 7-, 14-, or 28-day curing ages) of cementitious composites and no studies have been done to investigate how graphene materials affect the long-term mechanical properties (e.g. curing ages of 3 months, 6 months, 9 months or over) of cementitious composites. Moreover, as demonstrated in Chapters 2-4, there is a high dependence of mechanical strengths of cement-based mortars on the dosages and sizes of PRG. Although the importance of the dosages and sizes of PRG for enhancing mechanical strengths of cement-based mortars has been confirmed, the effects of another important parameter in the design of cementitious composites, i.e. the water and cement ratio, on the enhancement rate of PRG-cement based mortars is still lack of understanding. From these combination current research gaps, it is necessary to have more in-depth studies on short-term and long-term mechanical and durability properties of PRG-cement based mortars prepared with different dosages of PRG and a different water/cement ratio compared to the design mixes of the previous studies shown in Chapters 2-4.

To address the above-mentioned research gaps, **t**his chapter of this thesis aims to explore how the PRG additive with different dosages influences on short-term and long-term mechanical and durability properties of cementitious-based mortars prepared. Six PRG dosages, i.e. 0%, 0.03, 0.05, 0.07, 0.1, and 0.3%, with the average particle size of 20μm and the water and cement ratio of 0.55 were used. In this study, a higher water and cement ratio compared to the previous studies presented in Chapters 2-4 (water and cement ratio of 0.485) is used to investigate how different design mixes influence the optimal dosage and the properties of the mortars. The study also performs several microanalyses on physicochemical and microstructural properties of the mortars to have a better understanding of microstructures of PRG-cement based composites. The outcomes of this study will provide better knowledge of the effects of PRG on mechanical and durability properties of cement mortars at short-term and long-term curing ages, which is

still lacking in existing research studies on PRG additives and cement-based composites. It also contributes to future studies on using PRG materials as an additive in cement-based composites to reinforce the performance of construction materials.

2. Experimental programs

2.1. Materials

The physical properties of PRGs manufactured by First Graphene Ltd (Perth, Australia) are shown in Table 1. General-purpose cement complied with Australian Standard AS 3972-2010 [17] was used as the binder of mortar mixes and its typical chemical properties are shown in Table 2. Natural sand with 2.36-mm maximum particle sizes was used as fine-aggregate of mortar mixes. MasterGlenium SKY 8100 complied with Australian Standard AS 1478.1-2000 [18] was used as the superplasticizer to improve the dispersion of PRGs in water.

Table 1. Physical properties of pristine graphene sheets.

ID	Particle Size-d50 (μm)	Thickness (nm)	Purity (%)	Poured bulk density (g/cm3)
Size 20μm	20	1-3	~98	~ 0.12

Table 2. Typical chemical properties of general-purpose cement.

Compounds	OPC (%)
CaO	63.28
SiO_2	19.95
Al_2O_3	4.79
Fe_2O_3	3.14
MgO	2.03
Na_2O	0.29
K_2O	0.4
SO_3	2.69
P_2O_5	0.04

2.2. Preparation of mortar composites

The design of the mortars mixes of cementitious composites is shown in Table 3. As shown in the table, there are six different PRG dosages with the water/cement ratio of 0.55 used in this study including 0% (the control mortar), 0.03, 0.05, 0.07, 0.1, and 0.3% by weight of cement binder. First, the aqueous solutions including water, superplasticizer and PRG were sonicated for 30 minutes by using Ultrasonication UIP1000hdT. Then, these solutions were gradually added to natural sand and binder (which were mixed four minutes) for 5 minutes. Next, all samples were vibrated for one minute after mounting to mitigate entrapped air during the mounting process. After that, they were covered with wet fabrics and plastic sheets to prevent moisture loss and were demounted after 24 hours cured at room temperature. Finally, all the samples continued to be cured in a fog room until testing days.

Table 3. Designed mixes of PRG-cement based mortars prepared with different PRG dosages.

Mix	PRG dosage (%)*	Water/cement ratio	Cement (kg/m3)	Water (kg/m3)	Sand (kg/m3)	Superplasticizer (kg/m3)
1	0	0.55	465	256	1545	1.4
2	0.03	0.55	465	256	1545	1.4
3	0.05	0.55	465	256	1545	1.4
4	0.07	0.55	465	256	1545	1.4
5	0.1	0.55	465	256	1545	1.4
6	0.3	0.55	465	256	1545	1.4

* The percentage of pristine graphene based on weight of cement binder.

2.3. Test methods

Different tests were conducted on all the mixes: compressive strength, flexural strength, direct tensile strength, water absorption, void, drying shrinkage, sulfate extension, water penetration for investigating mechanical and durability properties of the mortars. The cubes with the size of 50×50×50 mm^3 complied with ASTM C109/C109M-07 [19] were used for compression strength tests at 7, 28, 90, and 270 days. Dog-bone shaped samples, according to ASTM C307-03 [20], were used for direct tensile strength tests at 28 and 270 days. Prism specimens with size 40x40x160 mm complied with ASTM C348-18 [21] were used for flexural strength tests at 7, 28, 90, and 270 days. The test method according to ASTM C642-06 [22] was used for determining density, water absorption, and voids of mortar mixes at 28 days. 25×25×285 mm prisms were utilized to measure drying shrinkage and sulfate expansion (3% Na_2SO_4) at 7, 14, 21, 28, 56, 90, 120, 150, 180, 210, 240 and 270 days, complied with ASTM C596-09 [23], ASTM C1012-12 [24] and ASTM C490-13 [25]. Water penetration depths of the mortars at 28 days were referred to BS EN 12390-8:2009 [26] with the water pressure of 500 kPa applied in 72 hours; however, in order to ensure all the samples were tested at the same condition and the constant water pressure, the automatic triaxial test system was used for this permeability test as shown in Fig. 1. The values of each designed mix at testing days were calculated by averaging values obtained from three nominal identical samples of each mix.

Raman spectra and particle size distribution were respectively performed by using the HORIBA LabRAM HR Evolution and Mastersizer 2000-Malvern to evaluate the quality and particle sizes of PRGs. X-ray diffraction (XRD) was performed by using the Rigaku MiniFlex 600 X-Ray diffractometer to find the mineralogical characteristics of cement hydration products of the mortars and PRGs. Fourier transform infrared spectroscopy (FTIR) was conducted using the Nicolet 6700 to determine specific functional groups of PRG-cement based mortars. Scanning electron microscopy (SEM) were obtained by using the FEI Quanta 450 to analyze PRG sizes and surface morphologies of the mortars.

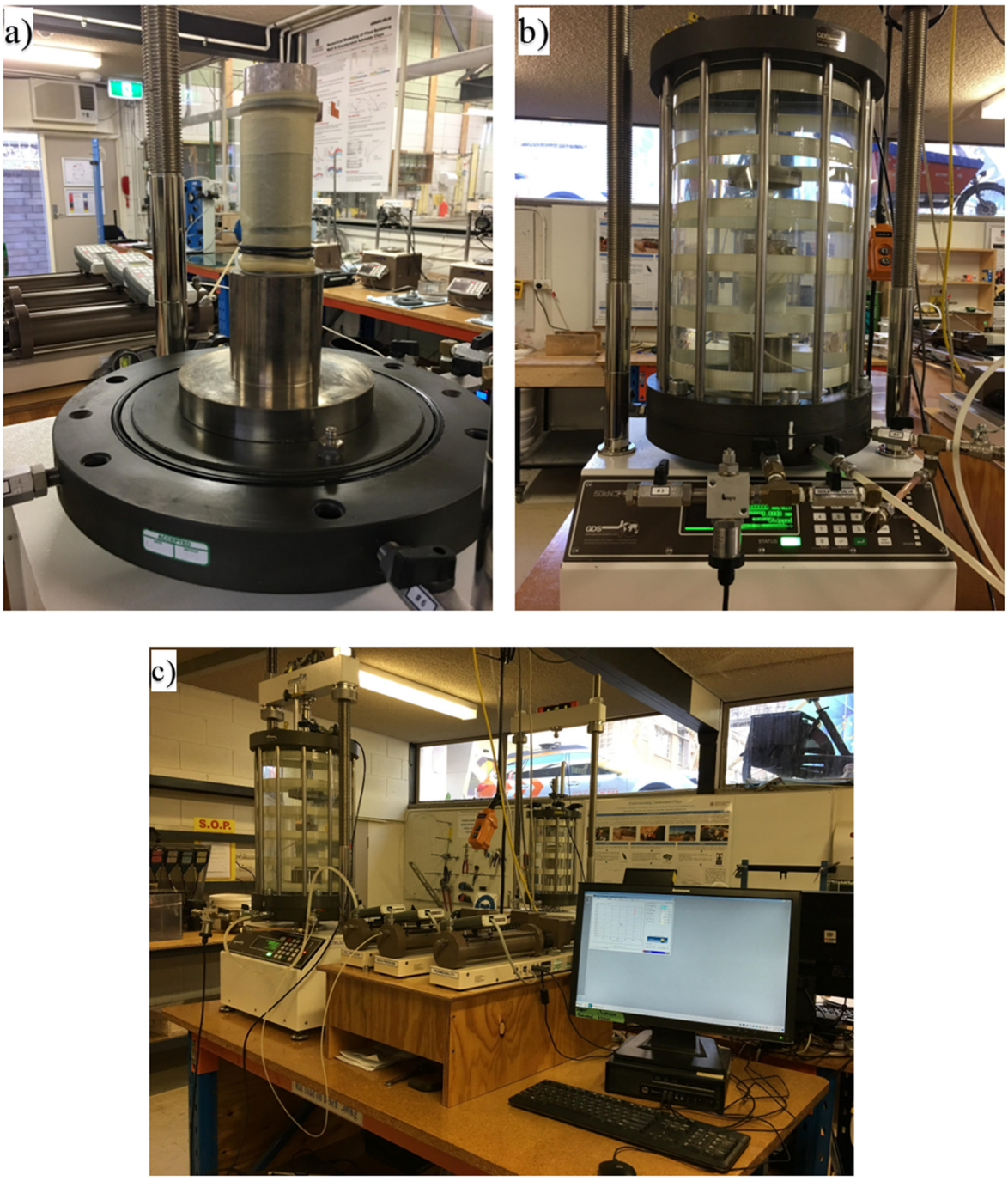

Fig. 1. Triaxial test equipment used for permeability test: (a) Sample preparation, (b) Triaxial cell pressure, (c) Automatic triaxial testing system.

3. Results and Discussion

3.1. Characteristics of PRGs

Fig. 2 shows the typical SEM image, particle size distribution, XRD pattern, and Raman spectrum of the PRG sample used for this study. As shown in Fig. 2(a), the irregular shape of

PRGs can be seen in the SEM image and its average particle size determined from the particle size distribution result is 20±8 μm. It can be seen in Fig. 2(b) that the typical peak of PRGs shown in the XRD result at the position 26.64°, showing that the d-spacing between layers is 0.334nm (based on the Bragg's Law), which is the same as the interplanar spacing of graphite [27, 28], showing the high crystalline structure and high quality of PRG sample. Moreover, the relative intensity ratios of $I_D/I_{D'}$ and I_{2D}/I_G of the PRG sample shown in Raman results in Fig. 2(c) are 1.23 and 0.36 respectively, and the narrow and symmetric 2D peak observed which is different from graphite with a broad and asymmetric 2D peak, showing that the PRG sample in this study does not have basal plane defects and contains few-layer sheets of graphene [29-32]. This presents the high-quality of the PRG sample used in this study and is consistent with its physical properties provided by the provider shown in Table 1.

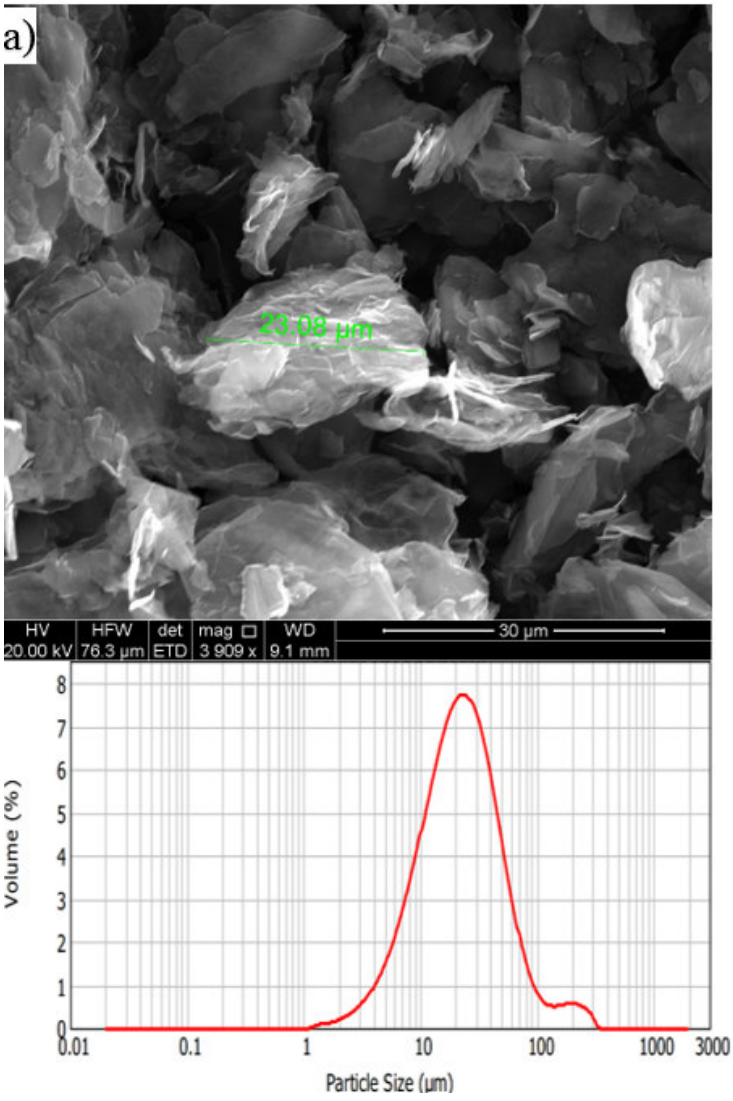
a)
23.08 µm
HV
20.00 kV
HFW
76.3 µm
det
ETD
mag
3 909 x
WD
9.1 mm
30 µm
Volume (%)
Particle Size (µm)
0.01
0.1
1
10
100
1000
3000

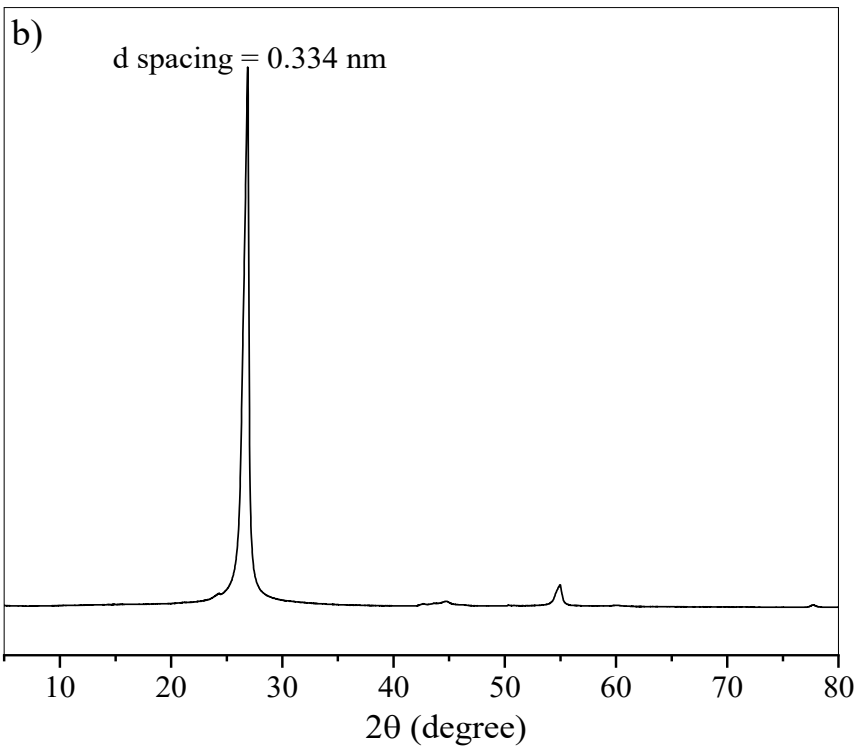
b)
d spacing = 0.334 nm
10
20
30
40
50
60
70
80
2θ (degree)

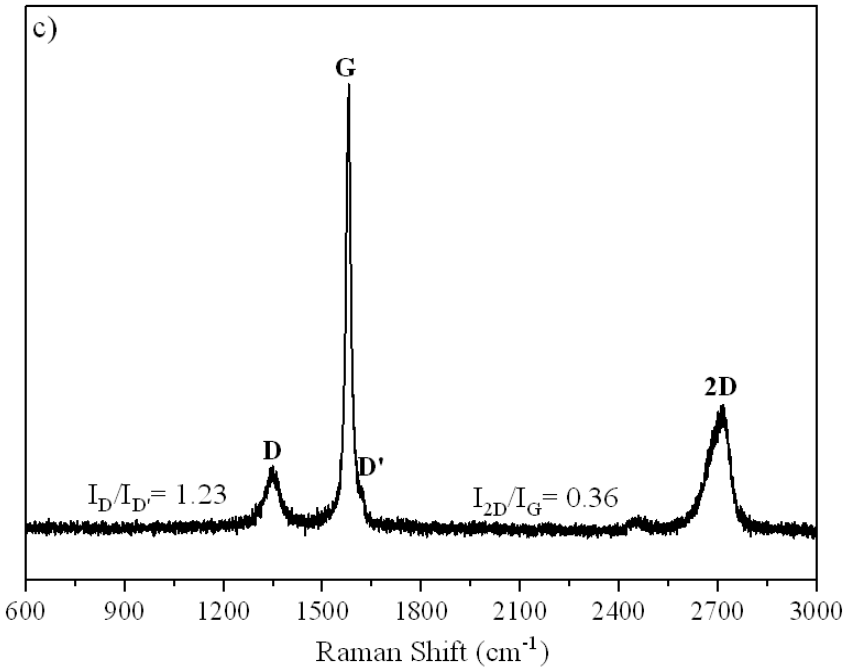

Fig. 2. (a) SEM image and particle size distribution, (b) XRD pattern and (c) Raman spectrum of PRG.

3.2. Mechanical properties of mortar mixes

3.2.1 Compressive strength

Fig. 3(a), (b) shows the compressive strength and enhancement compressive strength rate of the mortar mixes with different PRG dosages at 7-, 28-, 90-, and 270-day curing age. As shown in the figure, the compressive strengths of PRG-cement mortars depend on the PRG dosages and curing ages. Incorporating PRG dosages of from 0.03 to 0.07 into the mortars can increase their compressive strengths at all the testing days. The PRG dosage of 0.07% shows the highest compressive strengths at all curing ages, which are 36.6, 43.8, 43.9, and 39.6 MPa at 7, 28, 90, and 270 days, respectively. Compared to the results of the control mix at these curing ages, which are 34.5, 39, 41.2, and 36.5 MPa respectively, the strengths of the mix containing 0.07% PRG improve approximately 6.2, 12.5, 6.7, and 8.6% respectively. The improvement of those PRG-cement based mortars can be attributed to the enhancement of cementitious gels due to the closer distance between cement particles caused by van der Waals forces between PRGs [2, 12], and the improvement of PRG-cementitious gels due to adhesion friction forces between

surface areas of PRGs and cementitious gels which are consistent with previous experimental and molecular dynamic simulation research in PRG-cement based composites [12, 33]. When the PRG dosage used over the optimal dosage of 0.07%, there are significant decreases in compressive strengths of the mortars, which show negative enhancements in these mixes of 0.1% and 0.3% at different testing ages, which account for the agglomeration and formation of multi-layers PRGs in PRG solutions due to the influence of the van der Waals forces between PRGs resulting in the negative impact on the cement hydration process and the interaction of PRGs and cementitious gels [13, 34, 35]. It can also be seen in the figure that the compressive strengths of the mortar mixes increase with the curing age up to 90 days, and then decrease with the long-term curing age of 270 days. The fall in compressive strengths of the mortars at the long-term of curing age of 270 days can be attributed to the effect of calcium leaking in cement-based composites during a long-term curing process in a fog room. This is consistent with previous research on the influence of calcium leaking on the properties of cementitious composites [36-38].

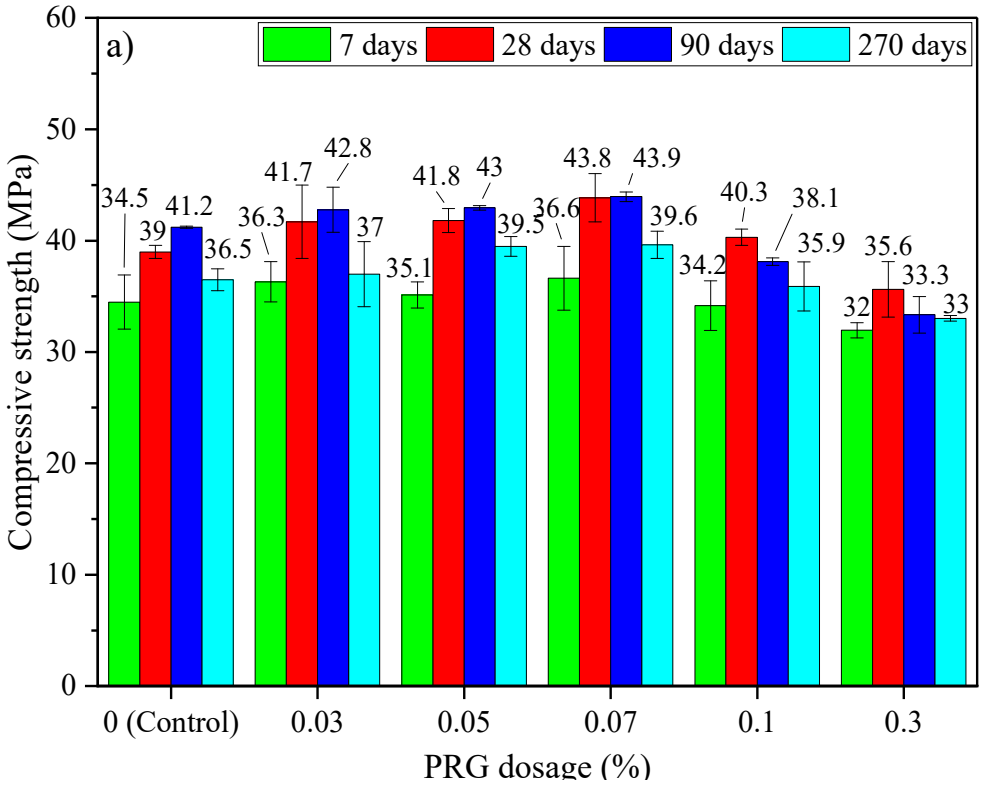

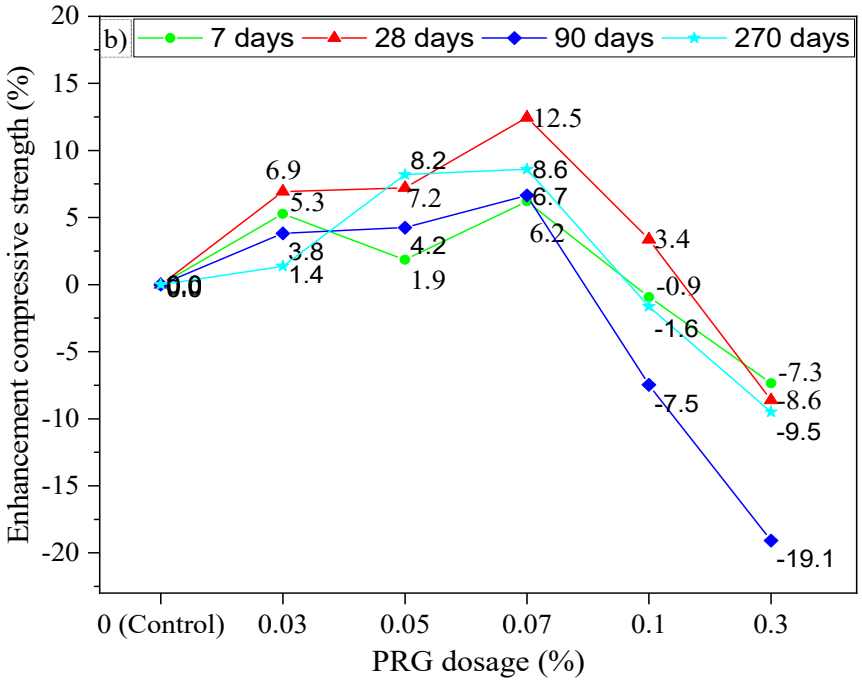

Fig. 3. (a) Compressive strength and (b) enhancement compressive strength of PRG-cement based mortars prepared with different PRG dosages at 7, 28, 90, and 270 days.

3.2.2 Flexural strength

The flexural strength and enhancement flexural strength rate of the mortars with different PRG dosages at curing ages of 7, 28, 90, and 270 days are shown in Fig. 4(a) and (b). As shown in the figure, the flexural strengths of PRG-cement based mortars are dependent on the PRG dosages and curing ages. The addition of PRGs into the mortars can slightly increase their flexural strengths at different curing ages. At the optimum dosage of 0.07% PRG, the 7-, 28-, 90-, and 270-day flexural strengths of the mortar are 6.03, 6.35, 6.68, and 7.21 MPa, respectively, which are 3.7, 4.0, 3.3, and 4.1% higher than the corresponding strengths of the control mortar (5.81, 6.1, 6.64, and 6.93 MPa respectively). The slight enhancement in flexural strengths of PRG-cement based mortars can be attributed to the benefit of PRGs in enhancing the development of crack paths in the cement matrix, resulting in the reduction of crack widths in structures. It can also be seen from the figure that the mixes containing 0.1% and 0.3% PRG show the slight decrease in 270-day flexural strengths compared to the control mix, which can account for the negative effect of the agglomeration and formation of multi-layers PRGs

resulting in the negative impact on the cement hydration process and the interaction of PRGs and cementitious gels [13, 34, 35].

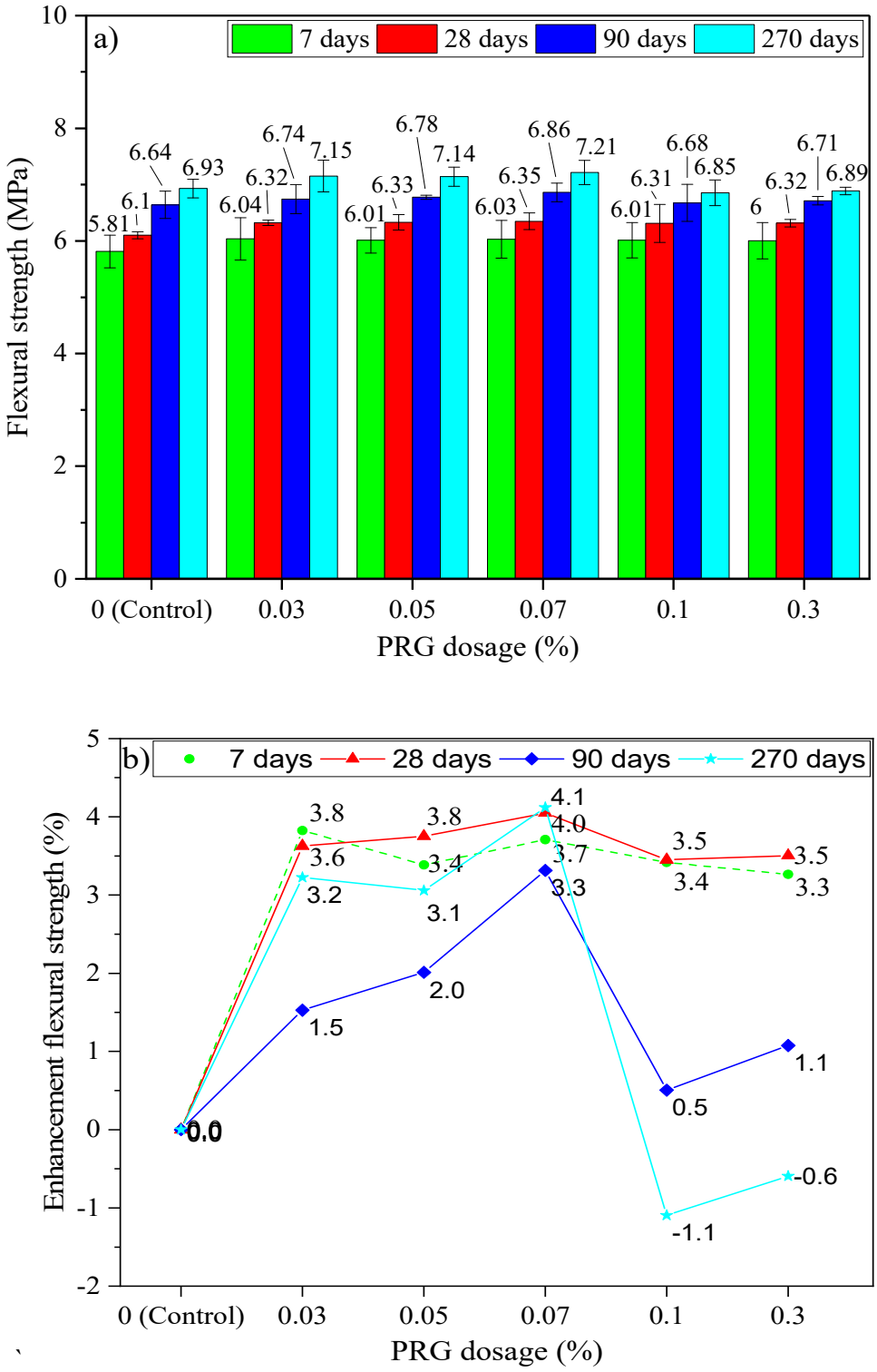

Fig. 4. (a) Flexural strength and (b) enhancement flexural strength of PRG-cement based mortars prepared with different PRG dosages at 7, 28, 90, and 270 days.

3.2.3 Tensile strength

Fig. 5(a), (b) shows the direct tensile strength and enhancement tensile strength rate of the mortars with different PRG dosages at the curing ages of 28 and 270 days. It can be seen in the figure that the trend in direct tensile strengths of the mortars is similar to that in flexural strengths which are dependent on the PRG dosages and curing ages. Incorporating PRGs into the mortars can improve their tensile strengths at 28-day and 270-day curing ages. The dosage of 0.07% PRG presents the highest strength enhancements at 28 and 270 days that are 3.79 and 4.14 MPa, respectively, which are 5.6 and 10% higher than the corresponding strengths of the control mix (i.e. 3.59 and 3.76 MPa respectively). The improvement in direct tensile strengths of PRG-cement based mortars can be attributed to the enhancement in PRG-cementitious gels due to adhesion friction forces between PRGs and cement gels that benefit the resistance from pull-out direct tensile forces. As also shown in the figure, when PRG used over the optimum dosage of 0.07%, the mixes containing 0.1% and 0.3% PRG show less improvements in tensile strengths compared to the others, which can be due to the negative effect of the poor dispersion of PRG suspension owing to the effect of the van der Waals forces between PRGs, leading to the agglomeration of PRGs and the formation of multi-layers PRGs and resulting in diminishing the interaction of PRGs and cementitious gels [13, 34, 35].

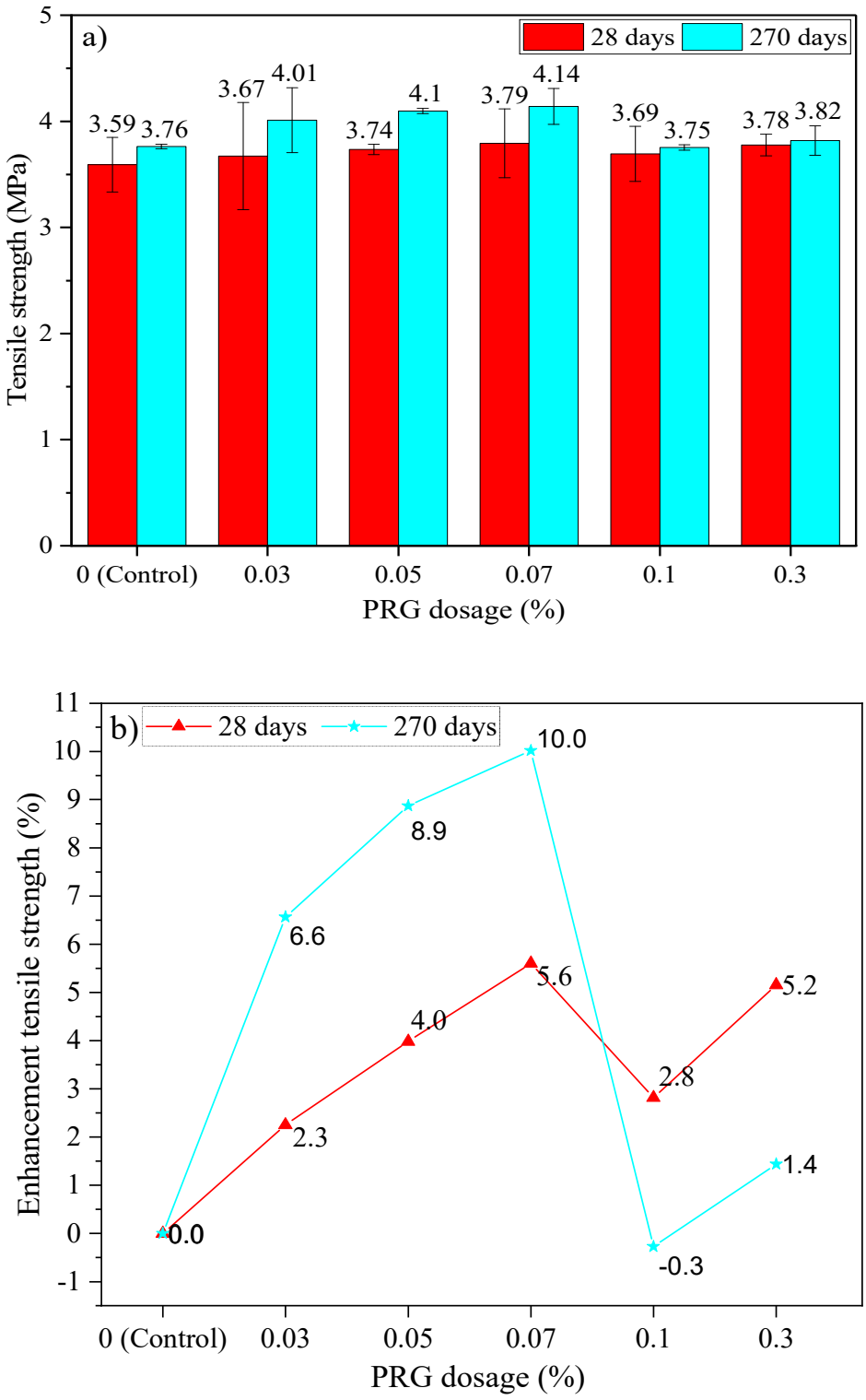

Fig. 5. (a) Direct tensile strength and (b) enhancement direct tensile strength of PRG-cement based mortars prepared with different PRG dosages at 28 days and 270 days.

3.3. Durability-related properties

3.3.1 Water absorption and voids

Fig. 6(a), (b) shows the results of water absorptions and voids (volume of permeable pore space) of the mortars with different PRG dosages at 28-day curing age. It can be seen in the figure that the water absorptions and voids of PRG-cement based mortars are dependent on the PRG dosage. Incorporating a small amount of PRG content into cement-based mortars results in a decrease in the water absorption and void of the mortars. The mixes containing 0.03, 0.05, and 0.07% PRG develop 11.1, 8.0, and 8.2% lower water absorptions than the control mix, respectively. However, when PRG is used over 0.07%, the water absorptions of the mixes with 0.1 and 0.3% PRG are 5.8 and 4.6% higher than the control. The trend of voids shown in Fig. 6(b) is similar to that of water absorptions. The addition of PRG of 0.03, 0.05, and 0.07% develop 10.6, 9.0, and 8.5% lower voids than the control, whereas the voids of the mixes containing 0.1 and 0.3% are 4.7 and 3.1% higher than the control. The lower water absorptions and voids of the mixes containing 0.03, 0.05, and 0.07% PRG are attributed to the higher content of hydration products in these mixes that consequently result in more compact microstructures and lower porosities.

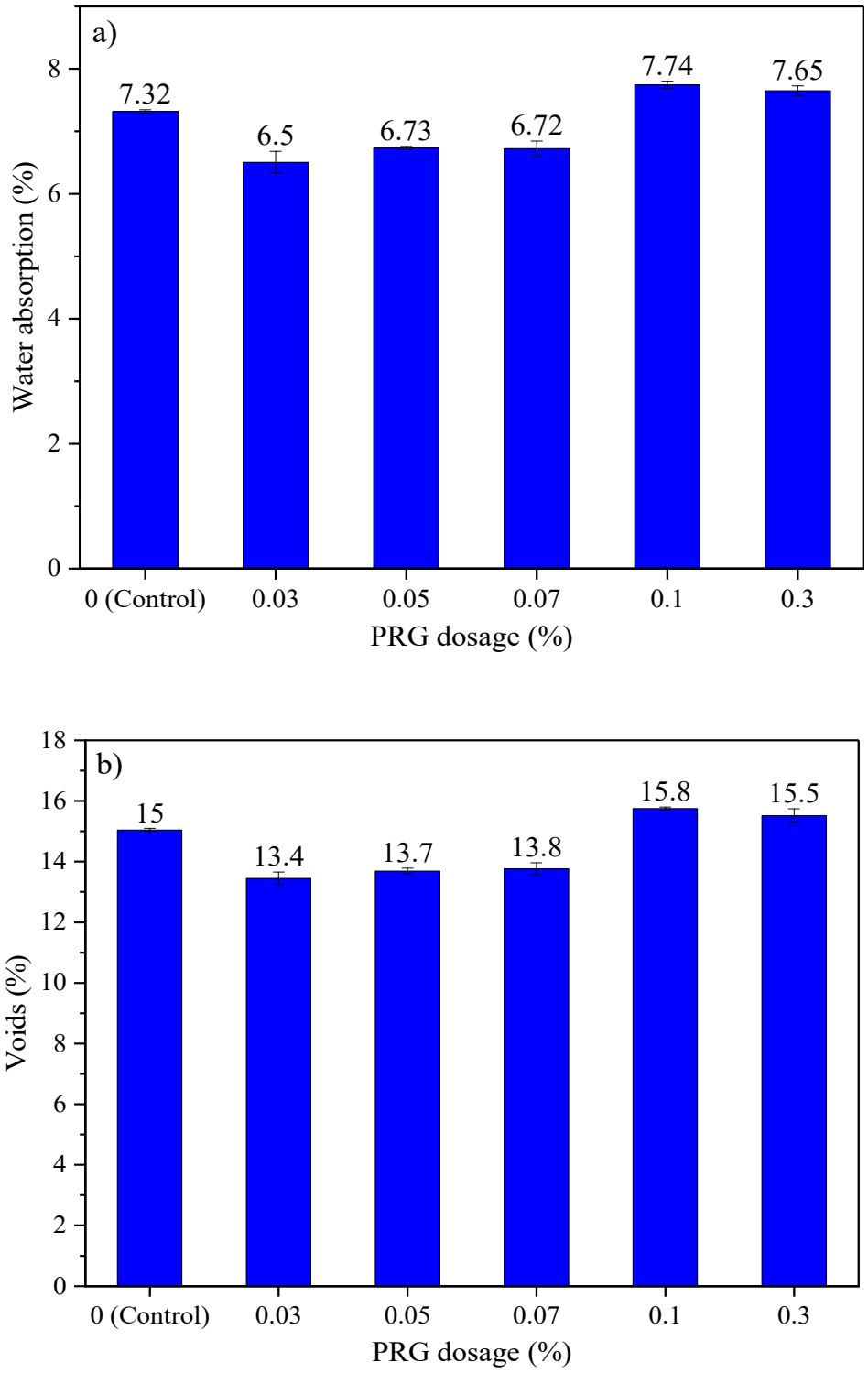

Fig. 6. (a) Water absorptions and (b) voids of PRG-cement based mortars prepared with different PRG dosages at 28 days.

3.3.2 Drying shrinkage

Fig. 7 presents the drying shrinkage of the mortars prepared with different PRG dosages at different curing ages. As shown in the figure, all the mixes develop high drying shrinkage at the early curing age of 7 days, and hence, gradually increase with curing ages and show steadily after 240 days. The addition of PRG to cement-based mortars does not show a clear positive effect on the results of drying shrinkage. Only two mixes containing 0.03% and 0.3% slightly develop lower drying shrinkage than the control throughout from 7-day to 270-day curing ages, which decrease approximately 7.5 and 7.0% at 7 days and 6.0% and 3.4% at 28 days respectively. There are no significant differences in the results of drying shrinkage between the other PRG mixes and the control. The reason for being no clear positive effect of PRG on drying shrinkage of the mortars can be attributed to the random distribution of PRGs in the cement matrix that can create tortuous paths in the cement matrix to prevent moisture loss during the drying shrinkage process. The mixes with a higher amount of PRG dosages can have more chances to increase tortuous paths in the cement matrix. However, it can be seen in the figure that the mix containing 0.03% PRG has lower drying shrinkage than those containing higher PRG dosages. This means that the moisture loss during the drying shrinkage process highly depends on the arrangement of PRGs in the cement matrix.

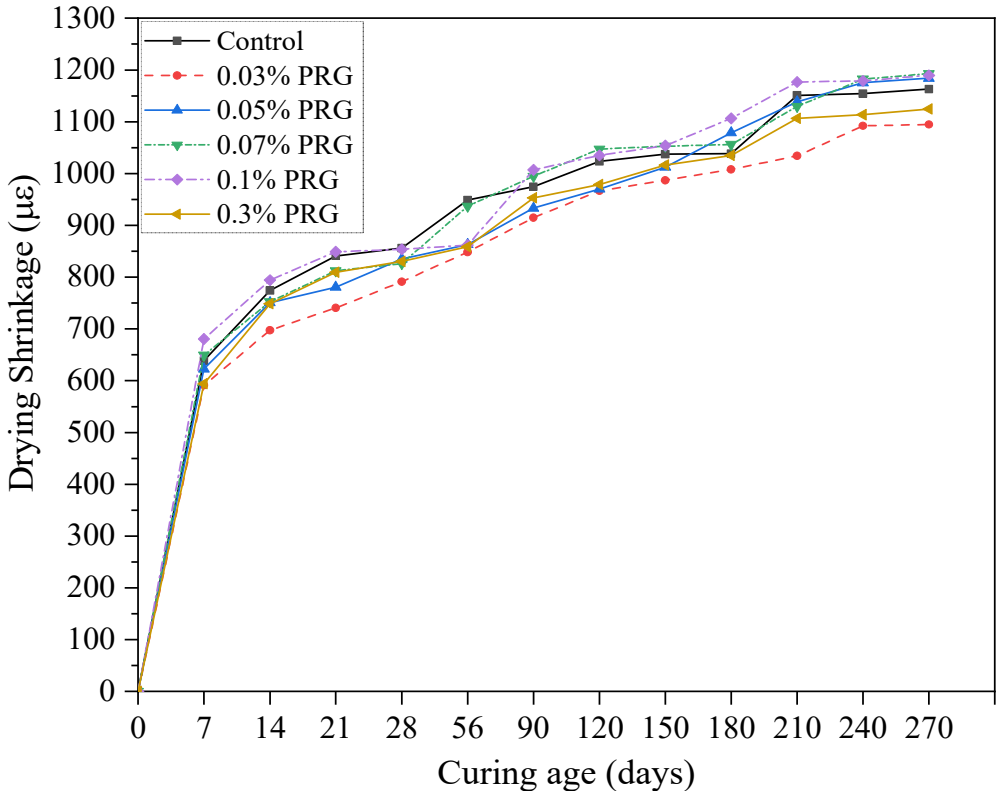

Fig. 7. Drying shrinkage of PRG-cement based mortars prepared with different PRG dosages at different ages.

3.3.3 Sulfate expansion

Fig. 8 shows the sulfate expansion of PRG-cement based mortars containing different PRG dosages immersed in the sodium sulfate solution at different curing ages. It can be seen in the figure that the incorporating of PRG into cement-based mortars generally shows the positive influence on resisting the sulfate solution. The mix containing 0.07% PRG shows the optimum dosage with the lowest sulfate expansion in the mortars, showing that its 7-day and 270-day sulfate expansion significantly develop approximately 40.3% and 43.7% lower than those of the control, respectively. There are no considerable differences in the long-term results of sulfate expansion between the other PRG mixes and the control. The benefit of PRG on sulfate expansion of cement-based mortars can be attributed to the positive effect of tortuous paths formed PRGs on impeding the penetration of sulfate ion in the cement matrix, resulting in a

lower amount of ettringite products created during the immersion process of mortars in the sulfate solution.

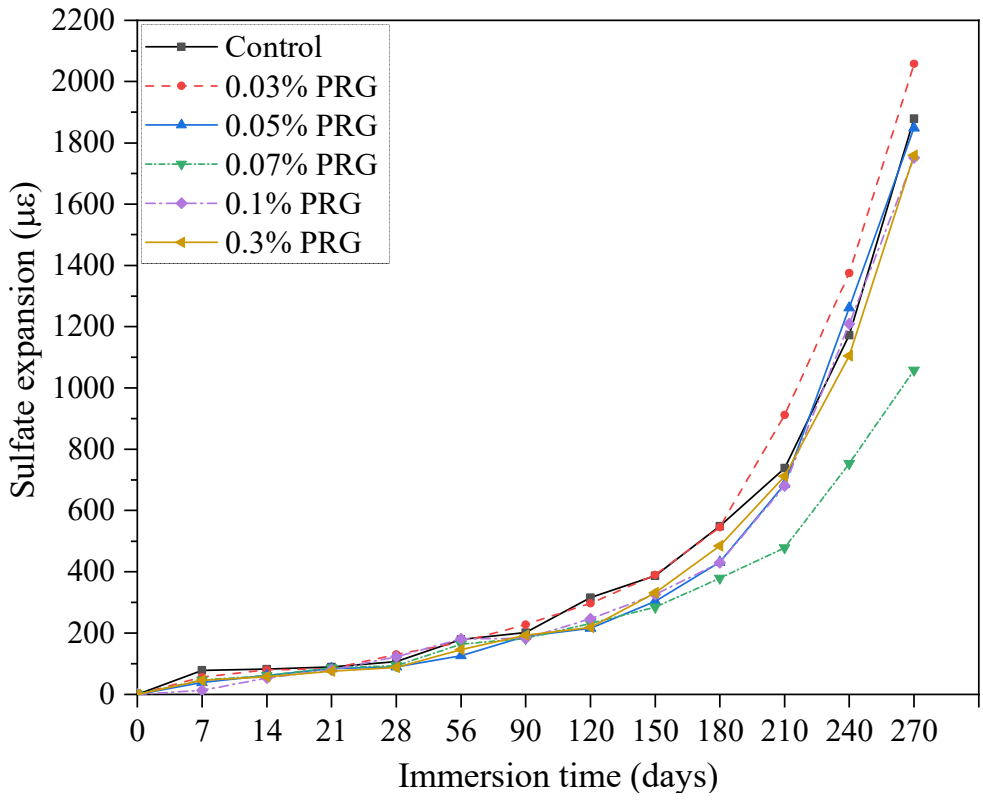

Fig. 8. Expansion of PRG-cement based mortars prepared with different PRG dosages immersed in the sulfate solution at different ages.

3.3.4 Water penetration

Table 4 shows the average water penetration depths of the mortars with different PRG dosages at 28 days. It is noted that this test was performed and controlled by the automatic triaxial testing system (as shown in Fig. 1) and the results of water penetration depths were calculated based on the ratio of the amount of water penetration into testing samples recorded by the system and areas of testing samples. As shown in Table 4, while the mix containing 0.03% PRG does not affect the water penetration depth of the cement mortar, the water penetration depth of the mixes with 0.05, 0.07, 0.1, and 0.3% PRG can decrease by 32.64, 4.02, 28.29, and 36.66% respectively compared to the control mix. The improved resistance to water penetration of PRG-cement

based mortars can be attributed to more tortuous paths for ingress of water that were formed by extensive barriers created from PRGs in the cement matrix.

Table 4. Average water penetration depth of hardened mortars with different PRG dosages at 28 days.

Mix	PRG dosage (%)	Penetrated water from triaxial test (mm3)	Average water penetration depth (mm)	Change as compared to the control (%)
1	0	4.06	2.00	
2	0.03	4.25	2.10	4.70
3	0.05	2.74	1.35	-32.64
4	0.07	3.89	1.92	-4.02
5	0.1	2.91	1.44	-28.29
6	0.3	2.57	1.27	-36.66

3.4. Microstructural analysis of cement-based mortars containing different PRG dosages

Complementary XRD, FTIR, and SEM characterizations were performed to examine the influence of different PRG dosages on the physicochemical and microstructure characteristics of the mortars. The four different PRG concentrations, including 0%, 0.03%, 0.07%, and 0.3%, representing the control mix, the mix with the lowest dosage, the optimal dosage based on mechanical results, and the mix with the highest dosage respectively, were selected for analysis

3.4.1 XRD and FTIR analysis

Fig. 9(a) shows the XRD patterns of the cement-based mortars with different dosages of PRG at 28 days. It is important to note that there are three main hydration products in the cement matrix created from the cement hydration process including calcium silicate hydrate (CSH), portlandite (CH), ettringite (Aft), and un-hydrated cement binder (Alite, belite) [12, 39, 40]. Among them, CSH gels are the main part contributing to mechanical strengths of cementitious composites. However, there are some difficulties in identifying them in XRD results because they are often as amorphous phases, but the content of CSH gels and the hydration degree of

the binder can be estimated by the content of portlandite and un-hydrated cement binder [12, 41, 42]. To ensure an equal percentage of natural sand in each sample of each mix, these XRD spectra were standardized to the equal intensity at the major peak of natural sand of 26.7° [12, 42, 43]. It can be seen in Fig. 9(a) that although all the samples have similar spectrum patterns with similar main crystalline phases confirmed, they also show slight differences in their intensities. The peaks of portlandite phases identified at 18.2°, 34.2° and 47.1° [12, 42, 44] of the mixes containing PRG show higher intensities than the control mix. This can be attributed to the beneficial effect of PRGs on the hydration of cement pastes [12, 42, 43], which is consistent with the mechanical results at 28 days of the mortars as discussed above in Section 3.2.

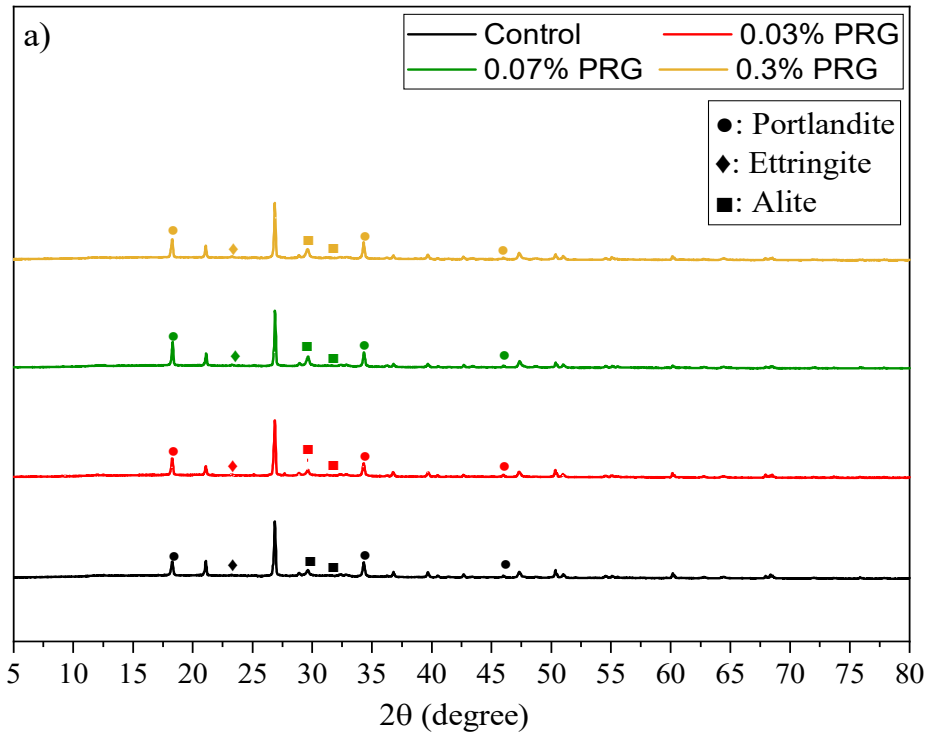

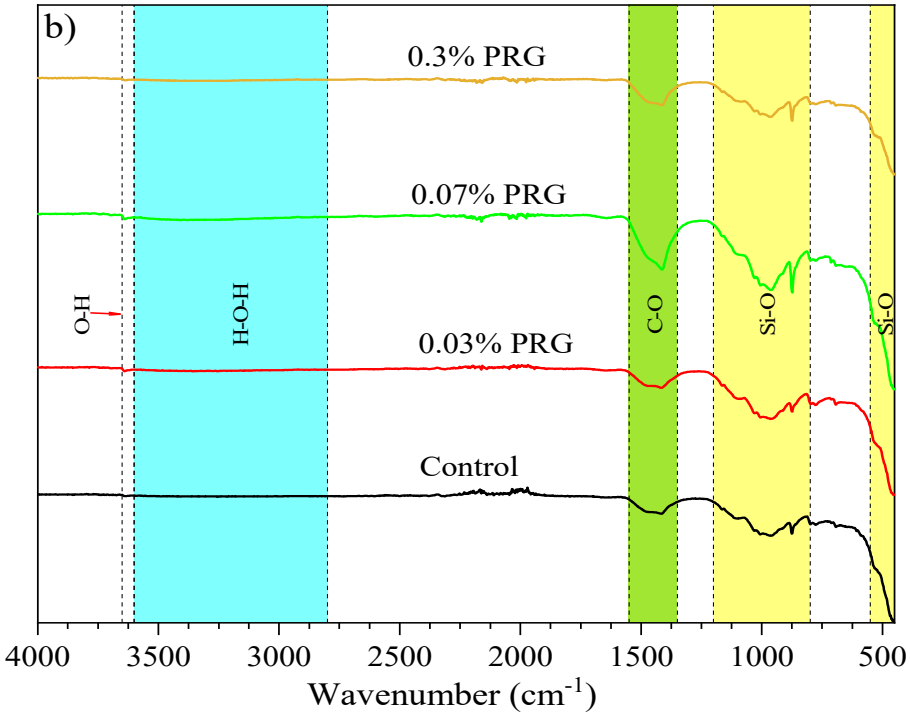

Fig. 9. (a) XRD patterns and (b) FTIR spectra of PRG-cement based mortars prepared with different PRG dosages at 28 days.

Fig. 9(b) presents the FTIR patterns of the different mortar mixes at 28 days. As shown in the figure, all the samples have similar spectra with some functional groups determined in the range of the band from 400 cm^{-1} to 4000 cm^{-1}, showing that there are no new distinguishing groups observed in all the samples, which are consistent with the results of XRD discussed above. It can also be seen in the figure that some functional groups are observed in these samples including Si-O bonds in CSH gels, which are in the ranges of 400-550 cm^{-1} and 800-1200 cm^{-1} [45, 46], and O-H bond in CSH gels and portlandite, which are in the ranges of 2800-3600 cm^{-1} [46, 47] and 3600-3650 cm^{-1} [45, 48], respectively. C-O bond in $(CO_3)^{2-}$ groups are observed in a range of 1350-1550 cm^{-1} [46, 47]. Although all the spectra show the same functional groups, it is evident from the figure that the intensities of the functional groups belong to CSH gels in the mixes containing PRG are higher than the control. This can account for the beneficial effect of PRG additive on the hydration of cement pastes, which is consistent with XRD results above and 28-day mechanical results of the mortars as discussed in Section 3.2.

3.4.2 SEM analysis

Fig. 10(a)-(h) shows the SEM images of different mortar mixes at 28 days. As shown in the figure, although SEM images of these mixes have similar components, they are different from how they are distributed and compacted in microstructures. The mixes containing 0% and 0.3% show less compact in their microstructures, which are large sizes in microcracks, less dense in the interfacial transition zones (ITZ), and larger contents of pores distributed in the cement matrix (Fig. 10(a), (b) and Fig. 10(g), (h), respectively), than those containing 0.03% and 0.07% (Fig. 10(c), (d) and Fig. 10(e), (f), respectively). It can also be seen from the figure that the mix with the dosage of 0.07% shows a better microstructure pattern with more compact, less microcracks observed, compared to the other samples. This can be due to a higher cement hydration degree of this mix, resulting in its stronger enhancement rates in mechanical strengths as discussed in Section 3.2.

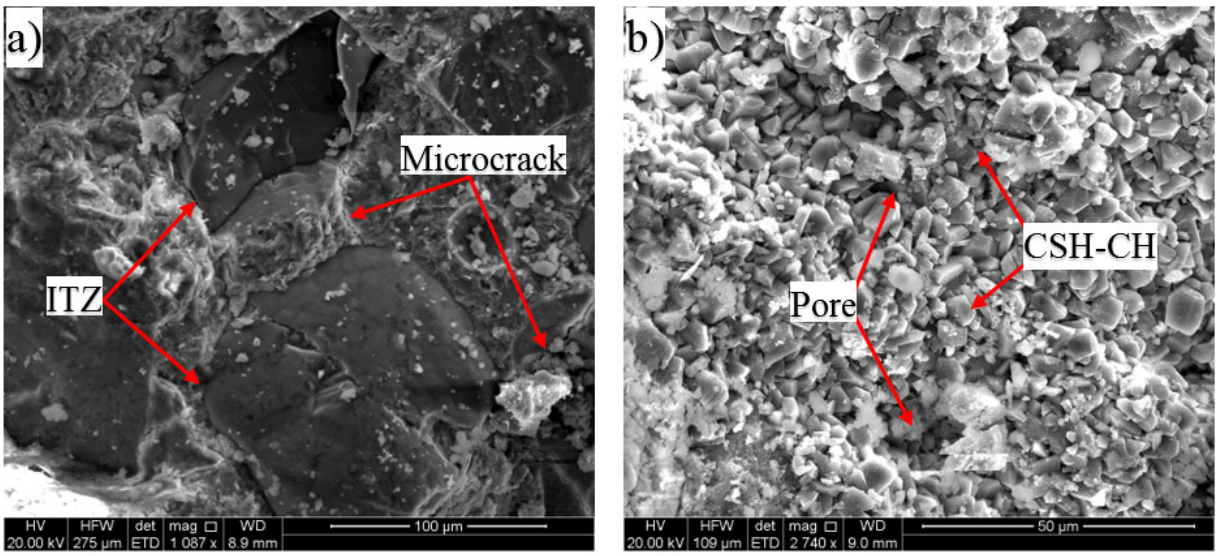

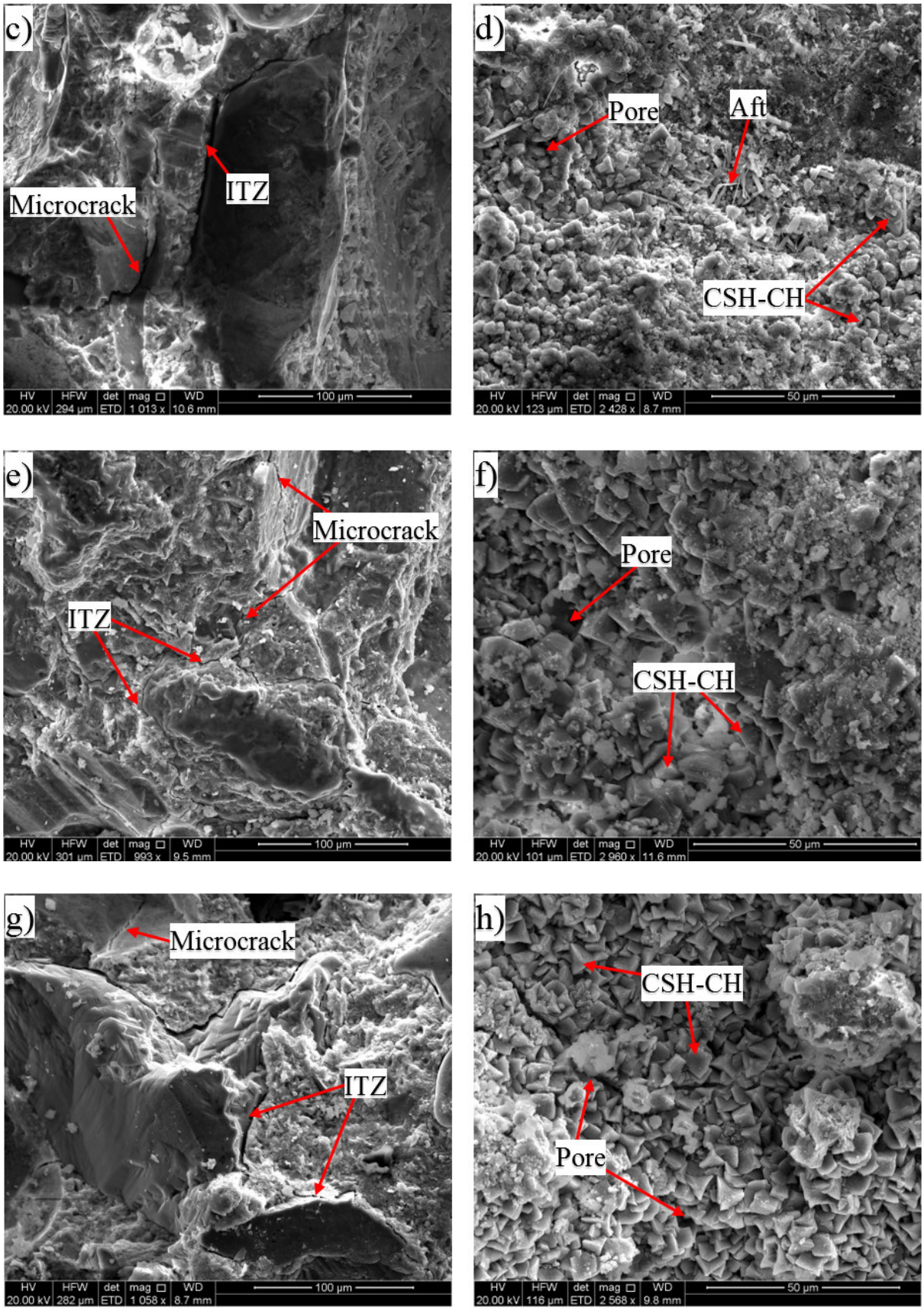

Fig. 10. SEM images of PRG-cement mortars prepared with different PRG dosages at 28 days: (a, b) control, (c, d) 0.03% PRG, (e, f) 0.07% PRG, (g, h) 0.3% PRG.

3.5. Further discussion

From the results of the mechanical and durability properties of cement-based mortars analyzed above, it can be concluded that the mechanical and durability properties of the mortars are dependent on the dosage of PRG. The addition of PRG to the mortars can improve the short-term and long-term mechanical and durability properties of cement mortars. The benefit of PRG additive for cementitious composites can be attributed to the improvement of cementitious gels thanks to the reduction of distances between cement particles in the cement matrix due to the effect of van der Waals forces between PRGs [2, 12, 49], together with the importance of adhesion friction forces created from surface areas of PRGs and cementitious gels [12]. This combination results in the development of microstructures of PRG-cement mortars, contributing to a better capacity in stress-distribution and the propagation of cracks in the mortars. However, when a large amount of PRG is used, the agglomeration of PRGs due to the effect of van der Waals forces between them will happen. This leads to the formation of multi-layers PRGs in the cement matrix, resulting in reducing the benefit of the interaction between PRGs and cementitious gels. Compared to the results presented in Chapter 4, although these studies were designed in different water and cement ratios and PRG sizes, the PRG dosage of 0.07% was identified as the optimum dosage for enhancing mechanical strengths of cement-based mortars in all the studies. Therefore, it can be concluded that if PRG additives used in cement-based mortars are high-quality materials, the optimized PRG dosage for enhancing mechanical strengths of PRG-cement based mortars will be independent with water and cement ratios as well as PRG sizes. However, it is also important to note that the enhancement strength rates of PRG-cement based mortars in this study are less significant. This could be due to the effects of PRG sizes or strengths of cementitious gels which are dependent on water and cement ratios. These influence factors should have further investigations in the future to have a better understanding of those factors on the enhancement of cement-based composites. In addition, based on the results of this study, it can be seen that 270-day compressive strengths of the

mortars were decreased after a long term curing in a fog room, which can be due to the calcium leaking of mortars during the long-term curing process. This is also an important factor that should have further studies on the effect of different curing conditions on the strengths of PRG-cement based composites to better understand the mechanism of this observed trend.

4. Conclusions

The results of this Chapter have presented the effects of the PRG dosages on short-term and long-term mechanical and durability properties of cement-based mortars. The following conclusions have been drawn from the results and discussion:

- The study confirmed the results from the previous studies that the properties of cement-based mortars are dependent on the dosage of PRG. The addition of PRG additive to cement-based mortars can enhance the compressive, flexural, and tensile strengths of the mortars at short-term and long-term curing ages. The PRG dosage of 0.07% is also identified as the optimized dosage for enhancing the mechanical strengths of the mortars prepared with the PRG size of 20μm and the water and cement ratio of 0.55.
- At the optimal dosage of 0.07%, 7-, 28-, 90-, and 270-day compressive and flexural strengths of the mix containing PRG increase approximately 6.2, 12.5, 6.7, and 8.6%, and 3.7, 4.0, 3.3, and 4.1% higher than those of the control mix, respectively. The 28-day and 270-day tensile strengths of the mortars at this dosage develop approximately 5.6 and 10% higher than the corresponding strengths of the control mix. The improvement in mechanical strengths of cement-based mortars can be attributed to the enhancement in PRG-cementitious gels thanks to the reduction of distances between cement particles in the cement matrix due to the effect of van der Waals forces between PRGs, and the importance of adhesion friction forces created from surface areas of PRGs and cementitious gels.
- When PRG is used over the optimal dosage of 0.07%, the addition of PRG to the mortars is either a negative influence on compressive strengths or a slight increase in flexural and

tensile strengths. This accounts for the effect of the agglomeration of PRGs in the cement matrix due to the van der Waals forces between PRGs.

- Incorporating a small number of PRG additives into cement-based mortars can decrease water absorptions and voids of the mortars. The mixes containing 0.03, 0.05, and 0.07% PRG develop 11.1, 8.0, and 8.2% & 10.6, 9.0, and 8.5% lower water absorptions & voids than the control mix, respectively. This benefit can be due to the higher content of hydration products in these mixes, leading to more compact microstructures and lower porosity in those mixes.
- The mixes containing 0.03% and 0.3% slightly develop lower drying shrinkage than the control throughout from 7-day to 270-day curing ages, which decrease approximately 7.5 and 7.0% at 7 days and 6.0% and 3.4% at 28 days, respectively. There are no significant differences in the results of drying shrinkage between the other PRG mixes and the control. The reason for being no clear positive effect of PRG on drying shrinkage of the mortars can be attributed to the random distribution of PRGs in the cement matrix that can create tortuous paths in the cement matrix to prevent moisture loss during the drying shrinkage process.
- The mix containing 0.07% PRG shows a significant decrease in the short-term and long-term sulfate expansion of cement-based mortars, which develop 40.3% and 43.7% lower sulfate expansion at 7 and 280 days than those of the control, respectively. The benefit of PRG on sulfate expansion of cement-based mortars can be attributed to the positive effect of tortuous paths formed PRGs on impeding the penetration of sulfate ion in the cement matrix, resulting in a lower amount of ettringite products created during the immersion process of mortars in the sulfate solution.
- The addition of PRG to cement-based mortars can improve the water penetration resistance of the mortars. The water penetration depth of the mixes containing 0.05, 0.07, 0.1, and 0.3% PRG can significantly decrease by 32.64, 4.02, 28.29, and 36.66%, respectively,

compared to the control mix. The improved resistance to water penetration of PRG-cement based mortars can be attributed to more tortuous paths for ingress of water that were formed by extensive barriers created from PRGs in the cement matrix.

- The results from XRD, FTIR, and SEM analyses show that the mechanical strengths of PRG-cement mortars correlate with their physicochemical and microstructure properties. The mixes with higher mechanical strengths show better patterns in their microstructures.

REFERENCES

[1] E. Shamsaei, F.B. de Souza, X. Yao, E. Benhelal, A. Akbari, W. Duan, Graphene-based nanosheets for stronger and more durable concrete: A review, Construction and Building Materials 183 (2018) 642-660.

[2] H. Yang, H. Cui, W. Tang, Z. Li, N. Han, F. Xing, A critical review on research progress of graphene/cement based composites, Composites Part A: Applied Science and Manufacturing 102 (2017) 273-296.

[3] B. Han, S. Sun, S. Ding, L. Zhang, X. Yu, J. Ou, Review of nanocarbon-engineered multifunctional cementitious composites, Composites Part A: Applied Science and Manufacturing 70 (2015) 69-81.

[4] A.K. Geim, K.S. Novoselov, The rise of graphene, Nature materials 6(3) (2007) 183-191.

[5] X. Li, Y.M. Liu, W.G. Li, C.Y. Li, J.G. Sanjayan, W.H. Duan, Z. Li, Effects of graphene oxide agglomerates on workability, hydration, microstructure and compressive strength of cement paste, Construction and Building Materials 145 (2017) 402-410.

[6] X. Li, Z. Lu, S. Chuah, W. Li, Y. Liu, W.H. Duan, Z. Li, Effects of graphene oxide aggregates on hydration degree, sorptivity, and tensile splitting strength of cement paste, Composites Part A: Applied Science and Manufacturing 100 (2017) 1-8.

[7] S. Lv, J. Liu, T. Sun, Y. Ma, Q. Zhou, Effect of GO nanosheets on shapes of cement hydration crystals and their formation process, Construction and Building Materials 64 (2014) 231-239.

[8] L. Zhao, X. Guo, C. Ge, Q. Li, L. Guo, X. Shu, J. Liu, Mechanical behavior and toughening mechanism of polycarboxylate superplasticizer modified graphene oxide reinforced cement composites, Composites Part B: Engineering 113 (2017) 308-316.

[9] B. Wang, R. Jiang, Z. Wu, Investigation of the mechanical properties and microstructure of graphene nanoplatelet-cement composite, Nanomaterials 6(11) (2016) 200.

[10] J. Tao, X. Wang, Z. Wang, Q. Zeng, Graphene nanoplatelets as an effective additive to tune the microstructures and piezoresistive properties of cement-based composites, Construction and Building Materials 209 (2019) 665-678.

[11] H. Du, S. Dai Pang, Enhancement of barrier properties of cement mortar with graphene nanoplatelet, Cement and Concrete Research 76 (2015) 10-19.

[12] V.D. Ho, C.-T. Ng, C.J. Coghlan, A. Goodwin, C. Mc Guckin, T. Ozbakkaloglu, D. Losic, Electrochemically produced graphene with ultra large particles enhances mechanical properties of Portland cement mortar, Construction and Building Materials 234 (2020) 117403.

[13] V.D. Ho, C.T. Ng, C.J. Coghlan, A. Goodwin, C. Mc Guckin, T. Ozbakkaloglu, D. Losic, Electrochemically produced graphene with ultra large particles enhances mechanical properties of Portland cement mortar, Construction and Building Materials 234 (2020).

[14] H. Du, H.J. Gao, S. Dai Pang, Improvement in concrete resistance against water and chloride ingress by adding graphene nanoplatelet, Cement and Concrete Research 83 (2016) 114-123.

[15] H. Du, S.T. Quek, S. Dai Pang, Smart multifunctional cement mortar containing graphite nanoplatelet, Sensors and Smart Structures Technologies for Civil, Mechanical, and Aerospace Systems 2013, International Society for Optics and Photonics, 2013, p. 869238.

[16] J.-L. Le, H. Du, S. Dai Pang, Use of 2D Graphene Nanoplatelets (GNP) in cement composites for structural health evaluation, Composites Part B: Engineering 67 (2014) 555-563.

[17] AS3972, General purpose and blended cements, Standard, Standard Australia, Australian Standard, 2010.

[18] AS1478.1, Chemical admixtures for concrete, mortar and grout - Admixtures for concrete, Australian Standard, 2000.

[19] ASTM-C109/C109M-07, Standard test method for compressive strength of hydraulic

cement mortars, ASTM International: USA 2008, 2008.

[20] ASTM-C307-03, Standard Test Method for Tensile Strength of Chemical-Resistant Mortar, Grouts, and Monolithic Surfacings Monolithic Surfacings, ASTM International, 2012.

[21] ASTM C 348–18, Standard Test Method for Flexural Strength of Hydraulic-Cement Mortars, Designation: C 348 (2010).

[22] ASTM C642-13, Standard test method for density, absorption, and voids in hardened concrete, (2013).

[23] ASTM C596-09, Standard Test Method for Drying Shrinkage of Mortar Containing Hydraulic Cement, (2017).

[24] ASTM C1012/C1012M, Standard Test Method for Length Change of Hydraulic Cement Mortars Exposed to a sulfate Solution, American Society for Testing and Materials Philadelphia, 2012.

[25] ASTM C490/C490M, Standard practice for use of apparatus for the determination of length change of hardened cement paste, mortar, and concrete., ASTM, West Conshohocken, PA (2013).

[26] BS EN 12390-8: 2009, Testing hardened concrete - Part 8: Depth of penetration of water under pressure, BRITISH STANDARD 8 (2009).

[27] N. Kothiyal, S. Sharma, S. Mahajan, S. Sethi, Characterization of reactive graphene oxide synthesized from ball–milled graphite: its enhanced reinforcing effects on cement nanocomposites, Journal of adhesion science and Technology 30(9) (2016) 915-933.

[28] T.T. Mai, C.N. Ha Thuc, H.H. Thuc, Preparation of graphene nano-layer by chemical graphitization of graphite oxide from exfoliation and preliminary reduction, Fullerenes, Nanotubes and Carbon Nanostructures 23(8) (2015) 742-749.

[29] A. Eckmann, A. Felten, A. Mishchenko, L. Britnell, R. Krupke, K.S. Novoselov, C. Casiraghi, Probing the nature of defects in graphene by Raman spectroscopy, Nano letters 12(8) (2012) 3925-3930.

[30] X. Liu, X. Wang, G. Licht, S. Licht, Transformation of the greenhouse gas carbon dioxide to graphene, Journal of CO2 Utilization 36 (2020) 288-294.

[31] Y. Shen, A.C. Lua, A facile method for the large-scale continuous synthesis of graphene sheets using a novel catalyst, Scientific reports 3(1) (2013) 1-6.

[32] A.C. Ferrari, J. Meyer, V. Scardaci, C. Casiraghi, M. Lazzeri, F. Mauri, S. Piscanec, D. Jiang, K. Novoselov, S. Roth, Raman spectrum of graphene and graphene layers, Physical review letters 97(18) (2006) 187401.

[33] S.J. Chen, C.Y. Li, Q. Wang, W.H. Duan, Reinforcing mechanism of graphene at atomic level: Friction, crack surface adhesion and 2D geometry, Carbon 114 (2017) 557-565.

[34] A. Gholampour, M.V. Kiamahalleh, D.N. Tran, T. Ozbakkaloglu, D. Losic, Revealing the dependence of the physiochemical and mechanical properties of cement composites on graphene oxide concentration, RSC Advances 7(87) (2017) 55148-55156.

[35] A. Gholampour, M. Valizadeh Kiamahalleh, D.N. Tran, T. Ozbakkaloglu, D. Losic, From Graphene Oxide to Reduced Graphene Oxide: Impact on the Physiochemical and Mechanical Properties of Graphene–Cement Composites, ACS applied materials & interfaces 9(49) (2017) 43275-43286.

[36] W. Lin, A. Cheng, R. Huang, C. Chen, X. Zhou, Effect of calcium leaching on the properties of cement-based composites, Journal of Wuhan University of Technology-Mater. Sci. Ed. 26(5) (2011) 990-997.

[37] C. Carde, R. François, Effect of the leaching of calcium hydroxide from cement paste on mechanical and physical properties, Cement and Concrete Research 27(4) (1997) 539-550.

[38] C. Carde, R. François, J.-M. Torrenti, Leaching of both calcium hydroxide and CSH from cement paste: Modeling the mechanical behavior, Cement and concrete research 26(8) (1996) 1257-1268.

[39] A.N. Junior, M.S. Lemos, R.D. Toledo Filho, E.d.M.R. Fairbairn, J. Dweck, Early stages hydration of high initial strength Portland cement, Journal of thermal analysis and calorimetry 113(2) (2013) 659-665.

[40] S. Lv, Y. Ma, C. Qiu, T. Sun, J. Liu, Q. Zhou, Effect of graphene oxide nanosheets of microstructure and mechanical properties of cement composites, Construction and building materials 49 (2013) 121-127.

[41] R. Jadhav, N. Debnath, Computation of X-ray powder diffractograms of cement components and its application to phase analysis and hydration performance of OPC cement, Bulletin of Materials Science 34(5) (2011) 1137-1150.

[42] S. Sharma, N. Kothiyal, Comparative effects of pristine and ball-milled graphene oxide on physico-chemical characteristics of cement mortar nanocomposites, Construction and Building Materials 115 (2016) 256-268.

[43] F. Rendell, R. Jauberthie, M. Grantham, Deteriorated concrete: Inspection and physicochemical analysis, Thomas Telford2002.

[44] J. Elena, M.D. Lucia, X-RAY Diffraction Study of hydration Processes in the Portland Cement, JAESVol 1 14.

[45] M. Horgnies, J. Chen, C. Bouillon, Overview about the use of Fourier transform infrared spectroscopy to study cementitious materials, WIT Trans. Eng. Sci 77 (2013) 251-262.

[46] P. Yu, R.J. Kirkpatrick, B. Poe, P.F. McMillan, X. Cong, Structure of calcium silicate hydrate (C-S-H): Near-, mid-, and far-infrared spectroscopy, Journal of the American Ceramic Society 82(3) (1999) 742-748.

[47] L. Fernández Carrasco, D. Torrens Martín, L. Morales, S. Martínez Ramírez, Infrared spectroscopy in the analysis of building and construction materials, InTech2012.

[48] S. Ghosh, S. Handoo, Infrared and Raman spectral studies in cement and concrete, Cement and Concrete Research 10(6) (1980) 771-782.

[49] Z. Pan, L. He, L. Qiu, A.H. Korayem, G. Li, J.W. Zhu, F. Collins, D. Li, W.H. Duan, M.C. Wang, Mechanical properties and microstructure of a graphene oxide–cement composite, Cement and Concrete Composites 58 (2015) 140-147.

CHAPTER 6:

INVESTIGATION OF THE INFLUENCE OF DIFFERENT PRISTINE GRAPHENE SIZES AND DESIGN MIXES ON ENHANCING MECHANICAL AND DURABILITY PROPERTIES OF PORTLAND CEMENT MORTARS CURED AT DIFFERENT CURING AGES

THE AIM AND OBJECTIVE OF THIS CHAPTER:

Aim: This chapter aims to explore the effect of different PRG sizes and design mixes on physicochemical, microstructural, mechanical, and durability properties of Portland cement-based mortars cured at short-term and long-term ages.

Objectives 1: investigating the influence of different PRG sizes and design mixes on short-term and long-term mechanical and durability properties of Portland cement-based mortars.

Objectives 2: analysing physicochemical and microstructural properties of PRG-cement based mortars to improve understanding of the impact of PRG sizes and design mixes on mechanical and durability properties of Portland cement-based mortars cured at short-term and long-term periods.

Revealing the effect of pristine graphene sizes on mechanical and durability properties of Portland cement-based mortars with curing ages

1. Introduction

As presented and analyzed in the previous studies shown in Chapters 2-5, it can be concluded that the addition of a small number of PRG materials to cement-based materials could enhance the mechanical strengths of PRG-cement based composites. For example, according to Ref. [1], incorporating 0.05% PRG into cement-based mortars could improve flexural strengths and compressive strengths of the mortars at 7 & 28 days by 23.5% & 16.8% and 7.5% & 1.3%, respectively. The influence of different dosages and sizes on the mechanical properties of cement-based composites has also been reported in few studies [2-4] and the studies of this thesis as shown in Chapters 2-5. An investigation into the effect of different PRG dosages on the cement-based paste showed that at the optimal PRG dosage of 0.06%, PRG could increase the 28-day compressive and flexural strength of the cement paste by 11% and 27.8%, respectively [4]**.** The effects of different dosages and sizes of PRG together with revealing the reinforcing mechanism of PRG for enhancing mechanical strengths of cement-based mortars have been investigated in the studies of this thesis and shown in Chapters 2-5. The results confirmed that the strengths of cement-based mortars are dependent on PRG dosages and sizes. At the optimal dosage of 0.07%, the mixes containing the ultra-large size of 73µm showed a significant influence on both 28-day compressive and tensile strengths of cement mortars, which could increase by 30.1% and 38.6% respectively. On the other hand, there are no significant effects on either compressive strengths or tensile strengths of the mix containing the PRG size of 5µm. The results in Chapter 4 also revealed that the reinforcing mechanism of PRG for enhancing mechanical strengths of cementitious composites is mostly attributed to adhesion friction forces between PRG sheets (PRGs) and cementitious gels, which highly depend on the surface area of the PRGs. The larger surface area of the PRGs will have a larger friction area

associated with cementitious gels, resulting in the improvement of the cement matrix around PRGs and creates interlock PRG-cementitious gels in a space network structure for better stress distribution and crack paths in the cement matrix. In addition to the advantages of PRG additives in mechanical properties of cementitious composites, the benefit of PRG in other properties also investigated in few recent studies**.** Du and Dai Pang [5] demonstrated that incorporating PRG into cement-based mortars could significantly decrease chloride migration coefficient and water penetration depth of mortars by 31% and 64%, respectively. The use of PRG in cement-based materials also improved the electrical conductivity of the composites, which could be used for structural health monitoring of structures **[**6**,** 7**]**.

To date, there have been still some limitations in the research field of PRG-cement based composites. First, although the durability properties are also important to service life, maintenance costs of construction structures, there have been few studies on durability properties of PRG-cement based composites. Second, most of the existing studies only have been focused on mechanical properties of cement-based composites at short-term curing ages (e.g. 7, 14, and 28 days). The results of this thesis shown in Chapter 5 are the first study on the effects of PRG dosages and sizes on mechanical and durability properties of cement-based mortars at the long-term curing ages (i.e. up to 270 days). Third, the effects of different design mixes of water and cement ratios, and different densities of PRG materials on enhancement strength rates of PRG-cement based composites have not been investigated in the literature. The results of this thesis presented in the previous Chapters 2-5 have confirmed some of the following points. The first thing is that although different sizes and design mixes were used in the studies of PRG-cement based mortars, the dosage of 0.07% is still identified as the optimized dosage of PRG in cement-based mortars. Another thing is that along with the dosages and sizes of PRG, the effects of design mixes of water and cement ratios can be an important factor that will affect enhancement rates of the properties of PRG-cement based mortars because they will impact on the strengths of cementitious gels, resulting in the influence on

strengths of the formation of PRG-cementitious gels. This can be revealed by a new study based on the continuous research of the study shown in Chapter 5 with different sizes and densities of PRG materials.

To address these research gaps, this Chapter of this thesis aims at exploring the effects of different sizes and densities of PRG on mechanical and durability properties of cementitious-based mortars at short-term and long-term curing ages. Several physicochemical and microstructural properties of the mortars were also performed to have a better understanding of the PRG-cement matrix. The results from this Chapter will provide better knowledge of how different sizes and densities of PRG and design mixes influence short-term and long-term properties of cement-based mortars. This will significantly contribute to future research on incorporating PRG in cementitious composites to enhance the performance of construction materials.

2. Experimental programs

2.1. Materials

The physical properties of three different sizes of PRG provided by First Graphene Ltd in Perth, Australia are shown in Table 1. Cement binder with the general-purpose type which was complied with Australian Standard AS 3972-2010 [8] was used for the design mixes and its typical chemical properties are shown in Table 2. Natural sand with 2.36-mm maximum particle sizes was used as fine aggregate of the mortars. MasterGlenium SKY 8100 complied with Australian Standard AS 1478.1-2000 [9] was used as the superplasticizer to improve the dispersion of PRGs in water.

Table 1. Physical properties of pristine graphene.

ID	Particle Size-d50 (μm)	Thickness (nm)	Purity (%)	Poured bulk density (g/cm3)
Size 20μm	20	1-3	~98	~ 0.12
Size 40μm	40	1-3	~98	~ 0.30
Size 73μm	73	1-3	~98	~ 0.12

Table 2. Typical chemical properties of general-purpose cement.

Compounds	OPC (%)
CaO	63.28
SiO_2	19.95
Al_2O_3	4.79
Fe_2O_3	3.14
MgO	2.03
Na_2O	0.29
K_2O	0.4
SO_3	2.69
P_2O_5	0.04

2.2. Specimens

The mix proportions of the mortars are shown in Table 3. As shown in the table, there are four mixes with different sizes of PRG at the optimized dosage of 0.07% and the water/cement ratio of 0.55 used in this study. The design was continued the study presented in Chapter 5 to investigate the effects of different sizes of PRG on mechanical and durability properties of cementitious-based mortars at short-term and long-term curing ages. The following procedure was applied in the mixing process of the mortars: the aqueous solutions including water, superplasticizer and PRG were sonicated for 30 minutes by using Ultrasonication UIP1000hdT.

Then, these solutions were gradually added for 5 minutes to natural sand and binder, which were mixed for four minutes. Next, all samples were vibrated for one minute after mounting to mitigate entrapped air during the mounting process. After that, they were covered with wet fabrics and plastic sheets to prevent moisture loss and were demounted after 24 hours cured at room temperature. Then, all the samples continued to be cured in a fog room until testing days.

Table 3. Designed mixes of PRG-cement based mortars prepared with different PRG sizes.

Mix	PRG dosage (%)*	Water/cement ratio	Cement (kg/m3)	Water (kg/m3)	Sand (kg/m3)	PRG (kg/m3)	Superplasticizer (kg/m3)
Control	0	0.55	465	256	1545	0	1.4
Size 20µm	0.07	0.55	465	256	1545	0.33	1.4
Size 40µm	0.07	0.55	465	256	1545	0.33	1.4
Size 73µm	0.07	0.55	465	256	1545	0.33	1.4

* The percentage of pristine graphene based on weight of cement binder.

2.3. Test methods

Different mechanical and durability tests of cement-based mortars were performed at different curing ages including compressive strength, flexural strength, direct tensile strength, water absorption, void, drying shrinkage, sulfate extension, and water penetration. Compression strength tests at 7, 28, 90, and 270 days with the cube sizes of 50×50×50 mm^3 complied with ASTM C109/C109M-07 [10]. Dog-bone shaped samples, according to ASTM C307-03 [11], were used for direct tensile strength tests at 28 and 270 days. Flexural strength tests at 7, 28, 90, and 270 days with the prism sizes of 40x40x160 mm complied with ASTM C348-18 [12]. The test method according to ASTM C642-06 [13] was used for determining density, water absorption, and voids of mortar mixes at 28 days. 25×25×285 mm prisms were utilized to measure drying shrinkage and sulfate expansion (3% Na_2SO_4) at 7, 14, 21, 28, 56, 90, 120, 150, 180, 210, 240 and 270 days, complied with ASTM C596-09 [14], ASTM C1012-12 [15] and ASTM C490-13 [16]. Water penetration depths of the mortars at 28 days were referred to BS

EN 12390-8:2009 [17]. To ensure all the samples tested at the same condition, the automatic triaxial test system was used for the water penetration test with the vertical water pressure of 500 kPa and applied in 72 h. The values of each designed mix at testing days were calculated by averaging values obtained from three nominal identical samples of each mix.

Scanning electron microscopy (SEM) were obtained by using the FEI Quanta 450 to analyze PRG sizes and surface morphologies of the mortars. X-ray diffraction (XRD) was performed by using the Rigaku MiniFlex 600 X-Ray diffractometer to find the mineralogical characteristics of cement hydration products of the mortars and PRGs. Raman spectra and particle size distribution were respectively performed by using the HORIBA LabRAM HR Evolution and Mastersizer 2000-Malvern to evaluate the quality and particle sizes of PRGs. Fourier transform infrared spectroscopy (FTIR) was conducted using the Nicolet 6700 to determine specific functional groups of PRG-cement based mortars. Results and Discussion

3. Results and Discussion

3.1. Characteristics of different PRG samples used for the study

Fig. 1 shows typical SEM images and particle size distribution of there PRG samples used for this study. As shown in the figure, the wrinkled and irregular shape of PRGs can be seen in the SEM images and their average particle sizes of 20µm, 40µm, and 73µm determined from the particle size distribution results are presented in Fig.1(a), (b), and (c), respectively. XRD patterns and Raman spectrum of three different sizes of PRG are shown in Fig. 2(a) and (b), respectively. As shown in Fig. 2(a), the typical peak of these PRG samples in XRD results are at the position 26.64°, resulting in the d-spacing between layers of 0.334nm (based on the Bragg's Law) [18, 19]. Besides, the relative intensity ratios of $I_D/I_{D'}$ and I_{2D}/I_G of these PRG samples of 20µm, 40µm, and 73µm shown in the Raman tests in Fig. 2(b) are 1.223 & 0.355, 1.387 & 0.374, and 1.544 & 0.395, respectively, which are respectively below 3.5 and 1, showing that the PRG sample in this study does not have basal plane defects and contains

mostly of few-layer sheets of graphene [20-23]. This presents the high-quality of the PRG sample used in this study. From Table 1, it is also important to note that although three PRG samples are in high-quality products with similar average thicknesses, they are different in sizes and densities (i.e. PRG size 40µm has the different density with PRG sizes of 20µm and 73µm).

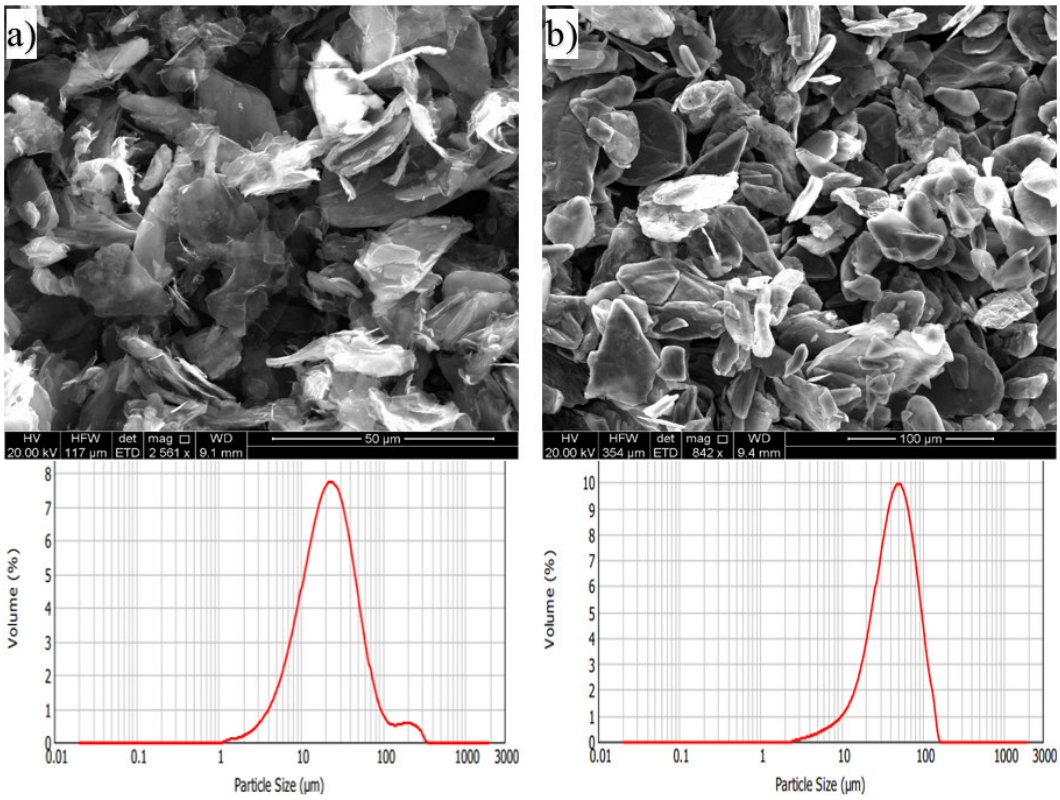

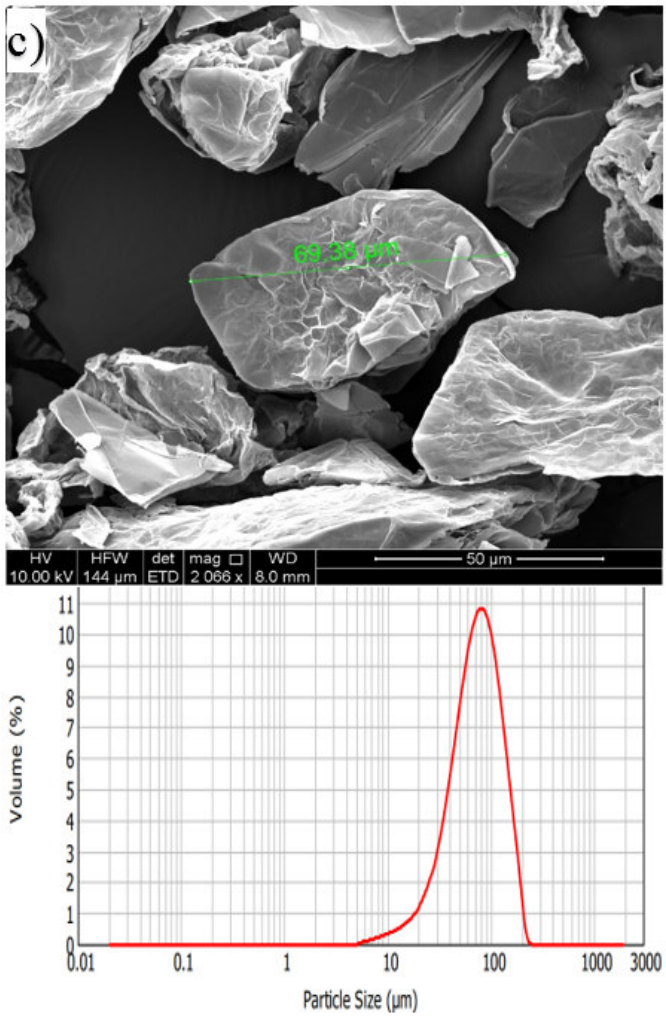

Fig. 1. (a) SEM images and particle size distribution of PRG: (a) size 20µm, (b) size 40µm, (c) size 73µm.

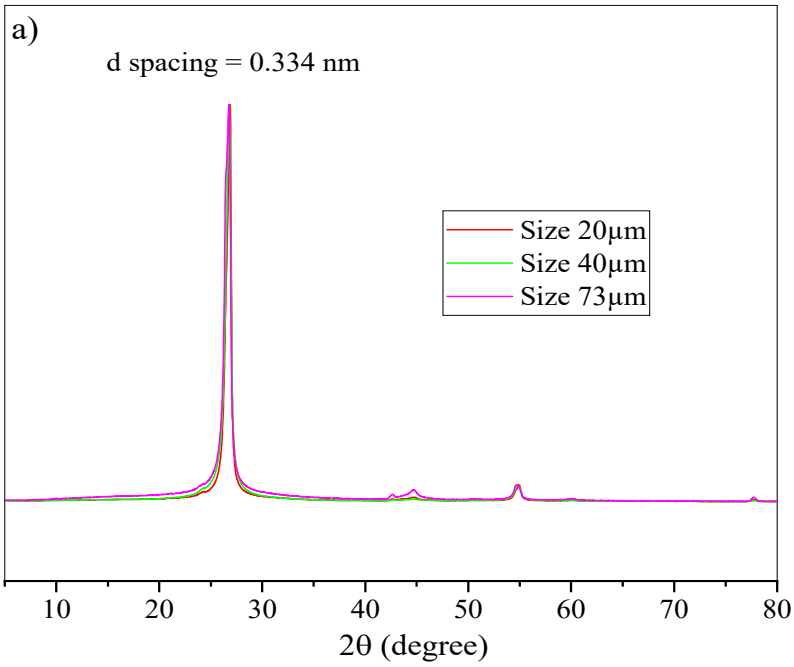

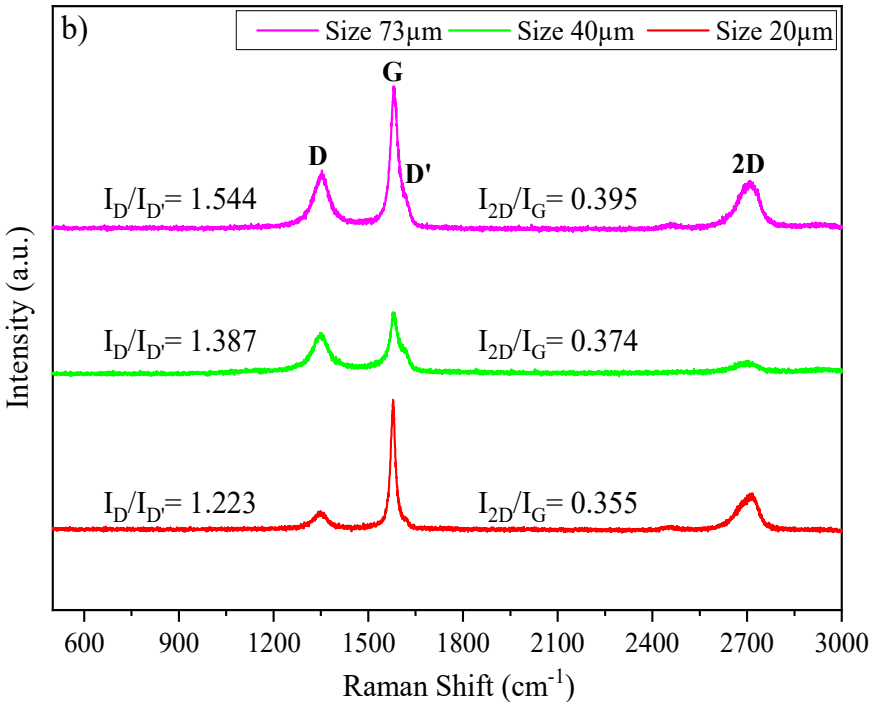

Fig. 2. (a) XRD patterns and (b) Raman spectra of different PRG sizes.

3.2. Mechanical properties of mortar mixes

3.2.1 Compressive strength

The compressive strengths and enhancement compressive strength rates of the mortars with different PRG sizes at 7-, 28-, 90-, and 270-day curing age are shown in Fig. 3(a), (b), respectively. As shown in the figure, the addition of PRG to the mortars can improve their compressive strengths, and their enhancement strength rates depend on the PRG sizes and curing ages. The mixes containing the PRG sizes of 20µm and 73µm shows higher enhancements than that with size 40µm. Although size 73µm presents the best improvement in 7-, 28-, 90-, and 270-day compressive strengths which are 6.9, 12.5, 7, and 18.4% higher than the control mix, respectively, there is a slight difference from the enhancement strength rates between PRG size 20µm and 73µm at all the testing days. The improvement of cement-based mortars when adding PRG can be attributed to the enhancement of cementitious gels due to the closer distance between cement particles caused by van der Waals forces between PRGs [24, 25], and the most important factor coming from adhesion friction forces between surface areas

of PRGs and cementitious gels which depends on the sizes of PRGs that is the larger surface area of PRGs has a larger friction area associated with cementitious gels, which are consistent with research in PRG-cement based composites [25, 26]. The lower enhancement of size 40µm could be due to its higher density compared to size 20µm and 73µm, resulting in the strong agglomeration and formation of multi-layers PRGs in the cement matrix due to van der Waals forces between PRGs that lead to a negative impact on the formation of PRG-cementitious gels [3, 27, 28]. From the results and analyses above, together with the results of shown in Chapters 2-5, it can be concluded that the enhancement compressive strength rate of PRG-cement based mortars depends on not only the dosages and sizes of PRG but also the design mix (water and cement ratios) and the density of PRG materials. As can also be observed in Fig. 3(a), compressive strengths of all the mixes increase up to 90 days, and then decrease with the long-term curing age of 270 days. This can be the influence of calcium leaking in cement-based composites during a long-term curing process in a fog room, which are in line with some studies in the literature about the calcium leaking of cementitious composites [29-31].

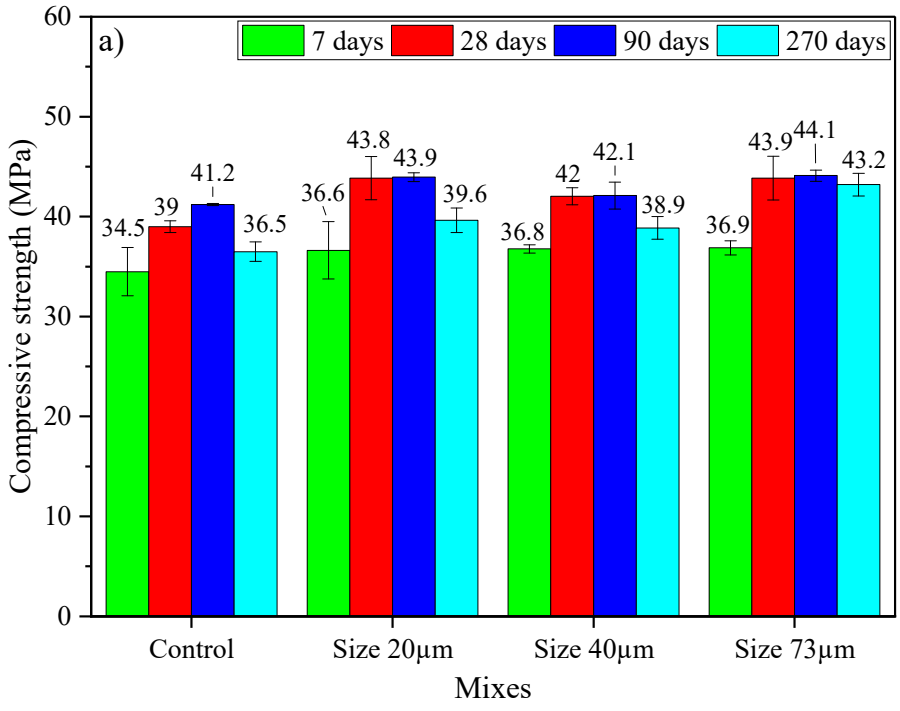

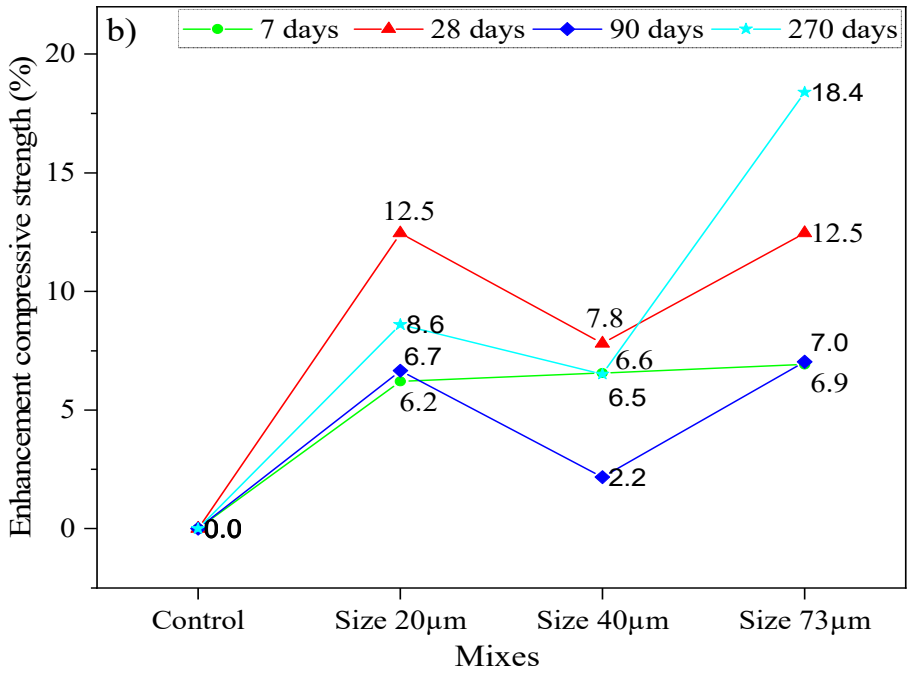

Fig. 3. (a) Compressive strength and (b) enhancement compressive strength of PRG-cement based mortars prepared with different PRG sizes at 7, 28, 90, and 270 days.

3.2.2 Flexural strength

Fig. 4(a), (b) shows 7-, 28-, 90-, and 270-day flexural strengths and enhancement flexural strength rates of the mortars with different sizes of PRG. It can be seen in the figure that incorporating PRG into cement-based mortars can enhance the compressive strengths of the mortars, and their enhancement strength rates depend on the PRG sizes and curing ages. The mixes with the PRG sizes of 20µm and 73µm shows higher enhancement rates than that with size 40µm. The mortar containing size 73µm shows the highest enhancement rate in 7-, 28-, 90-, and 270-day flexural strengths which are 1.1, 17.2, 12.2, and 8.1% higher than the control mix, respectively. While the mix with size 20µm can enhance 7-, 28-, 90-, and 270-day flexural strengths by 3.7, 4.0, 3.3, and 4.1%, that of size 40µm shows an increase by 0.3, 1.3, 0.1, 2.7% compared to the control, respectively. The enhancement in flexural strengths of PRG-cement based mortars can be due to the benefit of PRGs in enhancing the development of crack paths in the cement matrix, resulting in the reduction of crack widths in structures. In addition, the better enhancement of size 73µm than size 20µmand 40µm can account for the benefit of its

larger surface area to interact with cementitious gels, leading to better adhesion friction forces formed between PRGs and cementitious gels. This results in the effectiveness of stress distribution and can increase the path of crack developments. The least improvement of the mix with size 40µm can be due to its high-density property, resulting in a higher level of the agglomeration and formation of multi-layers PRGs. This leads to the negative impact on the cement hydration process and the interaction of PRGs and cementitious gels [3, 27, 28].

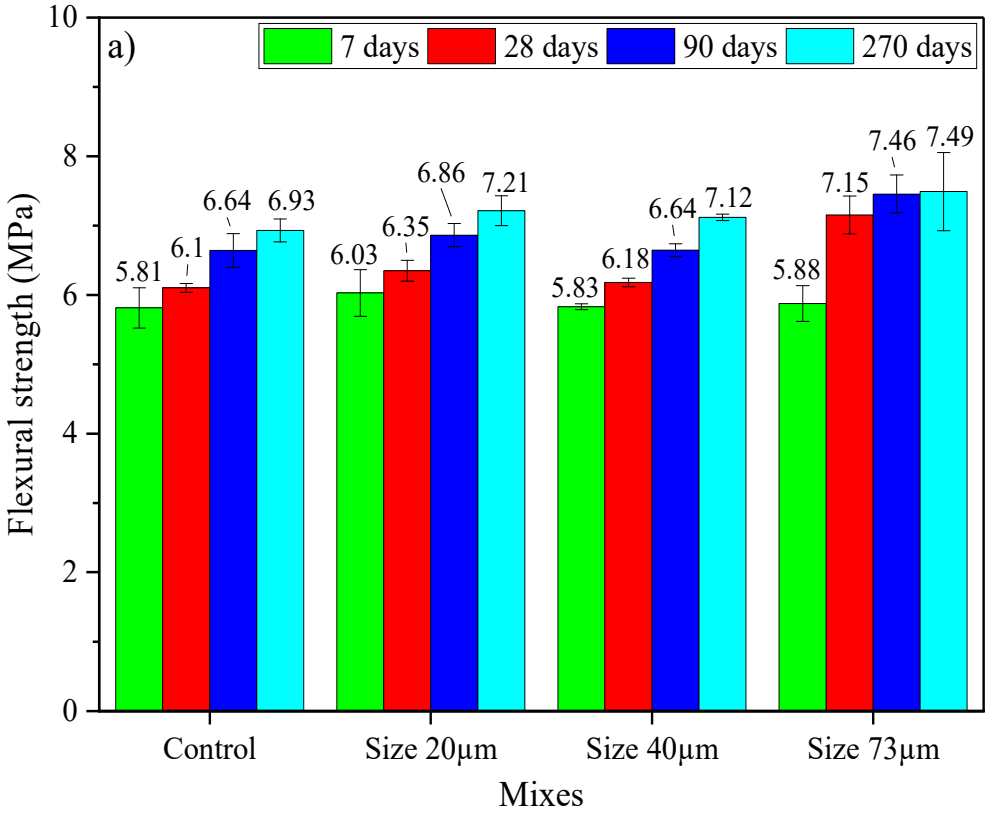

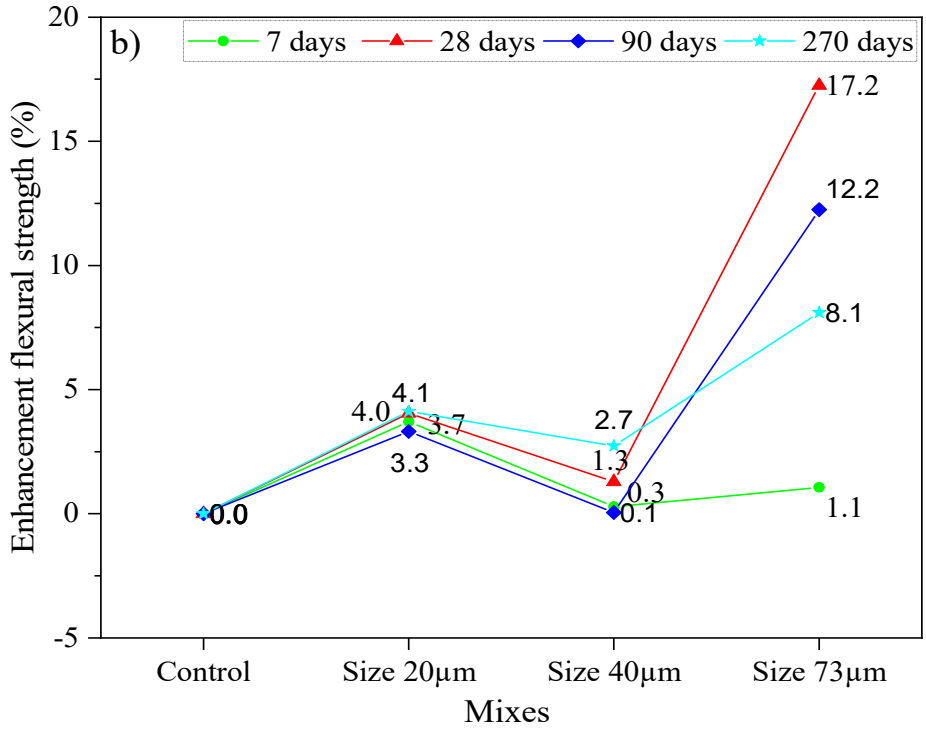

Fig. 4. (a) Flexural strength and (b) enhancement flexural strength of PRG-cement based mortars prepared with different PRG sizes at 7, 28, 90, and 270 days.

3.2.3 Tensile strength

28-, 270-day direct tensile strengths and enhancement tensile strength rates of the mortars with different sizes of PRG are shown in Fig. 5(a), (b). As shown in the figure, the addition of PRG to cement-based mortars can improve the direct tensile strengths of the mortars, and their enhancements depend on the PRG sizes and testing days. The PRG sizes of 20µm and 73µm show higher enhancement strength rates than PRG size 40µm. The mix with size 73µm shows the highest tensile enhancement at 28 and 270 days, which are 14.2 and 14.9% higher than the control mix, respectively. While the mix containing size 20µm can improve 28- and 270-day tensile strengths by 5.6 and 10%, the mix with size 40µm shows an increase by 2.5 and 3.9% compared to the control, respectively. The enhancement in direct tensile strengths of the mortars containing PRG can be attributed to the benefit of PRGs in improving PRG-cementitious gels, resulting in the development of crack paths in the cement matrix and the reduction of crack widths in structures. The mix with size 73µm shows the best tensile enhancement can account

for the benefit of its larger surface area to interact with cementitious gels, resulting in better adhesion friction forces formed between PRGs and cementitious gels. This can bring the effectiveness of stress distribution that will benefit for crack paths in the cement matrix. Size 40µm with the high density will lead to a higher level of the agglomeration and formation of multi-layers PRGs, resulting in the negative impact on the cement hydration process and the interaction of PRGs and cementitious gels [3, 27, 28]. This can be a reason for the lowest tensile enhancement rate of the mix with size 40µm.

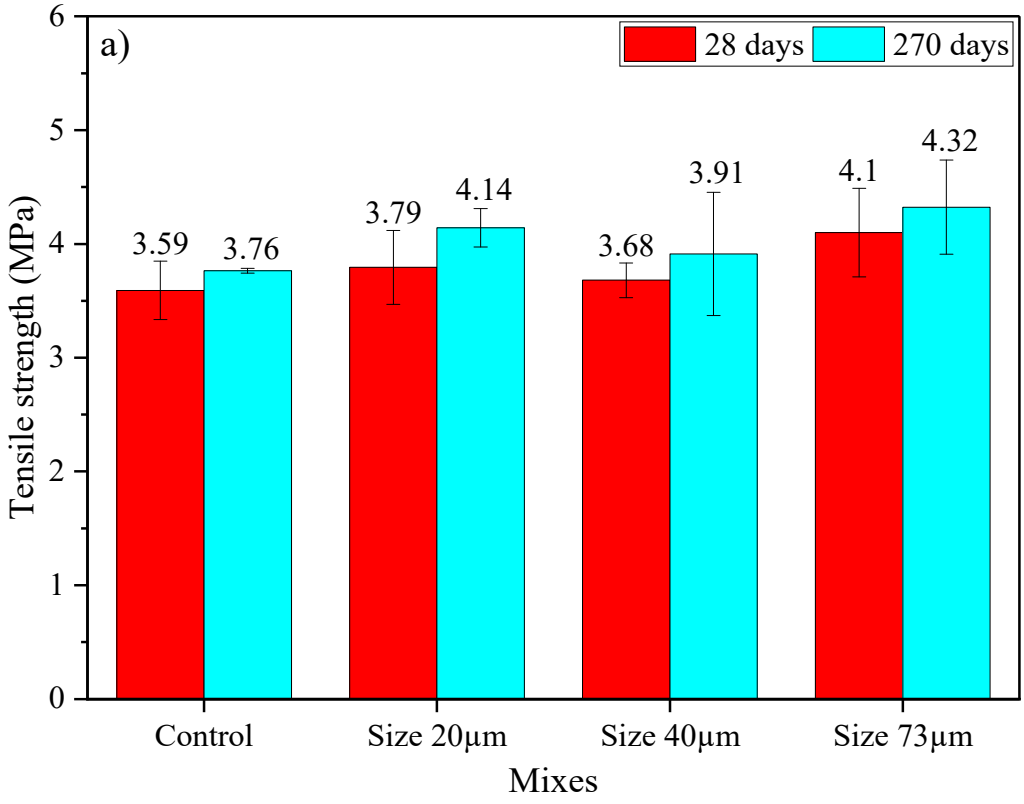

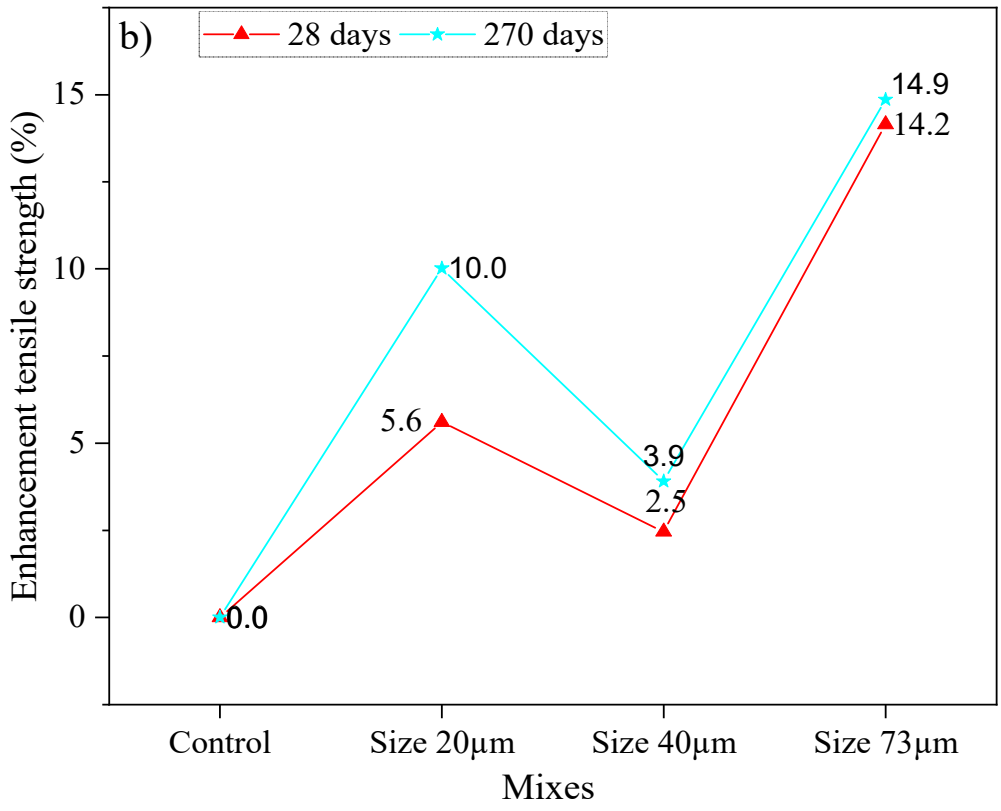

Fig. 5. (a) Direct tensile strength and (b) enhancement direct tensile strength of PRG-cement based mortars prepared with different PRG sizes at 28 days and 270 days.

3.3. Durability-related properties

3.3.1 Water absorption and voids

The results of 28-day water absorptions and voids of the mortars with different sizes of PRG are shown in Fig. 6(a), (b). As shown in the figure, the addition of a small amount of PRG to cement-based mortars results in a decrease in the water absorption and void of the mortars, and the decrease rate depends on the PRG size. The mixes containing the PRG sizes of 20µm and 73µm develop 8.15 & 8.28 % and 8.52 & 8.53 % lower water absorptions and voids than the control mix, respectively. The mix with size 40µm develops a lower enhancement of the water absorption and void than size 20µm and 73µm, which are approximately 2.55 and 3.5 %, respectively. The lower water absorptions and voids of the mixes containing PRG samples can be due to the higher content of hydration products in these mixes, resulting in more compact microstructures and lower porosities.

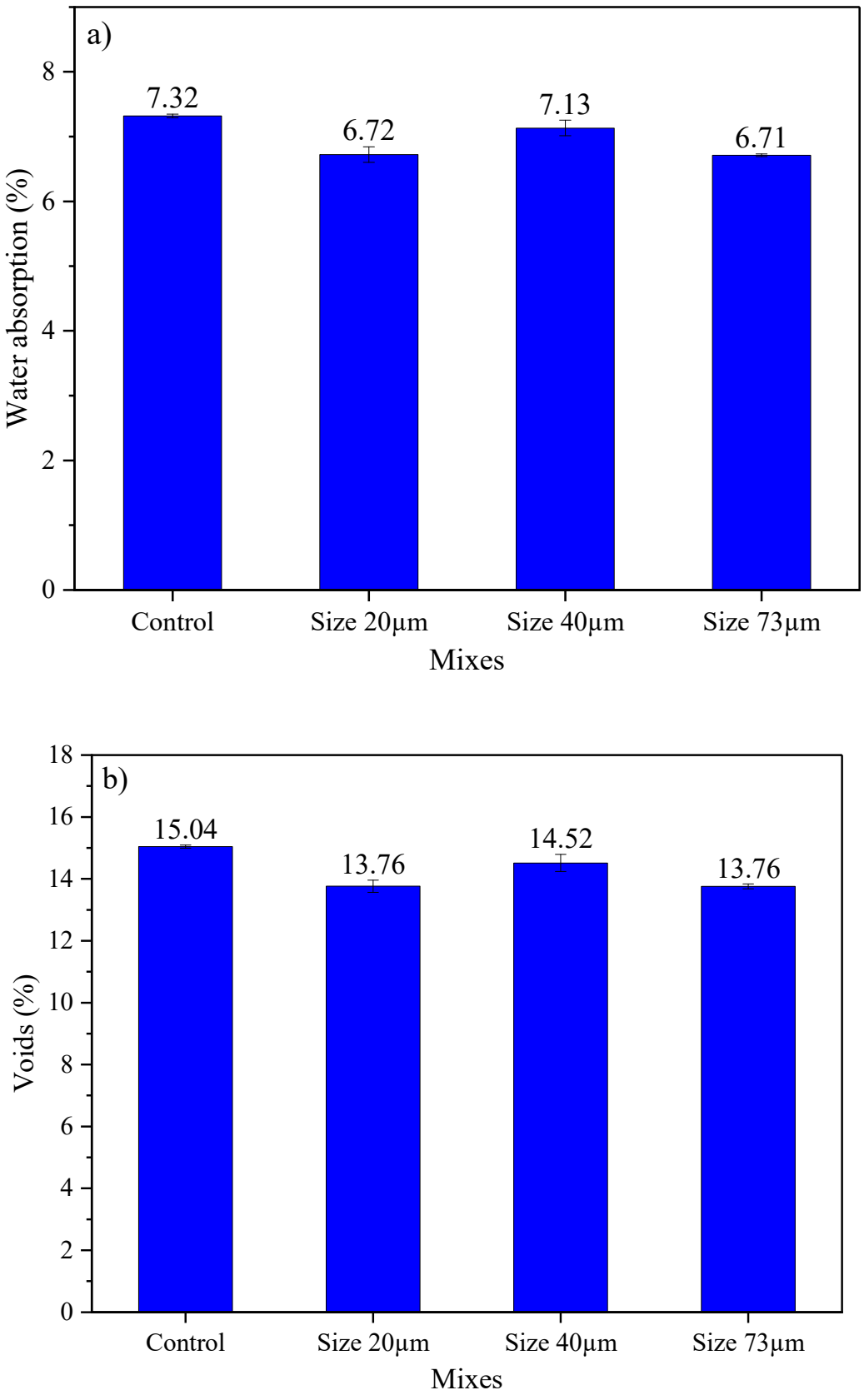

Fig. 6. (a) Water absorptions and (b) voids of PRG-cement based mortars prepared with different PRG sizes at 28 days.

3.3.2 Drying shrinkage

The drying shrinkage of the mortars with different sizes of PRG at different curing ages is shown in Fig. 7. It can be seen in the figure that the drying shrinkage of the mortars significantly develop at the early age of 7 days, and hence, gradually increase with the curing time and become steadier after 240-day curing age. There is no clear positive influence of PRG on the drying shrinkage results of cement-based mortars. Only the mix containing PRG size 73µm shows a slight improvement in the drying shrinkage throughout from 7-day to 270-day curing ages, which decrease approximately 1.0% at 7 days and 9.5% at 270 days respectively. The reason for being no clear positive effect of PRG on drying shrinkage of the mortars can be attributed to the random distribution of PRGs in the cement matrix that can create tortuous paths in the cement matrix to prevent moisture loss during the drying shrinkage process.

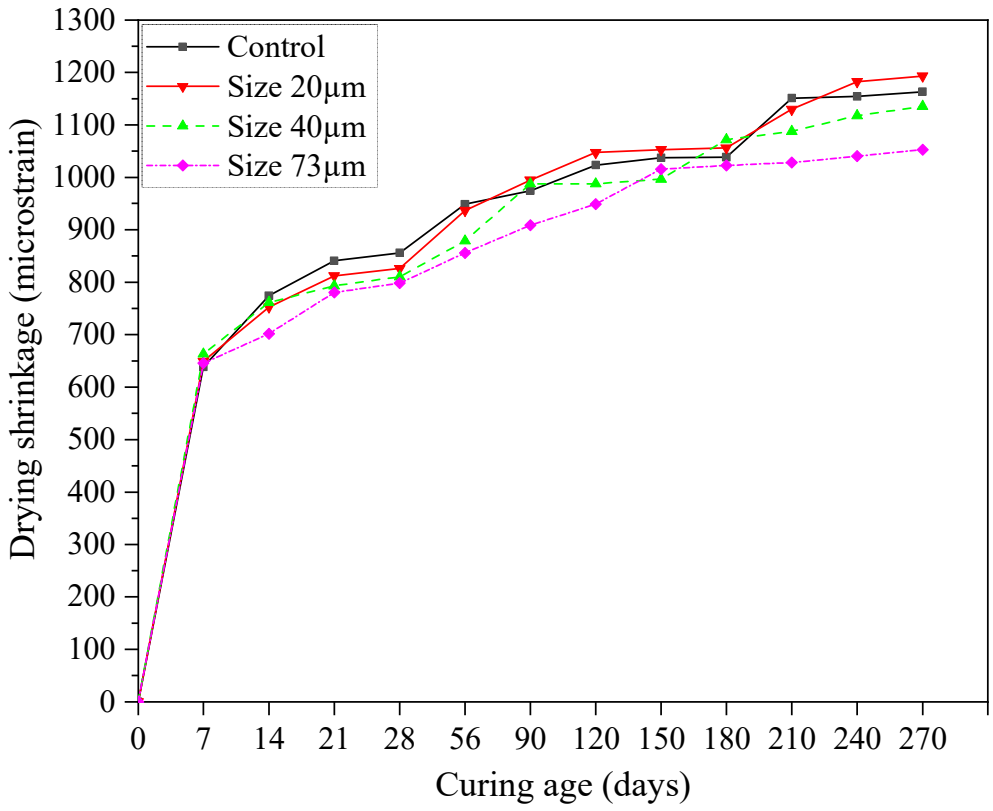

Fig. 7. Drying shrinkage of PRG-cement based mortars prepared with different PRG sizes at different ages.

3.3.3 Sulfate expansion

The sulfate expansion of the mortars containing different PRG sizes immersed in the sodium sulfate solution at different curing days is shown in Fig. 8. As shown in the figure, the mortars containing PRG materials present a positive influence on resisting the sulfate solution at all the curing ages. In general, the mix with size 73µm shows the best observation on sulfate expansion of the mortars, which decreases about 58.2% and 88.6% lower sulfate expansion at 7 days and 270 days, respectively, compared to the control mix. Besides, the mixes with size 20µm and 40µm can decrease 7-day & 270-day sulfate expansion by 40.3% & 43.7% and 82.1% & 51.5%, respectively. PRG materials can decrease sulfate expansion of cement-based mortars can be due to the positive effect of tortuous paths formed from PRGs on impeding the penetration of sulfate ion in the cement matrix, resulting in a lower amount of ettringite products created during the immersion process of mortars in the sulfate solution.

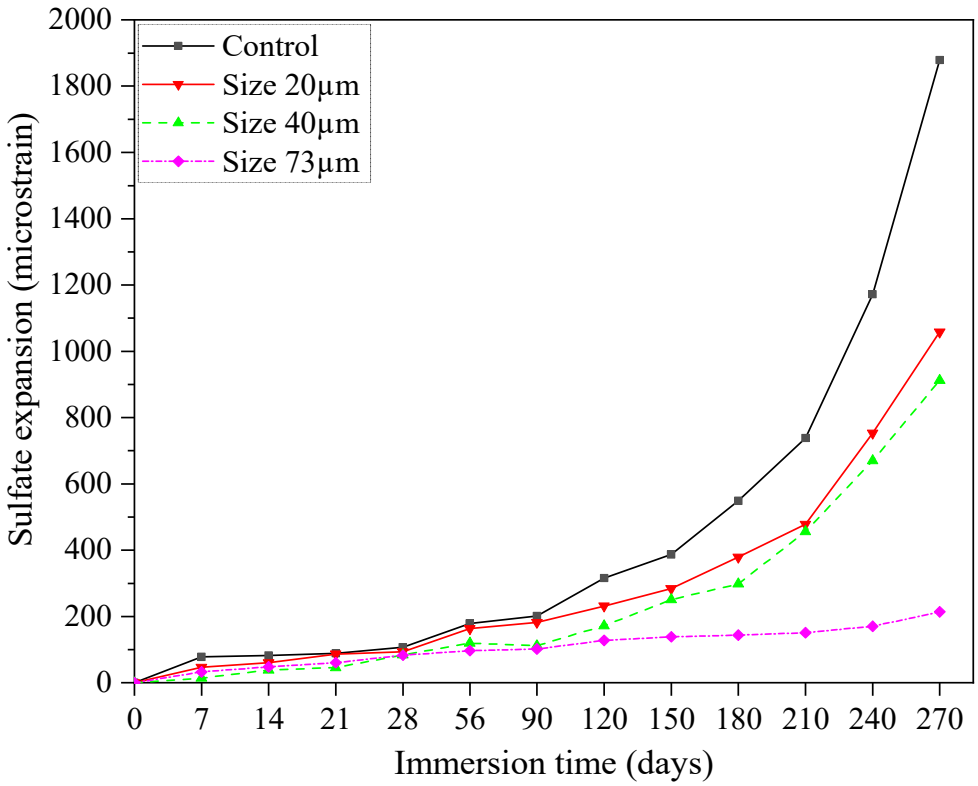

Fig. 8. Expansion of PRG-cement based mortars prepared with different PRG sizes immersed in the sulfate solution at different ages.

3.3.4 Water penetration

The average water penetration depths of the mortars with different sizes of PRG at 28 days are shown in Table 4. This test was performed and controlled by the automatic triaxial testing system, and the results of water penetration depths were calculated based on the ratio of the amount of water penetration into testing samples recorded by the system and areas of specimens. It can be seen in the Table that the addition of PRG to the mortars can decrease the water penetration depth into the mortar mixes. The mixes containing the PRG sizes of 20µm, 40µm, and 73µm develop 4.02, 47.71, and 46.25% lower water penetration depth at 28 days than that of the control mix, respectively. The improved resistance to water penetration of PRG-cement based mortars can be attributed to more tortuous paths for ingress of water that were formed by extensive barriers created from PRGs in the cement matrix.

Table 4. Average water penetration depth of hardened mortars with different PRG sizes at 28 days.

Mix	PRG dosage (%)	Penetrated water from triaxial test (mm3)	Average penetration depth (mm)	Change as compared to the control (%)
Control	0	4.06	2.00	
Size 20µm	0.07	3.89	1.92	-4.02
Size 40µm	0.07	2.12	1.05	-47.71
Size 73µm	0.07	2.17	1.07	-46.58

3.4. Physicochemical and microstructural analysis of PRG-cement based mortars containing different sizes of PRG

3.4.1 XRD and FTIR analysis

XRD patterns of the mortars containing different PRG sizes at 28 days are shown in Fig. 9(a). In the cement hydration process, calcium silicate hydrate (CSH), portlandite (CH), ettringite (Aft), and un-hydrated cement binder (Alite, belite) are its main hydration products [25, 32,

33]. The main part contributing to the strength of cementitious gels is CSH gels, but they could not recognize in these spectra because CSH gels often exist at amorphous phases in a cement matrix and it is thus hard to identify with XRD test. However, the content of CSH gels can be inferred from the contents of portlandite and un-hydrated cement particles [25, 34, 35]. It is important to note that these XRD spectra were standardized to the equal intensity at the major peak of natural sand of 26.7° for making the equal percentage of existing sand in all the samples [25, 35, 36]. As shown in the figure, portlandite phases are identified at the peaks of 18.2°, 34.2° and 47.1° [25, 35, 37], and the mixes with PRG additives show higher portlandite intensities than the control mix. This can be attributed to the beneficial effect of PRGs on the hydration of cement pastes [25, 35, 36], which is in line with the mechanical results at 28 days of the mortars as discussed in Section 3.2. Moreover, it can also be seen in Fig.9(a) that although the mixes containing the PRG sizes of 20µm and 40µm have the higher peak intensity of un-hydrated alite phases than the control, they still have a higher peak intensity of portlandite than the control. This could be because these mixes had a higher amount of belite hydrated in the cement hydration process than the control (i.e. (alite, belite) + H_2O $\rightarrow$ portlandite + CSH [25, 33]), contributing to a higher peak intensity of portlandite of this mix at the short-term mechanical strengths.

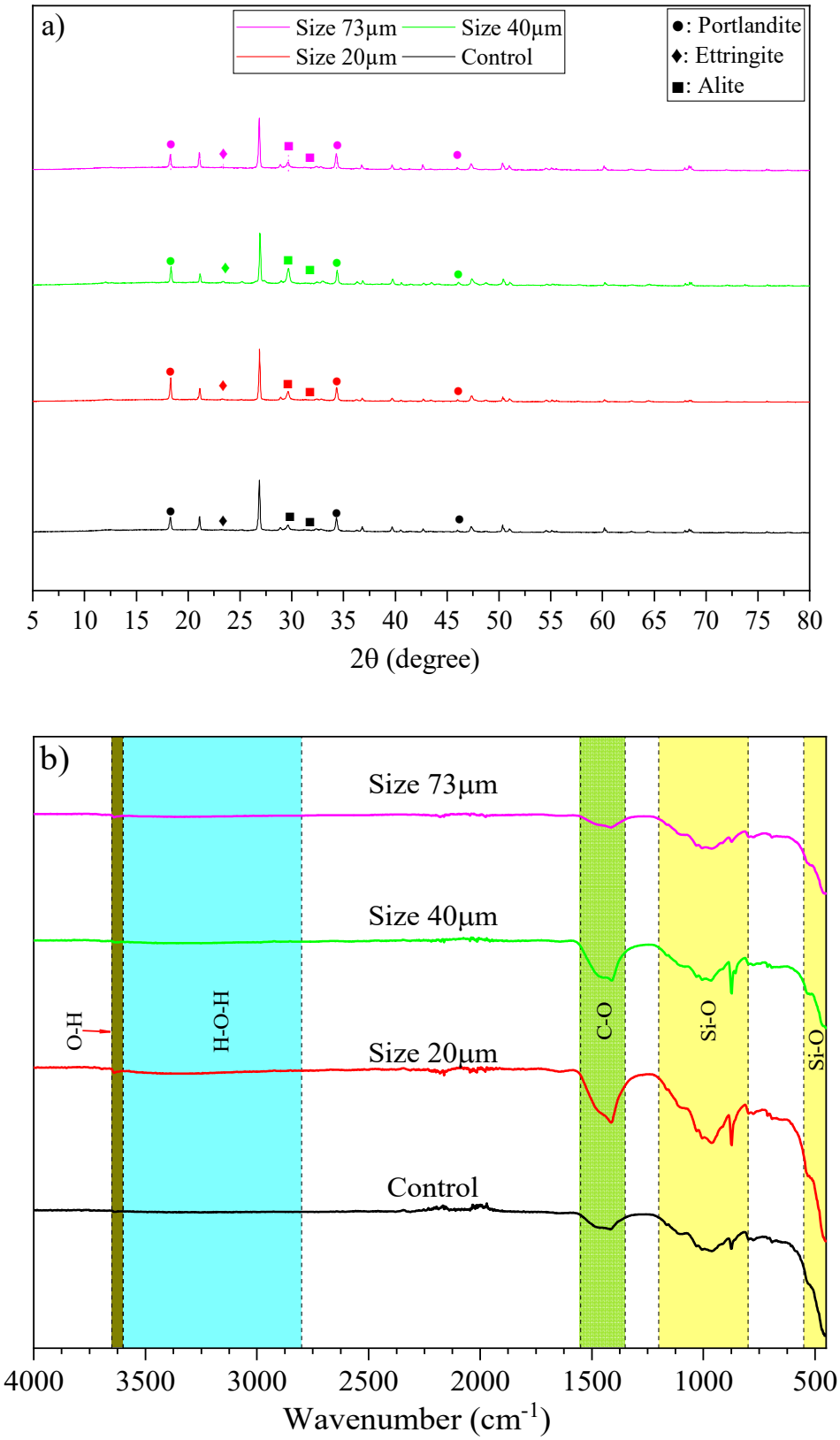

Fig. 9. (a) XRD patterns and (b) FTIR spectra of PRG-cement based mortars prepared with different PRG sizes at 28 days.

FTIR patterns at 28 days of the mortars containing different PRG sizes are shown in Fig. 9(b). It can be seen in the figure that all the samples have similar spectra with some functional groups determined in the range of the band from 400 cm^{-1} to 4000 cm^{-1}, showing that there are no new distinguishing groups observed in all the samples, which are consistent with the results of XRD discussed above. As can be observed in the figure, the group bands ranged 400-550 cm^{-1} and 800-1200 cm^{-1} are attributed to Si-O bonds in the CSH gels [38, 39]; the band ranged from 2800 to 3600 cm^{-1} represents O-H groups in H_2O belonging to CSH gels [39, 40]; the narrow band in the range of about 3600-3650 cm^{-1} corresponds to O-H bonds in portlandite [38, 41]; C-O bond in $(CO_3)^{2-}$ groups are observed in a range of 1350-1550 cm^{-1} [39, 40]. Although these mixes have similar spectra, the spectral intensities representing CSH gels (i.e. Si-O, H-O-H) and CH (i.e. O-H) in these mixes are slightly different, which show stronger intensities of the functional groups belong to CSH gels in the mixes containing PRG additives than the control mix. This may be attributed to the higher cement hydration degree in the mixes containing PRG materials, leading to the enhancement in mechanical strengths of those mixes compared to the control mix which is consistent with XRD results above and mechanical results of the mortars as discussed in Section 3.2.

3.4.2 SEM analysis

The SEM images at 28 days of the mortar mixes containing different sizes of PRG are shown in Fig. 10(a)-(h). As shown in the figure, although SEM images of these mixes have similar components, they are different from how they are distributed and compacted in microstructures. The control and size 40µm mixes not only show less compact in their microstructure, which are larger sizes in microcracks and less dense in the interfacial transition zones (ITZ) (Fig. 10(a) and (e), respectively) but also present larger contents of pores distributed in the cement matrix (Fig. 10(b) and (f), respectively) than the mixes containing the PRG sizes of 20µm and 73µm (Fig. 10(c, d) and (g, h), respectively). This can be attributed to a higher cement hydration

degree of these mixes than the others, resulting in the stronger enhancement rates in their mechanical strengths as discussed in Section 3.2.

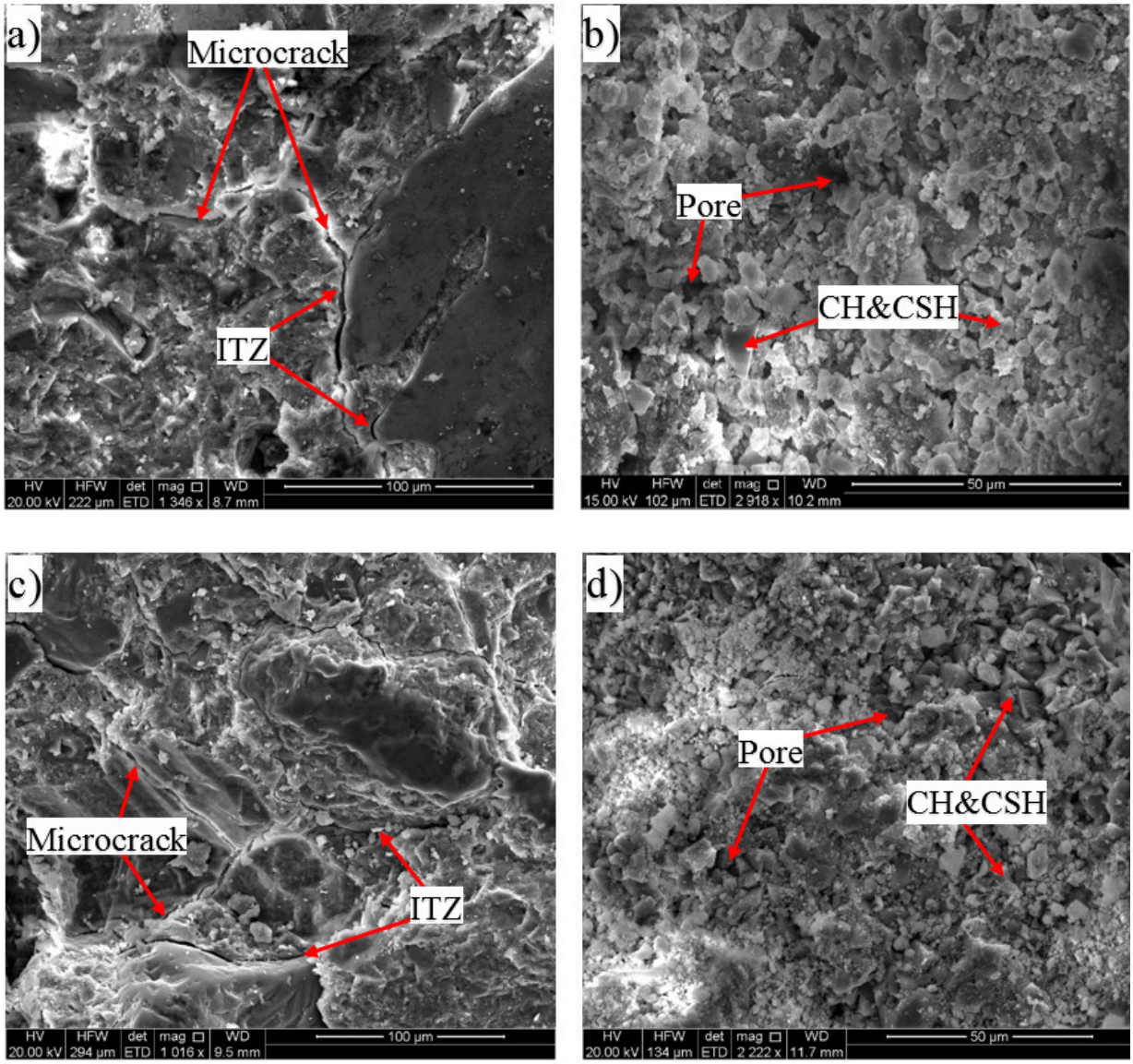

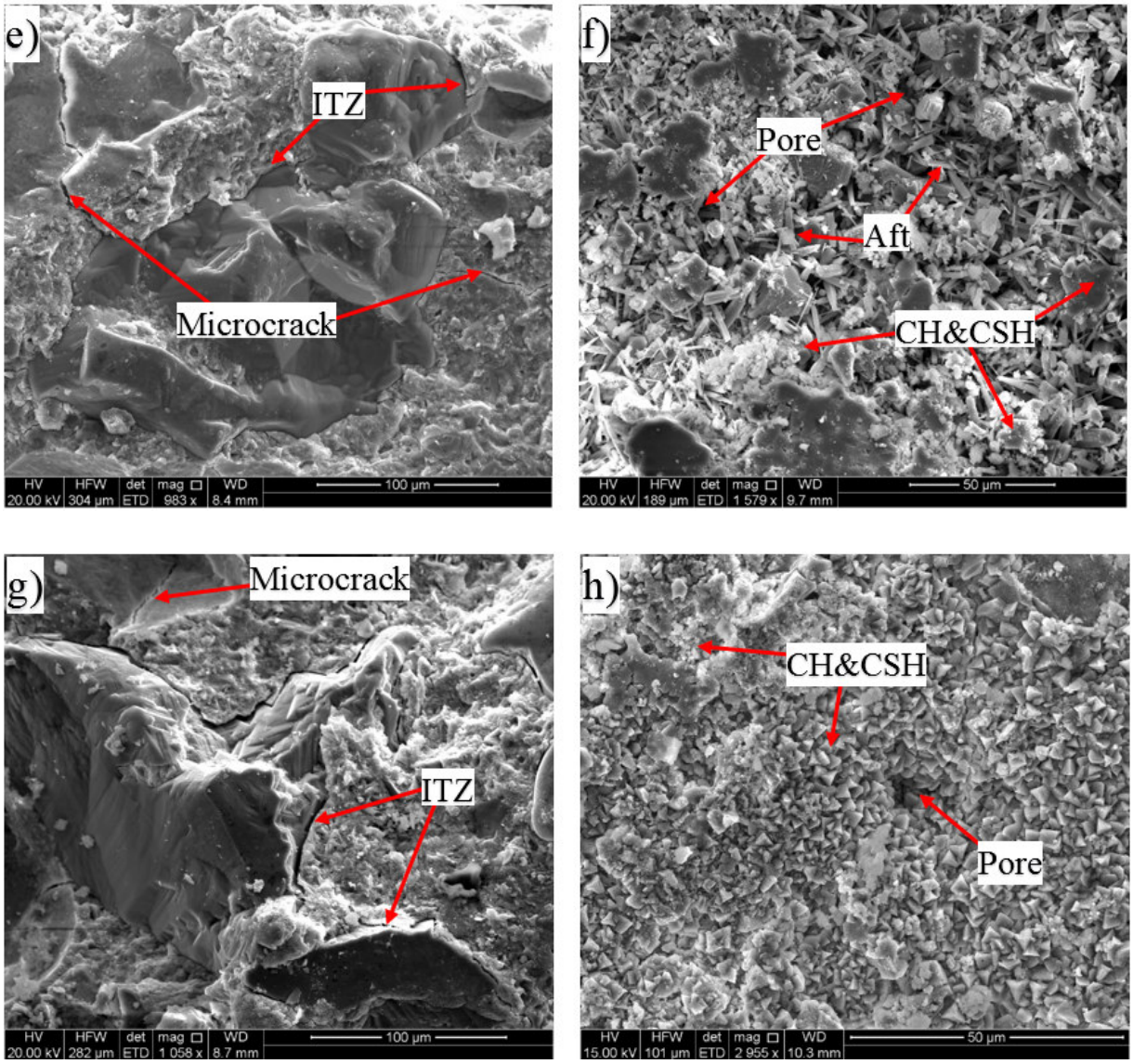

Fig. 10. SEM images of PRG-cement mortars prepared with different PRG sizes at 28 days: (a, b) control, (c, d) size 20µm, (e, f) size 40µm, (g, h) size 73µm.

3.5. Further discussion

From the results and discussion above, it can be concluded that the mortar mixes with different PRG sizes influence the results of the mechanical and durability properties of cement-based mortars. Incorporating PRG into cement-based mortars can enhance their mechanical and durability properties at short-term and long-term curing ages. The study also shows that properties of PRG samples will impact on the enhancement strength rates of cement-based mortars. When PRG materials with similar physical properties are used, the enhancement

strength rates of cement-based mortars containing the larger size (size 73µm) show better enhancement than the smaller size (size 20µm). In addition, the density of PRG materials also impacts on its enhancement in the mortars, shows that although size 20µm is smaller areas than size 40µm, the mix with size 20µm shows better enhancements than that with size 40µm because of the higher density of size 40µm. Moreover, it can be seen from the results of this study that the enhancement strength rates of cement-based mortars prepared with the ultra-large size 73µm in this study are less significant, compared to the results shown in Chapter 3. This can derive from the effect of water and cement ratios in the design mortars. Therefore, it can be concluded that the water and cement ratio is also an important factor that will impact on the properties of PRG-cement based composites. Therefore, further studies should consider the effects of all of these factors on the properties of cement-based composites containing PRG additives to better understand the mechanism of PRG-cement based composites so that the application of PRG as an additive in construction materials can be standardized in the near future.

4. Conclusions

The effects of the different sizes of PRG on the mechanical and durability properties of cement-based mortars with curing ages have been presented in this Chapter. The following conclusions have been drawn from the results and discussion:

- The mechanical properties of PRG-cement based mortars are dependent on the sizes and densities of PRG. Incorporating PRG into cement-based mortars can improve their compressive, flexural, and tensile strengths at short-term and long-term curing ages. The mixes containing the PRG sizes of 20µm and 73µm shows higher enhancements than that with size 40µm. The mix with the ultra-large size of 73µm presents the best improvement in 7-, 28-, 90-, and 270-day compressive strengths which are 6.9, 12.5, 7, and 18.4% higher than the control mix. There is a slight difference from the enhancement compressive

strength rates between the mix with PRG size 20µm and 73µm at 7-, 28-, 90-day, which are 6.2, 12.5, 6.7 respectively for size 20µm; whereas, there is a significant difference between them at 270-day, which is 8.6% for size 20µm compared to 18.4% for size 73µm.

- The enhancements in flexural and direct tensile strengths of the mortars show similar trends with their compressive strengths. The mix containing PRG size 73µm shows the best improvement in flexural and tensile strengths, followed by that of size 20µm and then 40µm. The enhancement in mechanical strengths of the mortars accounts for the improvement of compactness of mortars, which is due to the increase in cement hydration degrees, the reduction of distances between cement particles, and the most important part from adhesion friction forces between PRGs and cementitious gels which depend on the sizes of PRG. The lower enhancement of size 40µm could be due to its higher density compared to size 20µm and 73µm, resulting in the strong agglomeration and formation of multi-layers PRGs in the cement matrix due to van der Waals forces between PRGs that lead to a negative impact on the interaction between PRGs and the cement matrix. The results from mechanical strengths have confirmed the more benefit of the ultra-large size on the mechanical properties of the mortars at the long-term curing age compared to the smaller sizes.
- The results from compressive and tensile strengths at 28 days of the PRG size of 73µm between this study and the study in Chapter 3 have confirmed the high dependence of the strength enhancements of the mortars on water and cement ratios of the design mixes. 28-day compressive and tensile strengths of the mix containing PRG size 73µm with the ratio of 0.485 shows 30.1% and 38.6% respectively compared to the control mix; whereas, the companion mix with the ratio of 0.55 only show 12.5% and 14.2% respectively compared to the control mix.
- PRG materials also show the benefit to enhance the durability properties of cement-based mortars. Incorporating PRG into cement mortars can decrease the water absorption and

void of the mortars. The mixes containing the PRG sizes of 20µm and 73µm develop 8.15 & 8.28 % and 8.52 & 8.53 % lower water absorptions and voids than the control mix, respectively**.** The mix with size 40µm develops a lower enhancement of the water absorption and void than size 20µm and 73µm, which are approximately 2.55 and 3.5 %, respectively.

- There is no clear positive influence of PRG on the drying shrinkage results of cement-based mortars. Only the mix containing PRG size 73µm shows a slight improvement in the drying shrinkage throughout from 7-day to 270-day curing ages, which decrease approximately 1.0% at 7 days and 9.5% at 270 days, respectively. The reason for being no clear positive effect of PRG on drying shrinkage of the mortars can be attributed to the random distribution of PRGs in the cement matrix that can create tortuous paths in the cement matrix to prevent moisture loss during the drying shrinkage process.
- The mortars containing PRG materials present a positive influence on resisting the sulfate solution at all the curing ages. The mix with size 73µm shows the best observation on sulfate expansion of the mortars, which decreases about 58.2% and 88.6% lower sulfate expansion at 7 days and 270 days, respectively, compared to the control mix.
- The addition of PRG to the mortars can decrease the water penetration depth into the mortar mixes. The mixes containing the PRG sizes of 20µm, 40µm, and 73µm develop 4.02, 47.71, and 46.25% lower water penetration depth at 28 days than that of the control mix, respectively.

The results of this Chapter have not only provided a better understanding of incorporating PRG into cementitious composites, but they have also confirmed the benefit of PRG materials (especially for the ultra-large size of PRGs) on mechanical and durability properties of cementitious composites. The study has also provided a valuable orientation in studying PRG-cement based composites: although the quality, size, and density of PRG materials are important factors for improving the properties of PRG-cement based composites, other factors

such as water and cement ratios and curing conditions are also important to their enhancements that should be considered in future studies.

REFERENCES

[1] B. Wang, R. Jiang, Z. Wu, Investigation of the mechanical properties and microstructure of graphene nanoplatelet-cement composite, Nanomaterials 6(11) (2016) 200.

[2] J. Tao, X. Wang, Z. Wang, Q. Zeng, Graphene nanoplatelets as an effective additive to tune the microstructures and piezoresistive properties of cement-based composites, Construction and Building Materials 209 (2019) 665-678.

[3] V.D. Ho, C.T. Ng, C.J. Coghlan, A. Goodwin, C. Mc Guckin, T. Ozbakkaloglu, D. Losic, Electrochemically produced graphene with ultra large particles enhances mechanical properties of Portland cement mortar, Construction and Building Materials 234 (2020).

[4] W. Baomin, D. Shuang, Effect and mechanism of graphene nanoplatelets on hydration reaction, mechanical properties and microstructure of cement composites, Construction and Building Materials 228 (2019) 116720.

[5] H. Du, S. Dai Pang, Enhancement of barrier properties of cement mortar with graphene nanoplatelet, Cement and Concrete Research 76 (2015) 10-19.

[6] S. Sun, B. Han, S. Jiang, X. Yu, Y. Wang, H. Li, J. Ou, Nano graphite platelets-enabled piezoresistive cementitious composites for structural health monitoring, Construction and Building Materials 136 (2017) 314-328.

[7] J.-L. Le, H. Du, S. Dai Pang, Use of 2D Graphene Nanoplatelets (GNP) in cement composites for structural health evaluation, Composites Part B: Engineering 67 (2014) 555-563.

[8] AS3972, General purpose and blended cements, Standard, Standard Australia, Australian Standard, 2010.

[9] AS1478.1, Chemical admixtures for concrete, mortar and grout - Admixtures for concrete, Australian Standard, 2000.

[10] ASTM-C109/C109M-07, Standard test method for compressive strength of hydraulic

cement mortars, ASTM International: USA 2008, 2008.

[11] ASTM-C307-03, Standard Test Method for Tensile Strength of Chemical-Resistant Mortar, Grouts, and Monolithic Surfacings Monolithic Surfacings, ASTM International, 2012.

[12] ASTM C 348–18, Standard Test Method for Flexural Strength of Hydraulic-Cement Mortars, Designation: C 348 (2010).

[13] ASTM C642-13, Standard test method for density, absorption, and voids in hardened concrete, (2013).

[14] ASTM C596-09, Standard Test Method for Drying Shrinkage of Mortar Containing Hydraulic Cement, (2017).

[15] ASTM C1012/C1012M, Standard Test Method for Length Change of Hydraulic Cement Mortars Exposed to a sulfate Solution, American Society for Testing and Materials Philadelphia, 2012.

[16] ASTM C490/C490M, Standard practice for use of apparatus for the determination of length change of hardened cement paste, mortar, and concrete., ASTM, West Conshohocken, PA (2013).

[17] BS EN 12390-8: 2009, Testing hardened concrete - Part 8: Depth of penetration of water under pressure, BRITISH STANDARD 8 (2009).

[18] N. Kothiyal, S. Sharma, S. Mahajan, S. Sethi, Characterization of reactive graphene oxide synthesized from ball–milled graphite: its enhanced reinforcing effects on cement nanocomposites, Journal of adhesion science and Technology 30(9) (2016) 915-933.

[19] T.T. Mai, C.N. Ha Thuc, H.H. Thuc, Preparation of graphene nano-layer by chemical graphitization of graphite oxide from exfoliation and preliminary reduction, Fullerenes, Nanotubes and Carbon Nanostructures 23(8) (2015) 742-749.

[20] A. Eckmann, A. Felten, A. Mishchenko, L. Britnell, R. Krupke, K.S. Novoselov, C. Casiraghi, Probing the nature of defects in graphene by Raman spectroscopy, Nano letters 12(8) (2012) 3925-3930.

[21] X. Liu, X. Wang, G. Licht, S. Licht, Transformation of the greenhouse gas carbon dioxide to graphene, Journal of CO2 Utilization 36 (2020) 288-294.

[22] Y. Shen, A.C. Lua, A facile method for the large-scale continuous synthesis of graphene sheets using a novel catalyst, Scientific reports 3(1) (2013) 1-6.

[23] A.C. Ferrari, J. Meyer, V. Scardaci, C. Casiraghi, M. Lazzeri, F. Mauri, S. Piscanec, D. Jiang, K. Novoselov, S. Roth, Raman spectrum of graphene and graphene layers, Physical review letters 97(18) (2006) 187401.

[24] H. Yang, H. Cui, W. Tang, Z. Li, N. Han, F. Xing, A critical review on research progress of graphene/cement based composites, Composites Part A: Applied Science and Manufacturing 102 (2017) 273-296.

[25] V.D. Ho, C.-T. Ng, C.J. Coghlan, A. Goodwin, C. Mc Guckin, T. Ozbakkaloglu, D. Losic, Electrochemically produced graphene with ultra large particles enhances mechanical properties of Portland cement mortar, Construction and Building Materials 234 (2020) 117403.

[26] S.J. Chen, C.Y. Li, Q. Wang, W.H. Duan, Reinforcing mechanism of graphene at atomic level: Friction, crack surface adhesion and 2D geometry, Carbon 114 (2017) 557-565.

[27] A. Gholampour, M.V. Kiamahalleh, D.N. Tran, T. Ozbakkaloglu, D. Losic, Revealing the dependence of the physiochemical and mechanical properties of cement composites on graphene oxide concentration, RSC Advances 7(87) (2017) 55148-55156.

[28] A. Gholampour, M. Valizadeh Kiamahalleh, D.N. Tran, T. Ozbakkaloglu, D. Losic, From Graphene Oxide to Reduced Graphene Oxide: Impact on the Physiochemical and Mechanical Properties of Graphene–Cement Composites, ACS applied materials & interfaces 9(49) (2017) 43275-43286.

[29] W. Lin, A. Cheng, R. Huang, C. Chen, X. Zhou, Effect of calcium leaching on the properties of cement-based composites, Journal of Wuhan University of Technology-Mater. Sci. Ed. 26(5) (2011) 990-997.

[30] C. Carde, R. François, Effect of the leaching of calcium hydroxide from cement paste on mechanical and physical properties, Cement and Concrete Research 27(4) (1997) 539-550.

[31] C. Carde, R. François, J.-M. Torrenti, Leaching of both calcium hydroxide and CSH from cement paste: Modeling the mechanical behavior, Cement and concrete research 26(8) (1996) 1257-1268.

[32] A.N. Junior, M.S. Lemos, R.D. Toledo Filho, E.d.M.R. Fairbairn, J. Dweck, Early stages hydration of high initial strength Portland cement, Journal of thermal analysis and calorimetry 113(2) (2013) 659-665.

[33] S. Lv, Y. Ma, C. Qiu, T. Sun, J. Liu, Q. Zhou, Effect of graphene oxide nanosheets of microstructure and mechanical properties of cement composites, Construction and building materials 49 (2013) 121-127.

[34] R. Jadhav, N. Debnath, Computation of X-ray powder diffractograms of cement components and its application to phase analysis and hydration performance of OPC cement, Bulletin of Materials Science 34(5) (2011) 1137-1150.

[35] S. Sharma, N. Kothiyal, Comparative effects of pristine and ball-milled graphene oxide on physico-chemical characteristics of cement mortar nanocomposites, Construction and Building Materials 115 (2016) 256-268.

[36] F. Rendell, R. Jauberthie, M. Grantham, Deteriorated concrete: Inspection and physicochemical analysis, Thomas Telford2002.

[37] J. Elena, M.D. Lucia, X-RAY Diffraction Study of hydration Processes in the Portland Cement, JAESVol 1 14.

[38] M. Horgnies, J. Chen, C. Bouillon, Overview about the use of Fourier transform infrared spectroscopy to study cementitious materials, WIT Trans. Eng. Sci 77 (2013) 251-262.

[39] P. Yu, R.J. Kirkpatrick, B. Poe, P.F. McMillan, X. Cong, Structure of calcium silicate hydrate (C-S-H): Near-, mid-, and far-infrared spectroscopy, Journal of the American Ceramic Society 82(3) (1999) 742-748.

[40] L. Fernández Carrasco, D. Torrens Martín, L. Morales, S. Martínez Ramírez, Infrared spectroscopy in the analysis of building and construction materials, InTech2012.

[41] S. Ghosh, S. Handoo, Infrared and Raman spectral studies in cement and concrete, Cement

and Concrete Research 10(6) (1980) 771-782.

CHAPTER 7:

EXPLORING THE INFLUENCE OF THE GRAPHENE OXIDE ON ENHANCING MECHANICAL AND DURABILITY PROPERTIES OF AMBIENT-CURED ALKALI-ACTIVATED BINDER MORTARS PREPARED WITH DIFFERENT SANDS

THE AIM AND OBJECTIVE OF THIS CHAPTER:

Aim: This chapter aims to explore the effect of GO on mechanical, durability, and microstructural properties of FA/GGBS alkali-activated binder (AAB) mortars prepared with natural sand (NS) and lead smelter slag sand (LSS); and contributing to developing green construction materials by using waste-based materials to replace both cement binder and natural sand.

Objectives 1: investigating the influence of the addition of GO to AAB on compressive and tensile strengths, water absorption, and drying shrinkage of AAB mortars prepared with NS and LSS.

Objectives 2: analysing the microstructures of GO-AAB based mortars prepared with NS and LSS to gain understanding of the interaction mechanism of GO and AAB based mortars containing NS and LSS.

Statement of Authorship

Title of Paper	Influence of graphene oxide on the properties of ambient-cured alkali-activated binder mortars prepared with natural sand and lead smelter slag
Publication Status	☐ Published ☐ Accepted for Publication ☐ Submitted for Publication ☑ Unpublished and Unsubmitted work written in manuscript style
Publication Details	Ho, V. D., Gholampour, A., Losic, D., & Ozbakkaloglu, T. Influence of graphene oxide on the properties of ambient-cured alkali-activated binder mortars prepared with natural sand and lead smelter slag.

Principal Author

Name of Principal Author (Candidate)	Van Dac Ho		
Contribution to the Paper	Literature review, analysis of test results, and preparation of the manuscript		
Overall percentage (%)	50		
Certification:	This paper reports on original research I conducted during the period of my Higher Degree by Research candidature and is not subject to any obligations or contractual agreements with a third party that would constrain its inclusion in this thesis. I am the primary author of this paper.		
Signature		Date	25/03/2020

Co-Author Contributions

By signing the Statement of Authorship, each author certifies that:

i. the candidate's stated contribution to the publication is accurate (as detailed above);

ii. permission is granted for the candidate in include the publication in the thesis; and

iii. the sum of all co-author contributions is equal to 100% less the candidate's stated contribution.

Name of Co-Author	Aliakbar Gholampour		
Contribution to the Paper	Analysis and preparation of the manuscript.		
Signature		Date	27/03/2020

Name of Co-Author	Togay Ozbakkaloglu		
Contribution to the Paper	Conception of the research, analysis and interpretation of the results, review and revisions of the manuscript.		
Signature		Date	09/04/2020

Name of Co-Author	Dusan Losic		
Contribution to the Paper	Review of the manuscript.		
Signature		Date	11/04/2020

Journal paper 4 (In preparation)

Influence of graphene oxide on the properties of ambient-cured alkali-activated binder mortars prepared with natural sand and lead smelter slag

Van Dac Ho[1,2], Aliakbar Gholampour[3], Dusan Losic[2], Togay Ozbakkaloglu[4*]

[1]School of Civil, Environmental and Mining Engineering, The University of Adelaide, South Australia, 5005, Australia

[2]School of Chemical Engineering, The University of Adelaide, South Australia, 5005 Australia

[3]Department of Infrastructure Engineering, The University of Melbourne, Melbourne, VIC, Australia

[4]Ingram School of Engineering, Texas State University, San Marcos, TX, United States

*Corresponding author; Email address: togay.oz@txstate.edu

ABSTRACT

Using waste-based materials in concrete, such as fly ash (FA), ground granulated blast furnace slag (GGBS), and lead smelter slag (LSS), to replace Portland cement and natural sand (NS) offers great potential for reducing the environmental impact of concrete. In this study, the effects of graphene oxide (GO) additive on mechanical and durability properties of FA/GGBS-based alkali-activated binder (AAB) mortars that contain NS and LSS sand were assessed. Scanning electron microscopy and microstructural analyses were also performed on the mortars for assessing the reinforcement mechanism of GO in the composite matrix. The results show that the increase of GGBS content in AAB (i.e. 0%, 20% and 50% GGBS) results in a significant increase in compressive and tensile strengths, and a decrease in drying shrinkage, flowability, and water absorption of the mortars. It is found that mortars with 0.05% and 0.1% GO additives provide better mechanical and durability properties compared to the control mixes. It is also shown that oxygen functional groups of GO sheets have been reduced in alkaline solution and they were turned into the form of reduced graphene oxide (rGO) sheets, which result in a higher degree of wrinkling in their shapes. The better properties of AAB mortars containing GO additives are attributed to the improvement of the gel matrix formed through the combination of chemical and mechanical interactions between rGO sheets and the gel products. The outcomes of this study present great potential for the combined use of waste-based materials and GO additives in developing eco-friendly construction materials that can help in reducing the environmental effect of Portland cement and extraction of NS.

Keywords: Geopolymer mortars; Alkali-activated binders; Ground granulated blast furnace slag; Lead smelter slag; Fly ash; Mechanical and durability properties.

1. Introduction

Ordinary Portland cement (OPC), which is the most common binder of cementitious materials (Low, 2005), is one of the major contributors to greenhouse gases that accounts for 5% to 7% of the carbon dioxide (CO_2) emissions globally (Gholampour et al., 2019; Mehta and Meryman, 2009; Van den Heede and De Belie, 2012). As a result, much effort has been made in recent years to reduce the amount of CO_2 emissions associated with OPC products, such as improving cement plant efficiency (Van den Heede and De Belie, 2012), using supplementary cementitious materials (Lothenbach et al., 2011) and replacing OPC with waste-based materials (Shi et al., 2011; Shi et al., 2019; Van den Heede and De Belie, 2012). Meanwhile, over-exploitation of the natural sand (NS), which is the most commonly used fine aggregate in infrastructure, has been causing harmful environmental consequences on the ecosystem (Bravard et al., 2013; Sankh et al., 2014). Therefore, finding materials to alter NS has become imperative.

There has been considerable interest in applying waste-based materials in replacing OPC and NS in recent years (Gholampour et al., 2019). Waste materials such as ground granulated blast furnace slag (GGBS) and fly ash (FA) (Gholampour and Ozbakkaloglu, 2017), and lead smelter slag (LSS) (Atzeni et al., 1996; Tripathi et al., 2013) have shown great potential for the replacement of OPC and NS respectively to cut down the negative environmental impact of these materials (Gholampour et al., 2019). Some new materials to replace OPC in part or fully have been explored and alkali-activated binders (AABs) have been identified as one of the most promising of such materials. Geopolymers, which are the gels formed by alkali-activating low calcium materials such as FA, have drawn much attention thanks to their cost efficiency, high resistance to corrosion and the stability in chemical structures (Davidovits, 2008; Saafi et al., 2013). A major issue of FA used in geopolymers is that geopolymers containing FA develop low strengths under ambient curing conditions. For overcoming this limitation, researchers investigated combining FA with materials that have a high calcium oxide (CaO) content, such

as GGBS, in order to significantly improve their mechanical properties at the early stage (Deb et al., 2014; Gholampour et al., 2019; Jawahar and Mounika, 2016; Wardhono et al., 2015). Although FA/GGBS-based AAB composites can develop high compressive strengths, they still exhibit brittle behavior as well as low toughness, low flexural and tensile strength similar to OPC-based composites (Saafi et al., 2015). To address these limitations, researchers have explored the use of different additives to reinforce AAB, such as carbon fibers (Lin et al., 2008) or carbon nanotubes (Saafi et al., 2013). These additive materials have shown the ability to enhance the toughness, and flexural and tensile strength of AAB due to preventing the propagation and opening of cracks (Shaikh, 2013). However, carbon fibers and nanotubes have low specific surface areas, aspect ratios and limited interfacial connections in the gel matrix, resulting in weak bonding and arresting crack propagations in concrete (Cwirzen et al., 2009).

Graphene and its derivatives, i.e. graphene oxide (GO), reduced graphene oxide (rGO), and pristine graphene (PRG), have recently shown great potential for improving microstructures of cementitious materials owing to their outstanding properties of high mechanical properties, aspect ratios and large specific surface areas (Geim and Novoselov, 2007; Han et al., 2015). GO containing abundant oxygen functional groups on its surface is highly dispersive in polar liquids (Kim et al., 2012), therefore, its use to improve the properties of organic composites (Du and Cheng, 2012) or cementitious composites (Shamsaei et al., 2018) has received significant attention. However, the exploration of using GO in alkali-activated based materials has been very limited and only few studies have been worked on the properties of GO-based geopolymers (Saafi et al., 2015; Yan et al., 2016). Yan et al. (2016) studied the influence of different GO dosages on mechanical properties and microstructures of geopolymer pastes cured at 60 °C in 7 days. They showed that the mixes with 0.3% and 0.5% of GO could increase the flexural strength and fracture toughness of geopolymer pastes by 45.5% and 61.5%, respectively. Saafi et al. (2015) reported that 0.35% GO could increase the flexural strength, Young's modulus, and flexural toughness of geopolymer pastes cured at 60 °C for 24 h by

134%, 376%, and 56%, respectively. They also revealed that the alkaline environment in geopolymers reduced oxygen-containing functional groups in GO, resulting in the formation of rGO sheets (rGOs) and the creation of the cross-link between rGOs and geopolymer matrix that leads to improvements in mechanical properties of geopolymer composites. However, these two studies dealt with heat-cured geopolymer pastes and no research has been studied on the influence of GO additives on mechanical and durability properties of ambient-cured AAB mortars prepared with NS or its alternative LSS sand.

To address this research gap, this paper presents the first systematic study on the mechanical, durability and microstructural properties of ambient-cured AAB mortars containing NS and LSS reinforced with GO. The findings are promising and show the significant potential of using GO to address the current drawbacks of AAB composites. It also contributes to developing green construction materials by saving NS resources and reducing the negative environmental impacts of OPC.

2. Experimental Program

2.1. Materials

GGBS and FA class F were provided by Adelaide Brighton Cement Ltd, which were a by-product from Birkenhead Works and Leigh Creek Coal in South Australia, respectively. Their chemical compositions are shown in Table 1.

NS with maximum particle sizes was 2.13 mm, which was obtained from McLaren Vale Quarry in Fleurieu Peninsula. LSS with maximum particle sizes was 1.94 mm, which was sourced from Port Pirie in South Australia. They were used as fine aggregates in mortars. The particle size distribution and physical properties of the fine aggregates are presented in Fig. 1 and Table 2, respectively. The chemical composition of LSS is listed in Table 1. GO was produced from the oxidation of graphite flakes, which were obtained from Valence Industries Ltd. Australia, using the improved Hummer's method (Marcano et al., 2010).

The alkaline activator consisted of sodium hydroxide (NaOH) and sodium silicate (Na_2SiO_3) solutions. The ratio by weight of Na_2SiO_3/NaOH was 2.5, which was premixed by the supplier. The concentration of sodium hydroxide was 12 M, and sodium silicate with the ratio by weight of the silicon dioxide-to-sodium oxide ratio (SiO_2/Na_2O) was 3.

Table 1. Chemical composition of FA, GGBS, and LSS.

Compounds	FA (%)	GGBS (%)	LSS (%)
SiO_2	55.38	33.10	21.39
Al_2O_3	28.14	13.33	3.56
Fe_2O_3	3.31	0.69	28.10
CaO	3.45	42.83	23.11
MgO	1.85	5.57	5.44
Na_2O	2.30	0.27	0.27
K_2O	1.39	0.31	0.26
SO_3	0.32	1.81	-
P_2O_5	0.78	0.01	-
TiO_2	-	-	0.25
ZnO	-	-	9.47
PbO	-	-	4.06
LOI	3.08	2.08	4.09

FA: Fly ash

GGBS: Ground granulated blast furnace slag

LSS: Lead smelter slag

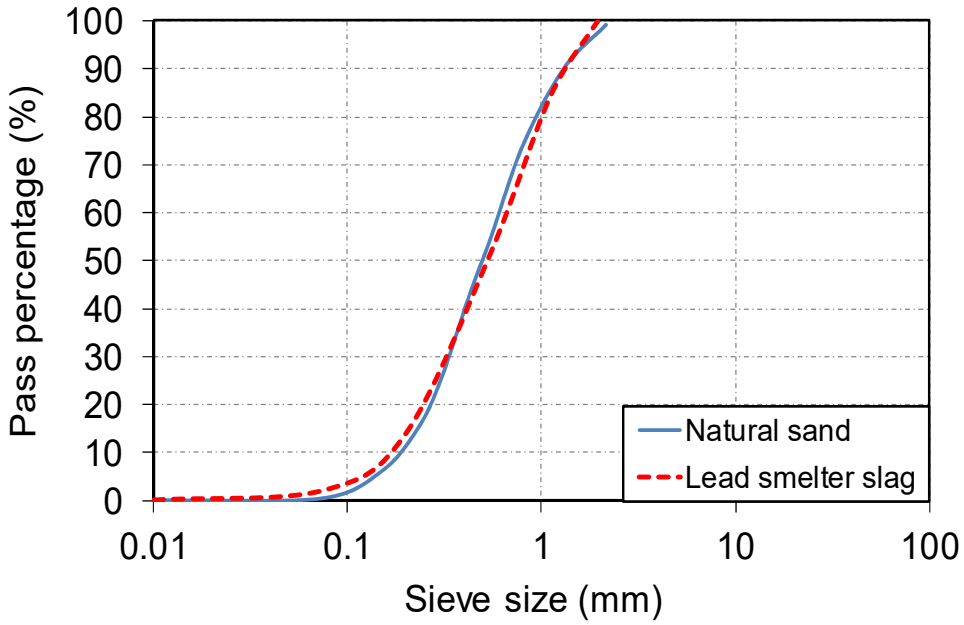

Fig. 1. Sieving test results of fine aggregates: Particle size distribution.

Table 2. Properties of fine aggregates.

Aggregate type	Maximum size (mm)	Specific gravity (SSD)	Water absorption (%)	Fineness modulus
NS	2.13	2.63	0.4	2.56
LSS	1.94	3.30	0.6	2.51

NS: Natural sand
LSS: Lead smelter slag

2.2. Mix design and preparation of AAB mortars

The details of the designed mixes are shown in Table 3. 18 unique mixtures of AAB mortars were prepared: nine mixes with NS and nine mixes with LSS. Binders were prepared with three different ratios including 100% FA, 80% FA/20% GGBS, and 50% FA/50% GGBS. An effective alkaline liquid-to-binder (l_{eff}/b) ratio of 0.45, 0.55, and 0.75 was used in 100% FA, 80% FA/20% GGBS, and 50% FA/50% GGBS mixes to achieve workable mixes, respectively. Two GO dosages of 0.05% and 0.1% were used in the mixes based on the comprehensive review of the literature, which revealed that 0.05-0.1% is the range of optimal graphene dosages on mechanical strengths of mortar composites without the considerable impact on the

agglomeration of nanomaterials because of van der Waals forces (Gholampour et al., 2017a; Ho et al., 2020; Shamsaei et al., 2018).

The mixes in Table 3 were labeled as following: NS and LS refer to natural sand and lead smelter slag used in the mixes, respectively; the numbers after them indicate the ratio of FA and GGBS binders used in each mix in percentage; the letters G0.05 and G0.1 stand for 0.05% and 0.1% of GO additives in each mix, respectively. For example, NS100 and LS100 represent the mixes prepared with 100% FA and NS, and 100% FA and LSS, respectively; LSS80/20G0.05 refers to the mix prepared with LSS, 80% FA and 20% GGBS, and 0.05% GO additive.

Table 3. Mix proportions and physical properties of mixes.

Mix	FA (kg/m^3)	GGBS (kg/m^3)	NS (kg/m^3)	LSS (kg/m^3)	GO* (g/m^3)	Na_2SiO_3 (kg/m^3)	NaOH (kg/m^3)	l_{eff}/b	Hardened density (kg/m^3)
NS100	570	–	1425	–	–	183	73	0.45	2190
NS80/20	444	111	1425	–	–	218	87	0.55	2213
NS50/50	265	265	1425	–	–	284	114	0.75	2241
NS100G0.05	570	–	1425	–	0.28	183	73	0.45	2209
NS100G0.1	570	–	1425	–	0.57	183	73	0.45	2212
NS80/20G0.05	444	111	1425	–	0.28	218	87	0.55	2218
NS80/20G0.1	444	111	1425	–	0.57	218	87	0.55	2223
NS50/50G0.05	265	265	1425	–	0.28	284	114	0.75	2249
NS50/50G0.1	265	265	1425	–	0.57	284	114	0.75	2256
LS100	570	–	–	1788	–	183	73	0.45	2437
LS80/20	444	111	–	1788	–	218	87	0.55	2476
LS50/50	265	265	–	1788	–	284	114	0.75	2513
LS100G0.05	570	–	–	1788	0.28	183	73	0.45	2444
LS100G0.1	570	–	–	1788	0.57	183	73	0.45	2453
LS80/20G0.05	444	111	–	1788	0.28	218	87	0.55	2483
LS80/20G0.1	444	111	–	1788	0.57	218	87	0.55	2491
LS50/50G0.05	265	265	–	1788	0.28	284	114	0.75	2520
LS50/50G0.1	265	265	–	1788	0.57	284	114	0.75	2528

* By weight of the binder

The procedure described below was applied to prepare the AAB mortars: first the alkaline solution and GO were mixed and sonicated for 30 minutes. After that, fine aggregates and binders were mixed in three minutes, and GO-alkaline solutions was then gradually added to the mixes for about five minutes including one minute for checking and stirring. All the specimens were vibrated for one minute by a vibration table for eliminating the entrapped air in the specimens during the process of mounting. The specimens were covered by plastic sheets for preventing the moisture loss and were demolded after 24 h of curing at room temperature. All the samples were continued curing in fog room at the ambient temperature of 23 ± 2 °C till the days of testing.

2.3. Testing methods

Different tests were conducted on all the mixes: flowability, compressive strength, direct tensile strength, water absorption, and drying shrinkage for investigating the fresh and hardened properties of AAB mortars. The flowability of all the fresh mortars was conducted immediately after mixings, based on ASTM C1437 (ASTM-C1437, 2015). For hardened mortars, the compressive and tensile strengths were associated with ASTM standards C109/C109M-07 (ASTM-C109/C109M-07, 2008) (50 mm cube samples at 7, 28, and 56 days) and C307-03 (ASTM-C307-03, 2012) (dog-bone shaped samples at 28 days), respectively. Cylinders with size 75x50 mm were utilized for water absorption tests at 28 days based on ASTM standard C1585-13 (ASTM C1585-13, 2013). 25×25×285 mm prisms were utilized to measure drying shrinkage at 7, 14, 21, and 28 days, complied with ASTM standard C596-09 (ASTM C596-09, 2017). Scanning electron microscopy (SEM) images were conducted by FEI Quanta 450 for analyzing the morphology of sands, binders, and the microstructure of AAB mortars. The results of each designed mix were determined by calculating the average of three nominally similar specimens.

3. Results and Discussion

3.1. Characterization of some key ingredients used for AAB mortars

Fig. 2(a) presents the X-ray diffraction (XRD) pattern of NS. It is shown in the figure that the XRD pattern of NS has no amorphous phases and sharp peaks are detected at the positions from 21.2° to 77.9°, denoting all the crystalline phases are quartz (SiO_2) of NS (Bahoria et al., 2018; Zainuri, 2015). Fig. 2(b) shows the XRD pattern of LSS. As shown in the figure, LSS has mostly amorphous phases and some peaks of the crystalline phases of Wustite (FeO) are detected at the positions of 37.02°, 42.86°, and 61.74°, which is consistent with characteristics of LSS shown previously (Zheng et al., 2014).

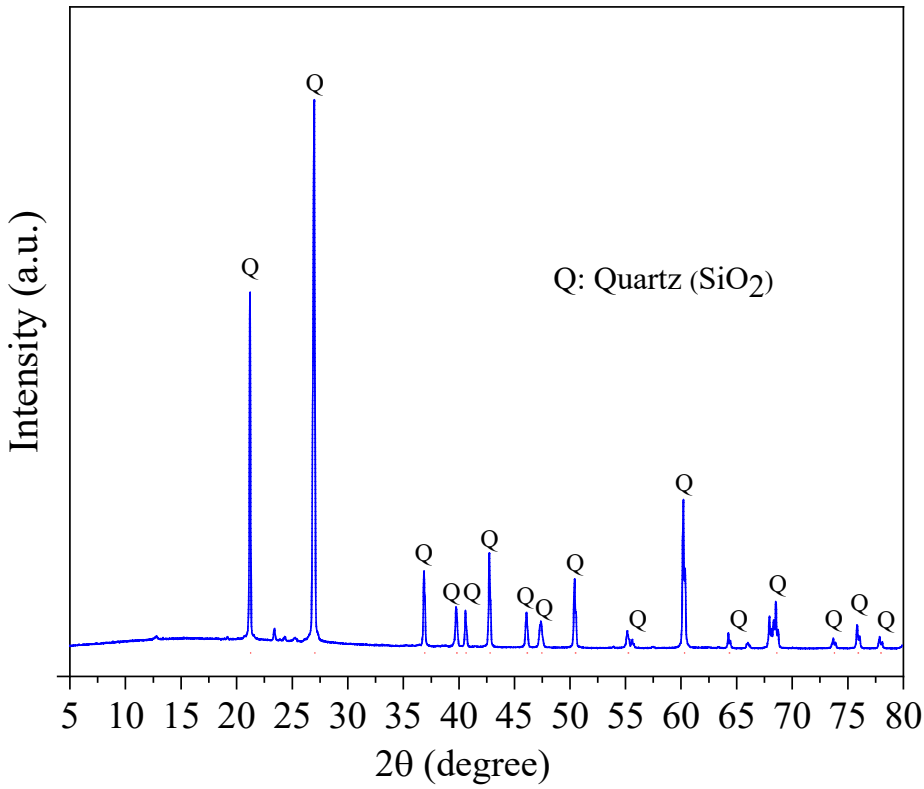

(a)

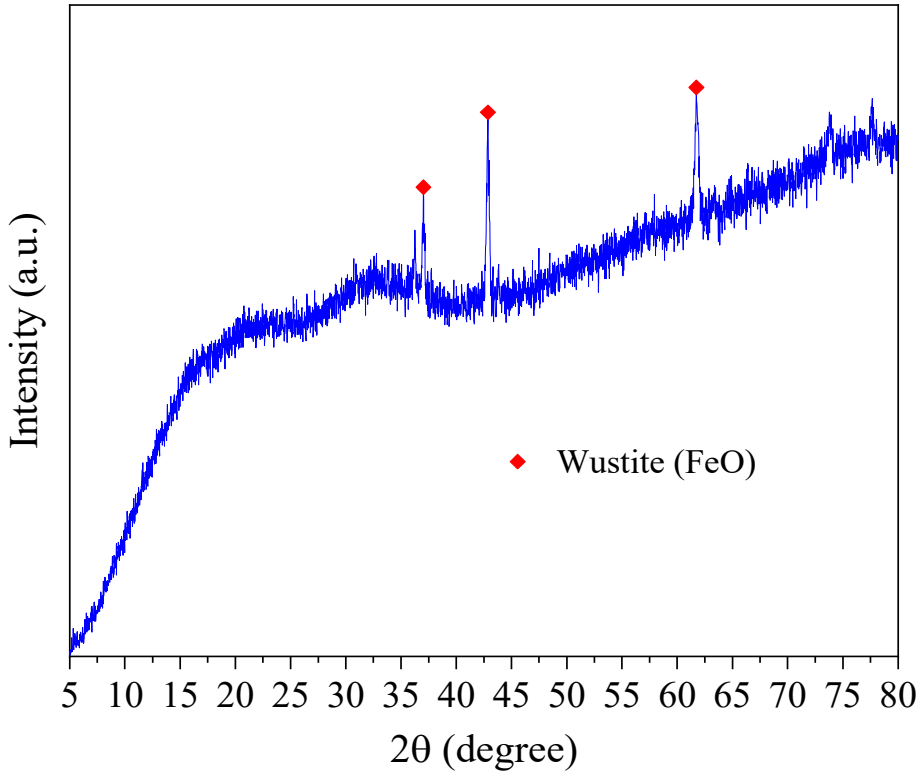

(b)

Fig. 2. X-ray diffraction patterns of: (a) NS and (b) LSS.

Fig. 3(a) shows the atomic force microscopy of GO sheets. As shown in the figure, the average size and thickness of GO are 1 μm and 1 nm, respectively. The images of graphite flakes and the final GO product in water solution (1 mg/ml) are presented in Fig. 3(b) and (c), respectively. It is shown in the figure that while the natural graphite flakes are dark in color, the final GO product in water is brown in color that shows the success of the oxidation of the natural graphite. Fig. 4(a)-(c) shows the typical images of GO obtained by transmission electron microscopy, XRD analysis, and thermogravimetric analysis (TGA), respectively. The typical wrinkling and irregular shape of GO sheets can be seen in Fig. 4(a). The scattering angle of GO in XRD shown in Fig. 4(b) is detected at 11.1°. Based on Bragg's Law, the d-spacing between layers of GO was 0.79 nm. The trends of the weight loss and the derivative weight change from TGA shown in Fig. 4(c) indicate the typical decomposition pattern of oxygen functional groups of GO (Tran et al., 2014).

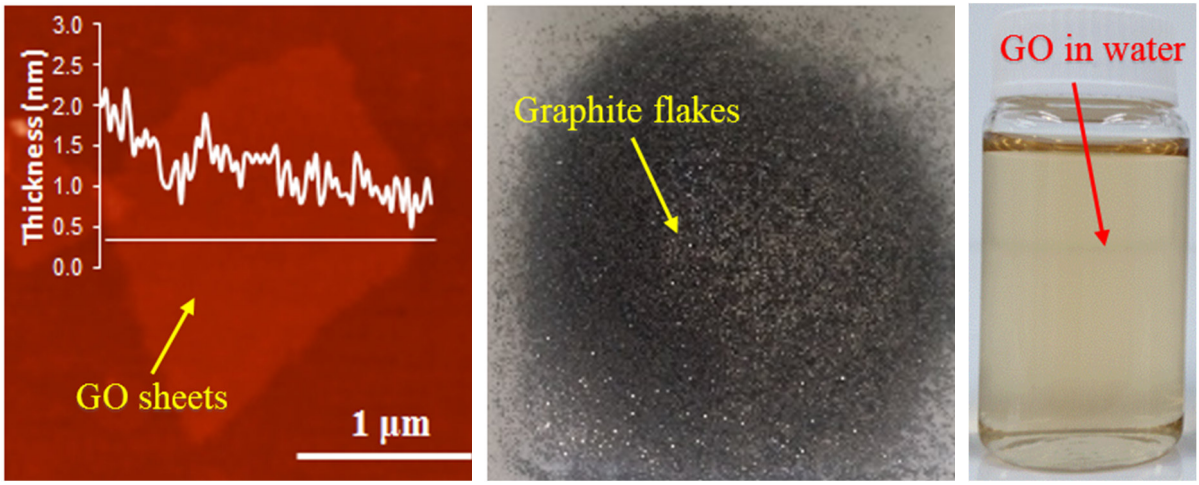

(a) (b) (c)

Fig. 3. (a) Atomic force microscopy image of GO sheets; photographs of (b) graphite flakes and (c) GO sheets in water solution (1 mg/ml).

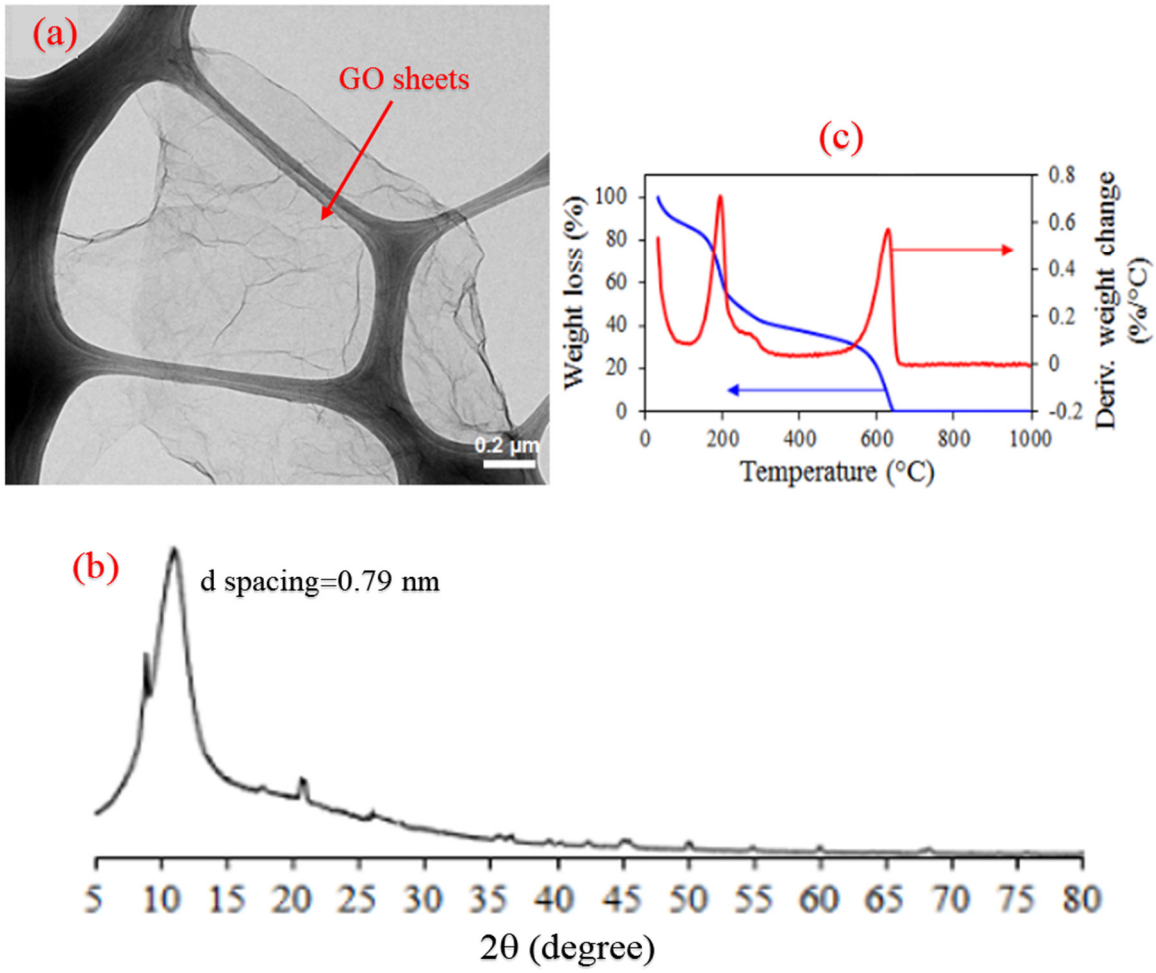

Fig. 4. a) Transmission electron microscopy image, (b) X-ray diffraction, and (c) Thermalgravimetric analysis plots of GO material used for mortar composites.

3.2. Flowability and hardened density of AAB mortars

The flowability results of different AAB mortars are presented in Fig. 5. The flow values were determined as the percentage of the increase in diameter of mortar spread from the original base of the conical mold. It can be seen that the flowability of the mortars with both sand types decreases when GGBS content (GGBS%) increases in the binder, which is attributed to the faster chemical reaction of GGBS in alkaline activator than that of FA, and also to the different morphologies of FA and GGBS (Nath and Sarker, 2014), which is discussed later in Section 3.5. Moreover, for each of the designed mixes, the addition of GO to AAB mortars decreases their flowability, and this rate of reduction increases with GO content. This is due to the large specific surface area of GO, causing more solution needed for lubricating GO's surfaces, which is consistent with the observations of previous researches on the influences of GO and PRG on the flow of conventional cement composites (Ho et al., 2020; Shang et al., 2015).

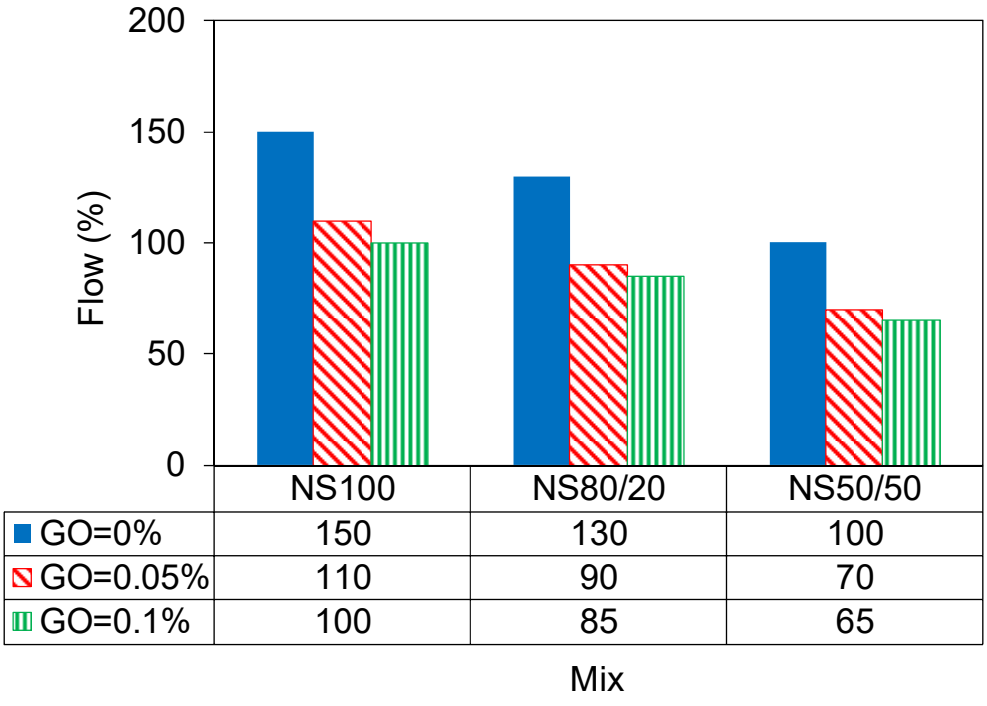

	NS100	NS80/20	NS50/50
GO=0%	150	130	100
GO=0.05%	110	90	70
GO=0.1%	100	85	65

(a)

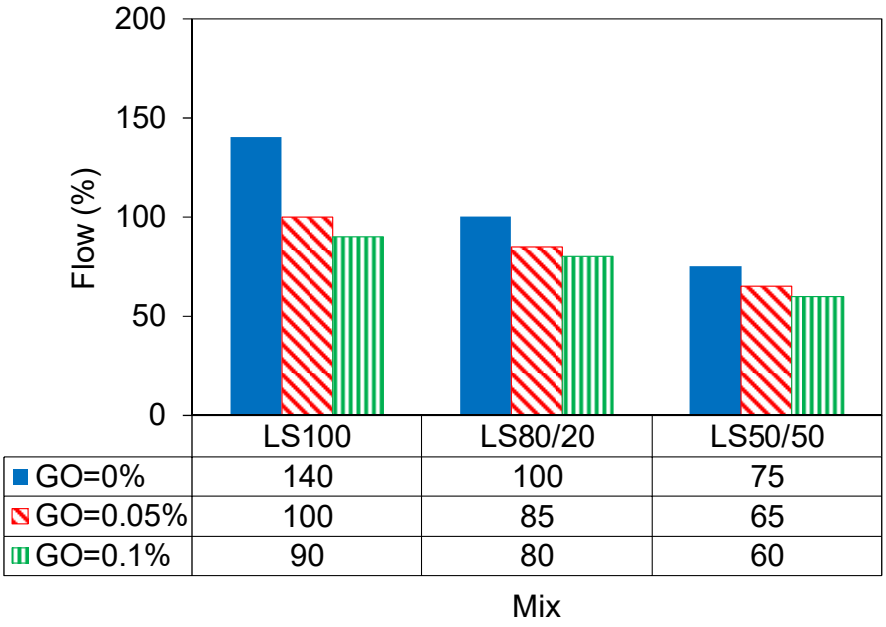

(b)

Fig. 5. Flowability test results of: (a) NS, (b) LSS group mixes.

As can be seen in Fig. 5(a), the NS100 mix without GO had the highest flowability in NS series. Incorporating GO led to a decrease in the flowability of NS mixes. The flowability of NS100, NS100G0.05, and NS100G0.1 were 50%, 57.1%, and 53.8% higher than those of mixes NS50/50, NS50/50G0.05, and NS50/50G0.1, respectively.

Fig. 5(b) shows that the LS100 mix without GO had the highest flowability in LSS series. The flowability of LSS mixes decreased with a rise in the GO content. The flowability of LS100, LS100G0.05, and LS100G0.1 mixes were 86.7%, 53.8%, and 50% higher than those of LS50/50, LS50/50G0.05, and LS50/50G0.1 mixes, respectively. Fig. 5 also shows that AAB mortars with NS had higher flowability than those with LSS. 100% FA, 80% FA/20% GGBS, and 50% FA/50% GGBS mixes containing LSS exhibited approximately 9%, 14%, and 16% lower flowability than those with NS, respectively. This is due to the higher angularity of LSS compared with that of NS, resulting in higher interparticle friction in LSS mixes in comparison with that in NS mixes (Tiwari et al., 2016), which is discussed later in Section 3.5.

Table 3 presents the hardened densities of different AAB mortars at 28 days. As shown in the table, the densities of the LSS mixes were higher values than those of the NS mixes, which is attributed to the higher specific gravity of LSS (see Table 2). Results also exhibit that increasing GGBS% caused an increased hardened density of the mortars.

3.3. Mechanical properties of AAB mortars

3.3.1. Compressive strength

The compressive strengths of the NS and LSS mixes at 7, 28, and 56 days are shown in Fig. 6(a) and (b), respectively. As shown, at all curing ages, the strength of different mortars increased with increasing GGBS% for both sand types. This is attributed to the rich content of CaO in GGBS in comparison with that in FA (as shown in Table 1), resulting in the formation of both reaction products of Na_2O-Al_2O_3-SiO_2-H_2O (N-A-S-H) and CaO-SiO_2-H_2O (C-S-H) (or C-A-S-H for their contraction form) in mixes with GGBS (Nath and Sarker, 2012). The figure also illustrates that the mixes with 100% FA had significantly lower compressive strengths than those with 50% FA/50% GGBS mixes at early curing ages for both NS and LSS mixes. This is because of the slow reactivity of FA at ambient curing, resulting in a weaker bond of N-A-S-H gels formed at early stages, which progressively improved with the curing duration (Temuujin et al., 2009).

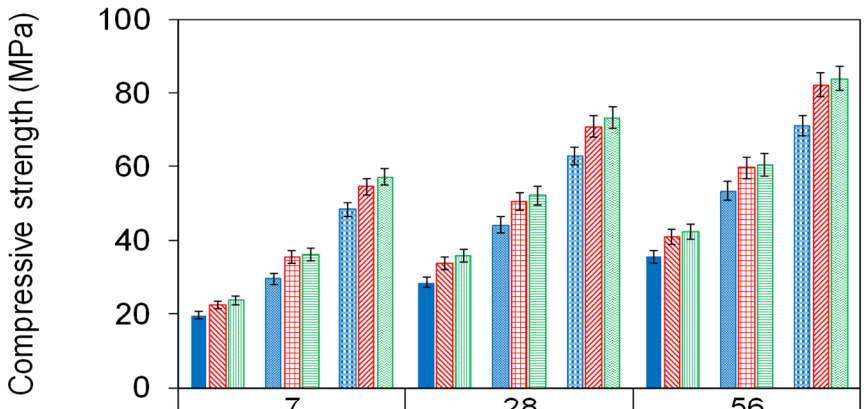

	7	28	56
NS100	19.7	28.6	35.5
NS100G0.05	22.4	33.9	41.1
NS100G0.1	23.7	35.8	42.3
NS80/20	29.5	44.1	53.4
NS80/20G0.05	35.4	50.5	59.7
NS80/20G0.1	36.2	52.1	60.5
NS50/50	48.4	62.9	71.1
NS50/50G0.05	54.6	70.9	82.2
NS50/50G0.1	57.2	73.3	83.9

Curing age (days)

(a)

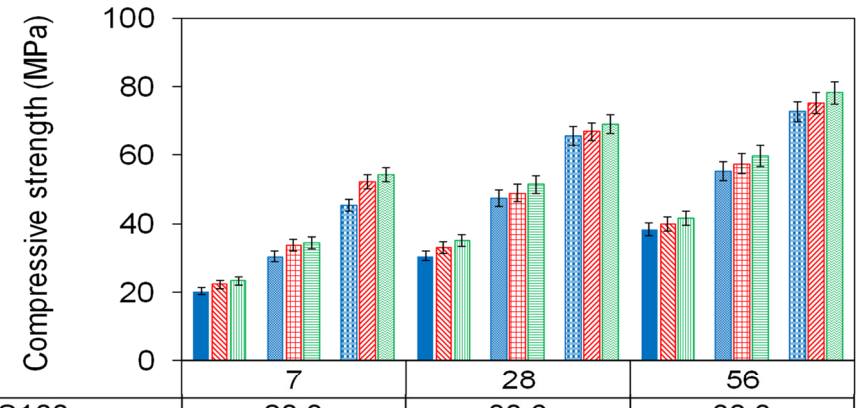

	7	28	56
LS100	20.3	30.6	38.3
LS100G0.05	22.3	33.1	39.8
LS100G0.1	23.3	35.1	41.7
LS80/20	30.4	47.5	55.2
LS80/20G0.05	33.7	48.9	57.5
LS80/20G0.1	34.3	51.5	59.8
LS50/50	45.4	65.6	72.7
LS50/50G0.05	52.2	66.8	75.1
LS50/50G0.1	54.3	68.9	78.1

Curing age (days)

(b)

Fig. 6. Variation of compressive strength of mixes with time: (a) NS, (b) LSS group mixes.

It is shown in Fig. 6(a) and (b) that incorporating GO in AAB mortars increased their compressive strengths in both NS and LSS mixes. In the NS series, compressive strengths of the mixes containing 0.05% GO at 7, 28, and 56 days were approximately 16, 15, and 14% higher than those containing 0% GO, respectively. In the LSS series, the mixes containing 0.05% GO had approximately 12, 4, and 4% higher 7-day, 28-day, and 56-day strengths than those containing 0% GO, respectively. It is also shown that increasing GO dosage from 0.05% to 0.1% caused a slight increase in strengths of the mortars. In the NS series, the mixes containing 0.1% GO exhibited approximately 4, 4, and 2% higher 7-day, 28-day, and 56-day strengths than those containing 0.05% GO, respectively. In the LSS series, compressive strengths of the mixes containing 0.1% GO at 7, 28, and 56 days were approximately 3, 5, and 4% higher than those containing 0.05% GO, respectively. The less significant increase in the compressive strengths of the mortars from 0.05% to 0.1% GO compared to those from 0% to 0.05% GO can be because of the lower dispersibility and higher agglomeration level of GO sheets in the mixes with 0.1% GO compared to those with 0.05% GO (Gholampour et al., 2017b), which will be discussed later in Section 3.5.

3.3.2. Direct tensile strength

Fig. 7(a) and (b) shows the 28-day direct tensile strengths of AAB mortars containing NS and LSS, respectively. As observed, the direct tensile strengths of the mixes increased with increasing GGBS% and GO dosage for both sand types. In the NS series, 50% FA/50% GGBS mixes containing 0, 0.05, and 0.1% GO exhibited approximately 26, 59, and 61% higher direct tensile strengths than the companion mixes with 100% FA, respectively. In the LSS series, the direct tensile strengths of 50% FA/50% GGBS mixes containing 0, 0.05, and 0.1% GO were approximately 23, 41, and 44% higher than those of the companion mixes with 100% FA, respectively.

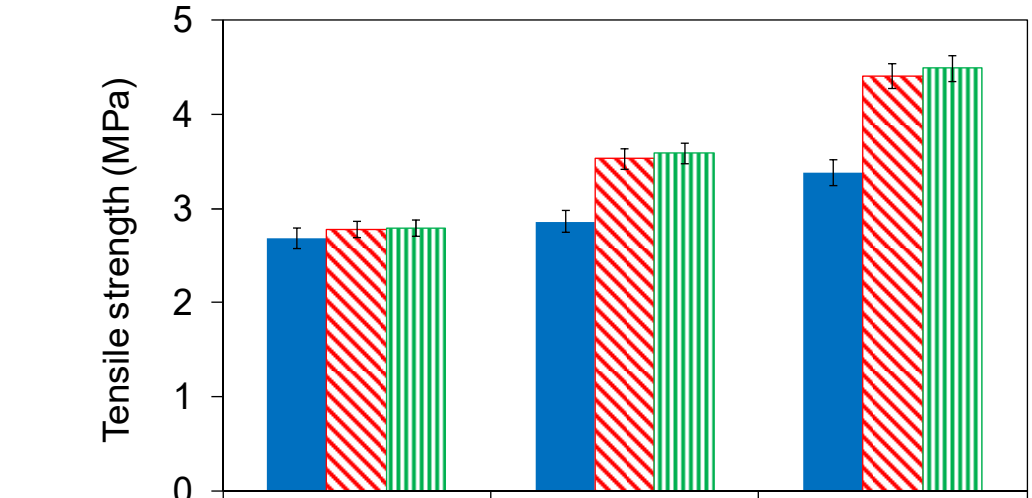

	NS100	NS80/20	NS50/50
GO=0%	2.68	2.86	3.38
GO=0.05%	2.78	3.53	4.41
GO=0.1%	2.79	3.59	4.49

Mix

(a)

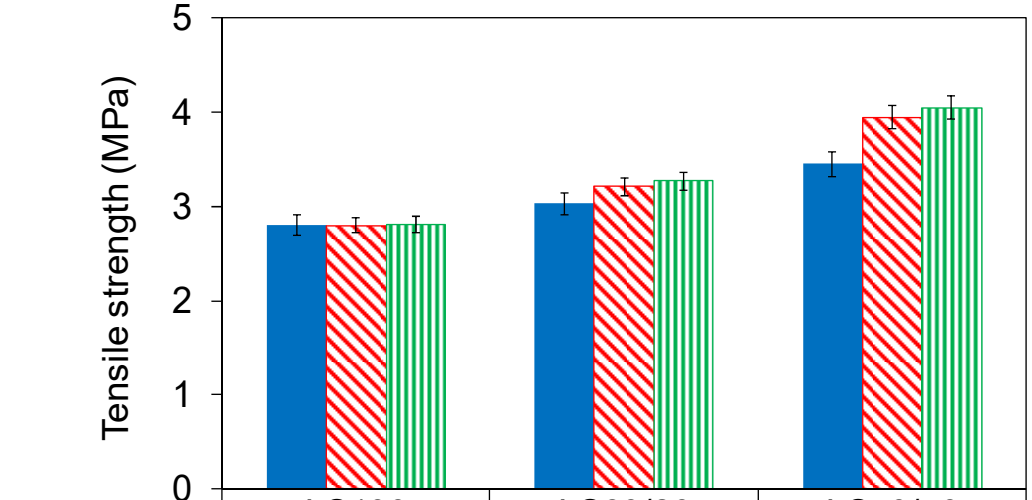

	LS100	LS80/20	LS50/50
GO=0%	2.80	3.03	3.45
GO=0.05%	2.80	3.21	3.95
GO=0.1%	2.81	3.27	4.05

Mix

(b)

Fig. 7. Direct tensile strength of mixes at 28 days: (a) NS, (b) LSS group mixes.

Fig. 7(a) and (b) shows that incorporating GO in AAB mortars increased their direct tensile strengths for both sand types, and this increase was more significant in the NS mixes than that in the LSS mixes, which is in line with the trends observed for compressive strengths at 28 days. Moreover, the strength enhancements were more pronounced in the mixes containing a higher GGBS% than those containing a lower GGBS%. In the NS series, the NS100G0.05, NS80/20G0.05, and NS50/50G0.05 mixes had approximately 4, 23, and 30% higher direct tensile strengths than the NS100, NS80/20, NS50/50 mixes, respectively. In the LSS series, incorporating 0.05% GO did not change the strength of LS100 mix, but the inclusion of 0.05% GO in LS80/20 and LS50/50 mixes resulted in an approximately 6% and 15% increase in the tensile strengths of the mortars, respectively. It is also shown in the figure that increasing GO dosage from 0.05% to 0.1% caused an approximately 2% increase in the direct tensile strengths of the mortars in both sand types. This indicates that an increase in the dosage of GO over 0.05% does not have a significant impact on tensile strengths of AAB mortars containing NS and LSS.

3.4. Durability properties

3.4.1. Water absorption

Fig. 8(a) and (b) shows the water absorption of AAB mortars containing NS and LSS at 28 days, respectively. As shown in the figure, for a given GO dosage, the absorption of the mixes decreased with increasing GGBS% for both sand types. This accounts for the larger content of hydration products (C-A-S-H) in the mortar mixes containing a higher GGBS%, resulting in the creation of a less porous microstructure compared to those containing a lower GGBS%, as discussed later in Section 3.5. In the NS series, 50% FA/50% GGBS mixes containing 0, 0.05, and 0.1% GO showed approximately 45, 34 and 37% lower water absorption than the companion mixes with 100% FA, respectively. In the LSS series, the water absorptions of 50% FA/50% GGBS mixes containing 0, 0.05, and 0.1% GO were approximately 39, 26, and 32% lower than those of the companion mixes with 100% FA, respectively. The figure also shows

that the water absorption of the LSS mixes without GO was slightly higher than that of the respective NS mixes, which can be explained by the higher water absorption of LSS than that of NS (shown in Table 2).

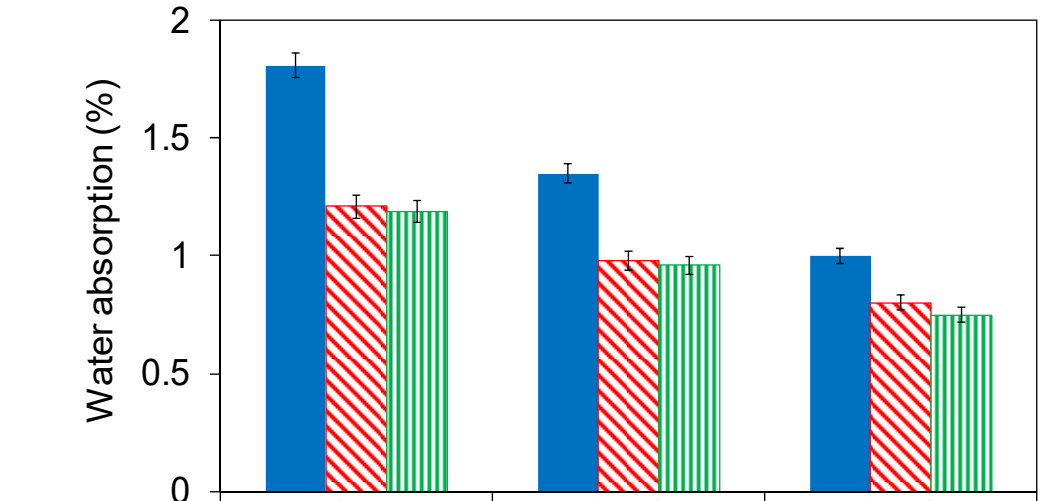

	NS100	NS80/20	NS50/50
GO=0%	1.81	1.35	1.00
GO=0.05%	1.21	0.98	0.80
GO=0.1%	1.19	0.96	0.75

Mix

(a)

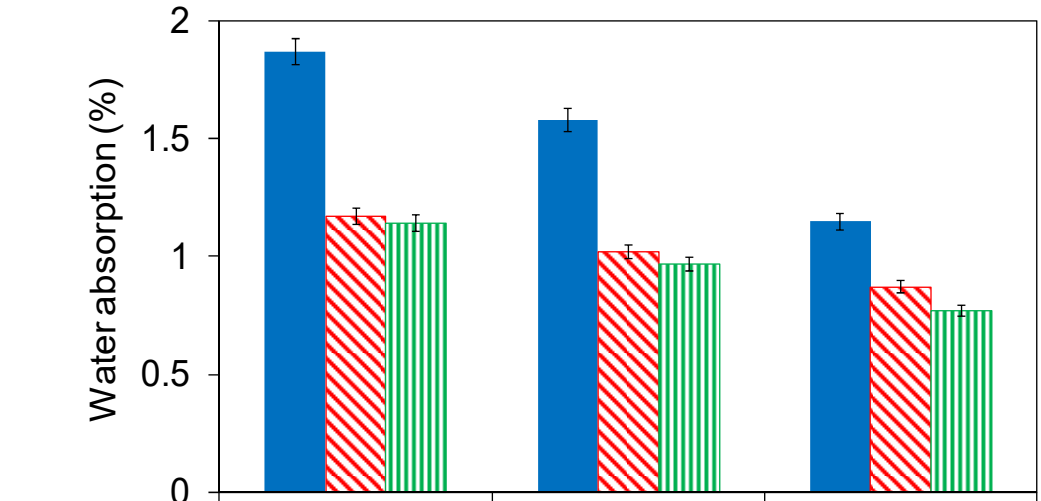

	LS100	LS80/20	LS50/50
GO=0%	1.87	1.58	1.15
GO=0.05%	1.17	1.02	0.87
GO=0.1%	1.14	0.97	0.77

Mix

(b)

Fig. 8. Water absorption of hardened mixes at 28 days: (a) NS, (b) LSS group mixes.

It is shown in Fig. 8(a) and (b) that, for a given binder type, incorporating GO in AAB mortars caused a decreased absorption for both sand types. This observation is attributed to the more compact microstructures of the mixes containing GO than those of the control mixes as a result of an improved gel matrix of the mortar, which is discussed in Section 3.5. NS100G0.05, NS80/20G0.05, and NS50/50G0.05 mixes had approximately 33, 27, and 20% lower water absorptions than NS100, NS80/20, NS50/50 mixes, respectively. For the LSS series, 100% FA, 80% FA/20% GGBS, and 50% FA/50% GGBS mixes containing 0.05% GO exhibited approximately 37, 35, and 24% lower water absorptions than those containing 0% GO, respectively.

It can also be observed in Fig. 8(a) and (b) that increasing GO dosage from 0.05% to 0.1% did not change the water absorption of the mortars significantly. In NS series, the water absorptions of 100% FA, 80% FA/20% GGBS, and 50% FA/50% GGBS mixes containing 0.1% GO were approximately 2, 2, and 6% lower than those containing 0.05% GO, respectively. In LSS series, LS100G0.1, LS80/20G0.1, and LS50/50G0.1 had approximately 3, 5, and 11% lower water absorptions than the companion mixes with 0.05% GO, respectively. These results indicate that an increase in the GO dosage over 0.05% does not have a considerable influence on the water absorption of AAB mortars containing NS and LSS, which is consistent with the trends observed for compressive and tensile strengths.

3.4.2. Drying shrinkage

Fig. 9 (a) and (b) shows the drying shrinkage of AAB mortars containing NS and LSS at different curing ages of 7, 14, 21, and 28 days, respectively. As shown in the figure, for a given GO dosage, the drying shrinkage of the mixes decreased when GGBS% increased for both sand types. This accounts for the larger content of hydration products (C-A-S-H) in the mortars

containing a higher GGBS%, resulting in a more compact microstructure and less interconnected capillary pore network of the gel matrix in the mixes, as discussed in Section 3.5. This observation agrees with the findings of previous research on the drying shrinkage of AAB concrete at ambient curing (Deb et al., 2015). The figure also shows that the drying shrinkage of the LSS mixes was lower than that of the NS mixes for a given binder type and GO dosage. This can be explained by the physical property of LSS with the honeycomb surfaces that can absorb and retain the alkaline solution during the curing process, resulting in superior moist conditions in the mixes containing LSS, which is discussed further in Section 3.5.

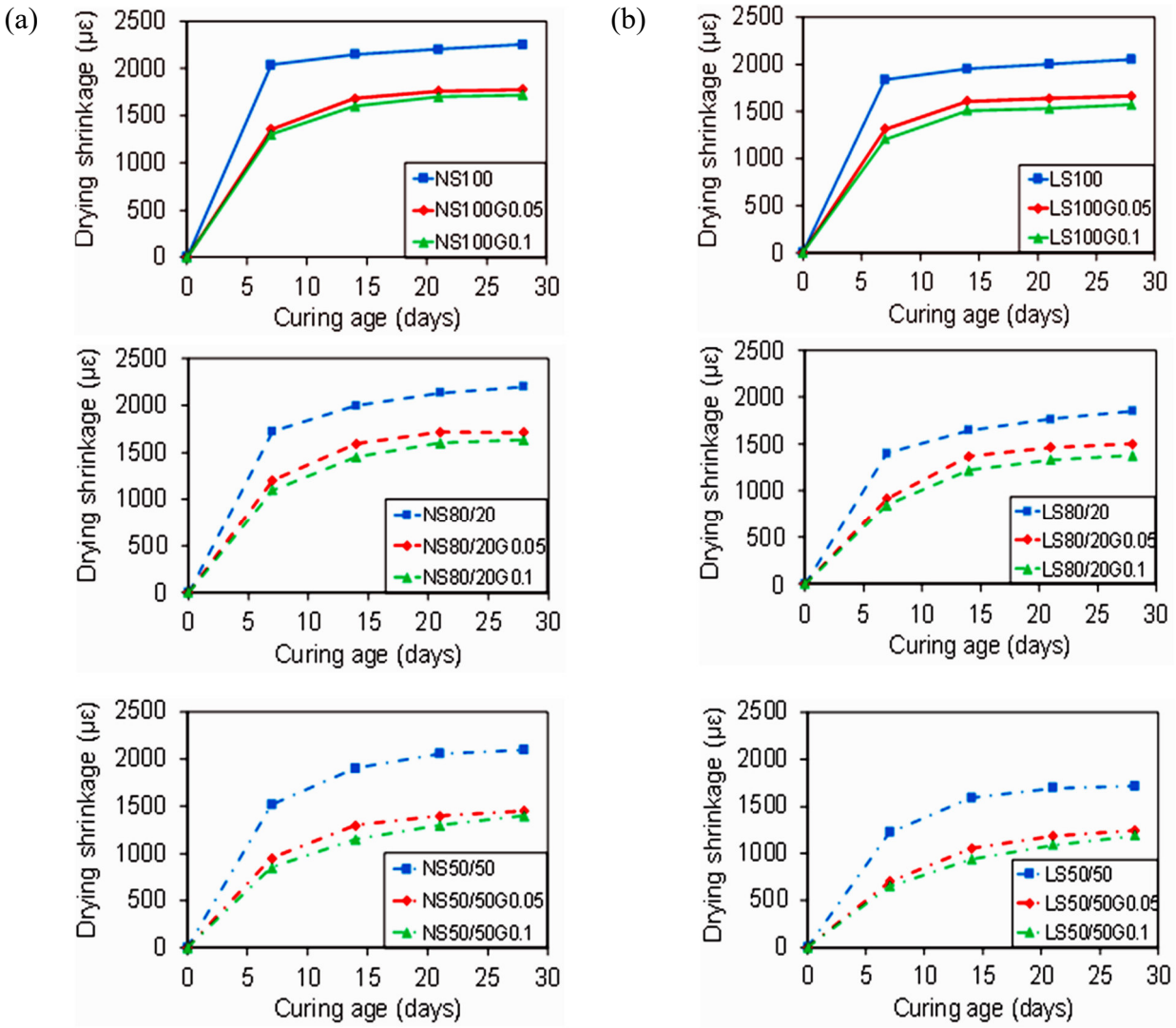

Fig. 9. Variation of drying shrinkage of mixes with time: (a) NS, (b) LSS group mixes.

As can be seen in Fig. 9 (a) and (b), incorporating GO into AAB mortars caused a decreased drying shrinkage of mortars for a given sand and binder type. As discussed in Section 3.4, this is because of the bridging effect of GO sheets over nanocracks and microcracks in the matrix of mixes containing GO compared to that of unreinforced mixes. In the NS series, the mixes containing 0.05% GO exhibited approximately 34, 25, 24, and 25% lower 7-day, 14-day, 21-day, and 28-day drying shrinkage than those containing 0% GO, respectively. In the LSS series, the drying shrinkage of the mixes containing 0.05% at 7, 14, 21, and 28 days was approximately 35, 23, 22, and 22% lower than those containing 0% GO, respectively. The figure also shows that increasing GO dosage from 0.05% to 0.1% caused a slight fall in the drying shrinkage of the mortars. In the NS series, the mixes containing 0.1% GO developed approximately 8, 8, 6, and 4% lower drying shrinkage at 7, 14, 21, and 28 days than those containing 0.05% GO, respectively. In the LSS series, the mixes containing 0.1% GO had approximately 8, 9, 8, and 6% lower 7-day, 14-day, 21-day, and 28-day drying shrinkage than those containing 0.05% GO, respectively. Similar to the trends of the strength and water absorption results, these observations suggest that an increase in the GO dosage over 0.05% does not have a significant positive influence on the drying shrinkage of AAB mortars.

3.5. SEM and microstructural analysis

The morphologies of FA, GGBS, NS, and LSS are presented in Fig. 10. As can be seen, FA had a spherical shape (Fig. 10(a)) and GGBS had a mostly irregular shape (Fig. 10(b)). LSS particles (Fig. 10(d)) were more irregular and angular in shape than NS particles (Fig. 10(c)), resulting in a higher interparticle friction among LSS particles compared to those among NS particles. This accounts for the lower flowability of LSS mixes in comparison with that of NS mixes discussed earlier. It is shown in Fig. 10(e) and (f) that the surface of LSS had a honeycomb structure that led to a higher moisture absorption in LSS mixes in comparison with that in NS mixes, thereby keeping the LSS mixes in a moister state. This can explain the higher absorption and lower shrinkage of LSS mixes compared to those of NS mixes.

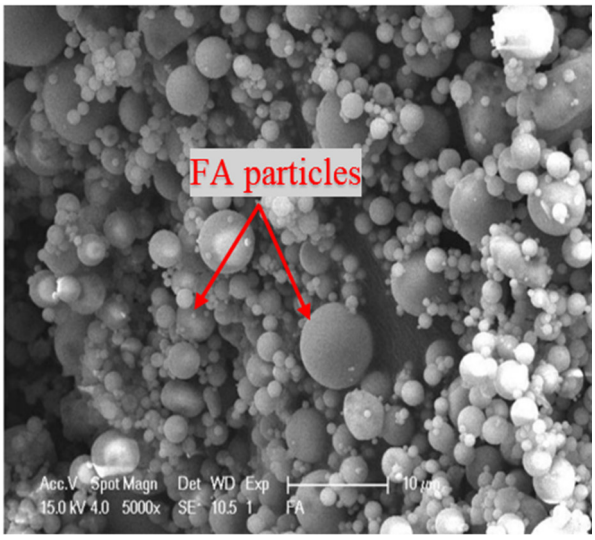
FA particles
Acc.V Spot Magn Det WD Exp
15.0 kV 4.0 5000x SE 10.5 1 FA

(a)

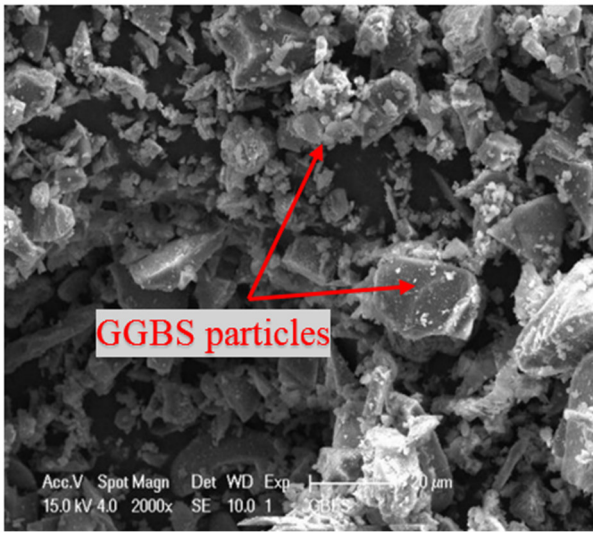
GGBS particles
Acc.V Spot Magn Det WD Exp
15.0 kV 4.0 2000x SE 10.0 1

(b)

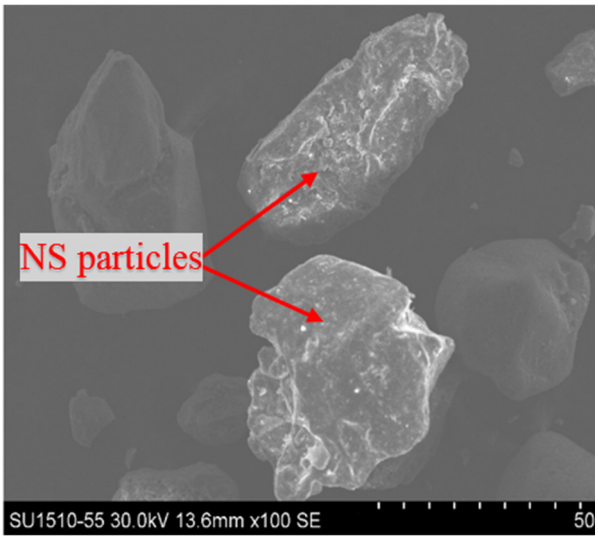
NS particles
SU1510-55 30.0kV 13.6mm x100 SE

(c)

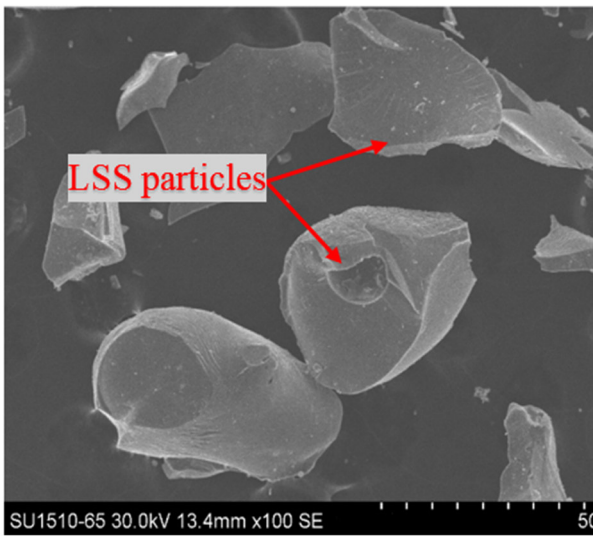
LSS particles
SU1510-65 30.0kV 13.4mm x100 SE

(d)

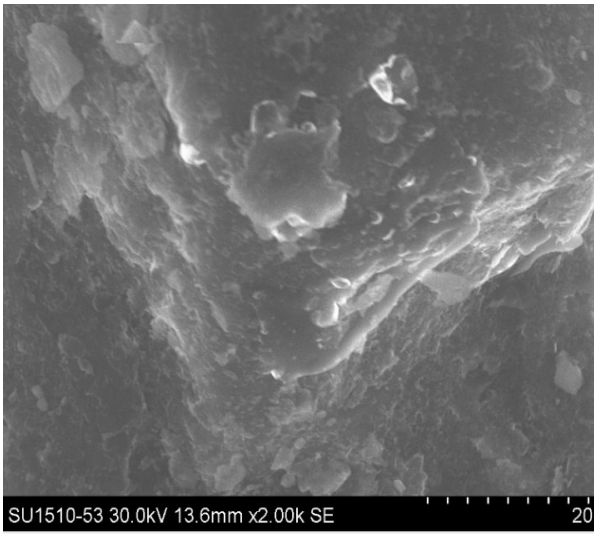
SU1510-53 30.0kV 13.6mm x2.00k SE

(e)

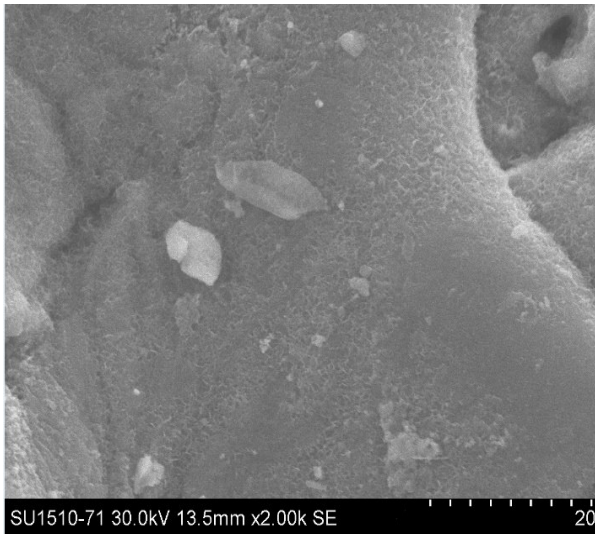
SU1510-71 30.0kV 13.5mm x2.00k SE

(f)

Fig. 10. SEM images of: particle shapes of: (a) FA, (b) GGBS, (c) NS, (d) LSS; and surfaces of: (e) NS, (f) LSS.

The typical SEM images of the AAB mortars surfaces containing NS and LSS without GO at 28 days are shown Fig. 11(a)-(f). As shown in the figure, for both sand types, although 80% FA/20% GGBS mixes (Fig. 11(b) and (e)) and 50% FA/50% GGBS mixes (Fig. 11(c) and (f)) had more capillary pores and wider microcracks than 100% FA mixes (Fig. 11(a) and (d)), their microstructures were more compact than 100% FA mixes. This can be due to the formation of stronger C-A-S-H gels in the gel matrices of the mixes containing GGBS compared to those without GGBS. This can explain the higher mechanical properties and lower drying shrinkage and water absorption of the mixes containing a higher GGBS%. It is also shown in the figure that the compactness of the microstructure of LSS mixes was similar to that of the NS mixes, which can explain why there were no considerable differences between mechanical strengths of these mixes as discussed earlier.

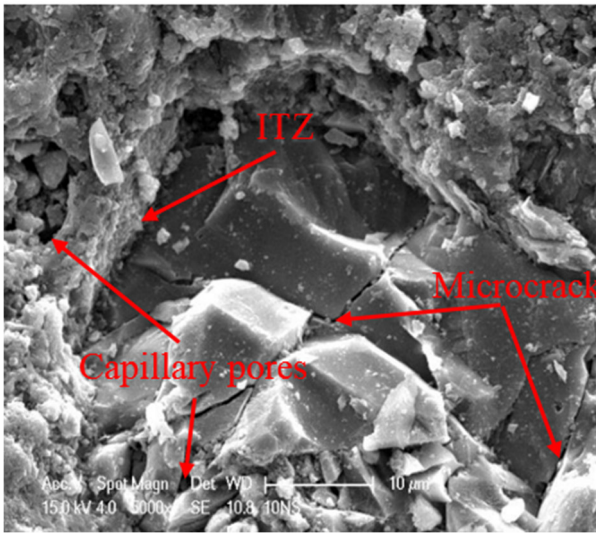

(a)

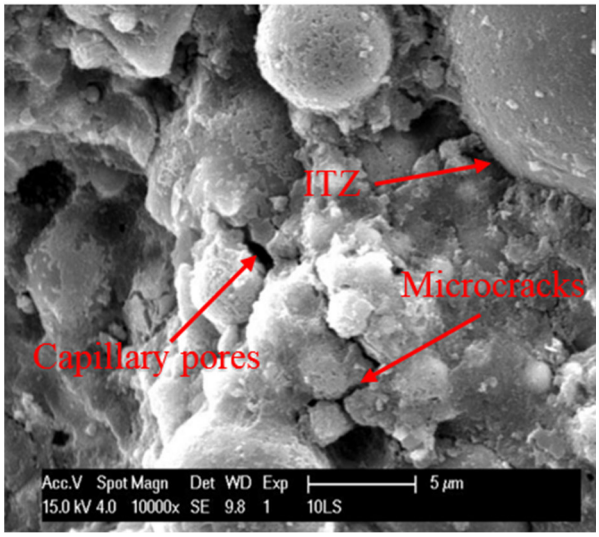

(d)

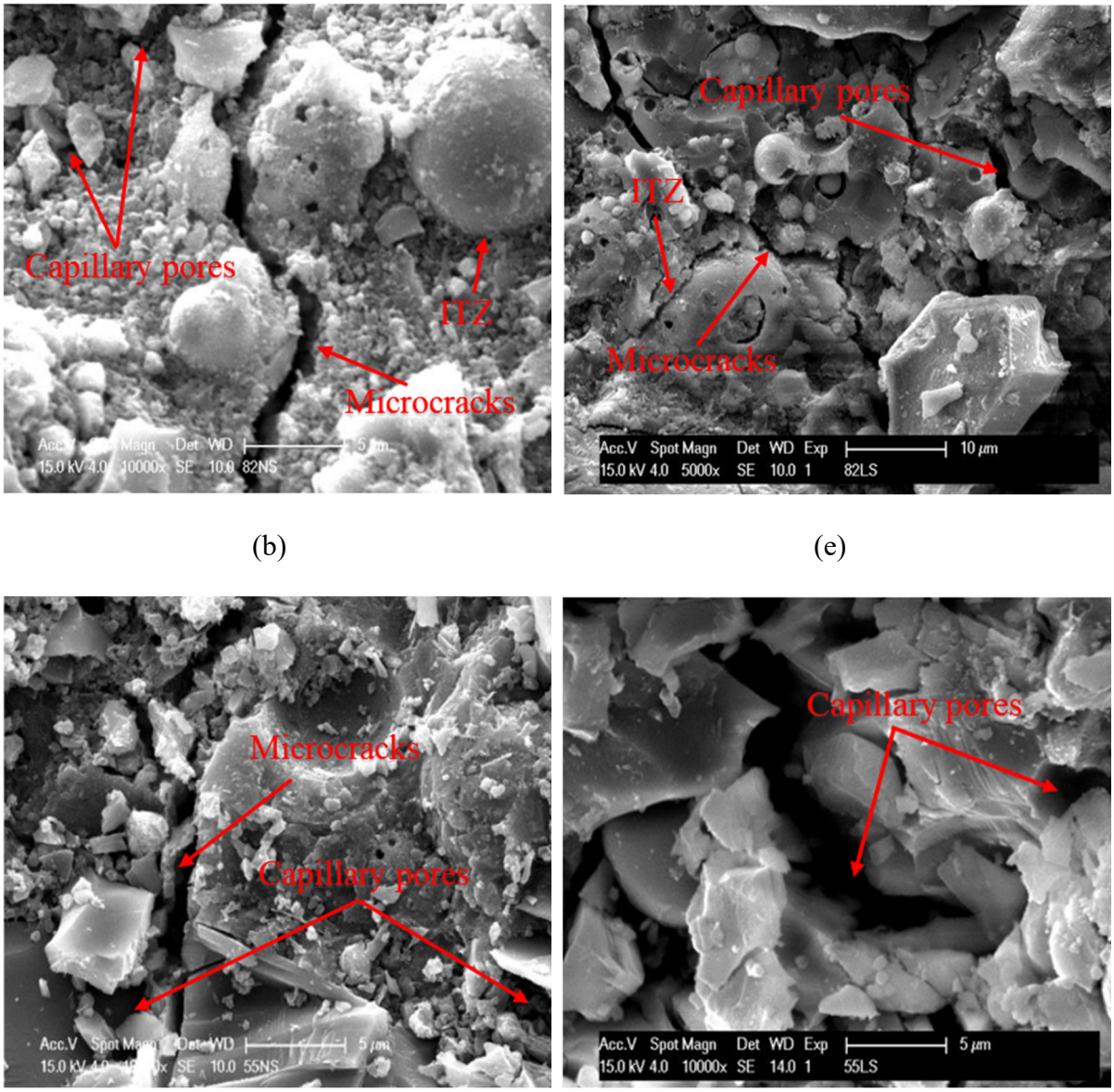

Fig. 11. SEM images of surfaces of mortar mixes containing: (a) NS100, (b) NS80/20, (c) NS50/50, (d) LSS100, (e) LSS80/20, (f) LSS50/50.

The effects of the liquid solutions on the physical structure and the dispersion of GO are shown in Fig. 12. The photographs of GO in alkaline and water solution just after sonication, and after four-hour sonication with the same GO dosage of 1 mg/ml are presented in Fig. 12(a) and (b), respectively. As shown in Fig. 12(a) and (b), GO sheets in water were brown in color and dispersed well without any recognizable sedimentation after four hours, whereas they were dark in color in alkaline solution and exhibited significant sedimentation after four hours. This

indicates that GO sheets have undergone deoxygenation with a loss of oxygen-containing groups (e.g. carboxyl, hydroxyl) in alkaline solution, resulting in the formation of rGO in alkaline solution (Saafi et al., 2015; Yan et al., 2016). Fig. 12(c) and (d) presents the microscopic images of GO sheets in alkaline solution. As shown in the figure, GO sheets exhibited a high degree of folding and wrinkling in alkaline solution because they turned into rGO sheets as a result of undergoing a reduction in their oxygen functional groups formed on their basal planes and edges during the improved Hummer's method (Bai et al., 2013; Saafi et al., 2015). The high degree of wrinkling of the sheets enhances the interaction and interlocking between rGO sheets and the gel matrix in AAB mortars (Galpaya et al., 2013; Saafi et al., 2015), resulting in the improvement in mechanical strengths and durability properties of AAB mortars. However, a rise in the GO dosage over 0.05% did not have a considerable influence on mechanical and durability properties of AAB mortars compared to the mixes with 0.05% GO. This is due to the lower dispersibility and higher agglomeration level of rGO sheets in the mixes, affecting their bond, interaction and interlocking in the gel matrix. This agrees with the observations of previous studies on GO, rGO and PRG in geopolymer and cementitious composites (Gholampour et al., 2017b; Ho et al., 2020; Kiamahalleh et al., 2020; Saafi et al., 2015; Yan et al., 2016).

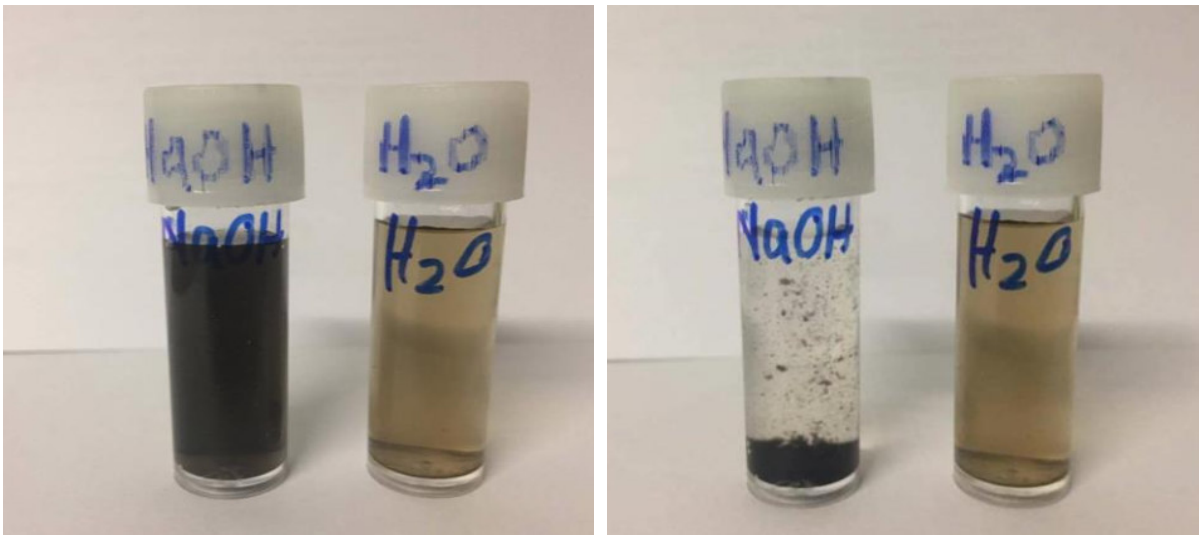

(a) (b)

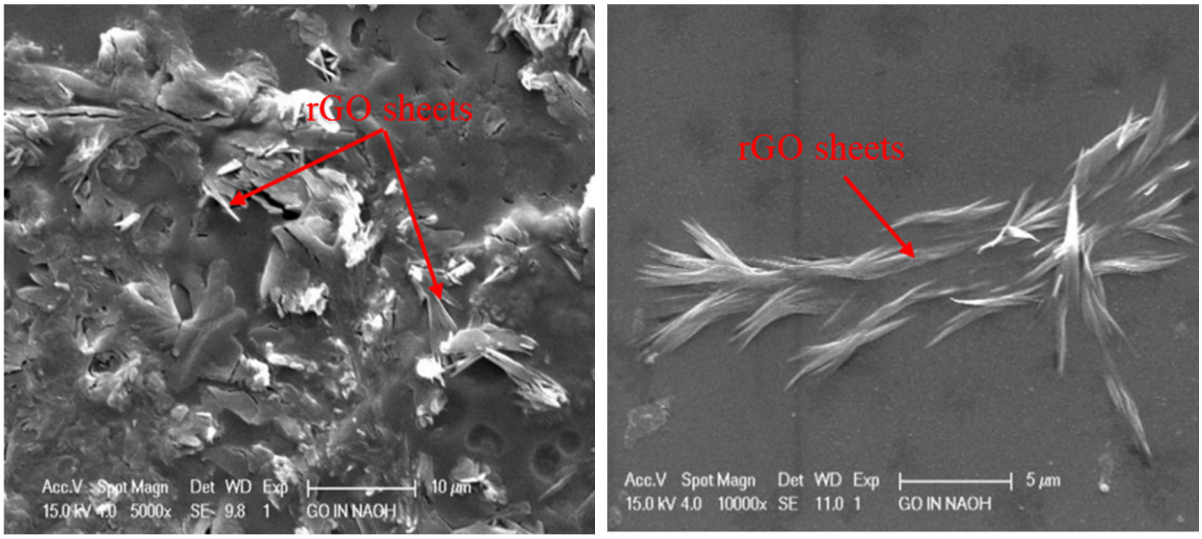

(c) (d)

Fig. 12. Photographs of GO dispersed in alkaline solution and in water: (a) just after sonication, (b) after 4 hours sonication; and (c, d) microscopic images of rGO in alkaline solution.

Fig. 13 illustrates typical SEM images of GO in the microstructures of AAB mortars containing NS and LSS at 28 days. It was difficult to observe the rGO sheets in the microstructures of the mortars because of their low content in the mortars. Fig. 13(a) shows the typical interaction between rGO and FA in the LS100G0.1 mix. It is evident from the figure that the rGO sheets absorbed and covered the surface of FA particles, indicating physiochemical interactions between reduced graphene oxide and fly ash in the matrix. This resulted in the positive effect of cross-linking and interlocking between them, enhancing the strengths of the gel matrix and microstructures of the composites (Hsu, 2008; Saafi et al., 2015). For the LSS groups, although the LS80/20G0.1 mix (Fig. 13(b) and (c)) had wider capillary pores than the LS80/20 mix (Fig. 11(e)), its microstructure was more compact with a lower amount of unreacted FA/GGBS. Similarly, the benefit of GO sheets can also be seen in the NS groups: the microstructures of the NS80/20G0.1 (Fig. 13(d)) and NS50/50G0.1 (Fig. 13(e)) mixes had a higher compactness than those of the mixes without GO additives of NS80/20 (Fig. 11(b)) and NS50/50 (Fig. 11(c)), respectively. These observations can explain why the mixes containing GO exhibited higher strengths, lower water absorptions and lower drying shrinkage than the mixes without GO.

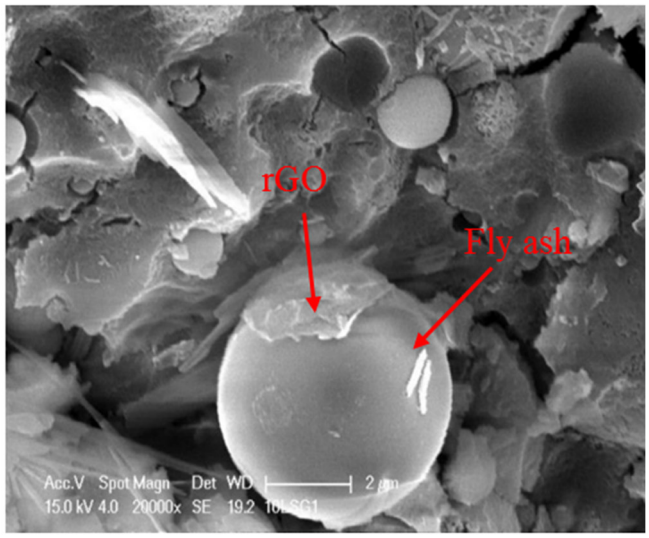
rGO
Fly ash
Acc.V Spot Magn Det WD 2 μm
15.0 kV 4.0 20000x SE 19.2

(a)

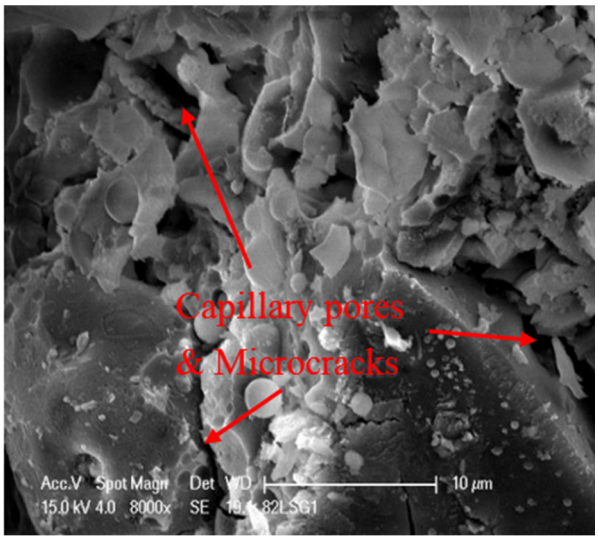
Capillary pores
& Microcracks
Acc.V Spot Magn Det WD 10 μm
15.0 kV 4.0 8000x SE

(b)

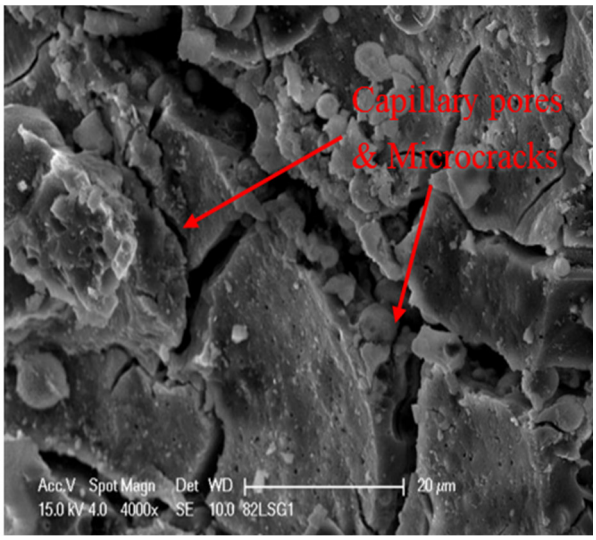
Capillary pores
& Microcracks
Acc.V Spot Magn Det WD 20 μm
15.0 kV 4.0 4000x SE 10.0 82LSG1

(c)

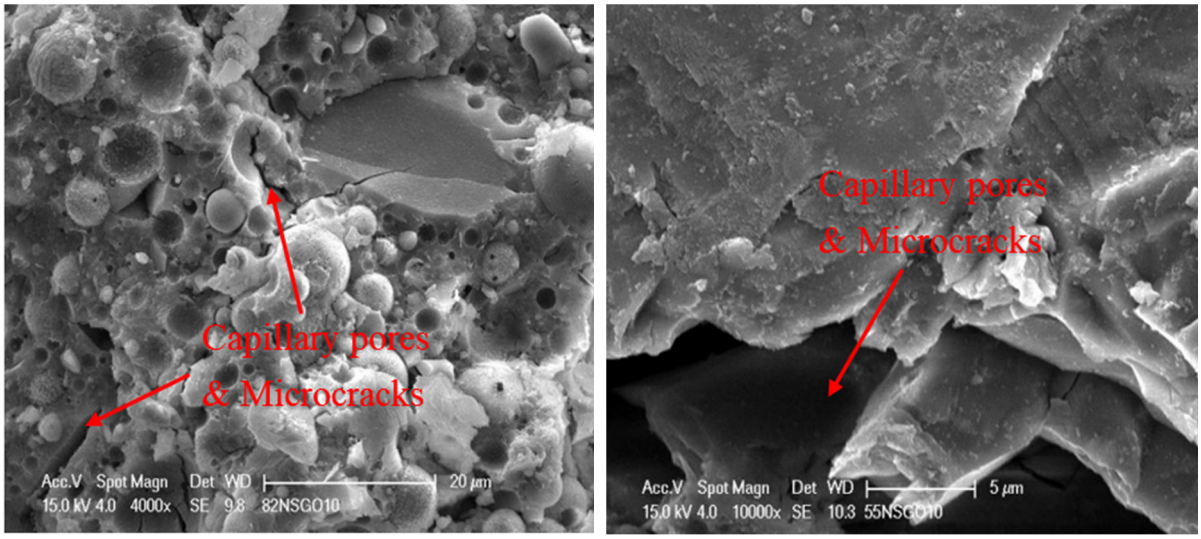

(d) (e)

Fig. 13. SEM images of surfaces of GO-based mortar composites: (a) rGO interacts with the binder in the matrix, (b, c) LSS mixes, (d, e) NSS mixes.

From the above analysis, it can be concluded that the addition of GO to AAB mortars had positive effects on mechanical strengths and durability properties of the mortars containing LSS and NS, which is due to the dominant effect of the chemical and mechanical interactions between rGO and the gel matrix (i.e. C-A-S-H). This results in improved strengths of the gel matrix, enhanced stress distribution, and impeded crack propagations from nanoscale to macroscale in the composites, which agrees with the observation from previous research on graphene materials in geopolymer and cementitious composites (Gholampour et al., 2017b; Ho et al., 2020; Ranjbar et al., 2015; Saafi et al., 2015; Yan et al., 2016).

4. Conclusions

This paper has presented the outcomes of the first study on the properties of fly ash/ground granulated blast furnace slag-based alkali-activated binder (AAB) mortars containing NS and LSS with GO additives. The following conclusions can be drawn from the presented results:

- The flowability of AAB mortars containing NS and LSS decreases with increasing GGBS% due to the faster chemical reaction of GGBS in alkaline solution than that of

FA. In addition, for a given binder type and GO dosage, AAB mortars with LSS exhibit lower flowability than those with NS, which is attributed to the higher angularity of LSS than that of NS. The addition of GO to AAB mortars decreases their flowability owing to the large specific surface area of GO that leads to an increased solution requirement to lubricate the surface of the particles.

- Increasing GGBS% increases compressive and tensile strengths of AAB mortars. For a given sand and binder type, the incorporation of 0.05% GO increases the strengths of AAB mortars, which is because of the improvement of the gel matrix resulting from chemical and mechanical interactions between rGO and gel products. Increasing GO dosage from 0.05% to 0.1% causes a slight increase in compressive and tensile strengths of mortars. These diminished benefits are because of the lower dispersibility and higher agglomeration level of rGO sheets in the mixes with 0.1% GO compared to those with 0.05% GO.
- An increased GGBS% and GO dosages causes a decreased water absorption of AAB mortars containing NS and LSS. This is due to the higher amount of hydration products (C-A-S-H gels) in the mortars containing a higher GGBS%, as well as the improvement of the gel matrix in the mixes containing GO additives, both resulting in a more compact microstructure of mortar mixes compared to those containing a lower GGBS% and no GO. However, there are only minor improvements in the absorption of the mortars are observed when the GO dosage is increased above a certain threshold (i.e. from 0.05% to 0.1%).
- The drying shrinkage of AAB mortars decreases with increasing GGBS%, which is due to the less interconnected capillary pore network of the gel matrix in the mixes containing a higher GGBS%. For a given binder type and GO dosage, the LSS mixes exhibit a lower drying shrinkage than the NS mixes, which is due to a better moisture retention of the LSS mixes resulting from honeycomb surfaces of LSS particles. The

addition of GO to AAB mortars causes a decreased drying shrinkage, with a further increase in the GO dosage from 0.05% to 0.1% resulting in only a slight decrease in drying shrinkage.

- The results of SEM and microstructural analyses show that mechanical and durability properties of AAB mortars have a close relationship with their physicochemical and microstructural properties. The incorporation of GO in AAB mortars results in the reduction of oxygen functional groups of GO sheets, which results in the formation of reduced graphene oxide sheets with a higher degree of wrinkling. The improvement of mechanical and durability properties of AAB mortars containing GO is attributed to the chemical and mechanical interactions between rGO sheets and the gel products, resulting in improved internal stress distributions and reduced crack propagations in the composites.

The results from this study have shown the great potential of using GO additives in AAB mortars containing NS and LSS for improving their mechanical and durability characteristics. These findings are expected to encourage future studies on the topic and make important contributions toward developing eco-friendly construction materials for reducing the environmental effect of OPC and extraction of NS.

Declaration of competing interest

The authors declare that there is no competing interest.

Acknowledgements

The authors acknowledge Hariz, Mesdames Rabbah, Yin, and Dinh for completing experimental work as part of their Honour's thesis.

References

ASTM-C109/C109M-07, 2008. Standard test method for compressive strength of hydraulic cement mortars. ASTM International: USA 2008.

ASTM-C307-03, 2012. Standard Test Method for Tensile Strength of Chemical-Resistant Mortar, Grouts, and Monolithic Surfacings Monolithic Surfacings. ASTM International.

ASTM-C1437, 2015. Standard Test Method for Flow of Hydraulic Cement Mortar. Standard, ASTM.

ASTM C596-09, 2017. Standard Test Method for Drying Shrinkage of Mortar Containing Hydraulic Cement.

ASTM C1585-13, 2013. Standard Test Method for Measurement of Rate of Absorption of Water by Hydraulic-Cement Concretes.

Atzeni, C., Massidda, L., Sanna, U., 1996. Use of granulated slag from lead and zinc processing in concrete technology. Cement and Concrete Research 26, 1381-1388.

Bahoria, B., Parbat, D., Nagarnaik, P., 2018. XRD Analysis of Natural sand, Quarry dust, waste plastic (ldpe) to be used as a fine aggregate in concrete. Materials Today: Proceedings 5, 1432-1438.

Bai, S., Shen, X., Zhu, G., Yuan, A., Zhang, J., Ji, Z., Qiu, D., 2013. The influence of wrinkling in reduced graphene oxide on their adsorption and catalytic properties. Carbon 60, 157-168.

Bravard, J.-P., Goichot, M., Gaillot, S., 2013. Geography of sand and gravel mining in the Lower Mekong River. First survey and impact assessment. EchoGéo.

Cwirzen, A., Habermehl-Cwirzen, K., Nasibulin, A., Kaupinen, E., Mudimela, P., Penttala, V., 2009. SEM/AFM studies of cementitious binder modified by MWCNT and nano-sized Fe needles. Materials Characterization 60, 735-740.

Davidovits, J., 2008. Geopolymer chemistry and applications. Geopolymer Institute.

Deb, P.S., Nath, P., Sarker, P.K., 2014. The effects of ground granulated blast-furnace slag blending with fly ash and activator content on the workability and strength properties of geopolymer concrete cured at ambient temperature. Materials & Design (1980-2015) 62, 32-39.

Deb, P.S., Nath, P., Sarker, P.K., 2015. Drying shrinkage of slag blended fly ash geopolymer concrete cured at room temperature. Procedia Engineering 125, 594-600.

Du, J., Cheng, H.M., 2012. The fabrication, properties, and uses of graphene/polymer composites. Macromolecular Chemistry and Physics 213, 1060-1077.

Galpaya, D., Wang, M., Yan, C., Liu, M., Motta, N., Waclawik, E.R., 2013. Fabrication and mechanical and thermal behaviour of graphene oxide/epoxy nanocomposites. Journal of Multifunctional Composites 1, 91-98.

Geim, A.K., Novoselov, K.S., 2007. The rise of graphene. Nature materials 6, 183-191.

Gholampour, A., Ho, V.D., Ozbakkaloglu, T., 2019. Ambient-cured geopolymer mortars prepared with waste-based sands: Mechanical and durability-related properties and microstructure. Composites Part B: Engineering 160, 519-534.

Gholampour, A., Kiamahalleh, M.V., Tran, D.N., Ozbakkaloglu, T., Losic, D., 2017a. Revealing the dependence of the physiochemical and mechanical properties of cement composites on graphene oxide concentration. RSC Advances 7, 55148-55156.

Gholampour, A., Ozbakkaloglu, T., 2017. Performance of sustainable concretes containing very high volume Class-F fly ash and ground granulated blast furnace slag. Journal of Cleaner Production 162, 1407-1417.

Gholampour, A., Valizadeh Kiamahalleh, M., Tran, D.N., Ozbakkaloglu, T., Losic, D., 2017b. From Graphene Oxide to Reduced Graphene Oxide: Impact on the Physiochemical and Mechanical Properties of Graphene–Cement Composites. ACS applied materials & interfaces 9, 43275-43286.

Han, B., Sun, S., Ding, S., Zhang, L., Yu, X., Ou, J., 2015. Review of nanocarbon-engineered multifunctional cementitious composites. Composites Part A: Applied Science and Manufacturing 70, 69-81.

Ho, V.D., Ng, C.T., Coghlan, C.J., Goodwin, A., Mc Guckin, C., Ozbakkaloglu, T., Losic, D., 2020. Electrochemically produced graphene with ultra large particles enhances mechanical properties of Portland cement mortar. Construction and Building Materials 234.

Hsu, T.-C., 2008. Adsorption of an acid dye onto coal fly ash. Fuel 87, 3040-3045.

Jawahar, J.G., Mounika, G., 2016. STRENGTH PROPERTIES OF FLY ASH AND GGBS BASED GEO POLYMER CONCRETE. Asian Journal of Civil Engineering (BHRC) 17, 127-135.

Kiamahalleh, M.V., Gholampour, A., Tran, D.N.H., Ozbakkaloglu, T., Losic, D., 2020. Physiochemical and mechanical properties of reduced graphene oxide–cement mortar composites: Effect of reduced graphene oxide particle size. Construction and Building Materials 250, 118832.

Kim, D.H., Yun, Y.S., Jin, H.-J., 2012. Difference of dispersion behavior between graphene oxide and oxidized carbon nanotubes in polar organic solvents. Current Applied Physics 12, 637-642.

Lin, T., Jia, D., He, P., Wang, M., Liang, D., 2008. Effects of fiber length on mechanical properties and fracture behavior of short carbon fiber reinforced geopolymer matrix composites. Materials Science and Engineering: A 497, 181-185.

Lothenbach, B., Scrivener, K., Hooton, R., 2011. Supplementary cementitious materials. Cement and concrete research 41, 1244-1256.

Low, M.-S., 2005. Material flow analysis of concrete in the United States. Massachusetts Institute of Technology.

Marcano, D.C., Kosynkin, D.V., Berlin, J.M., Sinitskii, A., Sun, Z., Slesarev, A., Alemany, L.B., Lu, W., Tour, J.M., 2010. Improved synthesis of graphene oxide. ACS nano 4, 4806-4814.

Mehta, P.K., Meryman, H., 2009. Tools for reducing carbon emissions due to cement consumption. Structure 1, 11-15.

Nath, P., Sarker, P., 2012. Geopolymer concrete for ambient curing condition, Australasian Structural Engineering Conference 2012: The past, present and future of Structural Engineering. Engineers Australia, p. 225.

Nath, P., Sarker, P.K., 2014. Effect of GGBFS on setting, workability and early strength properties of fly ash geopolymer concrete cured in ambient condition. Construction and Building materials 66, 163-171.

Ranjbar, N., Mehrali, M., Mehrali, M., Alengaram, U.J., Jumaat, M.Z., 2015. Graphene nanoplatelet-fly ash based geopolymer composites. Cement and Concrete Research 76, 222-231.

Saafi, M., Andrew, K., Tang, P.L., McGhon, D., Taylor, S., Rahman, M., Yang, S., Zhou, X., 2013. Multifunctional properties of carbon nanotube/fly ash geopolymeric nanocomposites. Construction and Building Materials 49, 46-55.

Saafi, M., Tang, L., Fung, J., Rahman, M., Liggat, J., 2015. Enhanced properties of graphene/fly ash geopolymeric composite cement. Cement and Concrete Research 67, 292-299.

Sankh, A.C., Biradar, P.M., Naghathan, S., Ishwargol, M.B., 2014. Recent trends in replacement of natural sand with different alternatives, Proceedings of the International Conference on Advances in Engineering and Technology, pp. 59-66.

Shaikh, F.U.A., 2013. Review of mechanical properties of short fibre reinforced geopolymer composites. Construction and Building Materials 43, 37-49.

Shamsaei, E., de Souza, F.B., Yao, X., Benhelal, E., Akbari, A., Duan, W., 2018. Graphene-based nanosheets for stronger and more durable concrete: A review. Construction and Building Materials 183, 642-660.

Shang, Y., Zhang, D., Yang, C., Liu, Y., Liu, Y., 2015. Effect of graphene oxide on the rheological properties of cement pastes. Construction and Building Materials 96, 20-28.

Shi, C., Jiménez, A.F., Palomo, A., 2011. New cements for the 21st century: The pursuit of an alternative to Portland cement. Cement and concrete research 41, 750-763.

Shi, C., Qu, B., Provis, J.L., 2019. Recent progress in low-carbon binders. Cement and Concrete Research 122, 227-250.

Temuujin, J.v., Van Riessen, A., Williams, R., 2009. Influence of calcium compounds on the mechanical properties of fly ash geopolymer pastes. Journal of hazardous materials 167, 82-88.

Tiwari, A., Singh, S., Nagar, R., 2016. Feasibility assessment for partial replacement of fine aggregate to attain cleaner production perspective in concrete: A review. Journal of Cleaner Production 135, 490-507.

Tran, D.N., Kabiri, S., Losic, D., 2014. A green approach for the reduction of graphene oxide nanosheets using non-aromatic amino acids. Carbon 76, 193-202.

Tripathi, B., Misra, A., Chaudhary, S., 2013. Strength and abrasion characteristics of ISF slag concrete. Journal of Materials in Civil Engineering 25, 1611-1618.

Van den Heede, P., De Belie, N., 2012. Environmental impact and life cycle assessment (LCA) of traditional and 'green'concretes: literature review and theoretical calculations. Cement and Concrete Composites 34, 431-442.

Wardhono, A., Law, D.W., Strano, A., 2015. The strength of alkali-activated slag/fly ash mortar blends at ambient temperature. Procedia Engineering 125, 650-656.

Yan, S., He, P., Jia, D., Yang, Z., Duan, X., Wang, S., Zhou, Y., 2016. Effect of reduced graphene oxide content on the microstructure and mechanical properties of graphene–geopolymer nanocomposites. Ceramics International 42, 752-758.

Zainuri, M., 2015. Synthesis of SiO2 nanopowders containing quartz and cristobalite phases from silica sands. Materials Science-Poland 33, 47-55.

Zheng, Y.-X., Liu, W., Qin, W.-Q., Kong, Y., Luo, H.-L., Han, J.-W., 2014. Mineralogical reconstruction of lead smelter slag for zinc recovery. Separation science and technology 49, 783-791.

CHAPTER 8: CONCLUSIONS AND RECOMMENDATIONS FOR FUTURE DIRECTIONS

1. Conclusions

This thesis aims at studying the effect of industrially produced pristine graphene (PRG) and graphene oxide (GO) on the properties of cement composites and fly ash (FA)/ground granulated blast furnace slag (GGBS) alkali-activated binder (AAB) composites, respectively. The results of this thesis have provided a better understanding of the application of graphene-based additives for the development of next-generation construction materials. This not only addresses the drawbacks of these composite materials but also contribute to creating eco-friendly construction materials that can reduce the environmental impact of using Portland cement and natural sand. The major research outcomes of this thesis are summarized below:

Pristine graphene additives in Portland cement mortars:

- Incorporating industrially produced PRG into cement mortars enhances their mechanical properties and the level of improvement depends on PRG concentrations. The highest enhancement rates of compressive and tensile strengths of cement mortars are achieved at the optimized dosage of PRG (i.e. 0.07%). However, further increases in PRG dosages (i.e. 0.1%, 0.3%) lead to a reduction in enhancement rates of the mechanical properties of cement mortars.
- The mechanical properties of cement mortars significantly depend on the sizes of PRG additives. Small sizes (e.g. 5μm) often show no considerable effects on compressive and tensile strengths of cement mortars. While medium (e.g. 23 μm) and large sizes (e.g. 43μm) have more advantages in tensile strengths than

compressive strengths, ultra-large sizes (e.g. 56µm, 73µm) present significant effects in both compression and tension properties.

- The sizes of PRG have a significant effect on the enhancement rates of mechanical strengths of the mortars, whereas they do not have a significant influence on the optimized PRG dosage for mechanical strengths of cement-based mortars. The dosage at 0.07% PRG is identified as the optimized concentration of PRG for enhancing mechanical strengths of cement-based mortars regardless of PRG sizes and design mixes.
- The strength enhancement rates of cement-based mortars depend on the dosages, sizes and densities of PRG and the design mix. The addition of PRG additive to cement-based mortars can enhance the compressive, flexural, and tensile strengths of the mortars at short-term and long-term curing ages. The mix containing PRG size 73µm shows the best improvement in mechanical strengths, followed by that of size 20µm and then 40µm. The lower level of enhancement for the mix with size 40µm is due to its higher density compared to size 20µm and 73µm, resulting in the strong agglomeration and formation of multi-layers PRGs in the cement matrix due to van der Waals forces between PRGs. This leads to a negative impact on the interaction between PRGs and the cement matrix.
- Incorporating a small amount of PRG additives into cement-based mortars can decrease water absorptions and voids of the mortars. However, there is no clear positive influence of different dosages and sizes of PRG on the drying shrinkage results of cement-based mortars. The mortars containing PRG materials present a positive influence on resisting the sulphate solution at all the curing ages. The addition of PRG to the mortars can decrease the water penetration depth into the mortar mixes. The ultra-large size shows the highest enhancement rates in

mechanical and durability properties of cement-based mortars at different curing ages.

- The improvement of PRG-cement mortars is due to the increase in the microstructure compactness of the cement matrix that comes from the strengthened PRG-cementitious gels as results of part from the rise in the hydration degree of cement pastes, and most from adhesion friction forces between pristine graphene sheets and calcium silicate hydrate gels.
- The less improvement in strengths of cement mortars when PRG is used over the optimized dosage is attributed to the effect of van der Watt forces, which cause agglomeration and poor adhesion friction forces between PRGs and the cement matrix.
- Incorporating PRG into cementitious composites as an additive not only improves their brittle properties but also reduces the mass of cement production. Therefore, this helps decrease carbon dioxide emission into the atmosphere associated with Portland cement production and alleviate global warming and climate change yearly.
- The results from this thesis have confirmed that the prominent benefit of industrially manufactured ultra-large PRG sizes to enhance mechanical and durability properties of cementitious composites, resulting in the potential of using PRG as a next-generation additive in cementitious composites that can improve the properties of building and construction materials.

Graphene oxide additives in FA/GGBS alkali-activated binder (AAB) mortars:

- Incorporating GO into AAB mortars as an additive increases compressive and tensile strengths of AAB mortars prepared with both natural sand (NS) and lead smelter slag (LSS) sand. Their enhancement rates increase with the percentage of

GGBS (GGBS%) in alkali-activated binders. There are no significant increases in compressive and tensile strengths of AAB mortars when rising the dosages of GO from 0.05% to 0.1%.

- The increase of GGBS% results in a decrease in water absorption and dry shrinkage of AAB mortars with both NS and LSS. These properties of the mortars are improved more when using GO as an additive. Also, there are inconsiderable improvements in water absorption and dry shrinkage of the mortars containing NS and LSS between 0.05% GO and 0.1% GO.
- The enhancement of mechanical and durability properties of AAB mortars prepared with NS and LSS and containing GO is due to the physical properties of the raw materials, chemical, and mechanical interactions between GO sheets and the gel productions in the alkali-activated matrix.
- The results of the thesis have shown the great potential of using GO as the additive in AAB mortars prepared with NS and LSS for improving their mechanical and durability properties, contributing to developing eco-friendly construction materials that can reduce the environmental impact of using Portland cement and natural sand.

2. Recommendations for future directions

Although this thesis has shown the promising potential of using PRG materials to enhance mechanical and durability properties of cement-based mortars as well as using GO to improve mechanical and durability properties of AAB mortars prepared with NS and LSS, some other properties of these types of materials still need further investigation. Therefore, future studies are recommended to contribute to the developments of next-generation construction materials with graphene additives, and hence, the practical application of these materials in the construction industry can be done in the near future.

- The influence of different dosages and sizes of industrially manufactured PRG on other properties (e.g. fracture toughness, elastic modulus, chloride resistance, electrical conductivity or fire resistance) of Portland cement composites. Besides, future research should also examine how different sizes of ultra-large PRG including sizes with hundreds of micrometers (i.e. 100, 150, or 200 μm) impact on the properties of cementitious composites in order to not only validate the results of the current study but also figure out the possible optimized size of PRG materials for the composites.
- The enhancement rate of cement composites with PRG additives also depends on the strength of PRG-cementitious gels. Therefore, the strength of cement pastes, which is based on water and cement ratios, is one of the main factors influencing PRG-cementitious gels. As a result, future studies should investigate how different water and cement ratios influence enhancement rates of mechanical and durability properties of cement composites prepared with PRG additives.
- Future studies can focus on exploring the effect of curing conditions on mechanical and durability properties of Portland cement composites at different curing ages. This point is necessary to find the best curing conditions for PRG-cement based composites so that PRG additives can keep the enhancement of PRG-cement composites during their longevity as required in practical applications.
- The influence of GO on other properties (e.g. fracture toughness, sulfate extension, corrosion resistance, fire resistance) and other long-term mechanical and durability properties of AAB composites should be explored to ensure that their benefits are consistent with time as the practical application.
- The investigation of the effect of different sizes and functional groups of GO on mechanical and durability properties of AAB composites. The results can help

determine the range of sizes and groups in GO that have a strong effect on the microstructures of the composites.

- The effect of different PRG concentrations and sizes on mechanical and durability properties of AAB composites also needs to have further investigation, and hence, it can provide a better understanding of the enhancement mechanism of PRG in AAB composites. The results from these studies can contribute to the developments of the next-generation construction materials with graphene additives, enhance the transition to practical applications, and help reduce the environmental impact of using Portland cement and natural sand.

APPENDICES

Appendix 1: Journal paper 1 (Published)

Construction and Building Materials 234 (2020) 117403

Contents lists available at ScienceDirect

Construction and Building Materials

journal homepage: www.elsevier.com/locate/conbuildmat

Electrochemically produced graphene with ultra large particles enhances mechanical properties of Portland cement mortar

Van Dac Ho [a,b,c], Ching-Tai Ng [a], Campbell J. Coghlan [b,c], Andy Goodwin [d], Craig Mc Guckin [d], Togay Ozbakkaloglu [a], Dusan Losic [b,c,*]

[a] School of Civil, Environmental and Mining Engineering, The University of Adelaide, South Australia 5005, Australia
[b] School of Chemical Engineering, The University of Adelaide, South Australia 5005, Australia
[c] ARC Research Hub for Graphene Enabled Industry Transformation, The University of Adelaide, South Australia 5005, Australia
[d] First Graphene Ltd, Suite 3, 9 Hampden Road, Nedlands, WA 6009, Australia

HIGHLIGHTS

- Pristine graphene (PRG) industrially produced by electrochemical process for cement mortar was explored.
- The ultra-large size of PRG particles in average of 56 ± 12 μm was confirmed.
- The 0.07% PRG is an optimal PRG dosage with 34.3% and 26.9% enhancement of compressive and tensile strengths at 28 days.
- PRG improves the microstructure of the cement matrix.
- A strong relationship between mechanical results and bonding gels, densities and arrangements of the crystals is revealed.
- PRG is promising a next-generation of additives in cementitious composites.

ARTICLE INFO

Article history:
Received 9 July 2019
Received in revised form 12 September 2019
Accepted 26 October 2019
Available online 29 November 2019

Keywords:
Pristine graphene
Cementitious composites
Compressive strengths
Tensile strengths
Hydration process
Microstructures

ABSTRACT

The effects of the dosages (0.01%, 0.03%, 0.05%, 0.07%, 0.1%, and 0.3% by weight of cement binder) of an ultra-large size (56 ± 12 μm) of pristine graphene (PRG) industrialy manufactured by electrochemical process on compressive and tensile strengths of cement mortars are presented. To have a better understanding of the reinforcement mechanism of PRG-cementitious gels, the physicochemical and microstructure analyses were performed. The results show that the addition of PRG to cement mortars improves their mechanical properties, with characteristic concentration dependence. The mortar mix with 0.07% PRG is identified as the optimal concentration, which provides 34.3% and 26.9% improvement in compressive and tensile strength at 28 days, respectively. This enhancement is attributed to the improvement of the hydration degree of cement paste, resulting in more Calcium Silicate Hydrate gel production. This also comes from the reinforcement of the adhesion bond that was created from friction forces between PRG sheets and cement gels, resulting in strengthening cement matrix composites and impeding crack propagations in the structure. However, with the further increases in PRG contents (i.e. 0.1%, 0.3%), the enhancement of mechanical properties of mortars is limited due to the impact of the van der Waals force on the sedimentation of PRG suspension, leading to the poor dispersion of the prepared PRG suspension. These results suggests that industrially produced pristine graphene by electrochemical process is a promising additive for improving performances of construction materials.

1. Introduction

Cementitious materials are one of the most commonly used materials in the construction industry due to their high compressive strength. However, they suffer from poor tensile strength, flexural strength, fracture toughness and brittleness giving rise to durability issues [1,2]. To overcome these issues, cement materials are augmented through the use of specific additives, reduction of water and cement ratios, and reinforcement materials such as steel, carbon and plastic fibers [3].

Recently, cementitious material development has focused on the incorporation of nanomaterials to not only enhance the

* Corresponding author at: School of Chemical Engineering, The University of Adelaide, South Australia 5005, Australia.
E-mail address: dusan.losic@adelaide.edu.au (D. Losic).

https://doi.org/10.1016/j.conbuildmat.2019.117403
0950-0618/

mechanical properties but also retard the propagation of cracks to generate a more durable composite [4]. These studies revealed two critical mechanisms [5], which affect the strength of cementitious materials in incorporating nanoparticles, such as nano-SiO_2 [6], nano-TiO_2 [7] and nano-$CaCO_3$ [8], into the cement matrix. The first is the high specific surface area of nanoparticles, which accelerates the progression of cement hydration and creates more Calcium Silicate Hydrate (CSH) gels. The second mechanism comes from the small particle size property, which allows them to act as a filler. This grants the material with a denser microstructure. However, nanoparticles with low aspect ratios lack competence in arresting the propagation of cracks from the nanoscale cracks, they are thus unable to enhance the reinforcement efficiency [9].

In addition to inorganic nanomaterials, carbon-based materials, such as nanofibers and nanotubes, have been investigated in cementitious composites as additives and demonstrated they can improve the mechanical properties [10,11]. However, these carbon materials showed some limitations to generate a full bonding with cementitious materials due to a lack of interfacial areas between them [12].

Graphene, a recently discovered two-dimensional (2D) carbon material, has many outstanding properties such as high electrical and thermal conductivity, high-temperature stability, high mechanical strength, ultra-large specific surface areas and high aspect ratios. Graphene is widely recognized to be an ideal additive to enhance performances of cementitious materials [13,14]. There are several different forms of graphene materials such as graphene oxide (GO), reduced graphene oxide (rGO), pristine graphene (PRG), doped graphene, and functionalized graphene that have different functionality and properties. The pristine graphene produced by a direct exfoliation process from graphite using electrochemical method has different properties compared with rGO, showing less defects, better crystallinity and conductivity. GO is an oxygenated derivate of graphene prepared by acid oxidation of graphite and is water-compatible and highly dispersible. This is one of the reasons why GO was preferentially explored as an additive for improving mechanical performances of cementitious composites. Wang, et al. [15] demonstrated that including 0.05% of GO in cement pastes can increase 40.4% and 90.5% in compressive and flexural strength at 28 days, respectively. This was confirmed by Lv, et al. [16]. They reported that GO can enhance strength and toughness properties of cement composites. Their results show that the compressive strength of cement paste with 0.06% GO is increased by 58.5% after 28 days, while the flexural strength is improved by 67.1% after 28 days with the mix having 0.04% GO concentration. Sharma and Kothiyal [17] reported that the compressive strength of the cement mortar with 0.1% GO additive is increased by 86.3% after 28 days. Recently few studies revealed the influence of different oxygen functional groups from GO on the phase composition and intermolecular interaction of cementitious materials to help early-age hydration characteristics of the composites [18,19]. Nevertheless, GO material has some limitations that could impact its performances in cementitious composites. It is less crystalline with a high level of defects and has mechanical properties that are considerably lower than those compared to PRG or rGO. Therefore, the application of PRG and rGO in cementitious composites is expected to be more beneficial for improving structural performances of cement-based materials [18,19].

Graphene materials, such as rGO and PRG, are highly hydrophobic and less dispersible in water compared to GO. This is the reason of being less attractive to be incorporated into cement composites to improve cement performances regardless of their better mechanical properties [20,21]. Recent studies proved that the rGO and PRG dispersion in aqueous solution can be improved by a combination of surfactants and ultrasonication method and could significantly enhance mechanical properties of cement materials [20,22]. For examples, Wang et al. [20] found that the addition of 0.05% PRG in cement mortar can improve compressive strength and flexural strength at 7 days, by 8% and 24%, respectively. Tong, et al. [23] showed that the compressive strength of cement mortar is improved by 19.9% after 28 days when adding 0.1% PRG by weight of cement. However, these earlier studies only focused on investigating the changes in mechanical properties of cementitious composites between the control mortar and the mix with a certain PRG content (e.g. 0.05 or 0.1%) but limited details about properties of used graphene materials [24]. In 2015, Du and Dai Pang [25] studied the properties of cement mortars with four different PRG dosages (i.e. 0%, 2.5%, 5.0% and 7.5% by weight of cement, with PRG size 8 μm), and showed that the addition of PRG can significantly decrease water penetration depth. However, their study indicates there are insignificant effects of PRG on compressive and flexural strengths of cement mortars. This is attributed to the high rate of PRG dosages used, resulting in the agglomeration of PRG sheets and forming multi-layers PRG sheets, which results in the hindrance to the interaction between PRG and cement matrix. A recent study of PRG-cement mortars with different PRG concentrations (i.e. 0%, 0.05%, 0.1%, 0.5% and 1% by weight of cement, with PRG size 5–10 μm) by Tao et al. [26] confirmed that cement mortar with 0.05% PRG additive can improve compressive strength and flexural strength at 28 days, by about 8.3% and 15.6%, respectively, but the strengths start decreasing when the PRG dosages are increased to exceed 0.05% owing to the agglomeration of PRG. Although these studies presented the dependence of the properties of PRG-cement mortars on PRG dosages, the characteristics of the mechanism behind this dependence have not been well understood. Compared to the proposed reinforcement mechanism of GO in cement composites, this is attributed to the strong interfacial adhesion between carboxyl, hydroxyl groups and cement matrix [27], which indicates that smaller size GO often shows a better enhancement rate in mechanical properties of cement composites than larger size GO as smaller size GO has more of these functional groups [17,24]. Unlike GO, graphene sheets of PRG materials have very few of oxygen groups located at the edges, where different mechanisms are involved with the friction adhesion forces between PRG sheets and cement matrix. Thus, the larger size of single PRG structure is proposed to have the better enhancement to the cement matrix. To date, no studies have been done to investigate the influence of the ultra-large size of PRG on mechanical properties of cement-based mortars. While graphene materials are slowly moving into industrial space with many graphene manufacturers around the world that are able to produce their large quantities, there is still a lack of studies using industrially manufactured graphene to improve performances of cementitiou.

To address these research gaps, the aim of this study is to investigate the use of industrially manufactured PRG produced by an electrochemical process with focus on studying the effects of the ultra-large size of PRG (i.e. 56 μm) and their dosages (i.e. from 0% to 0.3% by weight of cement binder) on the physicochemical and mechanical properties of PRG-cement mortars. Our hypothesis is that very large sheets of graphene with the size of several tens of micron will significantly improve the mechanical properties of cement. Most of the previous studies were based on PRG prepared in research laboratories with variable quality and less reproducible structural and mechanical characteristics. In this work, it is the first time to use industrially produced PRG manufactured by an electrochemical process that has recently been established by First Graphene Ltd in Perth, Australia, with the capacity of 100 t/year. To better understand the mechanism behind the positive effects of ultra-large PRG particles with different dosages on cement mortars, a series of microanalyses were completed using X-ray

diffraction analysis (XRD), Thermogravimetric analysis (TGA), Fourier transform infrared spectroscopy (FTIR), Scanning electron microscopy (SEM), and Ultraviolet–visible spectrophotometer (UV–vis). Industrial production of graphene has dramatically reduced the cost of producing graphene in large quantities, allowing it to be incorporated into industrial-scale materials, such as concrete. Hence, the promising results from this study will provide an attractive avenue to practical applications of graphene-based materials for a broad range of construction materials to enhance their mechanical and durability properties.

2. Experimental methods

2.1. Materials

The PRG with the physical properties shown in Table 1 were provided by First Graphene Ltd (Australia) from their industrial production plant. Ordinary Portland Cement (OPC), which is general purpose cement according to Australian Standard AS 3972-2010 [28], with the chemical composition shown in Table 2 were used as the binder of mortar mixes. Natural sand with a 2.36-mm maximum particle size was used as the fine aggregate, and its particle size distribution is presented in Table 3. MasterGlenium SKY 8100, which is the second generation polycarboxylic ether polymer superplasticizer in compliance with Australian Standard AS 1478.1-2000 [29], was used in all mortar mixes as a surfactant to increase the dispersion of PRG in aqueous solution and workability of mortars. The properties of the superplasticizer are shown in Table 4.

2.2. Preparation of PRG suspension

The aqueous solution for mortar mixes, including water, PRG and superplasticizer, was prepared following the steps: (i) MasterGlenium SKY 8100 was mixed and stirred in water within 2 min; (ii) PRG was then added and stirred for 2 min; (iii) the solution was then sonicated by Ultrasonicator UIP1000hdT for 30 min to create the aqueous solution for the mortar mixes.

2.3. Preparation of PRG-cement mortar composites

A total of seven unique mixes of PRG-cement based mortars were prepared. Their detailed mix proportions are described in Table 5. As shown in the table, there are seven concentrations of PRG used, i.e. 0% (as the plain mortar), 0.01, 0.03, 0.05, 0.07, 0.1 and 0.3% by weight of cement binder. These seven concentrations were designed based on a comprehensive literature review, which focused on investigating the effects of graphene's derivative (e.g. GO, rGO, PRG) on properties of cementitious materials [19,30].

To prepare the mortar mixes, the procedures described below were adopted to improve the uniform of the cement matrix: natural sand and OPC were mixed together for four minutes, and then the aqueous solution (preparation procedures as described in Section 2.2) was gradually added to the mortars and continued mixing together within five minutes, which contained one minute to check and stir the mixes. All samples after mounting were vibrated for one minute to eliminate the entrapped air in samples during mounting. All specimens were demounted after 24 h cured in room temperature and covered with wet fabric sheets to prevent the loss of moisture. They continued to be cured in a fog room under the ambient temperature of 23 ± 2 °C until the testing days (i.e. at 7 days and 28 days).

The labels of the PRG-cement based mortar mixes shown in Table 5 are designed as follows: the PRG letter is used to refer to pristine graphene in the mixes. The number after the PRG letter stands for the proportion of PRG calculated by the weight of Portland cement in the mixes. To illustrate, PRG0 and PRG0.07 are the mortar mixes prepared with 0% (i.e. the control mix) and 0.07% PRG by the weight of cement, respectively.

Table 2
Chemical composition of ordinary Portland cement (OPC).

Compounds	OPC (%)
CaO	63.28
SiO_2	19.95
Al_2O_3	4.79
Fe_2O_3	3.14
MgO	2.03
Na_2O	0.29
K_2O	0.4
SO_3	2.69
P_2O_5	0.04

2.4. Characterization of microstructural tests

2.4.1. Scanning electron microscopy and particle size measurements

SEM was obtained by using the FEI Quanta 450, which analyzes and provides high-resolution images of surface topography. The SEM analysis was conducted at 28 days, and SEM specimens were cut from the samples of PRG-cement mortars at 28-day mechanical tests with the dimensions of about 5 × 5 × 5 mm to analyze their surface morphologies and microstructures. All these specimens were dried and then coated by a 5 nm-thick platinum layer to enhance the quality of SEM images. Particle size measurement of PRG dispersions was measured in triplicate by a Nanosight NS300 (Malvern Instruments) coupled with a green laser (532 nm) using the O-ring top-plate sample chamber configuration. The pre-installed Nanoparticle Tracking Analysis (NTA) software version 3.3 took into account the Brownian motion trajectory of the particles to measure its size.

2.4.2. X-ray diffraction analysis

XRD was conducted by using the Rigaku MiniFlex 600 X-Ray diffractometer to find the mineralogical characteristics (i.e. the crystalline phases) of materials (i.e. OPC, natural sand, PRG, and hydration products of PRG-cement mortars). The XRD was worked at conditions 40 kV and 15 mA, 2θ = 5°–80° at 0.02° step size. The XRD specimens were collected from remnant pieces of PRG-cement mortars at 28-day compression tests, and then, they were dried in the oven for one day, then ground, and sieved into fine powders (i.e., < 10 μm) for analysis.

2.4.3. Thermogravimetric analysis

TGA was performed by using the TGA Q500 instrument to investigate the effects of PRG on the hydration process of cement composites at 7 and 28 days. About 20 mg of the powder (i.e. < 10 μm) of mortar mixes was heated from room temperature to

Table 1
Physical properties of pristine graphene supplied by First Graphene ltd.

ID	Average particle size (μm)	Thickness (nm)	Purity (%)	Bulk density (g/cm^3)
PRG-70	56 ± 12	1–3	98.3	0.1

Table 3
Particle size distribution of natural sand.

Mesh size (mm)	2.36	1.18	0.6	0.15	0.075
Cumulative passing (%)	96.7	84.6	62.2	4.5	0.4

Table 4
Properties of superplasticizer (MasterGlenium SKY 8100).

pH	Boiling temperature (°C)	Density at 20 °C (kg/dm^3)	Flash point (°C)	Vapour pressure at 20 °C (hPa)	Solid content (mass, %)
6.4	≥100	1.06	>100	23	30.7

Table 5
Mix proportions of the cement mortar composites.

Mix	Pristine graphene (%)*	Water/cement ratio	Cement (kg/m^3)	Water (kg/m^3)	Pristine graphene (kg/m^3)	Sand (kg/m^3)	Superplasticizer (kg/m^3)
PRG0	0	0.485	527	256	0.0	1448	1.4
PRG0.01	0.01	0.485	527	256	0.1	1448	1.4
PRG0.03	0.03	0.485	527	256	0.2	1448	1.4
PRG0.05	0.05	0.485	527	256	0.3	1448	1.4
PRG0.07	0.07	0.485	527	256	0.4	1448	1.4
PRG0.1	0.1	0.485	527	256	0.5	1448	1.4
PRG0.3	0.3	0.485	527	256	1.6	1448	1.4

* The percentage of pristine graphene based on weight of cement binder.

900 °C with the heating rate of 10 °C per minute under the nitrogen atmosphere condition. The outcomes of the TGA analysis are able to identify the contents of evaporable water (i.e. free water covers outer surfaces of cement composites) and non-evaporable water (i.e. the water content bound by products (e.g. portlandite, calcium silicate hydrate gels) of the cement hydration process). Based on the proportion of the weight loss of testing samples, the hydration degree of cement pastes of the control and PRG-cement samples was calculated (the details are discussed later in Section 3.4.2).

2.4.4. Fourier transform infrared spectroscopy

FTIR was performed by using the Nicolet 6700 to determine specific functional groups and their intensities in samples, including PRG, cement, sand, powder cementitious materials at 28 days. The infrared spectrum was obtained by using the support of the spectrum analysis software, which shows spectrums in transmission mode with the range of frequency in wavenumber from 400 cm^{-1} to 4000 cm^{-1}.

2.4.5. Ultraviolet-visible spectrophotometer

UV–vis was obtained by using Shimadzu UV-1601 to investigate the dispersion of PRG aqueous solution, varying with the time between two methods: 30 min sonicated by Ultrasonication UIP 1000hdT (Hielscher, Germany) and without sonication. The percentage of the transmittance of PRG aqueous solution determined by UV–vis varies with time is used to provide a quantitative analysis of the dispersity or sedimentation of the solution.

2.5. Flowability test and mechanical property tests

The flow test of fresh mortars was performed immediately after mixed mortars, according to ASTM C1437 [31]. The dimensions of the truncated cone mold are top diameter 70 mm, height 50 mm, and bottom diameter 100 mm. The truncated cone mold was filled with fresh mortars by layers and tamped by a tamper to ensure uniform filling of the mold, then the mold was raised vertically, and the mean horizontal spreads of fresh mortars were recorded. This test was conducted to investigate the flowability of PRG-cement mortar mixes. For hardened cement composites, the compressive strength was determined at 7 and 28 days by carrying out compressive tests. A typical 50 mm cube was used according to the ASTM standard C109/C109M-07 [32]. The direct tensile test with a dog-bone shaped sample was also conducted at 7 days and 28 days in accordance with the ASTM standard C307-03 [33]. These tests were performed to identify the effect of PRG concentrations on mechanical properties of PRG-cement based mortars. The compressive and tensile strengths were determined from the averaged values of three nominally identical specimens for each mix proportion.

3. Results and discussion

3.1. Characterization of industrial manufactured pristine graphene (PRG) materials

The morphology and physical properties of industrially produced PRG material used in this study are summarized in Fig. 1 and Table 1, which show their morphology, particle size and crystallinity. The graphene particle has irregular shaped structures and the average particle size of the graphene sheets is 56 ± 12 μm and a carbon content of >98.3%. From Fig. 1(c), the XRD pattern shows the crystalline phase of PRG at the scattering angle $2\theta = 26.64°$. The interplanar spacing between layers (i.e. d-spacing) calculated based on the Bragg's Law is 0.334 nm, which is the same as the interplanar spacing of Graphite [24,34], showing a high quality of PRG used in the study.

The observations of the sedimentation of PRG in aqueous solution with times between 30 min sonicated and without sonicated at the same 0.03% PRG content based on the percentage of transmittance of these solutions from UV–vis analysis are shown in Fig. 2. It is important to note that a solution with a lower percentage of the transmittance with time presents for better dispersion of PRG aqueous solution with time. As shown in Fig. 2(a), without a sonication, the transmittance is high at the early stage about 30%, and continues rising remarkably with time about 70% and 90% after 4 h and 24 h, respectively. In Fig. 2(b), 30 min sonicated, the transmittance values are low, and rise very slowly with time compared to no sonication, which is about 0.5%, 2.5%, and 25% after sonication, 4 h, and 24 h respectively. From the photos in Fig. 2(c) and (d), we can note that the suspension of PRG aqueous solution

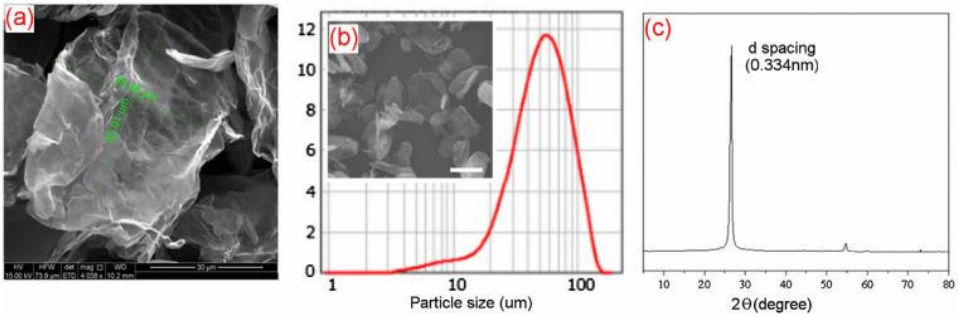

Fig. 1. (a) High resolution SEM images showing the size of single PRG particlce and b) Low resolution SEM image (bar scale 50um) and PRG particle size distribution (C) XRD pattern of PGR material.

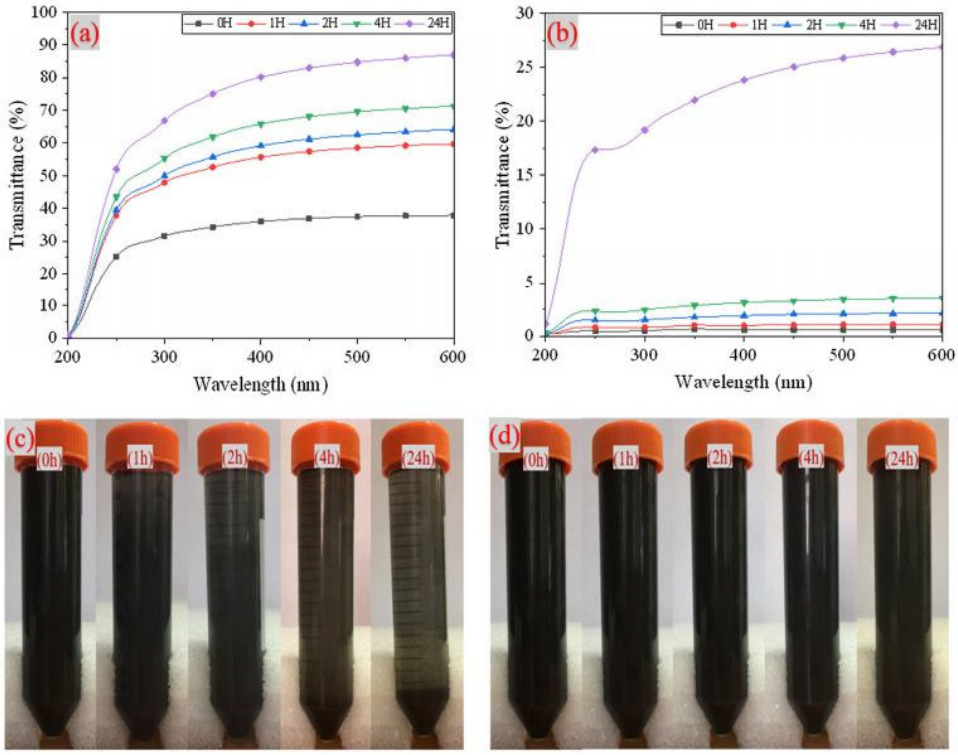

Fig. 2. Variation of transmittance of pristine graphene suspension at 0.03% PRG with time from UV–Vis test: (a) without sonication, and (b) 30 min sonication. Photographs of PRG aqueous suspension after 0 h, 1 h, 2 h, 4 h, and 24 h: (c) without sonication, and (d) 30 min sonication.

without a sonication shows a clear variation of sedimentation following the time whereas it is hard to observe the change of the sedimentation of the one with 30 min sonicated. The results from UV–vis and observed photos indicate that the PRG aqueous solution is much more stable and well dispersed with the sonication method than without sonication, especially within 4 h after the sonication, which is important to be able to create mixes with high quality because of the effects of initial setting time characteristic of OPC on cementitious composites [35].

3.2. Effects of PRG on the flowability of PRG-cement mortar composites

Fig. 3 presents the flowability of the mortar mixes with different concentrations of PRG. As shown in the figure, the flowability of the mortars reduces with an increase in the PRG contents, and the mean value of the flowability of the control mix is 135 mm, which is 22.7% higher compared to the mix with the addition of 0.3% PRG (mean value of the flowability is 110 mm). The decrease of the flowability of the mixes with the rise in the PRG contents is

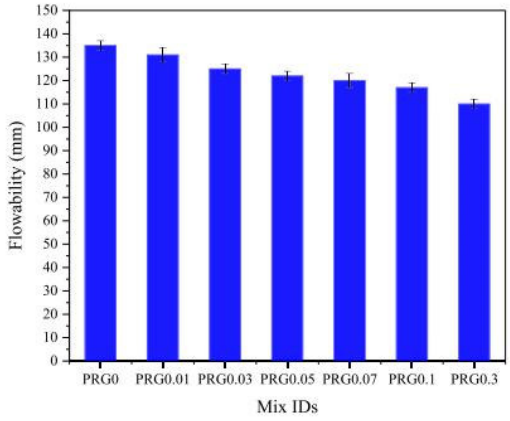

Fig. 3. Flowability test results of fresh mortars with different PRG contents.

attributed to the large specific surface area of PRG, resulting in more amount of water required to lubricate their surface sheets, which is in agreement with the previous research studies on the effects of nanomaterials (e.g. GO, nano-SiO2, PRG) on the flowability of the cement matrix [19,20].

3.3. Effects of PRG on mechanical properties of PRG-cement mortar composites

The 7 and 28 days compressive test results of the control mix and the mixes with different PRG concentrations, and their enhancement strengths compared to the control mortar are shown in Fig. 4. It can be seen that the addition of PRG to the mortar mixes results in an increase in the compressive strength of the cementitious composites for both 7 and 28 days compressive test results. The optimal concentration of PRG is at 0.07% PRG, which is 50.0 MPa and 56.3 MPa at 7 and 28 days, respectively. Compared to these tests with the control mix at the same test days, which is 36.5 MPa and 42 MPa, the results show that the strength is enhanced about 36.8% at 7 days and 34.3% at 28 days, respectively.

The trend of the compressive strengths of the mortars at 7 and 28 days decreases when the PRG contents beyond the optimum value (i.e. 0.07% PRG). The graph in Fig. 4(b) shows that the compressive test results at 7 days of the PRG-cement mortar mixes with the PRG concentrations under the optimum value have lower enhancement strength rates than those at 28 days. Whereas, the trend is upside-down for the mixes with the PRG contents beyond 0.07% PRG.

Fig. 5 describes the 7 and 28 days tensile test results of the different mortar mixes, and their enhancement strengths compared to the control mix. As shown in the figure, the tensile strength of the PRG-cement mortars increases with an increase in the PRG concentrations at all curing ages. It is evident from Fig. 5 that the optimal concentration of PRG is at 0.07% PRG, which is 3.9 MPa at 7 days and 4.6 MPa at 28 days, compared to these testing days of the control mix, which is 3.1 MPa and 3.6 MPa, respectively. This enhancement in tensile strengths equates to about 25.3% at 7 days and 26.7% at 28 days. Fig. 5(a) also shows that the tensile strength of the PRG-cement mortars starts dropping when the PRG contents beyond 0.07% PRG. From Fig. 5(b), the enhancement strength rates of the tensile test results at 7 days of the PRG-cement mortar mixes are higher than those at 28 days, except for the mixes PRG0.01 and PRG0.07.

The observed improvement in the compressive and tensile strengths of the PRG-cement mortar composites with the highest strength at the PRG0.07 mix, which will be discussed in more details in Section 3.4, could be explained by the following reasons: (i) the enhanced cement gels of the cement matrix composite owing to: (1) the improvement of the hydration degree of cement pastes due to the high specific surface area of PRG sheets, resulting in better spreading water to cement particles, which is similar with the observation of previous studies on mechanical properties of GO and cementitious composites [9,30]; (2) the closer of cement particles in the cement matrix caused by the van der Waals forces between PRG sheets, resulting in an enhancement of strengths of cement gels [30,36]; (ii) the improvement of bonding gels comes from the improved interfacial friction and interconnecting behavior between the crystals of the hydration products in cement gels, which was created from a part of the covalent bonds between some COOH groups in PRG and cement gels (this is similar to other studies observed in a combination of carbon nanotube and GO and Portland cement [9,37]), and most from friction forces between the

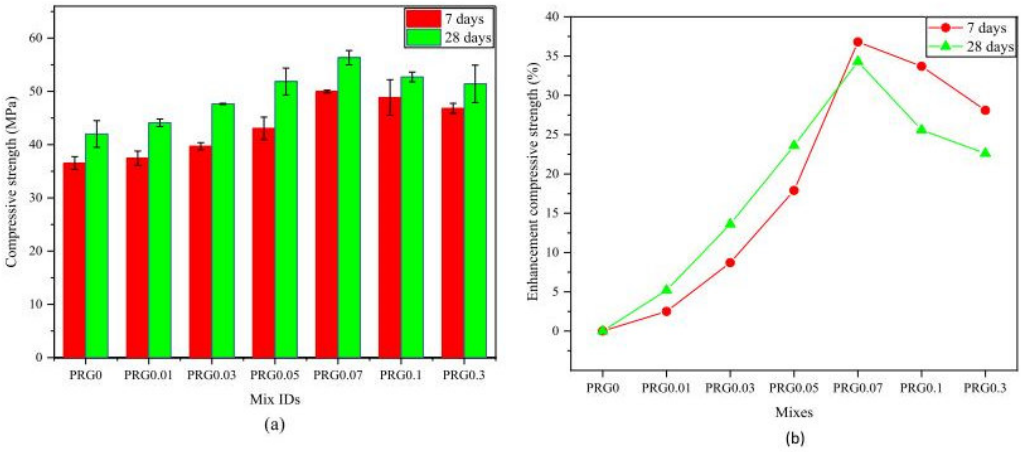

Fig. 4. (a) Compressive strength and (b) enhancement compressive strength of PRG-cement mortars with different proportions of PRG at 7 and 28 days.

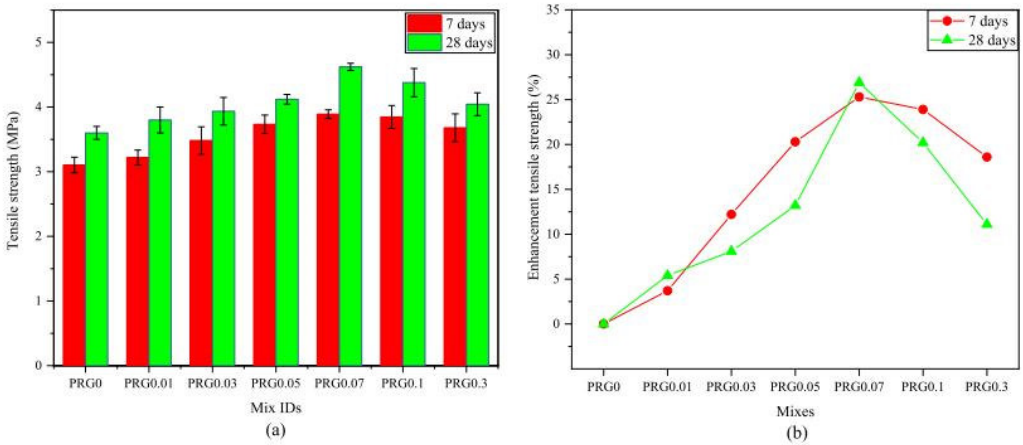

Fig. 5. (a) Tensile strength and (b) enhancement tensile strength of PRG-cement mortars with different proportions of PRG at 7 and 28 days.

areas of PRG sheets and cement gels (this was reported in previous research by using the molecular dynamics simulation method [38,39]), resulting in being able to enhance the stress distribution and impeding the propagation of cracks from nanoscale to microscale and macroscale in the cement matrix [19,20]. Nevertheless, the mixes with the high PRG concentrations, which are beyond the optimum value, i.e. PRG0.1 and PRG0.3, lead to poor dispersion resulting in the re-stacking of PRG sheets due to the effect of the van der Waals force. This is attributed to the creation of multi-layers PRG sheets with a thicker thickness that results in poor interfacial friction and interconnecting behaviour, and thus, reduces the compressive and tensile strengths. This is in line with previous findings on GO and cement composites [19,40].

The axial compressive stress and strain relationship of the mortar mixes with different PRG concentrations at 28 days is shown in Fig. 6. The curves show that for a given PRG concentration, the compressive strength increases with an increase in the PRG content, and reaches the highest strength with the PRG0.07 mix, and then, starts decreasing in strengths when the PRG contents beyond

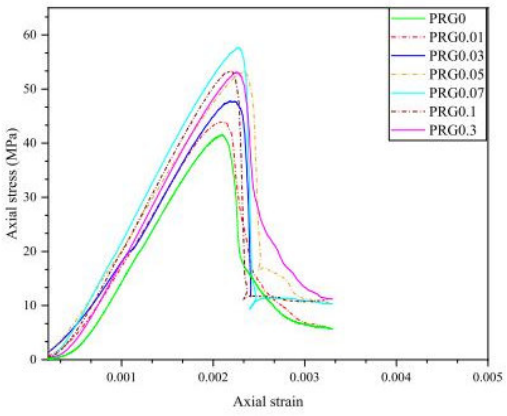

Fig. 6. The axial stress and axial strain relationship of mortar mixes with different PRG contents at 28-day compressive testing.

this optimal value. It is important to note that the stress-strain curves can also show the estimated elastic modulus of materials, deduced from the ratio between stress and strain which are taken at about 40% of the ultimate compressive strength. Therefore, from Fig. 6, it is concluded that the elastic modulus of the PRG-cement based mortars is higher than the plain mortar, and the mix with a higher compressive strength presents a higher elastic modulus. This trend is consistent with the widespread relationship between compressive strength and elastic modulus in solid materials as shown in other research or standards [19,41].

3.4. Microstructure and characterization of PRG-cement mortar composites

The influence of the PRG concentrations on the mechanical properties of cement mortar composites at microscale was evaluated using microstructural tests: XRD, TGA, FTIR, and SEM. These tests were designed and conducted by four different contents of PRG as follows: 0 (the control mix), 0.03% (as shown the transparently effective effect of PRG), 0.07% (the optimum PRG content based on the experimental results from mechanical tests), 0.3% (the maximum PRG content).

3.4.1. XRD analysis

The XRD patterns of OPC, sand, and PRG-cement mortar mixes are shown in Fig. 7. As shown in Fig. 7(a), the peaks detected in the XRD pattern for the natural sand are at positions: from 21.2°, 26.7°, 36.7°, to 77.9° etc., which indicates crystalline phases of quartz in natural sand [42,43]. Fig. 7(a) also shows that the peaks of diffraction spectra for OPC powder identified the following main phases: (i) Alite ($3CaO.SiO_2$, C_3S) at positions: from 29.5°, 32.3°, etc. to 62.4°; (ii) Belite ($2CaO.SiO_2$, C_2S) at positions: 30.2°, and 32.7°; (iii) Tricalcium aluminate ($3CaO.Al_2O_3$, C_3A) at 23.1° and 32.3°; (iv) Tetracalcium aluminateferrite ($4CaO.Al_2O_3.Fe_2O_3$, C_4AF) at 12.3°; and Gypsum ($CaO.SO_3{\cdot}2H_2O$) at 11.8°. It is also notable from the figure that C_3S shows the major content in the OPC powder, followed by C_2S, C_3A, C_4AF, and Gypsum, respectively. These identified phases and characteristics are in agreement with previous studies on the OPC components and its hydration process using the XRD analysis [44,45].

In cementitious composites, the main products of the hydrated cement paste are portlandite ($Ca(OH)_2$, CH) and calcium silicate

hydrate (CSH), which contribute to mechanical properties of cementitious composites, and part of ettringite. The brief hydration reaction process can be seen in Eqs. (1) and (2) in Section 3.4.2. The XRD patterns of the mortar mixes with different PRG concentrations, i.e. PRG0, PRG0.03, PRG0.07, PRG0.3, are shown in Fig. 7(b). Although they have similar types of hydrated productions, their contents are different, resulting in different mechanical strengths (as discussed before in Section 3.3). It is important to note that CSH gels often stay at the amorphous phases, the XRD analysis is thus limited to identify CSH phases [20,45]. However, the content of CSH gels can be estimated based on the amount of CH (as shown in Eq. (1) in Section 3.4.2), and the amount of the un-hydrated cement (e.g. alite) [24,45,46]. The degree of the hydration process of cement mortars can be estimated by the amount of the crystalline phases of CH in XRD analysis results. In order to make the equal percentage of natural sand existed in each sample of each mix, the major peak of natural sand at the position 26.7° of each mix was standardized to have equal intensity in all spectra of all the mixes [17,46].

Fig. 7(b), (c) shows that the detected peaks at the scattering angles of 18.2°, 34.2°, and 47.1° correspond with CH phases [44,46]. Fig. 7(c) shows that the intensities of these peaks for portlandite in the mixes having PRG (i.e. PRG0.03, PRG0.07, and PRG0.3) are higher than the control mix (i.e. PRG0), and are augmented with the increase of the PRG contents. It reaches the highest value at the PRG0.07 mix, and then decreases when the PRG concentration beyond 0.07% (i.e. PRG0.3). This suggests that the mixes containing PRG contents have higher degrees of the hydra-

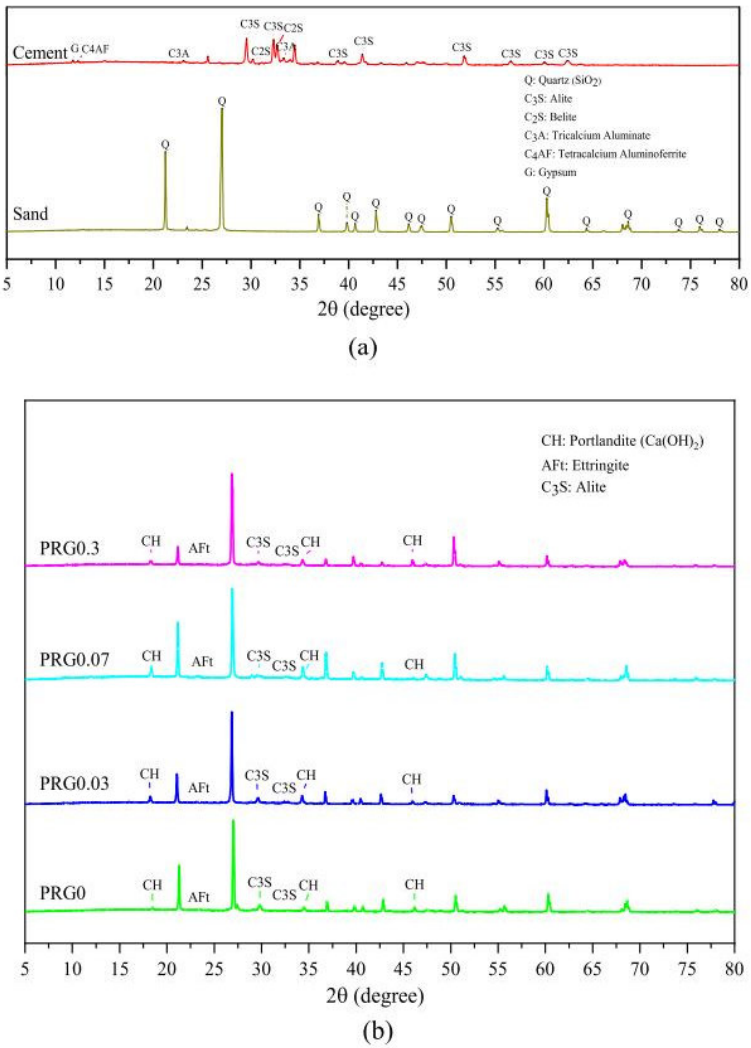

Fig. 7. Powder XRD patterns of: (a) natural sand and original Portland cement; (b) PRG-cement composites with different PRG contents (i.e. 0%, 0.03%, 0.07%, and 0.3%) at 28 days; (c) insets of portlandite and tricalcium silicate details of different PRG-cement composites at 28 days.

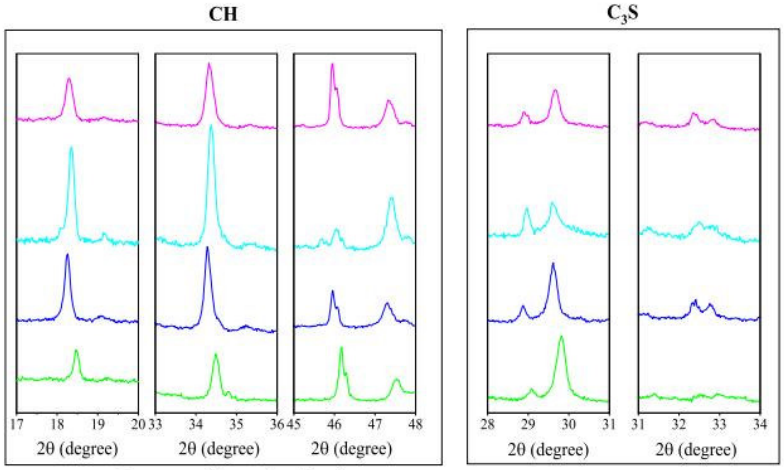

Summary of intensity of peaks

ID	PRG0	PRG0.03	PRG0.07	PRG0.3
CH	5390	8037	11848	8908
C_3S	3848	3770	3456	3616

(c)

Fig. 7 (*continued*)

tion of cement pastes than the control (as will be also validated by TGA, FTIR results), which is consistent with the studies on graphene and cementitious composites in literature [20,46].

Moreover, the major peaks of un-hydrated alite ($2\theta = 29.5°$, 32.3°) in these mixes detailed in Fig. 7(c) show that the control mix has the highest intensity of the amount of un-hydrated alite than the others, which is followed by PRG0.03, PRG0.3, and PRG0.07, respectively. This shows that PRG can accelerate the degree of the hydration of cement pastes and create more CSH gels in cementitious materials [17,45,46]. In summary, the XRD analysis results are in agreement with the growth trend of the mechanical strengths of PRG-cement mortar composites discussed previously in Section 3.3.

3.4.2. TGA analysis

TGA is another well-known method used to analyze the hydration degree of cementitious composites, which is based on the content of portlandite and non-evaporable water calculated from samples [47,48]. According to previous studies on cementitious composites [24,49], the brief chemical reactions of the hydration performance of OPC and the decomposition reactions of its hydration products summarized below can provide a better understanding to identify different phases in TGA analysis results.

$$(C_3S, C_2S) + H_2O \rightarrow CH + CSH \quad (1)$$

$$(C_3A, C_4AF) + Gypsum(CaO.SO_3.2H_2O) + H_2O \rightarrow AFt + AFm(monosulphoaluminate)\frac{n!}{r!(n-r)!} \quad (2)$$

$$(CSH) \rightarrow C_3S + H_2O \quad (3)$$

$$Ca(OH)_2 \rightarrow CaO + H_2O \quad (4)$$

$$CaCO_3 \rightarrow CO_2 + H_2O \quad (5)$$

$$Ca(OH)_2 + CO_2 \rightarrow CaCO_3 + H_2O \quad (6)$$

Fig. 8(a), (b) shows the TGA analysis results of cement composites at 7 and 28 days of curing age, respectively. As shown in Fig. 8 (b), from the derivative weight change cures, it can be divided into four main loss mass phases: (i) the mass loss below 145 °C is referred to as evaporable water and part of bound water [50,51]; (ii) the mass loss in the range from 145 °C to 200 °C is attributed to CSH gels (Eq. (3)) [20,48]; (iii) from 350 °C to 500 °C is related to the decomposition of portlandite (Eq. (4)) [47,52]; (iv) the mass loss in the range of 600–700 °C is referred to the composition of $CaCO_3$ (Eq. (5)) [48,49]. The non-evaporable water and portlandite contents can be estimated by the following equations [47,48]:

$$M_{non-water} = M_{145°C} - M_{900°C}(\%) \quad (7)$$

$$M_{CH} = \frac{74}{18} * ML_{CH} + \frac{74}{44} * ML_{CaCO3}(\%) \quad (8)$$

where: (i) $M_{145\ °C}$, $M_{900\ °C}$, and $M_{non\text{-}water}$ present for the mass loss of sample at 145 °C, 900 °C, and non-evaporable water in percentage, respectively. (ii) ML_{CH} and ML_{CaCO3}, present for the mass loss in percentage due to the decomposition of portlandite and $CaCO_3$ phases, respectively; M_{CH} stands for the content of portlandite in percentage, $\frac{74}{18}$ and $\frac{74}{44}$ stand for factors showed the ratios of molecular weight of water in the decomposition phases of portlandite and $CaCO_3$ (as referred to Eqs. (4) to (6)).

Based on Eqs. (7) and (8), the amount of portlandite and non-evaporable water of samples at 7 and 28 days are shown in Fig. 8 (a), (b). The contents of portlandite and non-evaporable water increase with an increase in the curing ages, i.e. 7 and 28 days, in all the samples, regardless of the PRG concentrations in the mixes,

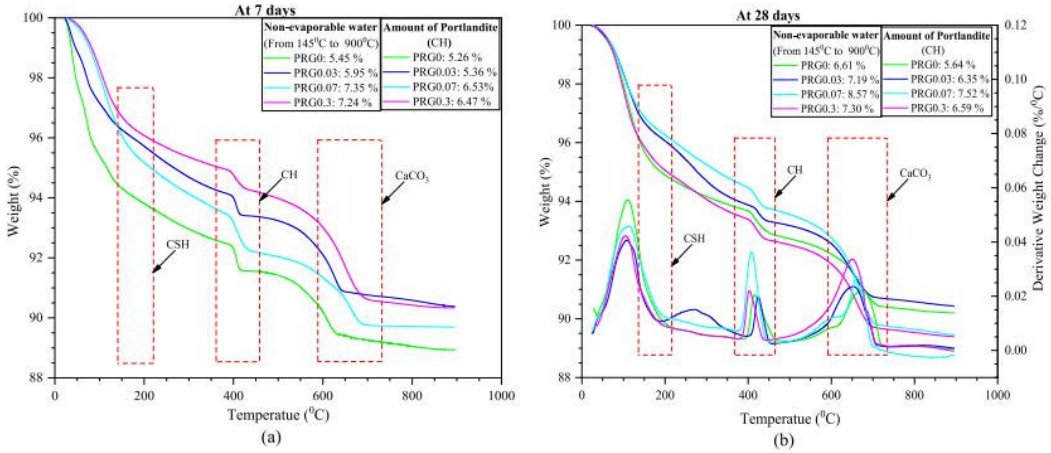

Fig. 8. TGA cures show the weight loss as variation of temperature of PRG-cement composites with different PRG contents (i.e. 0%, 0.03%, 0.07%, and 0.3%) at different days: (a) 7 days; (b) 28 days.

which is in line with other studies on cementitious composites [19,48]. The PRG mixes show higher percentages of portlandite and non-evaporable water than the control at all curing times. In addition, it is evident from the figures that these proportions increase with an increase in the PRG contents. The highest proportion is achieved in the PRG0.07 mix, and then decreased when using beyond this PRG concentration (i.e. PRG0.3), which is consistent with the observed results in the mechanical strengths and XRD analysis (as discussed before in Sections 3.3 and 3.4.1). In summary, from the TGA analysis results, the PRG can accelerate the hydration degree of cementitious composites, which is in agreement with the previous finding in graphene and cement matrix composites [19,20,47].

3.4.3. FTIR analysis

The FTIR spectra of natural sand, OPC, and PRG are shown in Fig. 9(a). The major bands observed for natural sand are: the asymmetrical bending vibration of Si—O—Si at about 470 cm^{-1}; the band at about 520 cm^{-1} attributed to the asymmetrical bending vibration of Si—O—Al; the symmetrical bending variation of Si—O observed at about 692 cm^{-1} presents the crystalline form of quartz in natural sand; the band from 750 to 810 cm^{-1} is attributed to the symmetrical stretching variation of Si—O; and the asymmetrical stretching variation from about 950 to 1100 cm^{-1} for Si—O. All observed bands for natural sand from FTIR analysis results are in agreement with previous studies on natural sand using infrared spectrum [53,54].

For OPC, the bands at about 450 cm^{-1} and 525 cm^{-1}correspond to out-of-plane and in-plane bending vibrations of Si—O bonds and stretching vibration from about 800 cm^{-1} to 1000 $cm^{-1}$with peaks at about 879 and 935 cm^{-1} correspond to Si—O bonds within the SiO_4 groups. These bands are attributed to C_3S and C_2S main constituents in OPC [55–57]; the Al—O bending vibration at about 720 cm^{-1} is belong to AlO_4 groups in C_3A composition in OPC [55,56]; two bending vibrations at about 600 and 650 cm^{-1} and the stretching band from about 1050 to 1150 cm^{-1} correspond to the S—O bonds within SO_4 tetrahedral groups, belong to the gypsum constituent in OPC [56,57]; the stretching variation from 1370 cm^{-1} to 1520 cm^{-1} is attributed to $(CO_3)^{2-}$ in OPC [57].

The major bands of PRG showed the stretching vibrations: from about 1000 cm^{-1} to about 1240 cm^{-1}, which represents the appearance of alkoxy groups (C—O); about from 1300 cm^{-1} to 1600 cm^{-1} corresponds to aromatic double carbon groups (C═C); about 1700 cm^{-1} and from 2500 cm^{-1} to 3600 cm^{-1} refers to the carboxyl (C═O) and hydroxyl (O–H) groups, respectively. This shows that the existing of carboxylic acid groups (i.e. COOH) in PRG are in agreement with other studies on graphene composites [58,59].

Fig. 9(b), (c) shows the FTIR spectra of the plain mix and PRG-cement mixes at 28 days of curing age. The group bands in the ranges of 400–550 cm^{-1} and 800–1200 cm^{-1} represent for Si—O bonds in the CSH gels [55,60]. A broad band from 2800 to 3600 cm^{-1} attributed to O–H groups in water molecules belongs to CSH gels in the mixes [55,56,60]. The narrow vibration in the range of about 3500–3600 cm^{-1} corresponds to O—H bonds in CH (portlandite) [55], and C—O bonds in $(CO_3)^{2-}$ groups observed in a range of 1350–1550 cm^{-1} [56,60]. From Fig. 9(b), (c), it is evident that the intensities of spectra represented for CSH gels (i.e. Si—O, H—O—H), CH (i.e. O—H), and $CaCO_3$ (i.e. $(CO_3)^{2-}$) in PRG-cement mixes (i.e. PRG0.03, PRG0.07, PRG0.3) are stronger than those of the control mix (PRG0). This is attributed to higher hydration degrees in PRG-cement pastes, which results in the enhancement of mechanical properties of the PRG mixes. This is consistent with mechanical properties, XRD, TGA results discussed before, and in agreement with previous studies on graphene in cementitious composites [56,58,60]. Moreover, at a given PRG concentration, the intensity of the spectrum of PRG0.07 shows the strongest band, followed by PRG0.3 and PRG0.03 respectively. This is consistent with the trend curves of the mortar mixes in compressive and tensile strengths as discussed earlier in Section 3.3.

3.5. SEM cross-sectional analysis

The SEM images of cracking patterns of the mortar mixes, i.e. PRG0, PRG0.03, PRG0.07, and PRG0.3, at 28 days at 50 μm and 30 μm magnification are shown in Fig. 10. The density and width of micro-cracks lead to a reduction in bonding, interconnecting, and interfacial friction properties of cementitious composites as shown in these SEM images. The control mix (Fig. 10(a), (b)) shows a higher degree of cracks both in the density and size and the lower compactness of the microstructure than those in PRG0.03, PRG0.07, and PRG0.3, as shown in Fig. 10(c)–(h), resulting in the

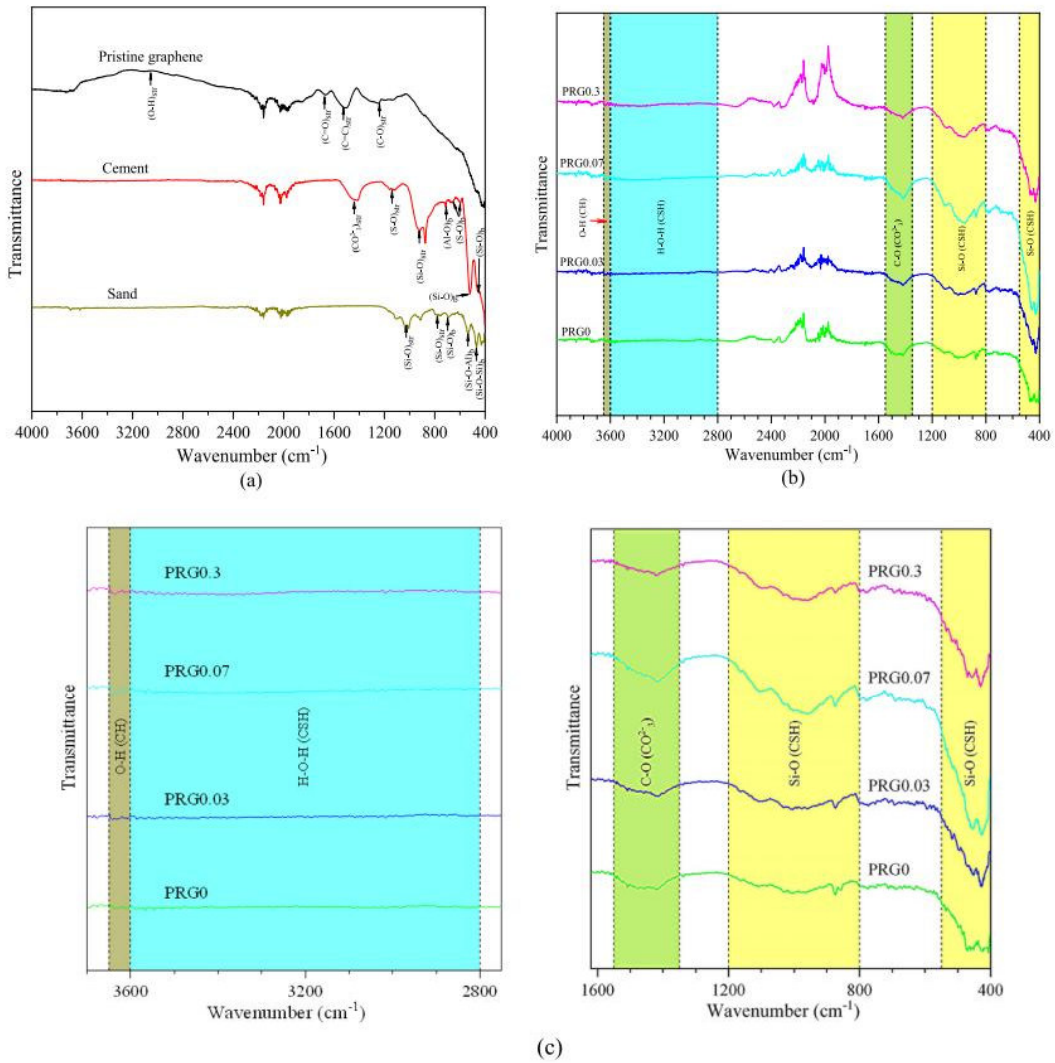

Fig. 9. FTIR spectra of: (a) PRG, OPC and NS; (b, c) PRG-cement composite mixes with different PRG contents (i.e. 0%, 0.03%, 0.07%, and 0.3%) and their insets at 28 days.

lower strengths of the control mix than the others. Thus, the PRG-cement based mortars with better microstructures have the efficient capacity in crack bridging, crack branching and stress distribution, and also impeding crack propagations in structures, which leads to significant enhancement of compressive and tensile strengths. This is consistent with the results discussed in previous sections and also in agreement with the observations of other studies on graphene and cement materials [17,19,20,47].

Fig. 11 shows the high magnification at 10 μm and 5 μm of SEM images of the mortar mixes with different PRG concentrations, i.e. 0%, 0.03%, 0.07%, and 0.3%, at 28-day curing age. The SEM images show four main compositions of the microstructures of the samples: CSH gels have tetrahedral and polyhedral shapes; CH has hexagonal shapes; Aft has needle-rod shapes; and pores intercalate between crystals [16,17,24]. It can be observed that they have similar types of the compositions in microstructures while the density and distribution of these components in each sample are different. For PRG0 shown in Fig. 11(a), (b), it not only shows fewer contents and smaller sizes of CSH and CH crystals, but also consists of significant numbers of pores in its microstructure. This leads to smaller mechanical strengths than those of the PRG-cement mixes (as consistent with the results discussed in the previous sections).

By the addition of the 0.03%, 0.07%, and 0.3% PRG content (Fig. 11(c)–(h)), there are apparent changes in their microstructures with larger sizes and enhanced densities of crystals, also more compactness. The best observation in the change of the microstructure can be seen in PRG0.07 (Fig. 11(e), (f)), which is the densest, and followed by PRG0.3 (Fig. 11(g), (h)) and PRG0.03

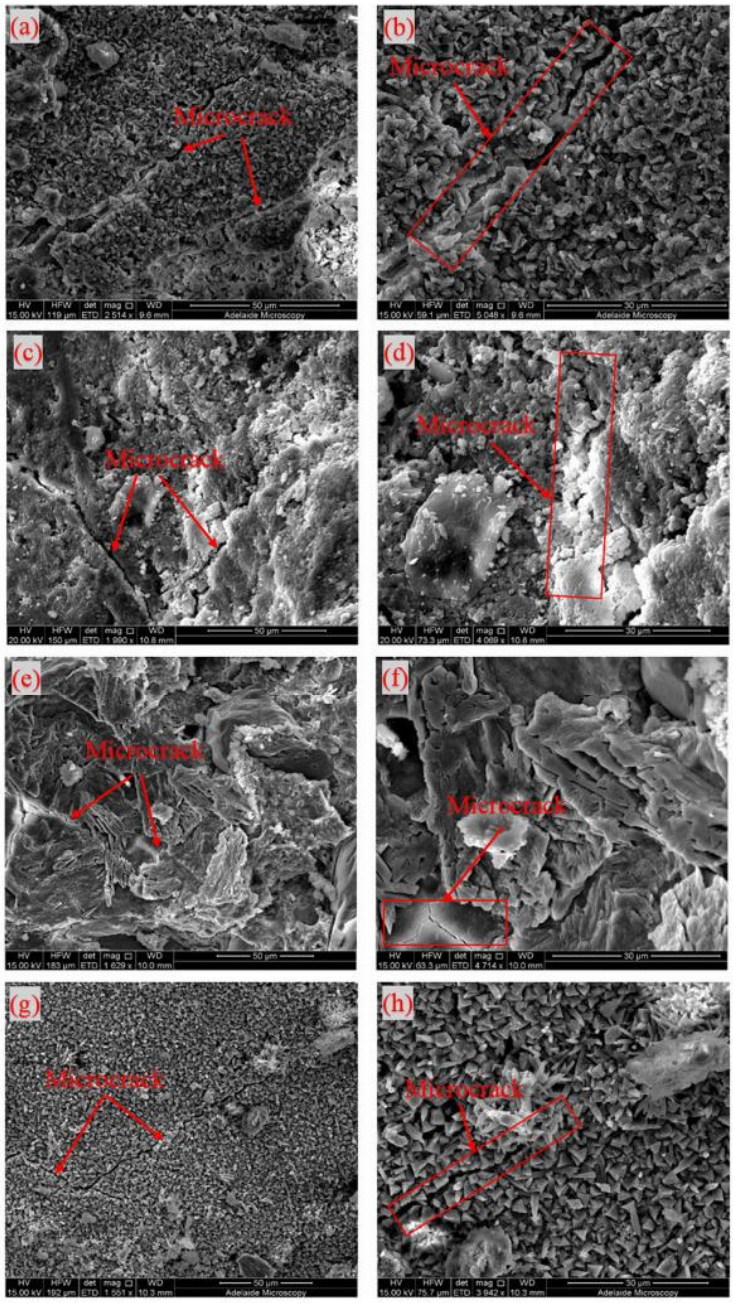

Fig. 10. SEM images of cracking patterns at 50 μm and 30 μm magnification of PRG-cement mortar mixes with different PRG contents (i.e. 0%, 0.03%, 0.07%, and 0.3%) at 28 days: (a, b) PRG0; (c, d) PRG0.03; (e, f) PRG0.07; (g, h) PRG0.3.

(Fig. 11(c), (d)). This is because PRG0.07 not only shows the highest degree of the cement hydration, which was discussed earlier in XRD, TGA, and FTIR results, but also comes from the mechanical adhesive friction forces between PRG sheets and cement gels,

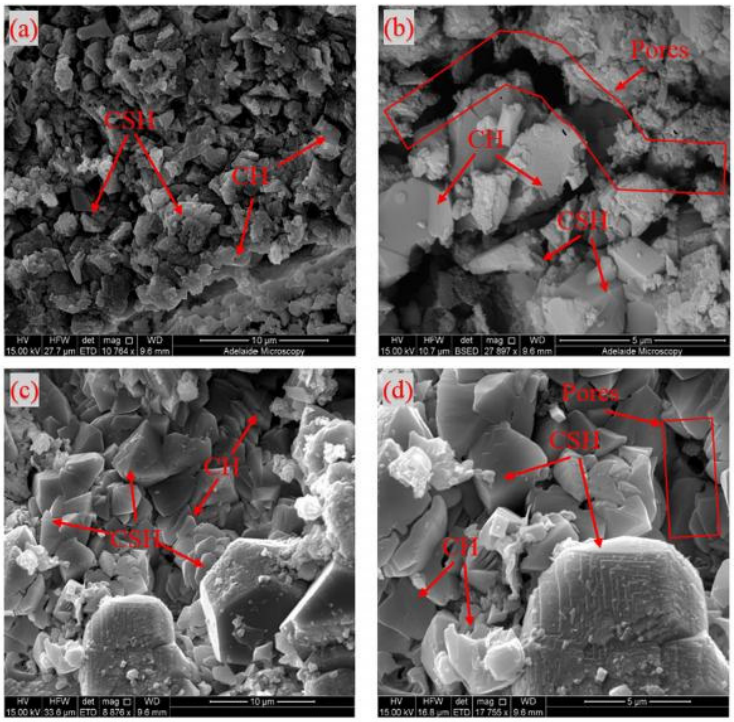

Fig. 11. High magnification at 10 μm and 5 μm of SEM images of PRG-cement mortar mixes with different PRG contents (i.e. 0%, 0.03%, 0.07%, and 0.3%) at 28 days: (a, b) PRG0; (c, d) PRG0.03; (e, f) PRG0.07; (g, h) PRG0.3.

resulting in the strong interconnection across the compositions of cement matrix composites.

When PRG concentration is increased up to 0.3%, it leads to poor dispersion. The agglomeration of PRG sheets occurs due to the effect of the van der Waals force. This creates multi-layers PRG sheets with thicker thickness, and hence, it prevents PRG sheets to contribute to improve the degree of the cement hydration process and to interact with the crystals compositions of cement gels. This leads to the reduction in mechanical strengths, which is in line with the results discussed in the previous sections and previous studies on a combination of graphene and cementitious composites [19].

4. Conclusions

The results of the investigation on the effects of different concentrations of industrially produced PRG by electrochemical exfoliation of graphite on the physicochemical and mechanical properties of PRG-cement mortar composites have been presented. The following key conclusions have been drawn based on the results and discussions in the study:

(1) The first study of the ultra-large size of PRG particles in average of 56 ± 12 μm produced by this industrial process has been confirmed that there is a significant enhancement of the ultra-large PRG size to mechanical properties of cementitious composites, compared to all previous studies using graphene based materials.
(2) It has been shown that the addition of PRG to cement mortars can improve their mechanical properties and the level of improvement depends on PRG contents. The 0.07% PRG mix has been identified as the optimal PRG concentration in this study, which provides 34.3% and 26.9% enhancement of compressive and tensile strengths at 28 days, respectively.
(3) PRG has improved the microstructure of the cement matrix, which comes from the rise in the hydration degree of cement pastes and the adhesive friction forces between PRG sheets and cement gels, and has also impeded crack propagations in the structures.
(4) The mixes with the PRG contents, which are higher of the optimal value (i.e. 0.07%), lead to poor dispersion resulting in the agglomeration of PRG sheets. This limits the improvement of the mechanical strengths.
(5) The results from XRD, TGA, FTIR, and SEM analyses have shown that there is a strong relationship between mechanical results and bonding gels, densities and arrangements of the crystals in the microstructures.

The results and findings from this study have suggested a promising capability of industrially manufactured PRG using electrochemical process due to their unique properties to be used as a next-generation of additives in cementitious composites. This could improve the properties of building materials, such as mechanical, durability, conductivity, and shielding properties. We are currently in the process of investigating the effects of the different contents, sizes and types of PRG on these properties, and the findings will be presented in separate studies.

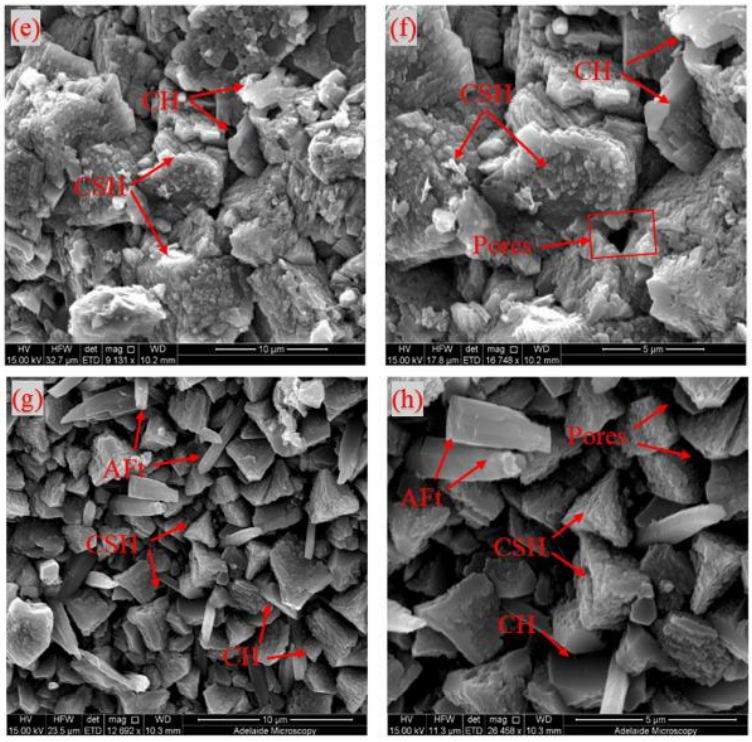

Fig. 11 (*continued*)

Declaration of Competing Interest

The authors declare that they have no known competing financial interests or personal relationships that could have appeared to influence the work reported in this paper.

Acknowledgements

This work is supported and funded by the ARC Research Hub for Graphene Enabled Industry Transformation (Grant IH150100003) and First Graphene Ltd. The authors also thank the Schools of Civil, Environmental and Mining Engineering and Chemical Engineering and Advanced Materials at the University of Adelaide for supporting this work. The authors also acknowledge Adam Ryntjes as the technical support in the experimental works.

References

[1] M.S. Choi, S.-T. Kang, B.Y. Lee, K.-T. Koh, G.-S. Ryu, Improvement in predicting the post-cracking tensile behavior of ultra-high performance cementitious composites based on fiber orientation distribution, Materials 9 (10) (2016) 829.
[2] R.V. Sagar, B.R. Prasad, S.S. Kumar, An experimental study on cracking evolution in concrete and cement mortar by the b-value analysis of acoustic emission technique, Cem. Concr. Res. 42 (8) (2012) 1094–1104.
[3] H. Du, H.J. Gao, S. Dai Pang, Improvement in concrete resistance against water and chloride ingress by adding graphene nanoplatelet, Cem. Concr. Res. 83 (2016) 114–123.
[4] M.S. Konsta-Gdoutos, Z.S. Metaxa, S.P. Shah, Multi-scale mechanical and fracture characteristics and early-age strain capacity of high performance carbon nanotube/cement nanocomposites, Cem. Concr. Compos. 32 (2) (2010) 110–115.
[5] F. Sanchez, K. Sobolev, Nanotechnology in concrete–a review, Constr. Build. Mater. 24 (11) (2010) 2060–2071.
[6] T. Ji, Preliminary study on the water permeability and microstructure of concrete incorporating nano-SiO 2, Cem. Concr. Res. 35 (10) (2005) 1943–1947.
[7] L. Senff, D. Tobaldi, S. Lucas, D. Hotza, V. Ferreira, J. Labrincha, Formulation of mortars with nano-SiO 2 and nano-TiO 2 for degradation of pollutants in buildings, Compos. B Eng. 44 (1) (2013) 40–47.
[8] W. Li, Z. Huang, T. Zu, C. Shi, W.H. Duan, S.P. Shah, Influence of nanolimestone on the hydration, mechanical strength, and autogenous shrinkage of ultrahigh-performance concrete, J. Mater. Civ. Eng. 28 (1) (2015) 04015068.
[9] Z. Pan, L. He, L. Qiu, A.H. Korayem, G. Li, J.W. Zhu, F. Collins, D. Li, W.H. Duan, M. C. Wang, Mechanical properties and microstructure of a graphene oxide–cement composite, Cem. Concr. Compos. 58 (2015) 140–147.
[10] B.M. Tyson, R.K. Abu Al-Rub, A. Yazdanbakhsh, Z. Grasley, Carbon nanotubes and carbon nanofibers for enhancing the mechanical properties of nanocomposite cementitious materials, J. Mater. Civ. Eng. 23 (7) (2011) 1028–1035.
[11] M.S. Konsta-Gdoutos, C.A. Aza, Self sensing carbon nanotube (CNT) and nanofiber (CNF) cementitious composites for real time damage assessment in smart structures, Cem. Concr. Compos. 53 (2014) 162–169.
[12] M.A. Rafiee, W. Lu, A.V. Thomas, A. Zandiatashbar, J. Rafiee, J.M. Tour, N.A. Koratkar, Graphene nanoribbon composites, ACS Nano 4 (12) (2010) 7415–7420.
[13] S. Lv, L. Deng, W. Yang, Q. Zhou, Y. Cui, Fabrication of polycarboxylate/graphene oxide nanosheet composites by copolymerization for reinforcing and toughening cement composites, Cem. Concr. Compos. 66 (2016) 1–9.
[14] B. Han, S. Sun, S. Ding, L. Zhang, X. Yu, J. Ou, Review of nanocarbon-engineered multifunctional cementitious composites, Compos. Part A Appl. Sci. Manuf. 70 (2015) 69–81.
[15] Q. Wang, J. Wang, C.-X. Lu, B.-W. Liu, K. Zhang, C.-Z. Li, Influence of graphene oxide additions on the microstructure and mechanical strength of cement, New Carbon Mater. 30 (4) (2015) 349–356.
[16] S. Lv, S. Ting, J. Liu, Q. Zhou, Use of graphene oxide nanosheets to regulate the microstructure of hardened cement paste to increase its strength and toughness, CrystEngComm 16 (36) (2014) 8508–8516.

[17] S. Sharma, N. Kothiyal, Influence of graphene oxide as dispersed phase in cement mortar matrix in defining the crystal patterns of cement hydrates and its effect on mechanical, microstructural and crystallization properties, RSC Adv. 5 (65) (2015) 52642–52657.
[18] S. Lv, J. Liu, T. Sun, Y. Ma, Q. Zhou, Effect of GO nanosheets on shapes of cement hydration crystals and their formation process, Constr. Build. Mater. 64 (2014) 231–239.
[19] A. Gholampour, M.V. Kiamahalleh, D.N. Tran, T. Ozbakkaloglu, D. Losic, Revealing the dependence of the physiochemical and mechanical properties of cement composites on graphene oxide concentration, RSC Adv. 7 (87) (2017) 55148–55156.
[20] B. Wang, R. Jiang, Z. Wu, Investigation of the mechanical properties and microstructure of graphene nanoplatelet-cement composite, Nanomaterials 6 (11) (2016) 200.
[21] K. Chu, W.-S. Li, H. Dong, Role of graphene waviness on the thermal conductivity of graphene composites, Appl. Phys. A 111 (1) (2013) 221–225.
[22] Z. Metaxa, Polycarboxylate based superplasticizers as dispersant agents for exfoliated graphene nanoplatelets reinforcing cement based materials, J. Eng. Sci. Tech. Rev. 8 (2015) 1–5.
[23] T. Tong, Z. Fan, Q. Liu, S. Wang, S. Tan, Q. Yu, Investigation of the effects of graphene and graphene oxide nanoplatelets on the micro-and macro-properties of cementitious materials, Constr. Build. Mater. 106 (2016) 102–114.
[24] S. Lv, Y. Ma, C. Qiu, T. Sun, J. Liu, Q. Zhou, Effect of graphene oxide nanosheets of microstructure and mechanical properties of cement composites, Constr. Build. Mater. 49 (2013) 121–127.
[25] H. Du, S. Dai Pang, Enhancement of barrier properties of cement mortar with graphene nanoplatelet, Cem. Concr. Res. 76 (2015) 10–19.
[26] J. Tao, X. Wang, Z. Wang, Q. Zeng, Graphene nanoplatelets as an effective additive to tune the microstructures and piezoresistive properties of cement-based composites, Constr. Build. Mater. 209 (2019) 665–678.
[27] E. Shamsaei, F.B. de Souza, X. Yao, E. Benhelal, A. Akbari, W. Duan, Graphene-based nanosheets for stronger and more durable concrete: a review, Constr. Build. Mater. 183 (2018) 642–660.
[28] AS3972, General, purpose and blended cements Standard, Standard Australia, Australian Standard 2010.
[29] AS1478.1, Chemical admixtures for concrete, mortar and grout - Admixtures for concrete Australian Standard 2000.
[30] H. Yang, H. Cui, W. Tang, Z. Li, N. Han, F. Xing, A critical review on research progress of graphene/cement based composites, Compos. Part A Appl. Sci. Manuf. 102 (2017) 273–296.
[31] ASTM-C1437, Standard, Test Method for Flow of Hydraulic Cement Mortar 2015 ASTM Standard
[32] ASTM-C109, C109M-07, Standard, test method for compressive strength of hydraulic cement mortars ASTM International: USA 2008, 2008.
[33] ASTM-C307-03, Standard, Test Method for Tensile Strength of Chemical-Resistant Mortar, Grouts, and Monolithic Surfacings Monolithic Surfacings, ASTM International 2012.
[34] N. Kothiyal, S. Sharma, S. Mahajan, S. Sethi, Characterization of reactive graphene oxide synthesized from ball–milled graphite: its enhanced reinforcing effects on cement nanocomposites, J. Adhes. Sci. Technol. 30 (9) (2016) 915–933.
[35] H. Du, S. Dai Pang, Dispersion and stability of graphene nanoplatelet in water and its influence on cement composites, Constr. Build. Mater. 167 (2018) 403–413.
[36] M. Wang, R. Wang, H. Yao, Z. Wang, S. Zheng, Adsorption characteristics of graphene oxide nanosheets on cement, RSC Adv. 6 (68) (2016) 63365–63372.
[37] Z. Lu, D. Hou, L. Meng, G. Sun, C. Lu, Z. Li, Mechanism of cement paste reinforced by graphene oxide/carbon nanotubes composites with enhanced mechanical properties, RSC Aadv. 5 (122) (2015) 100598–100605.
[38] D. Hou, Z. Lu, X. Li, H. Ma, Z. Li, Reactive molecular dynamics and experimental study of graphene-cement composites: structure, dynamics and reinforcement mechanisms, Carbon 115 (2017) 188–208.
[39] S.J. Chen, C.Y. Li, Q. Wang, W.H. Duan, Reinforcing mechanism of graphene at atomic level: friction, crack surface adhesion and 2D geometry, Carbon 114 (2017) 557–565.
[40] C. Lu, Z. Lu, Z. Li, C.K. Leung, Effect of graphene oxide on the mechanical behavior of strain hardening cementitious composites, Constr. Build. Mater. 120 (2016) 457–464.
[41] B. Code, ACI 318-11 Building Code Requirements for Structural Concrete and Commentary, American Concrete Institute, Retrieved 8, 2012.
[42] B. Bahoria, D. Parbat, P. Nagarnaik, XRD analysis of natural sand, quarry dust, waste plastic (ldpe) to be used as a fine aggregate in concrete, Mater. Today Proc. 5 (1) (2018) 1432–1438.
[43] M. Zainuri, Synthesis of SiO2 nanopowders containing quartz and cristobalite phases from silica sands, Mater. Sci. Poland 33 (1) (2015) 47–55.
[44] J. Elena, M.D. Lucia, X-RAY Diffraction Study of hydration Processes in the Portland Cement, JAESVol 1 14.
[45] R. Jadhav, N. Debnath, Computation of X-ray powder diffractograms of cement components and its application to phase analysis and hydration performance of OPC cement, Bull. Mater. Sci. 34 (5) (2011) 1137–1150.
[46] S. Sharma, N. Kothiyal, Comparative effects of pristine and ball-milled graphene oxide on physico-chemical characteristics of cement mortar nanocomposites, Constr. Build. Mater. 115 (2016) 256–268.
[47] L. Zhao, X. Guo, C. Ge, Q. Li, L. Guo, X. Shu, J. Liu, Investigation of the effectiveness of PC@ GO on the reinforcement for cement composites, Constr. Build. Mater. 113 (2016) 470–478.
[48] L. Zhao, X. Guo, Y. Liu, C. Ge, L. Guo, X. Shu, J. Liu, Synergistic effects of silica nanoparticles/polycarboxylate superplasticizer modified graphene oxide on mechanical behavior and hydration process of cement composites, RSC Adv. 7 (27) (2017) 16688–16702.
[49] F.G.S. Silva, R.A.F. Junior, J.S. da Silva, K.W. Pinto, H.M.C. Andrade, J. Dweck, J.P. Gonçalves, Hydration of the equilibrium catalyst (Ecat) calcium hydroxide system, J. Therm. Anal. Calorim. 120 (2) (2015) 1089–1098.
[50] V.S. Ramachandran, J.J. Beaudoin, Handbook of Analytical Techniques in Concrete Science and Technology: Principles, Techniques and Applications, Elsevier, 2000.
[51] P. Mounanga, A. Khelidj, A. Loukili, V. Baroghel-Bouny, Predicting Ca (OH) 2 content and chemical shrinkage of hydrating cement pastes using analytical approach, Cem. Concr. Res. 34 (2) (2004) 255–265.
[52] W. Wongkeo, P. Thongsanitgarn, P. Chindaprasirt, A. Chaipanich, Thermogravimetry of ternary cement blends, J. Therm. Anal. Calorim. 113 (3) (2013) 1079–1090.
[53] J. Hlavay, K. Jonas, S. Elek, J. Inczedy, Characterization of the particle size and the crystallinity of certain minerals by ir spectrophotometry and other instrumental methods: II, Investigations on quartz and feldspar, Clays Clay Miner. 26 (2) (1978) 139–143.
[54] G. Anbalagan, A. Prabakaran, S. Gunasekaran, Spectroscopic characterization of Indian standard sand, J. Appl. Spectrosc. 77 (1) (2010) 86–94.
[55] M. Horgnies, J. Chen, C. Bouillon, Overview about the use of Fourier transform infrared spectroscopy to study cementitious materials, WIT Trans. Eng. Sci 77 (2013) 251–262.
[56] L. Fernández Carrasco, D. Torrens Martín, L. Morales, S. Martínez Ramírez, Infrared spectroscopy in the analysis of building and construction materials, InTech 2012.
[57] P.A. Bhat, N. Debnath, Theoretical and experimental study of structures and properties of cement paste: the nanostructural aspects of C-S-H, J. Phys. Chem. Solids 72 (8) (2011) 920–933.
[58] A. Gholampour, M. Valizadeh Kiamahalleh, D.N. Tran, T. Ozbakkaloglu, D. Losic, From graphene oxide to reduced graphene oxide: impact on the physiochemical and mechanical properties of graphene-cement composites, ACS Appl. Mater. Interfaces 9 (49) (2017) 43275–43286.
[59] R. Gao, N. Hu, Z. Yang, Q. Zhu, J. Chai, Y. Su, L. Zhang, Y. Zhang, like graphene-Ag composite films with enhanced mechanical and electrical properties, Nanoscale Res. Lett. 8 (1) (2013) 32.
[60] P. Yu, R.J. Kirkpatrick, B. Poe, P.F. McMillan, X. Cong, Structure of calcium silicate hydrate (C-S-H): near-, mid-, and far-infrared spectroscopy, J. Am. Ceram. Soc. 82 (3) (1999) 742–748.

Appendix 2: Journal paper 2 (Published)

Construction and Building Materials 264 (2020) 120188

Contents lists available at ScienceDirect

Construction and Building Materials

journal homepage: www.elsevier.com/locate/conbuildmat

Influence of pristine graphene particle sizes on physicochemical, microstructural and mechanical properties of Portland cement mortars

Van Dac Ho [a,b,c], Ching-Tai Ng [a], Togay Ozbakkaloglu [d], Andy Goodwin [e], Craig McGuckin [e], Ramesh U. Karunagaran [b,c], Dusan Losic [b,c,*]

[a] School of Civil, Environmental and Mining Engineering, The University of Adelaide, South Australia 5005, Australia
[b] School of Chemical Engineering, The University of Adelaide, South Australia 5005 Australia
[c] ARC Research Hub for Graphene Enabled Industry Transformation, The University of Adelaide, South Australia 5005 Australia
[d] Ingram School of Engineering, Texas State University, United States
[e] First Graphene Ltd, Suite 3, 9 Hampden Road, Nedlands WA 6009, Australia

HIGHLIGHTS

- Pristine graphene (PGR) enhances compressive and tensile strengths of cement mortars.
- Mechanical strengths of cement mortars strongly depend on the sizes of PRG.
- Larger size PRG improves the compactness of microstructures of cement mortars.
- Ultra-large sizes of PRG show the significant influence on mechanical strengths.

ARTICLE INFO

Article history:
Received 7 April 2020
Received in revised form 1 July 2020
Accepted 7 July 2020

Keywords:
Pristine graphene
Cement mortar
Mechanical properties
Acceleration
Microstructure

ABSTRACT

This paper aims to study the effect of the size of pristine graphene (PRG) particles on the compressive and tensile strengths of cement-based mortars and to gain better understandings of the mechanism behind the enhancement of these properties. PRG industrially manufactured by the electrochemical process with a variety of particle sizes including 5 μm, 43 μm, 56 μm, and 73 μm was used at the optimal dosage of 0.07% by weight of cement binder. The results indicate that mechanical strengths of cement mortars at 7 and 28 days considerably depend on the size of PRG. The mixes with size 56 μm and 73 μm show significant influence on both compressive and tensile strengths of cement mortars, which increase approximately 34.3% and 30.1% at 28-day compressive strengths, and 26.9% and 38.6% at 28-day tensile strengths, respectively. On the other hand, the mix with size 43 μm of PRG addition exhibits a significant increase only in tensile strength, and there are no significant effects on either compressive strengths or tensile strengths of the mix containing 5 μm particles. The observed enhancement in the mechanical properties of cement mortars by large PRG sizes is attributed to the improvement of cement hydration level, the reduction of cement particles' distance in cement gels because of the effect of van der Waals forces between PRG sheets, and the mechanical adhesion forces between PRG sheets and cement gels. The results from this study indicate that PRG is not only a promising additive in practical application for building materials to improve the current drawbacks of cement composites, but also a feasible option to support the reduction of cement mass used in cement composites, which could reduce the CO_2 footprint and amount of CO_2 emission into the atmosphere.

1. Introduction

The most commonly used materials in the construction industry are cementitious composites. Although they are strong in compressive strength, they are weak in tensile and corrosive properties [1]. Researchers have proposed different approaches and additives to improve their properties such as using plastic, carbon fibers [2,3], nanoparticles [4], carbon nanofibers and nanotubes [5,6]. However, these additives were unable to effectively improve properties of cementitious composites due to limitations in bonding and arresting microcracks [5–7]. Moreover, the core component of cementitious composites, which is Portland cement,

* Corresponding author at: School of Chemical Engineering, The University of Adelaide, South Australia 5005 Australia.
E-mail address: dusan.losic@adelaide.edu.au (D. Losic).

https://doi.org/10.1016/j.conbuildmat.2020.120188
0950-0618/

is also one of the factors contributing to a major amount of carbon dioxide (CO_2) into the atmosphere that causes greenhouse gases. Global Portland cement production is estimated at 4 billion tons per year which the largest man-made material in the world [8–10]. It was reported that one ton of Portland cement production could release about one ton of carbon dioxide [11,12], which accounts for about 7% of CO_2 release globally [8,9,11,13]. Therefore, developing approaches and new additives to improve the properties of cement composites and reduce the amount of cement consumption in order to decrease CO_2 emission have attracted significant research interests. Improving only 1–2% in the reduction of CO_2 release by enhancing properties of cement composites could make a significant contribution to climate change.

To address these problems, several measures were explored by researchers such as improving cement plant production efficiency or using supplementary materials [4,14,15]. There have been intense studies in using supplementary materials to enhance properties of cement composites and reduce the mass of cement consumption with many publications in recent decades, including using fly ash, ground granulated blast furnace slag, nanoparticles or graphene materials [4,16–20]. Among them, graphene and its derivatives (i.e. graphene oxide (GO), reduced graphene oxide (rGO) and pristine graphene (PRG), as two-dimensional materials, have shown the great potential for improving properties of cementitious materials owing to their outstanding properties of high mechanical and conductivity properties, large specific surface areas and aspect ratios [16,18,21,22]. These studies showed graphene additives could significantly enhance key properties of cement composites such as compressive and tensile strengths, chloride penetration, and electrical conductivity [16,18]. It is important to note that there are significant differences in structural, chemical, mechanical and electrical properties of these graphene materials. While the properties of GO materials, produced from oxidized graphite are well known, the difference between graphene nanoplatelets produced from rGO and PRG materials has not been well described in research papers because both are termed as graphene nanoplatelets or flakes. PRG made by an electrochemical process from graphite materials preserves its original pristine structure. Thus, it has different properties compared with graphene nanoplatelets from rGO sheets that are also produced from graphite materials by different methods using harsh acids and oxidants to make GO which is reduced to rGO by followed a thermal or chemical process. The result are a significant level of defects and less crystallinity in the properties of graphene (rGO) nanoplatelets.

For GO studies, Li et al. [23] showed that incorporating of 0.04% GO into cement paste produced a 14% improvement in its compressive strength at 28 days, and there was no positive effect on its compressive strengths when the incorporation of GO below 0.03%. Another study performed by Wang et al. [24] reported that cement paste and cement mortar with 0.05% GO additive showed the highest enhancement rates in their compressive and flexural strengths, which could increase by 40.4% & 90.5% and 24.4% & 70.5% in compressive & flexural strengths of cement paste and cement mortar at 28 days, respectively. Although a significant process has been made in studying the effects of GO additives on properties of cement composites, the mechanism between GO and cement composites in the strength improvement has not been studied in-depth [18]. Few studies have recently explored the influence of oxygen functional groups from GO on the mechanism of the intermolecular interaction between GO sheets and the cementitious matrix, resulting in the improvement in the properties of cement composites [16,25,26]. Besides, the effects of different GO dosages and sizes on microstructures of cement mortars were also revealed in the study performed by Sharma and Kothiyal [27]. They showed that the mix with a smaller GO size (i.e. 100 nm) improved compressive strength by 86% at 1% GO concentration. This improvement was more than that of using the larger GO size (i.e. 900 nm) at the same dosage, which was improved by 63% only. This enhancement was explained by the effects of a larger level of oxygen-functional groups (e.g. carboxyl, hydroxyl) of GO with the smaller size compared to those with the larger size, resulting in stronger chemical adhesion forces between them and cement gels in the cement matrix [16,28].

In the case of PRG additives, recent studies on a combination of PRG and cement composites have shown great potential in strength improvement in PRG-cement composites [16,18]. These studies were mainly focused on the effects of dosages with limited numbers of studies revealing the influence of other parameters such as the sizes, number of layers, functional groups and the mechanism of the strength improvement of cement composites. In the study performed by Wang et al. [29], which only compared compressive strengths of cement mortars between the control and the mix with 0.05% PRG, compressive and flexural strengths at 7 days of the mortar with 0.05% PRG was respectively improved by 8% and 24%. Another study with four different PRG concentrations (i.e. 0%, 2.5%, 5.0%, and 7.5%) performed by Du and Dai Pang [30] showed that the incorporation of PRG into cement mortars could considerably decrease water penetration depth whereas there were insignificant effects of PRG on compressive and flexural strengths of cement mortars, which was due to the agglomeration of PRG coming from the high PRG dosages rate used. In 2019, Tao et al. [31] combined cement mortars with five different PRG dosages (i.e. 0%, 0.05%, 0.1%, 0.5%, and 1%) and revealed that 0.05% PRG additive was the optimal dosage and could respectively improve compressive and flexural strengths of the mortar at 28 days by 8.3% and 15.6%, however, the strengths started decreasing when PRG dosages over 0.05% owing to the agglomeration of PRG.

Even though these studies show a strong dependence of the properties of cement composites on PRG dosages, the mechanisms of this dosage dependence have not been clearly explained. Additionally, unlike GO, rGO and PRG sheets (PRGs) have very few oxygen-functional groups that indicate a different mechanism to enhance the cement matrix, which is likely based on friction adhesion forces between PRGs and cementitious gels [32]. Also, all the studies on PRG-cement composites from the literature have used PRGs with the average size varying from 5 μm to 25 μm [16,18,29,31], with no study has been exploring how an ultra-large size influences on strength improvement in PRG-cement composites, and revealing its enhancement mechanism. Our previous study [32] was the first study investigating the effects of dosages using the ultra-large PRG size (56um) on mechanical, microstructural and physicochemical properties of cement-based mortars. The study showed that at the optimal concentration (0.07% PRG), compressive and tensile strengths at 28 days of the mortar mix with PRG size 56um could enhance 34.3% and 26.9%, respectively. The study also revealed that the strengthening mechanism of cement mortars with the ultra-large PRG size was mostly due to friction adhesion forces between PRGs and cementitious gels. Compared with GO materials that have high levels of defects, high costs and environmental impact in production, and weaker mechanical properties [33,34], PRG materials have low levels of defects, stronger crystalline and mechanical properties and can be produced by an environmentally sustainable process in high quality at industrial scales with much lower costs. Therefore, PRG materials are expected to be more acceptable to be applied for building and infrastructure materials. This is a strong motivation to have more studies on the effects of other parameters of PRGs on properties of cementitious composites.

Table 1
Physical properties of different PRG sizes supplied by First Graphene Ltd.

ID	Particle	Thickness	Purity	Poured bulk density
	Size-d50 (μm)	(nm)	(%)	(g/cm3)
Size 5 μm	5	1–3	~98	~ 0.11
Size 43 μm	43	1–3	~98	~ 0.13
Size 56 μm	56	1–3	~98	~ 0.12
Size 73 μm	73	1–3	~98	~ 0.12

To address the above-mentioned research gaps, this study aims to explore the effects of different PRG sizes, which was industrially manufactured by an electrochemical process, on compressive and tensile strengths of cement mortars. The objectives of the study not only consider a range of PRG sizes including 5 μm, 43 μm, 56 μm, and 73 μm on these properties, but also evaluate their effects on physicochemical and microstructural properties of the mortars. The outcomes of this study will provide better understandings of the strengthening mechanism of compressive and tensile strengths of cement mortars, which is still lacking in the case of research of PRG-cement composites. The results of this study will contribute to future studies on using PRGs as additives in cement composites to enhance the performance of construction materials. The reduced mass of Portland cement in the binder of cement composites as a result of strength improvements due to the addition of PRGs will result in a reduction of the environmental impact of Portland cement products thanks to reduced CO_2 emission.

2. Experimental programs

2.1. Materials

The physical properties of four different PRG sizes provided by First Graphene Ltd in Perth, WA, Australia are shown in Table 1. From the table, it is important to note that although they are different in sizes, the other properties are similar. General purpose cement provided by Adelaide Brighton Cement LTD and complied with Australian Standard AS 3972–2010 [35] was used as the binder of mortar mixes and its typical chemical properties are shown in Table 2. Natural sand with 2.36-mm maximum particle sizes was used as fine-aggregate of mortar mixes. MasterGlenium SKY 8100 complied with Australian Standard AS 1478.1–2000 [36] was used as the superplasticizer to improve the dispersion of PRGs in water.

Table 2
Typical chemical properties of general purpose cement.

Compounds	OPC (%)
CaO	63.28
SiO_2	19.95
Al_2O_3	4.79
Fe_2O_3	3.14
MgO	2.03
Na_2O	0.29
K_2O	0.4
SO_3	2.69
P_2O_5	0.04

2.2. Specimens

In this study, we designed the mixes with different PRG sizes at the optimal dosage (0.07% PRG), which is based on our previous study [32] on the effects of PRG concentrations on mechanical properties of cement mortars, to investigate the effects of different PRG sizes on mechanical, physicochemical, and microstructural properties of cement mortars. The details of the designed mixes of cementitious composites are shown in Table 3. As shown in the table, the four different PRG sizes considered in this study are a small size 5 μm, a large size 46 μm, and two ultra-large sizes 56 μm and 73 μm. Prior to the mixing of the mortars, the aqueous solutions including water, superplasticizer and PRG were sonicated for 30 min by using Ultrasonication UIP1000hdT. Then, these solutions were gradually added for 5 min to natural sand and binder, which were mixed for four minutes. All samples were vibrated for one minute after mounting to mitigate entrapped air during the mounting process. After that, they were covered with wet fabrics and plastic sheets to prevent moisture loss and were demounted after 24 h cured at room temperature. After that, all the samples continued to be cured in a fog room until testing days.

2.3. Test methods

Compressive and tensile strengths were tested at 7 and 28 days to investigate the influence of different PRG sizes on cement mortars. For compression, 50 × 50 × 50 mm^3 cubes complied with ASTM C109/C109M-07 [37] were used. Dog-bone shaped samples, according to ASTM C307-03 [38], were used for tensile tests. The values of each designed mix at testing days were calculated by averaging values obtained from three nominal identical samples of each mix. Scanning electron microscopy (SEM) were obtained by using the FEI Quanta 450 to analyze PRG sizes and surface morphologies of the mortars. X-ray diffraction (XRD) was performed by using the Rigaku MiniFlex 600 X-Ray diffractometer to find the mineralogical characteristics of cement hydration products of the mortars and PRGs. Fourier transform infrared spectroscopy (FTIR)

Table 3
Designed mixes of cementitious composites.

Mix	Pristine Graphene (%)*	Graphene size (μm)	Cement(kg/m3)	Water (kg/m3)	Pristine Graphene (kg/m3)	Sand (kg/m3)	Superplasticizer (kg/m3)
Control			527	255.6	0.000	1448	1.4
Size 5 μm	0.07	5	527	255.6	0.369	1448	1.4
Size 43 μm	0.07	43	527	255.6	0.369	1448	1.4
Size 56 μm	0.07	56	527	255.6	0.369	1448	1.4
Size 73 μm	0.07	73	527	255.6	0.369	1448	1.4

* The percentage of pristine graphene based on weight of cement binder.

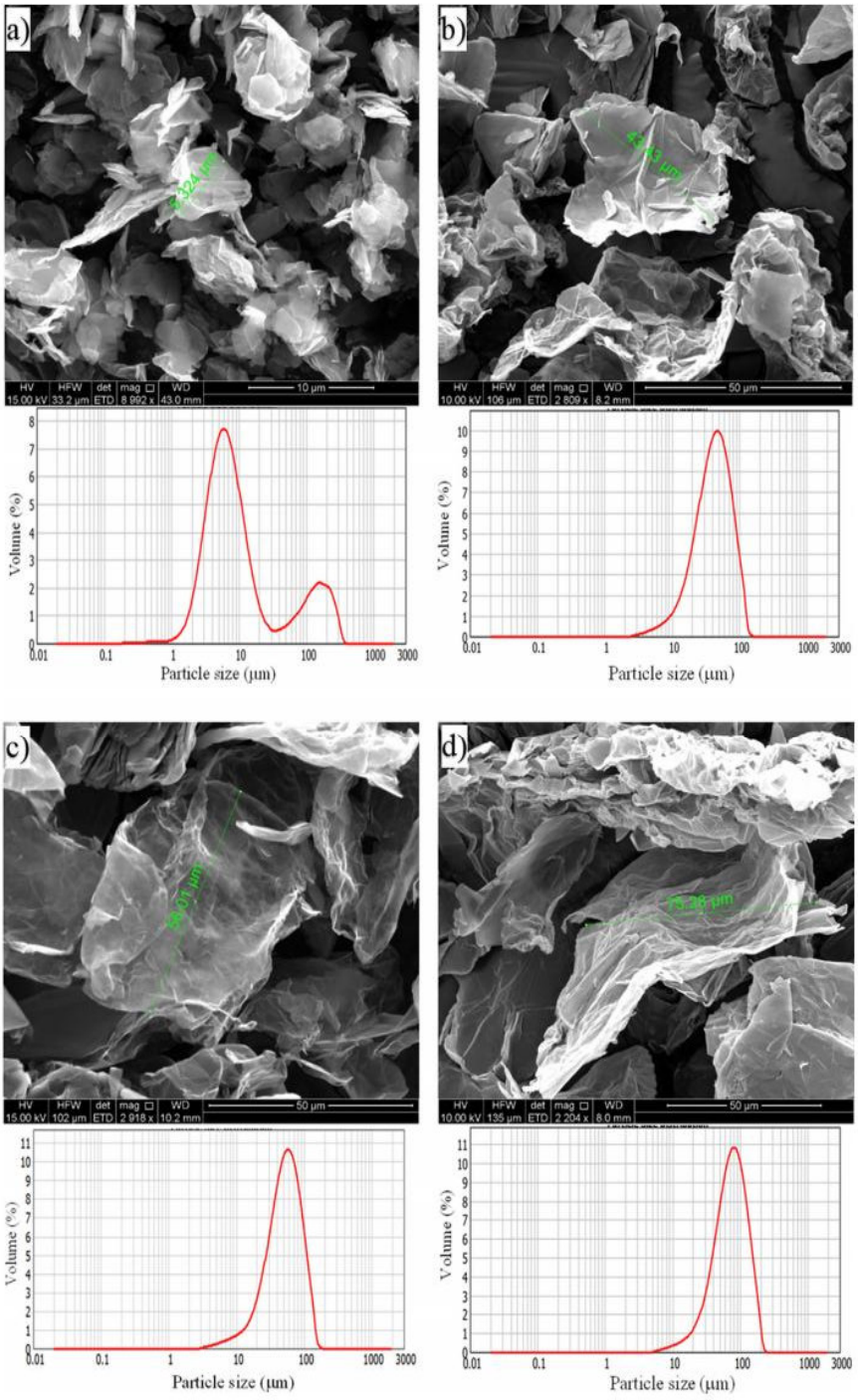

Fig. 1. SEM images and particle size distribution of PRG: (a) size 5 μm, (b) size 43 μm, (c) size 56 μm, (d) size 73 μm.

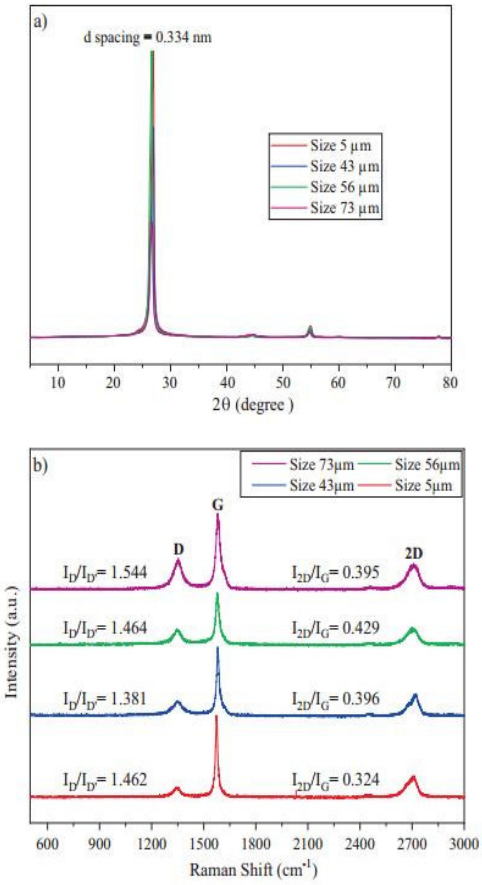

Fig. 2. (a) XRD patterns and (b) Raman spectra of different PRG sizes.

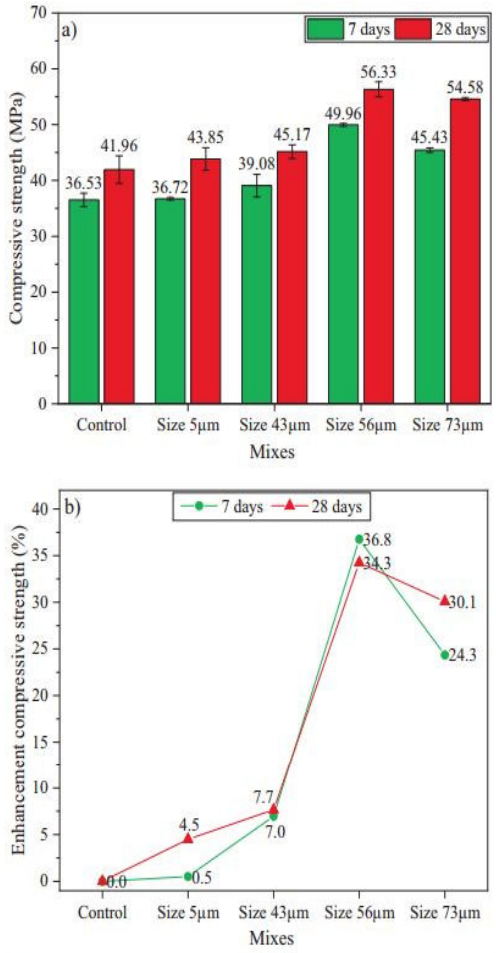

Fig. 3. (a) Compressive strength and (b) enhancement compressive strength at 7 and 28 days of different PRG sizes.

was conducted using the Nicolet 6700 to determine specific functional groups of PRG-cement based mortars. Raman spectra and particle size distribution (PSD) were respectively performed by using the HORIBA LabRAM HR Evolution and Mastersizer 2000 - Malvern to test the number of layers and particle sizes of PRGs. Analysis of variance (ANOVA) method was also used to evaluate how significant effects of different PRG sizes on compressive and tensile strengths of PRG-cement based mortars.

3. Results and discussion

3.1. Characteristics of PRGs

Fig. 1 shows typical SEM images and related PSD graphs of four PRG samples used for this study. As shown in the figure, their average particle sizes determined from SEM and PSD data are 5 ± 2 µm (Fig. 1(a)), 43 ± 8 µm (Fig. 1(b)), 56 ± 12 µm (Fig. 1(c)) and 73 ± 13 µm (Fig. 1(d)), and the PRG structures show wrinkled and irregular shapes with few layer thicknesses. Their XRD patterns presented in Fig. 2(a) show the typical peaks of these PRGs at the position 26.64°, resulting in their d-spacing between layers is 0.334 nm that can contribute to a few layers of PRGs [28,39]. Fig. 2(b) shows the Raman spectra of different PRG sizes. As shown in the figure, the relative intensity ratios of $I_D/I_{D'}$ and I_{2D}/I_G of all the PRG samples are respectively below 3.5 and 1. These mean that these PRG samples don't have basal plane defects [40] and contain mostly several layers (from four layers) [41], showing the high quality of PRGs used in this study and being consistent with their average thickness and other properties provided by the provider.

3.2. Mechanical properties of PRG-cement based mortars

Compressive strengths and their enhancement rates at 7 and 28 days of the mortars with different PRG sizes are shown in Fig. 3. As shown in Fig. 3(a) and (b), the addition of PRGs has a positive effect on compressive strengths of the mortars at 7 and 28 days regardless of PRG sizes. The mix with size 56 µm shows the highest compressive strength at 7 days and 28 days (49.96 MPa and 56.33 MPa respectively), which increase approximately 36.8% and 34.3%, respectively, in comparison with the control mix that is 36.53 MPa and 41.96 MPa. A similar trend is observed in size 73 µm, which rises approximately 24.3% and 30.1% at 7 days and 28 days, respectively. However, the mixes with size 5 µm and 43 µm present low enhancement rates in compressive strengths of cement based mortars at both testing days, which are respectively approximately 0.5% and 4.5% for size 5 µm, and 7% and 7.7% for size 43 µm. Therefore, it is concluded that the ultra-

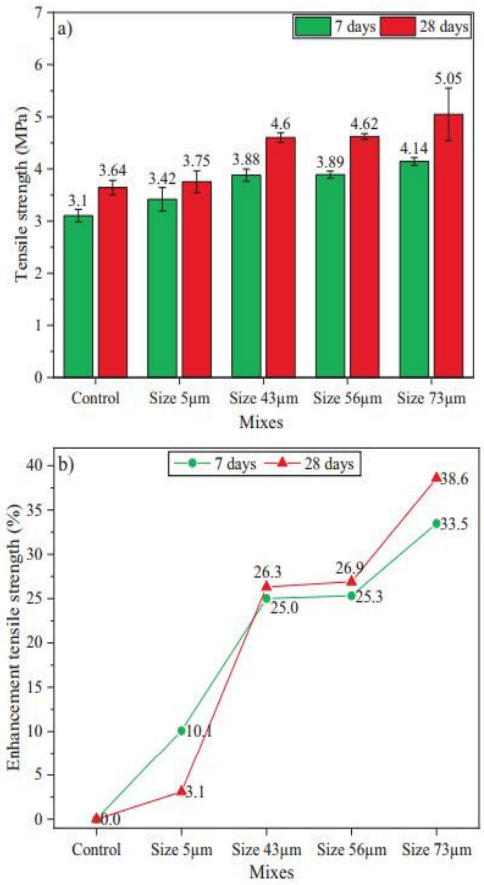

Fig. 4. (a) Tensile strength and (b) enhancement tensile strength at 7 and 28 days of different PRG sizes.

large sizes (56 μm and 73 μm) have a stronger influence on compressive strengths of cementitious composites than those of the small size and large size (5 μm and 43 μm), which will be discussed in Section 3.3.

Fig. 4 presents tensile strengths and their enhancement rates at 7 days and 28 days of the mortars with different PRG sizes. Fig. 4 (a), (b) shows that tensile strengths of the PRG-cement mortars of different PRG sizes at both testing days increase with the addition of PRG, and their enhancement strength rates depend on the sizes of PRGs. The size 73 μm mix shows the highest values in direct tensile strengths at 7 days (4.14 MPa) and 28 days (5.05 MPa), which enhance approximately 33.5% and 38.6%, respectively, compared to the control mix (3.1 MPa at 7 days and 3.67 MPa at 28 days). The size 43 μm and 56 μm mixes show similar enhancement rates in tensile strengths of the mortar mixes at 7 and 28 days, which respectively increase approximately 25% and 26.3% for size 43 μm, and 25.3% and 26.9% for size 56 μm. In contrast, the mix with size 5 μm presents the lowest enhancement in tensile strengths at both testing days, which are approximately 10.1% at 7 days and 3.1% at 28 days. In summary, it is evident from the results that the large size (43 μm) and ultra-large sizes (56 μm and 73 μm) shows significant enhancement on tensile strengths of the cement mortars whereas the small size (5 μm) presents less enhancement on tensile strengths of cementitious composites, which will be further discussed in Section 3.3.

3.3. Physicochemical, microstructural and ANOVA analyses of PRG-cement mortars with different sizes of PRGs

3.3.1. XRD, FTIR and SEM characterizations

The XRD patterns of the mortars with different sizes of PRGs at 28 days are shown in Fig. 5(a). It is important to note that these XRD spectra were standardized to the equal intensity at the major peak of natural sand of 26.7° for making the equal percentage of existing sand in all the samples [32,42]. Also, only main crystalline phases that relate to the cement hydration process were marked in XRD patterns to avoid a distraction from the analysis (most of the remaining peaks, such as 21.2°, 36.7°, or 77.9°, indicate crystalline phases of quartz [32]). As shown in Fig. 5(a), all the samples have similar spectrum patterns, showing similar main crystalline phases confirmed including cement hydration products (i.e. Portlandite and Ettringite) and un-hydrated cement (i.e. Alite). This means the addition of PRGs into cementitious composites does not create any new crystalline phases in the cement matrix. Moreover, the main cement hydration product in cementitious composites is calcium silicate hydrate (CSH) gels could not recognize in these spectra because CSH gels often exist at amorphous phases in a cement matrix and it is thus hard to identify with XRD test [29,43]. However, CSH contents can be inferred from the contents of portlandite and alite phases [32,42]. It can also be seen from the figure that the portlandite phases in the mixes with size 43 μm, 56 μm and 73 μm show higher intensities than the others. This observation, together with the fewer contents of alite in these mixes (size 43 μm, 56 μm and 73 μm) compared with those in the other mixes (control and size 5 μm), can result in higher degrees of the hydration of cement pastes in these mixes than the control and size 5 μm mixes [32,42]. This could account for the better enhancement in compressive and tensile strengths of the large size and ultra-large sizes than the others due to higher CSH gels created, as discussed above in Section 3.2. Moreover, it can also be seen in Fig. 5(a) that although the mix with size 5 μm has the higher peak intensity of un-hydrated alite phases than the control, it still has a higher peak intensity of portlandite than the control. This could be because the mix with size 5 μm had a higher amount of belite hydrated in the cement hydration process than the control (i.e. (alite, belite) + H_2O → portlandite + CSH [28,32]), contributing to a higher peak intensity of portlandite of this mix at the short-term mechanical strengths.

Fig. 5(b) shows the FTIR patterns of the mixes with different PRG sizes at 28 days. As shown in the figure, all the samples have similar spectra with some functional groups determined in the range of the band from 400 cm^{-1} to 4000 cm^{-1}, showing that there are no new distinguishing groups observed in all the samples, which are consistent with the results of XRD discussed above and the previous research [44]. From the figure, some functional groups are observed in these samples including Si-O bonds in CSH gels, which are in the ranges of 400–550 cm^{-1} and 800–1200 cm^{-1} [45,46], and O–H bond in CSH gels and portlandite, which are in the range of 2800–3600 cm^{-1} [46,47] and 3600–3650 cm^{-1} [45,48]. C-O bond in $(CO_3)^{2-}$ groups are observed in a range of 1350–1550 cm^{-1} [46,47], which indicates the appearance of $CaCO_3$ in these samples due to the chemical reaction between cement products and carbon dioxide during the curing and testing period. These $CaCO_3$ structures can also be observed as growing on the surface of portlandite and CSH crystals as flower-like shapes structures presented in Fig. 6(j) [32,49,50]). Although all the spectra show the same functional groups, it is evident from the figure that the intensities of functional groups belonging to CSH gels in the mixes with PRGs are higher than the control. This could be attributed to higher hydration degrees of cement binder in the mortars with PRGs additive, resulting in the improvement in

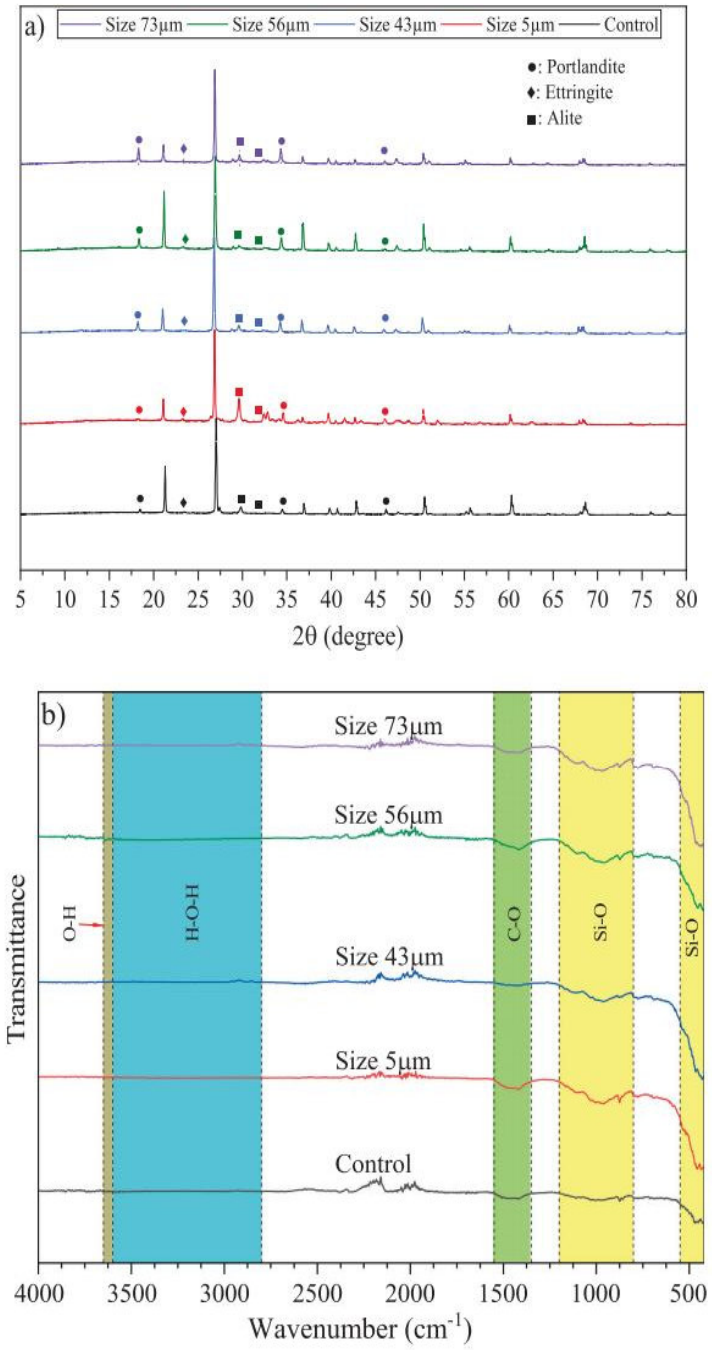

Fig. 5. (a) XRD and (b) FTIR of PRG-cement mortars with different PRG sizes at 28 days.

compressive and tensile strengths of these mixes as discussed above in Section 3.2.

SEM images of microstructures of the mortars with different sizes of PRGs at 28 days are shown in Fig. 6. It is evident from the figure that although these samples show similar components in their SEM images, they are different from how these components are distributed and compacted. In particular, the control mix and size 5 μm mix not only show less compact in the microstructure, which is large sizes in microcracks and less dense in the interfacial transition zones (ITZ) (Fig. 6(a) and (c)), but also present smaller sizes of crystal components and larger contents of pores distributed in the cement matrix (Fig. 6(b) and (d)) than

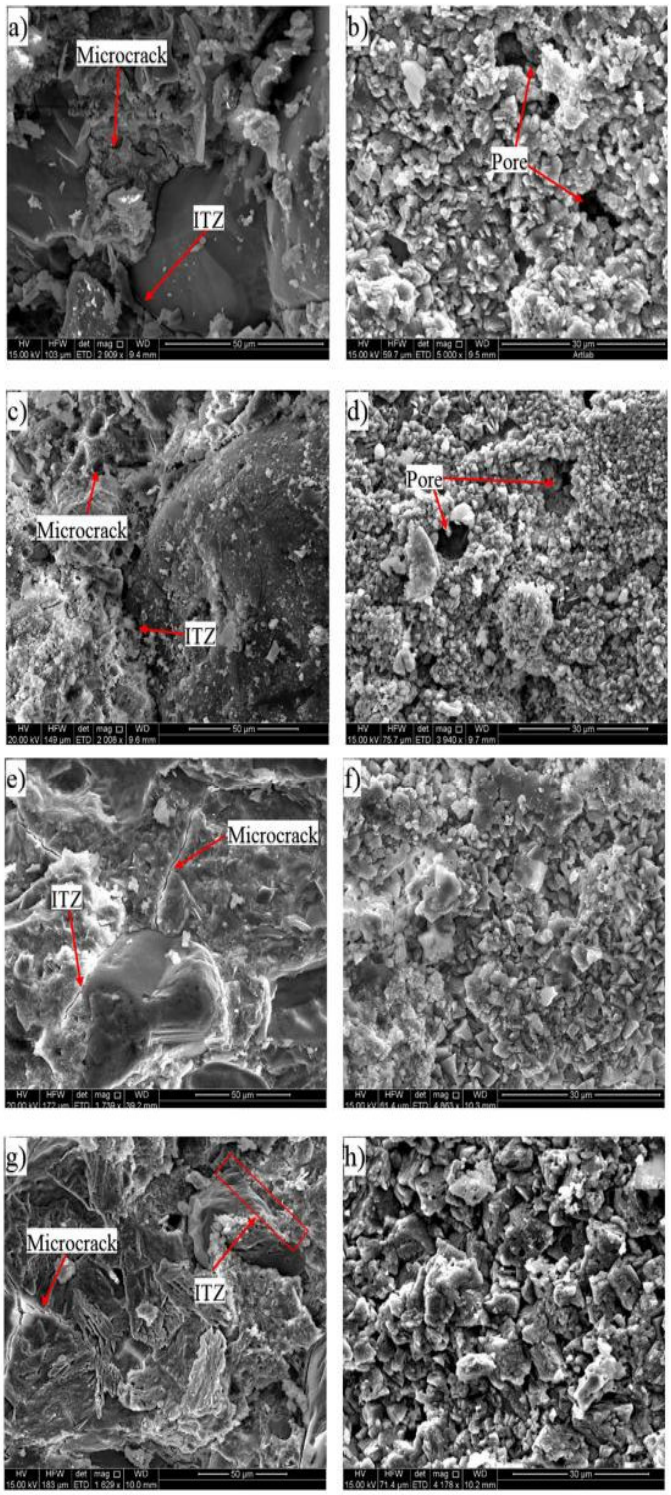

Fig. 6. SEM images of PRG-cement mortars with different PRG sizes at 28 days: (a, b) control, (c, d) size 5 μm, (e, f) size 43 μm, (g, h) size 56 μm, (i, j) size 73 μm.

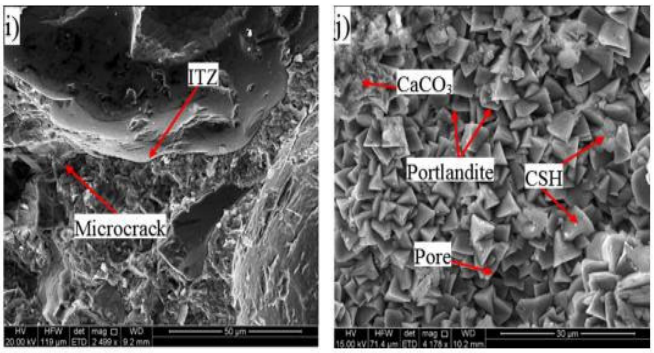

Fig. 6 (*continued*)

the others (Fig. 6(e)-(j)). It can also be seen from the figure that the mixes with size 56 μm (Fig. 6(g), (h)) and 73 μm (Fig. 6(i), (j)) show the most compact in the cement matrix of the mortars with typical components, followed by the size 43 μm mix (Fig. 6(e), (f)). This is attributed to the higher cement hydration degree and a stronger connection between PRGs and cement gels in the cement matrix of these mixes than the others, resulting in their stronger enhancement rates in compression and tension [29,32,51] as discussed in Section 3.2.

From the above observations and analyses, it can be concluded that physicochemical, microstructural and mechanical properties of cement-based mortars are strongly dependent on the sizes of PRGs additives. The benefits of PRG additives in the cement matrix could come from the combination of the following reasons: (1) a part of the enhancement in the cement hydration process due to the better spreading water of PRGs in a cement matrix, and the reduction of distances between cement particles in cement gels because of the effect of van der Waals forces between PRGs [18,32,51]; (2) most of the mechanical adhesion forces created from the friction forces between surfaces of PRGs and cement gels [32], suggesting that PRGs with larger sizes will have stronger friction adhesion forces due to having larger surface areas to connect with cement gels (e.g. 5 μm × 5 μm (25 μm^2), 73 μm × 73 μm (5329 μm^2)), resulting in their better enhancement rates in mechanical strengths of cement composites as discussed in Section 3.2. This type of friction forces between PRGs and cement gels was also identified by previous research in simulation studies using molecular dynamics simulation methods [52,53]. Therefore, PRGs can reinforce cement gels in cementitious composites, integrating PRGs into cement gels to create PRG-cementitious gels in the cement matrix, resulting in the improvement of microstructures of the PRG-cement mortars and contributing to a better capacity in stress-distribution and propagation of cracks of these PRG-cement mixes.

3.3.2. ANOVA analysis to evaluate the benefit of different sizes of PRGs on compressive and tensile strengths of cement mortars

The ANOVA analysis by applying the Dunnett method is used to determine whether the enhancement of different sizes of PRGs on compressive and tensile strengths of cement mortars is statistically significant or not. This analysis method is based on the null hypothesis theory with a significant level of 0.05 to assess how significant differences between the mortar mixes, which is detailed in previous studies [54,55]. The results of the ANOVA analyses for compressive strengths at 7 days and 28 days of the different mixes are shown in Table 4. As can be seen from the table, only the ultra-large sizes mixes (size 56 μm and 73 μm) are significant improvements in compressive strengths at both testing days compared to the others (their P-values < 0.05). Moreover, while the size 56 μm mix shows the most benefit at the 7 days test because it shows significant difference even with the size 73 μm (i.e. P-value = 0.009), there is no significant difference between them at 28 days (i.e. P-value = 0.186).

Table 5 presents the results of the ANOVA tests at 7 days and 28 days for tensile strengths of the different mortars. It is evident from the table that the mixes with size 43 μm, 56 μm and 73 μm show significant benefit in tensile strengths at both testing days compared with the control. In addition, the size 73 μm mix presents the strongest effect at the age of 7 days compared to size 43 μm (i.e. P-value = 0.026) and size 56 μm (i.e. P-value = 0.03), whereas there are no significant differences between these PRG sizes on tensile strengths at 28-day.

In summary, it is evident from all the above analyses that compressive and tensile strengths of cement based mortars at 7 days and 28 days strongly depend on the sizes of PRG additives. While the small size (5 μm) does not show any significant influence on compressive and tensile strengths of the cement mortars at both testing days, the large size (43 μm) only shows a significant influence on tensile strengths at both testing days. In contrast, the

Table 4
Assessment of effects of different PRG sizes on compressive strengths of PRG-cement mortars at 7 days and 28 days using ANOVA tests.

Difference of levels	7-day compression			28-day compression		
	Difference of means	T-Value	Adjusted P-Value	Difference of means	T-Value	Adjusted P-Value
Size 5 μm - Control	0.19	0.21	0.998	1.89	1.41	0.464
Size 43 μm - Control	2.55	2.88	0.051	3.22	2.40	0.111
Size 56 μm - Control	13.43	15.21	0.000	14.37	10.72	0.000
Size 73 μm - Control	8.90	10.07	0.000	12.62	9.42	0.000
Size 56 μm - Size 43 μm	10.88	11.05	0.000	11.16	12.96	0.000
Size 73 μm - Size 43 μm	6.35	6.44	0.002	9.41	10.93	0.000
Size 73 μm - Size 56 μm	−4.53	−4.6	0.009	−1.75	−2.03	0.186

Table 5
Assessment of effects of different PRG sizes on tensile strengths of PRG-cement mortars at 7 days and 28 days using ANOVA tests.

Difference of levels	7-day tension			28-day tension		
	Difference of means	T-Value	Adjusted P-Value	Difference of means	T-Value	Adjusted P-Value
Size 5 μm - Control	0.31	2.88	0.051	0.11	0.54	0.949
Size 43 μm - Control	0.78	7.15	0.000	0.96	4.62	0.003
Size 56 μm - Control	0.79	7.24	0.000	0.98	4.72	0.003
Size 73 μm - Control	1.04	9.57	0.000	1.41	6.77	0.000
Size 56 μm - Size 43 μm	0.01	0.13	0.990	0.02	0.09	0.996
Size 73 μm - Size 43 μm	0.26	3.62	0.026	0.45	1.86	0.230
Size 73 μm - Size 56 μm	0.25	3.49	0.030	0.43	1.77	0.256

ultra-large sizes (56 μm and 73 μm) show a significant influence on both compression and tension at all the testing days. This confirms the strong benefit of the ultra-large sizes on the mechanical properties of cementitious composites.

3.3.3. Prediction the benefit of PRG additive to reduce the amount of Portland cement used in building materials

As mentioned in the Introduction Section, the use of Portland cement accounts for about 7% of CO_2 emission into the atmosphere globally, causing greenhouse gases. Thus, it is important to find methods to reduce the amount of cement used in building materials without impacting on requirements of their designed strengths. In this case, PRG appears as a promising additive for building materials to reduce the amount of Portland cement used globally. From the previous sections, it can be concluded that the addition of PRGs to cement mortars can enhance their mechanical strengths. The ultra-large sizes (56 μm and 73 μm) show the significant improvement in both compressive and tensile strengths at all the testing days.

As discussed in Section 3.2, the size 56 μm mix can enhance the 28-day compressive and tensile strengths of the mortar up to 56.33 MPa (↑34.3%) and 4.62 MPa (↑26.9%) compared to the control mix 41.96 MPa and 3.67 MPa, respectively. In practice, we often use the compressive strength at 28 days as the most important parameter to design for new constructions. As shown in Table 3, the mass of Portland cement in 1 m^3 of cement mortars for the current design mixes is 527 kg, and the compressive strength at 28 days of the control mix is 41.96 MPa. Based on compressive strengths of cement pastes and water/cement ratio of mortars, we can predict compressive strengths of cement mortars and one of the precise design-oriented models for predicting was proposed by Kargari et al. [56], which considers different formulas for different cement paste classes. In this study, we used the cement paste with 45 MPa at 28-day compressive strength. According to Kargari et al. [56], the formula used to predict compressive strengths of cement mortars with cement paste class 42.5 MPa is shown below:

$$f'_{c28} = 25.32(1/(W/C)-0.443) \quad (1)$$

where W/C means water and cement ratios. The water and cement ratio we used in this study is 0.485. According to the formula above, the compressive strength of the cement mortar is 40.1 MPa, which is only a 2.31% error compared to the experimental result (41.96 MPa). If we simply assume that the required compressive strength for designing building construction is 56.33 MPa. From Equation (1), the requirement of water and cement ratio for the cement mortar calculated is 0.375. Thus, the mass of Portland cement for the practical design mix with the above water and cement ratio (0.375) is 610 kg. This means if we use 369 g PRG size 56 μm as the additive for 1 m^3 cement mortar with 0.485 water/cement ratio, we can reduce about 83 kg (↓15.75%) Portland cement for the required compressive strength at 0.375 water/cement ratio. As reported in Refs. [8–10], it takes approximately 4 billion tons of cement production in the world yearly, and thus, PRG additive can support to reduce the mass of cement production down to 3.37 billion tons, which can decrease approximately 1.1% of the CO_2 emission caused by cement production every year. This will be a significant contribution to mitigate greenhouse gases, which accounts for the global warming gases and climate change. However, this contribution should consider that some impact on CO_2 and environmental footprint coming from the graphene manufacturing process. The production of pristine graphene powders used in this paper is industrially manufactured using the electrochemical process by First Graphene Ltd that has several advantages providing significantly lower footprints compared with other graphene materials (GO and rGO) using chemical oxidation/reduction-based manufacturing processes [57]. Firstly, this process utilizes the world's highest purity vein graphite with a carbon content greater than 98% of total graphitic carbon which is used directly without a further process that excludes extensive graphite processing footprint (gridding, flotation). Secondly, the electrochemically produced process of PRG from this graphite is a single-step process that is closed-loop, therefore, all electrolytes are recovered and reused. Due to the extremely high carbon content of the graphite used in the system, the kWh per each kilogram of produced PRG is extremely low with a very high conversion from graphite to graphene approaching 100% conversion. One of disadvanatges of PGR materials are their high hydrophobicity and their lower dispersions in water that can result in the non-uniform distribution in the cement matrix. The use of special dispersants or superplasticisers as we used in this work, is shown could address this problem, but it is necessary to develop better methods by using additional additives or advanced mixing methods to create composites with improved uniform distribution.

4. Conclusions

The effects of different sizes of PRGs on physicochemical, microstructural and mechanical properties of cement-based mortars have been presented and evaluated in this study. Based on the results and discussion above, the following conclusions have been drawn:

1. The addition of PRGs additive to cement-based mortars enhances their compressive and tensile strengths at 7 days and 28 days. The enhancement accounts for the improvement of compactness of mortars, which is due to the increase in cement hydration degrees, the reduction of distances between cement particles, and the most important part from mechanical adhesion forces between PRGs and cement gels.

2. Compressive and tensile strengths of the cement mortars considerably depend on the sizes of PRGs additive. While the small size (5 μm) presents no significant effect on both mechanical tests, the large size (43 μm) only shows a significant influence on tensile strengths. The ultra-large sizes (56 μm and 73 μm) have shown the most prominent benefit to compressive and tensile strengths at both testing days.

3. The results from XRD, FTIR, and SEM analyses show that compressive and tensile strengths PRG-cement mortars have a close

relationship with their physicochemical and microstructure properties. The higher mechanical strengths they are, the better microstructures they have.

4. The use of PRGs in cement composites as an additive can support to reduce the mass of cement production, and thus decrease the amount of the CO_2 emission into the atmosphere caused by cement production, contributing to mitigating the global warming gases and climate change yearly.

The results from the study confirm the prominent benefit of the ultra-large sizes on mechanical properties of cementitious composites. This provides the potential to apply ultra-large PRG sizes to cementitious composites as additives to not only enhance both compressive and tensile strengths but also contribute to alleviating the global warming gases. The study also contributes to providing a fast track in studying PRG and cement composites to investigate the influence of PRGs on other properties of cementitious composites, such as permeability, toughness, shrinkage, or corrosion; therefore, the application of this promising additive in practice for building materials could complete soon.

Declaration of Competing Interest

The authors declare that they have no known competing financial interests or personal relationships that could have appeared to influence the work reported in this paper.

Acknowledgements

This work is supported and funded by the ARC Research Hub for Graphene Enabled Industry Transformation (IH 1500003) and First Graphene Ltd (Perth, WA, Australia). The authors also thank the Schools of Civil, Environmental and Mining Engineering and School of Chemical Engineering and Advanced Materails at the University of Adelaide for supporting this work. The authors also acknowledge Adam Ryntjes and Dale Hodson as the technical support in the experimental works.

References

[1] H.F.W. Taylor Cement chemistry 2 1997 Thomas Telford Publishing
[2] D. Chung, Comparison of submicron-diameter carbon filaments and conventional carbon fibers as fillers in composite materials, Carbon 39 (8) (2001) 1119–1125.
[3] E.T. Dawood, M. Ramli, High strength characteristics of cement mortar reinforced with hybrid fibres, Constr. Build. Mater. 25 (5) (2011) 2240–2247.
[4] P. Stynoski, P. Mondal, C. Marsh, Effects of silica additives on fracture properties of carbon nanotube and carbon fiber reinforced Portland cement mortar, Cem. Concr. Compos. 55 (2015) 232–240.
[5] A. Cwirzen, K. Habermehl-Cwirzen, A. Nasibulin, E. Kaupinen, P. Mudimela, V. Penttala, SEM/AFM studies of cementitious binder modified by MWCNT and nano-sized Fe needles, Mater. Charact. 60 (7) (2009) 735–740.
[6] B.M. Tyson, R.K. Abu Al-Rub, A. Yazdanbakhsh, Z. Grasley, Carbon nanotubes and carbon nanofibers for enhancing the mechanical properties of nanocomposite cementitious materials, J. Mater. Civ. Eng. 23 (7) (2011) 1028–1035.
[7] M.S. Konsta-Gdoutos, C.A. Aza, Self sensing carbon nanotube (CNT) and nanofiber (CNF) cementitious composites for real time damage assessment in smart structures, Cem. Concr. Compos. 53 (2014) 162–169.
[8] K. Rashid, S. Farooq, A. Mahmood, S. Iftikhar, A. Ahmad, Moving towards resource conservation by automated prioritization of concrete mix design, Constr. Build. Mater. 236 (2020) 117586.
[9] R. Maddalena, J.J. Roberts, A. Hamilton, Can Portland cement be replaced by low-carbon alternative materials? A study on the thermal properties and carbon emissions of innovative cements, J. Clean. Prod. 186 (2018) 933–942.
[10] M. Schneider, M. Romer, M. Tschudin, H. Bolio, Sustainable cement production—present and future, Cem. Concr. Res. 41 (7) (2011) 642–650.
[11] G.L. Golewski, Generalized fracture toughness and compressive strength of sustainable concrete including low calcium fly ash, Materials 10 (12) (2017) 1393.
[12] P.K. Mehta, H. Meryman, Tools for reducing carbon emissions due to cement consumption, Structure 1 (1) (2009) 11–15.
[13] A. Gholampour, V.D. Ho, T. Ozbakkaloglu, Ambient-cured geopolymer mortars prepared with waste-based sands: Mechanical and durability-related properties and microstructure, Compos. B Eng. 160 (2019) 519–534.
[14] P. Van den Heede, N. De Belie, Environmental impact and life cycle assessment (LCA) of traditional and 'green'concretes: literature review and theoretical calculations, Cem. Concr. Compos. 34 (4) (2012) 431–442.
[15] B. Lothenbach, K. Scrivener, R. Hooton, Supplementary cementitious materials, Cem. Concr. Res. 41 (12) (2011) 1244–1256.
[16] E. Shamsaei, F.B. de Souza, X. Yao, E. Benhelal, A. Akbari, W. Duan, Graphene-based nanosheets for stronger and more durable concrete: A review, Constr. Build. Mater. 183 (2018) 642–660.
[17] T.H.Y. Nguyen, K. Tsuchiya, D. Atarashi, Microstructure and composition of fly ash and ground granulated blast furnace slag cement pastes in 42-month cured samples, Constr. Build. Mater. 191 (2018) 114–124.
[18] H. Yang, H. Cui, W. Tang, Z. Li, N. Han, F. Xing, A critical review on research progress of graphene/cement based composites, Compos. A Appl. Sci. Manuf. 102 (2017) 273–296.
[19] O. Karahan, Transport properties of high volume fly ash or slag concrete exposed to high temperature, Constr. Build. Mater. 152 (2017) 898–906.
[20] A. Gholampour, T. Ozbakkaloglu, Performance of sustainable concretes containing very high volume Class-F fly ash and ground granulated blast furnace slag, J. Cleaner Prod. 162 (2017) 1407–1417.
[21] B. Han, S. Sun, S. Ding, L. Zhang, X. Yu, J. Ou, Review of nanocarbon-engineered multifunctional cementitious composites, Compos. A Appl. Sci. Manuf. 70 (2015) 69–81.
[22] A.K. Geim, K.S. Novoselov, The rise of graphene, Nat. Mater. 6 (3) (2007) 183–191.
[23] X. Li, Y.M. Liu, W.G. Li, C.Y. Li, J.G. Sanjayan, W.H. Duan, Z. Li, Effects of graphene oxide agglomerates on workability, hydration, microstructure and compressive strength of cement paste, Constr. Build. Mater. 145 (2017) 402–410.
[24] Q. Wang, J. Wang, C.-X. Lu, B.-W. Liu, K. Zhang, C.-Z. Li, Influence of graphene oxide additions on the microstructure and mechanical strength of cement, New Carbon Mater. 30 (4) (2015) 349–356.
[25] S. Lv, J. Liu, T. Sun, Y. Ma, Q. Zhou, Effect of GO nanosheets on shapes of cement hydration crystals and their formation process, Constr. Build. Mater. 64 (2014) 231–239.
[26] A. Gholampour, M.V. Kiamahalleh, D.N. Tran, T. Ozbakkaloglu, D. Losic, Revealing the dependence of the physiochemical and mechanical properties of cement composites on graphene oxide concentration, RSC Adv. 7 (87) (2017) 55148–55156.
[27] S. Sharma, N. Kothiyal, Influence of graphene oxide as dispersed phase in cement mortar matrix in defining the crystal patterns of cement hydrates and its effect on mechanical, microstructural and crystallization properties, RSC Adv. 5 (65) (2015) 52642–52657.
[28] S. Lv, Y. Ma, C. Qiu, T. Sun, J. Liu, Q. Zhou, Effect of graphene oxide nanosheets of microstructure and mechanical properties of cement composites, Constr. Build. Mater. 49 (2013) 121–127.
[29] B. Wang, R. Jiang, Z. Wu, Investigation of the mechanical properties and microstructure of graphene nanoplatelet-cement composite, Nanomaterials 6 (11) (2016) 200.
[30] H. Du, S. Dai Pang, Enhancement of barrier properties of cement mortar with graphene nanoplatelet, Cem. Concr. Res. 76 (2015) 10–19.
[31] J. Tao, X. Wang, Z. Wang, Q. Zeng, Graphene nanoplatelets as an effective additive to tune the microstructures and piezoresistive properties of cement-based composites, Constr. Build. Mater. 209 (2019) 665–678.
[32] V.D. Ho, C.-T. Ng, C.J. Coghlan, A. Goodwin, C. Mc Guckin, T. Ozbakkaloglu, D. Losic, Electrochemically produced graphene with ultra large particles enhances mechanical properties of Portland cement mortar, Constr. Build. Mater. 234 (2020) 117403.
[33] S. Chuah, Z. Pan, J.G. Sanjayan, C.M. Wang, W.H. Duan, Nano reinforced cement and concrete composites and new perspective from graphene oxide, Constr. Build. Mater. 73 (2014) 113–124.
[34] Y. Zhu, S. Murali, W. Cai, X. Li, J.W. Suk, J.R. Potts, R.S. Ruoff, Graphene and graphene oxide: synthesis, properties, and applications, Adv. Mater. 22 (35) (2010) 3906–3924.
[35] AS3972, General purpose and blended cements, Standard, Standard Australia, Australian Standard, 2010.
[36] AS1478.1, Chemical admixtures for concrete, mortar and grout - Admixtures for concrete, Australian Standard, 2000.
[37] ASTM-C109/C109M-07, Standard test method for compressive strength of hydraulic cement mortars, ASTM International: USA 2008, 2008.
[38] ASTM-C307-03, Standard Test Method for Tensile Strength of Chemical-Resistant Mortar, Grouts, and Monolithic Surfacings Monolithic Surfacings, ASTM International, 2012.
[39] T.T. Mai, C.N. Ha Thuc, H.H. Thuc, Preparation of graphene nano-layer by chemical graphitization of graphite oxide from exfoliation and preliminary reduction, Fullerenes, Nanotubes and Carbon Nanostructures 23(8) (2015) 742-749.
[40] A. Eckmann, A. Felten, A. Mishchenko, L. Britnell, R. Krupke, K.S. Novoselov, C. Casiraghi, Probing the nature of defects in graphene by Raman spectroscopy, NANOLett. 12 (8) (2012) 3925–3930.
[41] Y. Shen, A.C. Lua, Sci. Rep. 3 (1) (2013) 1–6.
[42] S. Sharma, N. Kothiyal, Comparative effects of pristine and ball-milled graphene oxide on physico-chemical characteristics of cement mortar nanocomposites, Constr. Build. Mater. 115 (2016) 256–268.
[43] R. Jadhav, N. Debnath, Computation of X-ray powder diffractograms of cement components and its application to phase analysis and hydration performance of OPC cement, Bull. Mater. Sci. 34 (5) (2011) 1137–1150.

[44] J. Wang, J. Tao, L. Li, C. Zhou, Q. Zeng, Thinner fillers, coarser pores? A comparative study of the pore structure alterations of cement composites by graphene oxides and graphene nanoplatelets, Compos. A Appl. Sci. Manuf. 130 (2020).
[45] M. Horgnies, J. Chen, C. Bouillon, Overview about the use of Fourier transform infrared spectroscopy to study cementitious materials, WIT Trans. Eng. Sci 77 (2013) 251–262.
[46] P. Yu, R.J. Kirkpatrick, B. Poe, P.F. McMillan, X. Cong, Structure of calcium silicate hydrate (C-S-H): Near-, mid-, and far-infrared spectroscopy, J. Am. Ceram. Soc. 82 (3) (1999) 742–748.
[47] L. Fernández Carrasco, D. Torrens Martín, L. Morales, S. Martínez Ramírez, Infrared spectroscopy in the analysis of building and construction materials, InTech2012.
[48] S. Ghosh, S. Handoo, Infrared and Raman spectral studies in cement and concrete, Cem. Concr. Res. 10 (6) (1980) 771–782.
[49] J. Jiang, Q. Zheng, D. Hou, Y. Yan, H. Chen, W. She, S. Wu, D. Guo, W. Sun, Calcite crystallization in the cement system: morphological diversity, growth mechanism and shape evolution, PCCP 20 (20) (2018) 14174–14181.
[50] S. Lv, H. Hu, J. Zhang, X. Luo, Y. Lei, L. Sun, Fabrication of GO/cement composites by incorporation of few-layered GO nanosheets and characterization of their crystal/chemical structure and properties, Nanomaterials 7 (12) (2017) 457.
[51] Z. Pan, L. He, L. Qiu, A.H. Korayem, G. Li, J.W. Zhu, F. Collins, D. Li, W.H. Duan, M. C. Wang, Mechanical properties and microstructure of a graphene oxide–cement composite, Cem. Concr. Compos. 58 (2015) 140–147.
[52] S.J. Chen, C.Y. Li, Q. Wang, W.H. Duan, Reinforcing mechanism of graphene at atomic level: Friction, crack surface adhesion and 2D geometry, Carbon 114 (2017) 557–565.
[53] D. Hou, Z. Lu, X. Li, H. Ma, Z. Li, Reactive molecular dynamics and experimental study of graphene-cement composites: Structure, dynamics and reinforcement mechanisms, Carbon 115 (2017) 188–208.
[54] V. Bewick, L. Cheek, J. Ball, Statistics review 9: one-way analysis of variance, Critical Care 8 (2) (2004) 130.
[55] C.W. Dunnett, A multiple comparison procedure for comparing several treatments with a control, J. Am. Stat. Assoc. 50 (272) (1955) 1096–1121.
[56] A. Kargari, H. Eskandari-Naddaf, R. Kazemi, Effect of cement strength class on the generalization of Abrams' law, Structural Concrete 20 (1) (2019) 493–505.
[57] R. Arvidsson, D. Kushnir, B.r.A. Sandén, S. Molander, Prospective life cycle assessment of graphene production by ultrasonication and chemical reduction, Environmental science & technology 48(8) (2014) 4529-4536.